UNIVERSITÀ DEGLI STUDI DI MILANO

Doctorate School in Chemical Sciences and Technologies

Department of Chemistry

PhD course in Chemical Sciences – XXVI cycle

Advanced Materials for Electrode Modification in Trace Electroanalysis

PhD Candidate

VALENTINA PIFFERI

Tutor: Dr. Luigi FALCIOLA

PhD course Coordinator: Prof. Emanuela LICANDRO

Director of the School: Prof. Silvia ARDIZZONE

A.A. 2012-2013

TABLE OF CONTENTS

1. EXTENDED ABSTRACT 6

2. INTRODUCTION 22

2.1. TRACE ANALYSIS 22
2.2. ELECTROANALYTICAL TECHNIQUES 23
2.3. AIM OF THE THESIS 25

3. SCREEN-PRINTED-ELECTRODES 26

3.1. INTRODUCTION 26
3.2. PLATINUM-BASED ELECTRODES: FURAN DETERMINATION 29
3.2.1. Furan 29
3.2.2. Materials and methods 31
3.2.3. Results and Discussion 31
3.2.4. Conclusions 36
3.3. CARBON-BASED AND PLATINUM-BASED ELECTRODES: BENZIDINES DETERMINATION 38
3.3.1. Benzidine and its derivatives 38
3.3.2. Materials and Methods 41
3.3.3. Results and Discussion 42
3.3.4. Conclusions 54
3.4. BISMUTH OXIDE-BASED ELECTRODES: CHROMIUM DETERMINATION 56
3.4.1. Chromium 56
3.4.2. Materials and Methods 59
3.4.3. Results and Discussion 59
3.4.4. Conclusions 68
3.5. GOLD-BASED ELECTRODES: ARSENIC DETERMINATION 70
3.5.1. Arsenic 70
3.5.2. Materials and Methods 71
3.5.3. Results and Discussion 72
3.5.4. Conclusions 78

4. NANOMATERIALS 80

4.1. CARBON-BASED NANOMATERIALS 84
4.1.1. Introduction 84
4.1.2. Carbon Nanotubes 86
4.1.2.1. Introduction 86
4.1.2.2. Materials and Methods 89
4.1.2.3. Results and Discussion 90

4.1.2.4. Conclusions 123
4.2. METALLIC AND SEMICONDUCTOR NANOPARTICLES 126
4.2.1. Introduction 126
4.2.2. Gold Nanoparticles and Carbon Nanotubes 128
4.2.2.1. Gold 128
4.2.2.2. Materials and Methods 129
4.2.2.3. Results and Discussion 130
4.2.2.4. Conclusions 141
4.2.3. Synthetic Silver Nanoparticles 143
4.2.3.1. Silver 143
4.2.4. Silver Nanoparticles on Nafion 145
4.2.4.1. Materials and Methods 145
4.2.4.2. Results and Discussion 146
4.2.4.3. Conclusions 154
4.2.5. Silver Nanoparticles on Carbon Nanotubes 156
4.2.5.1. Materials and Methods 156
4.2.5.2. Results and Discussion 157
4.2.5.3. Conclusions 165
4.2.6. Titanium Dioxide and Carbon Nanotubes 166
4.2.6.1. Titanium dioxide 166
4.2.6.2. Materials and Methods 167
4.2.6.3. Results and Discussion 168
4.2.6.4. Conclusions 178

5. CONDUCTING POLYMERS 180

5.1. INTRODUCTION 180
5.2. ELECTRON CONDUCTING POLYMERS 184
5.2.1. Poly(Brilliant Green) 184
5.2.2. Materials and Methods 186
5.2.3. Results and Discussion 189
5.2.4. Conclusions 209
5.3. CATION CONDUCTING POLYMERS 211
5.3.1. Poly(Aryl Ether Sulfone) 211
5.3.2. Materials and Methods 213
5.3.3. Results and Discussion 214
5.3.4. Conclusions 232

6. CONCLUSIONS 234

7. REFERENCES 238

8. APPENDIXES 265

8.1. ANALYTICAL PARAMETERS 265

8.2. ELECTROANALYTICAL TECHNIQUES (OUTLINES) 266

8.2.1. Cyclic Voltammetry (CV) 266

8.2.2. Electrochemical Impedance Spectroscopy (EIS) 267

8.2.3. Other voltammetric or amperometric techniques 267

8.3. LIST OF PAPERS AND CONGRESS COMMUNICATIONS 268

9. ACKNOWLEDGEMENTS 271

1. Extended abstract

Trace analysis [1] (*i.e.* the analysis of analytes in concentration low enough to cause difficulty, generally under 1 ppm) albeit very challenging, in the last years has shown a tremendous growth, prompted by the urgent need of many International Organizations (US Environmental Protection Agency EPA, U.S. Food and Drug Administration FDA, European Food Safety Authority EFSA, World Health Organization WHO) looking for new analytical techniques for the detection of different molecules in different and increasingly more complex matrixes. Trace analysis is therefore a basic and fundamental technique in many scientific and technological areas, from the environmental monitoring, the food safety and the clinical diagnosis to the national security and the forensic investigation.

The determination of trace analytes requires reliable and robust analytical methods characterized by high level of sensitivity, precision, accuracy, selectivity and specificity. Among different analytical techniques suitable for this purpose, such as mass spectrometry, which is characterized by high accuracy and sensitivity and low limits of detection, **electroanalytical techniques** and particularly those based on pulsed voltammetry, seem to be a promising independent alternative in terms of very high precision, accuracy and sensitivity, simplicity of use, portability, easy automation and possibility of *on-line* and *on-site* monitoring without sample pre-treatments and low costs. These methods are no more confined to the detection of inorganic species and have been already and successfully employed for the determination of organic compounds and environmental carcinogens [2, 3, 4], as the Jirí Barek UNESCO

Laboratory of Environmental Electrochemistry and the Trace Element Satellite Centre haves amply demonstrated in the last decades.

In this context, two quite recent technological developments have enhanced the chances of progress and growth of electroanalitycal methodologies for trace analysis:

- **the screen-printing microfabrication technology** [5, 6], which offers the possibility of large-scale mass production of extremely inexpensive, disposable and reproducible electrochemical sensors increasing the potentialities of the voltammetric techniques, since it allows to work with small amounts of samples, considerably reducing the analytical costs and facilitating *on-line* and *on-site* monitoring;

- the use of **nanosized and/or nanostructured materials** sometimes combined with the use of **polymeric materials for the modification of electrodes**, with the aim of increasing the affinity for the analyte, increasing sensitivity, lowering the limits of detection and minimizing or completely avoiding interferences.

This PhD thesis has sought to provide a contribution in this framework, trying to enhance the technological potentialities of electroanalytical methodologies in the field of inorganic and organic trace analysis, with the use of screen-printed electrodes and electrodes modified by nanomaterials and/or polymeric membranes.

SCREEN-PRINTED electrodes

Different types of screen-printed electrodes (SPEs) were employed for the determination of organic and inorganic carcinogenic hazardous compounds, included in the Priority Pollutants

List of many countries. In particular, the following analytes have been the subject of the study: furan, benzidines, chromium and arsenic.

Furan, a volatile oxygen-containing heterocyclic compound, was classified as a possible human carcinogen by the International Agency for Research on Cancer (IARC) in 1995, with the liver as primary target organ. It is unintentionally produced, together with dioxin, during most forms of combustion. For this reason, it falls into the Organic Persistent Pollutants list of Stockholm Convention. It is also formed during the thermal degradation of carbohydrates in foods [7], such as jarred baby foods, coffee, canned meat and toasted bread. The standard analytical procedure [8] for the detection of furan is based on GC/MS, which reaches the very low detection limits required by the analytical problem, but it is affected by results overestimation since furan can be produced during the heating required by the technique.

A new electroanalytical method based on Square Wave Voltammetry (frequency of 100-200 Hz) at Pt disk and Pt-SPE covered by Nafion was studied. Furan shows an oxidation peak in acetonitrile at 1.85-1.95 V (SCE) for Pt disk and 1.95 V (SCE) for Pt-SPE. Both electrodes display a good linear correlation in the dynamic range between 1.02 ppm and 68.07 ppm. Pt disk presents a problem of saturation for higher concentration. The detection limits are quite good (0.11 ppm for Pt disk and 0.52 ppm for Pt-SPE), while apparent recovery factors (in both cases > 95%) are better than those determined for the conventional GC/MS method. The applicability of the new method in a real matrix was tested using Pt-SPE covered with Nafion membrane for experiments in coffee, spiked with known quantities of furan. Good calibration plot (R^2 = 0.997) and apparent recovery factor (102 %) were obtained also in this case.

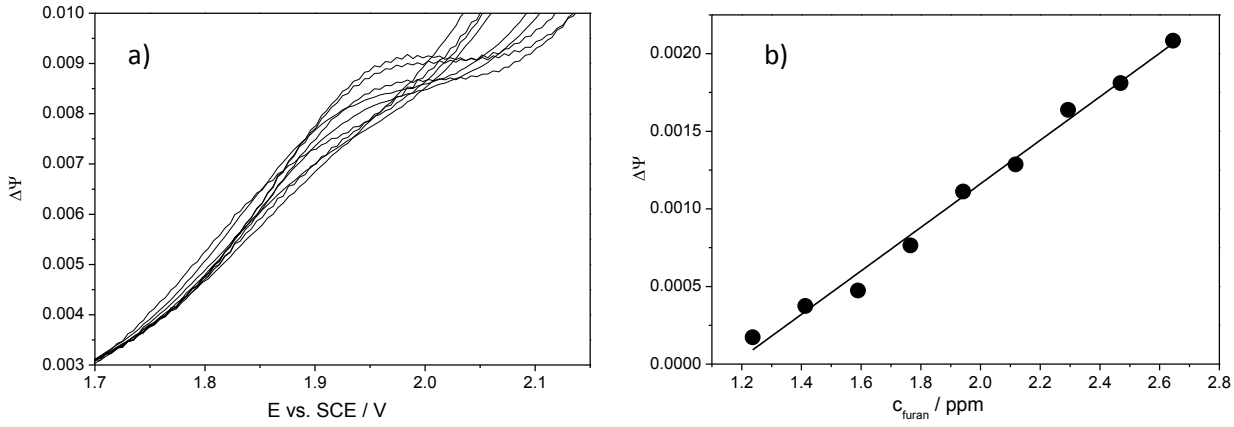

Figure 1.1. Square Wave Voltammetries of furan in acetonitrile with TBAP 0.1 M on Pt-SPE (a) and linear relationship between peak height and furan concentration (b).

Benzidine is an organic synthetic compound which exists as an odourless, white or slightly reddish crystalline solid and that evaporates slowly, especially from water and soil. Benzidine and its derivatives are employed in many fields but the main use remains the synthesis of azo-dyes, by coupling benzidine with phenols and amines [9], which are widely employed in textile, printing, leather, paper making, drug and food industries and can be released in the effluents and wastewaters. Benzidine was identified as a carcinogenic agent [10] for human urinary bladder by IARC because its oxidation by human enzymes can permit its binding with DNA. Furthermore, its derivatives generate benzidine through reduction by intestinal and environmental microorganisms. Though production and use of azo-dyes were forbidden in many countries since 1970s, their use in companies of emerging countries is still increasing, thus affecting the work place of many environments.

Electrochemical techniques for the detection of benzidine were tested at standard electrodes (Platinum and GC) with promising results [11, 12]. Benzidine and its derivatives (*o*-tolidine, *o*-toluidine, tetrametylbenzidine) were detected by Differential Pulse Voltammetry (DPV) using

Carbon-based Screen-Printed Electrodes (C-SPE) in comparison with Glassy Carbon electrodes. Cyclic voltammograms of these molecules show that the reaction is a bielectronic chemical and electrochemical reversible one for benzidine, *o*-tolidine and tetrametylbenzidine, while it is monoelectronic and irreversible for *o*-toluidine. The four molecules display different peak potential position, due to the presence or absence of electrodonating groups, tetrametylbenzidine characterized by the lower peak potential, followed by *o*-tolidine, benzidine and finally *o*-toluidine. In the case of the detection with DPV and C-SPE, all molecules show excellent linearity in the linear dynamic range 2 ppb-18 ppb ($R^2 > 0.9$), high accuracy (with apparent recovery factors very close to 100%) and very low detection limits (0.33 ppb for benzidine, 1.45 ppb for tetrametylbenzidine, 0.43 ppb for *o*-tolidine and 123 ppb for *o*-toluidine). Since the innovative technique seems to be very reliable and each molecule presents a different peak position, an interesting research development was the study of the behaviour of the mixture of the four molecules. Cyclic voltammograms show that they can be revealed at the same time and that their response remains linear and with a good correlation ($R^2 > 0.99$), also when they are present contemporaneously. Preliminary results using DPV display four observable peaks.

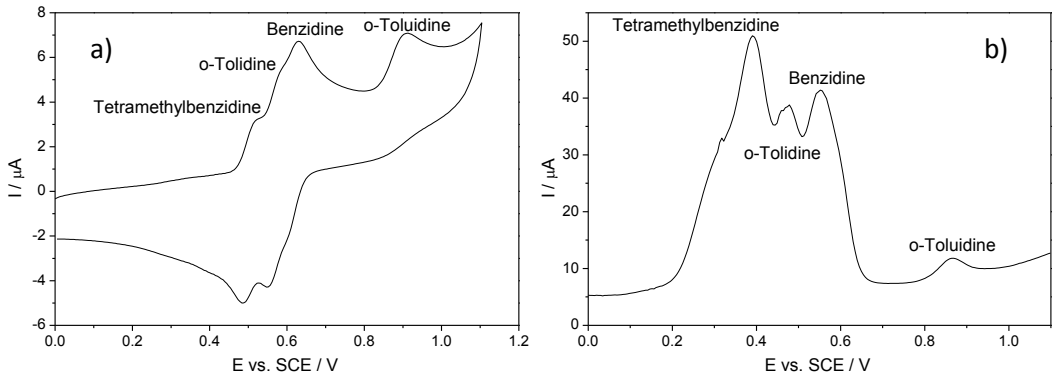

Figure 1.2. Cyclic (a) and differential pulse (b) voltammograms of all benzidines.

Chromium, particularly its hexavalent species, is a carcinogenic and mutagenic pollutant and it is located in the Priority Pollutants List of many countries. It is employed in several industrial processes (metal plating, leather tanning, paint making) and it can be especially found in waste waters. Therefore, in recent years, many efforts have been made to develop efficient and accurate techniques for its determination [13]. For this purpose mercury electrodes are widely used in association with voltammetric stripping techniques preceded by cathodic or anodic preconcentration steps, especially in the presence of chromium complexing agents. Nowadays, mercury tends to be replaced by other less toxic materials [14]. A promising alternative seems to be the environmentally friendly bismuth electrode [15, 16], since it presents an electrochemical behaviour very similar to mercury, in particular in the wide cathodic potential window.

Commercially available bismuth Screen-Printed Electrodes (Bi-SPE) were employed using Square Wave Voltammetry (SWV) to develop a new technique for the detection of Cr(VI), using pyrocatechol violet (PCV) as Cr(VI) complexing agent and electroactive probe and HEDTA as Cr(III) complexing agent to remove possible Cr(III) interferences. This innovative method was compared with the traditional procedure based on Differential Pulse Adsorptive Stripping Voltammetry (DPAdSV) at Hanging-Mercury Drop Electrode (HMDE). Many differences can be envisaged: first of all, PCV displays at Bi-SPE an intensive reduction peak at -1.18 V, which increases for consecutive additions of Cr(VI), in contrast with the decrease observed in the case of HMDE in the same conditions. This behaviour can be explained assuming that the complex Cr(VI)-PCV is electroactive at Bi-SPE and non-electroactive at HMDE. Secondly, PCV at Bi-SPE can be revealed without stripping, which is instead a necessary step required when adopting

HMDE. The new method shows a very good linearity range (R^2 = 0.996) and accuracy (Apparent Recovery Factors around 102%) and its limit of detection is an order of magnitude lower than that using HMDE (0.28 ppb against 2.8 ppb). The applicability of the new optimized procedure was tested analyzing samples coming from Cr(VI) photocatalysis in liquid phase to follow the photoreduction of Cr(VI) from a concentration of 2.8 ppm to the complete disappearance. The analysis was performed with an analyte addition method (three addition of the sample) after a calibration plot built with 8 standard additions. This method allows distinguishing the performances of different types of photocatalysts. The same test was also performed at HMDE for comparison: the new technique displays better results since it is less affected by interferences of the complex matrix.

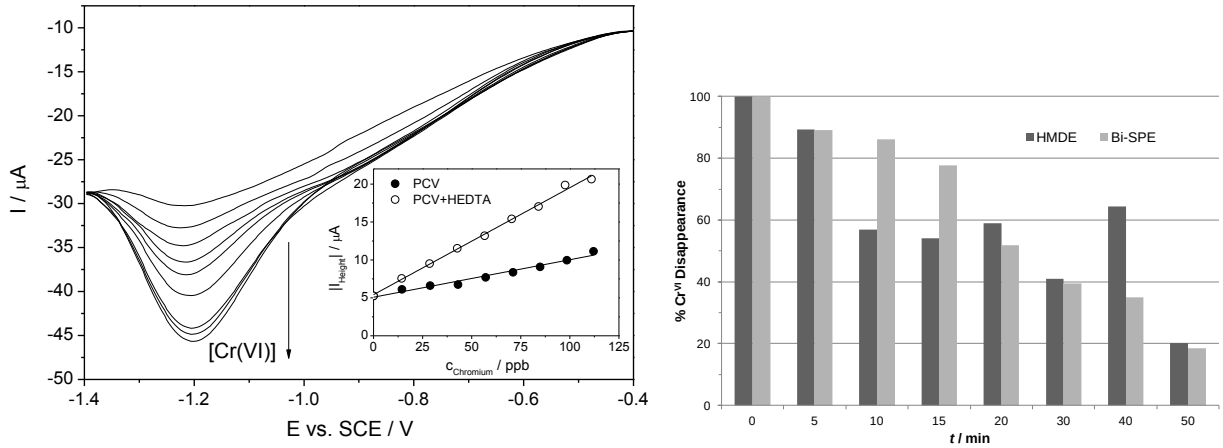

Figure 1.3. SW voltammograms at Bi-SPE for consecutive additions of Cr(VI) solution. Inset: calibration plots with (open circles) and without (full circles) HEDTA. Cr(VI) disappearance in T_400 photocatalytic test monitored by HDME and Bi-SPE.

Arsenic is a hazardous, dangerous and toxic compound, especially in its trivalent form, and arsenic contamination is widely recognized as a global health problem, ascribing it in the first places of the Priority Pollutants List. High levels of As can be found in soil, groundwater and drinking water, since arsenic derivatives are mainly used in agricultural poisons, such as

fungicides, insecticides, pesticides. Chronic arsenic exposure can cause a lot of health diseases, such as skin lesions, cancers, cardio-vascular system problems. For these reasons, many methods characterized by pros and cons are present in the Literature for As detection [17].

In this work, Gold-based screen-printed electrodes (Au-SPE) were used for the determination of As by Linear Sweep Voltammetry with a preconcentration step and a cleaning procedure. Citric acid was employed as supporting electrolyte instead of hydrochloric acid, which caused electrode damaging, and good calibration plots were obtained in the range 4.9-59 ppb, in particular for gold nanoparticles-based screen-printed electrodes. The optimized method was applied to As detection during its photocatalytic oxidation by titanium dioxide, allowing to discriminate among different types of photocatalysts.

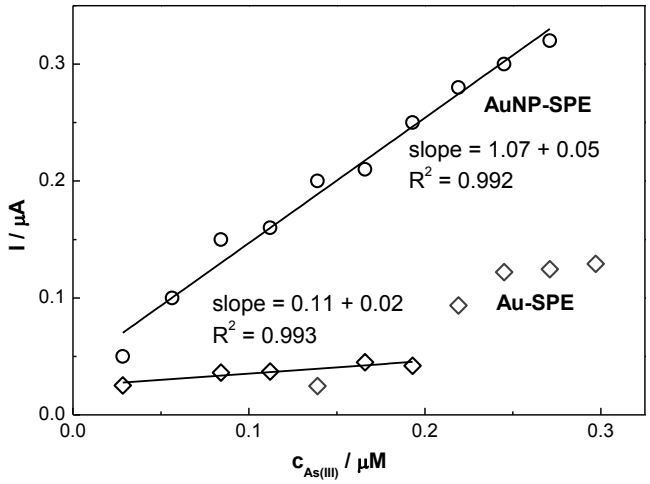

Figure 1.4. Calibration plots of Au-SPE and AuNP-SPE obtained for consecutive additions of As(III) solution.

ELECTRODES modified by NANOMATERIALS

An important advantage of electroanalytical techniques is the possibility to modify the working electrode with different types of advanced materials to increase the affinity for the analyte, to lower the limits of detection and to avoid interferences. In particular, during the last years,

nanomaterials appeared to be very promising for application in the field of sensors and biosensors. Among different types of nanomaterials, carbon nanotubes, metal and semiconductive nanoparticles, show very interesting properties and features for electrochemical performances and were chosen for the modification of electrodes to be used in selected trace electroanalytical applications.

All the new modified electrodes were firstly characterized and studied by Cyclic Voltammetry (CV) and Electrochemical Impedance Spectroscopy (EIS), in the presence or in the absence of a model probe molecule, in order to obtain important information about electrochemical properties and the behaviour of the electrode in solution and with the redox probe. After the characterization study, some electrodes were used as sensors for the determination of relevant compounds or pollutants at trace level.

Carbon nanotubes (CNT) [18, 19] are extensively employed in the electroanalytical field, due to their large surface area, electrocatalytic activity, fast electron transfer rate and easy functionalization. Since the procedure of purification with acids plays an important role for electrode performance, initially, a detailed study on different purification procedures was performed. 24 h sulfonitric mixture treatment appeared to be the best procedure for our CNTs yielding to materials characterized by an high metal nanoparticles removal, high amount of covalent acidity (responsible of CNTs activity), high surface area and mesoporosity. Moreover, the final removal of amorphous carbon by NaOH treatment highly improved the reversibility of the final electrodic device and favoured the diffusion mechanism of the process. The best type

of purified and activated CNTs was employed for applications in electroanalysis, in particular in the determination of some previously studied pollutants: *o*-toluidine, benzidine and furan.

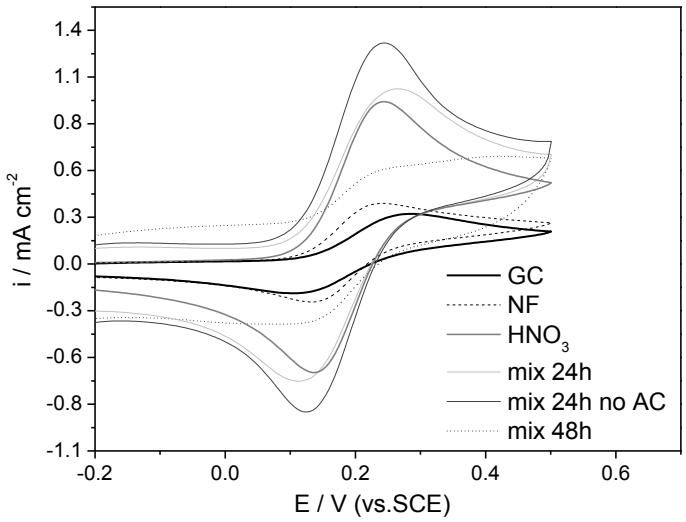

Figure 1.5. Cyclic voltammograms of CNTs after different purification methods.

o-toluidine was detected using Linear Sweep Voltammetry in the range 1.5-7 ppm with good correlation, obtaining a limit of detection of 0.16 ppm and excellent apparent recovery factors and repeatability, in comparison with carbon based-screen printed electrodes, which presented problems of fouling, probably due to polymerization products. This new method was used for the determination of *o*-toluidine during its photodegradation mediated by ZnO photocatalyst, showing better performances than C-SPE and comparable with HPLC. Moreover, the methodology was also employed to monitor *o*-toluidine absorption by cyclodextrine nanosponges based on hydrogel polyamidoamines (PAA), allowing to discriminate among various types of resins and to obtain absorption kinetic parameters.

Benzidine was determined by using Square Wave Voltammetry in the range 0.05-2.2 ppm, obtaining good correlation and good limits of detection at ppb level, with better apparent

recovery factors and repeatability in comparison with the previously optimized technique based on C-SPE.

In the case of furan, preliminary promising results were obtained with deposition of Pt nanoparticles on carbon nanotubes by cyclic voltammetry, but optimization of nanoparticles deposition procedure and application of other voltammetric techniques are still needed and are currently under investigation.

Metal and semiconductor nanoparticles [20] present unique peculiar properties, dependent on their size and shape, very different from bulk materials, such as high active surface area, high surface-to-volume ratio, selectivity, easy functionalization and electrocatalysis, and for these reasons they are extensively employed in electroanalysis. In this work, gold, silver and titanium dioxide nanoparticles were studied and characterized.

Gold nanoparticles, synthesized by colloidal procedure with or without a protective polymer on carbon nanotubes as support, showed in comparison with CNTs, an increase in the peak current and capacitance, followed by the decrease of charge transfer resistance. The polymer, if the content of gold is low, is detrimental for the electrochemical behaviour, probably because it isolates too much the gold nanoparticles. The best results were obtained with 1% Au or 5% Au-Polymer. The optimized electrode was tested for the determination of glycerol obtaining really promising preliminary results using cyclic voltammetry.

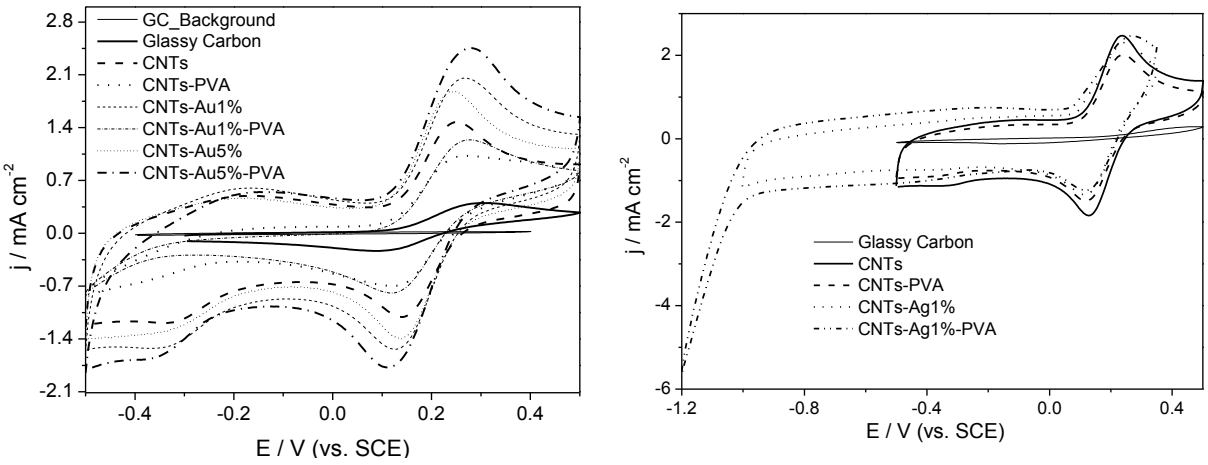

Figure 1.6. Cyclic voltammograms of Au (left) and Ag (right) nanoparticles and carbon nanotubes modified electrodes.

Silver nanoparticles were synthesized via colloidal method using two different supports: Nafion membrane and carbon nanotubes. In the case of Nafion, Ag nanoparticles show higher current intensity than bare electrode, probably due to higher surface area, a change in the diffusion mechanism from planar to convergent and small double layer formation. This electrode was tested for the determination of halothane and dichloromethane, showing promising preliminary results. In the case of CNTs, silver nanoparticles allowed the extension of the potential range towards negative values and peak currents were higher than the previous case with Nafion, showing the important contribute played by CNTs. Moreover, the use of a protective polymer (PVA) caused the decrease of the electrode activity, probably due to less available Ag nanoparticles.

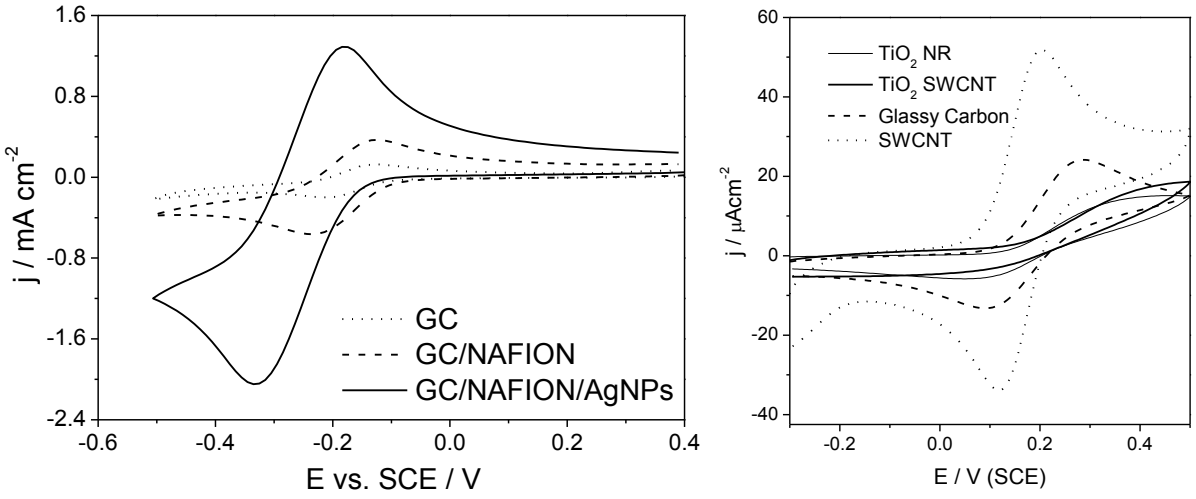

Figure 1.7. Cyclic voltammograms of silver nanoparticles (left) and titania nanorods (right) modified electrodes.

Titanium dioxide nanorods were studied in combination with single-walled carbon nanotubes, in the dark or under UV illumination, considering the photoactivity of titania. The best electrochemical performances were obtained for SWCNTs, since titania, as semiconductor brings a more resistive behaviour. Differences between dark and irradiation appeared only in the presence of titania, as expected. UV irradiation caused a change in the model probe molecule diffusion through the nanomaterials, probably ascribable to excited electrons of the titanium dioxide.

ELECTRODES modified by POLYMERIC MEMBRANES

Conducting polymers are polymeric systems characterized by ionic conductivity. They can be divided into two classes: electron and proton conducting polymers. Electron conducting polymers present a conjugated chain structure, with an extended π-bond system, leading to the formation of broad valence and conduction bands. Among all the types of electron conducting polymers, electroactive polymers seem to have the best qualities for the construction of

sensors [21, 22, 23]. Indeed, they can act as electron donors/acceptors, adding to the high conductivity, an electrocatalytic effect and a possibility of redox-mediation, showing both electronic and ionic conductivity in contact with the electrolyte solution.

Brilliant Green (BG), belonging to the triphenylmethane family, was chosen as electroactive polymer for the production of modified electrodes, in combination with CNTs and PEDOT [24], another non-redox electron conducting polymer. CNTs in combination with PEDOT gave the best electrochemical performance in terms of capacitance and low resistance, but when the determination of hydrogen peroxide was considered, electrode with CNTs and polyBG gave the best results for the presence of the redox centre (LoD around 30 ppb). This electrode was also tested as biosensor for glucose and ethanol, immobilizing on the electrode glucose oxidase (GOx) and alcohol oxidase (AlOx), respectively and showing very good results in comparison with the biosensors of the Literature, with limit of detections of 2 ppm for glucose and 1 ppm for ethanol. Moreover, the influence of oxygen was studied, obtaining better results in its presence for glucose detection and in its absence for ethanol determination, probably due to the aerobic or anaerobic character of the enzyme bacterium.

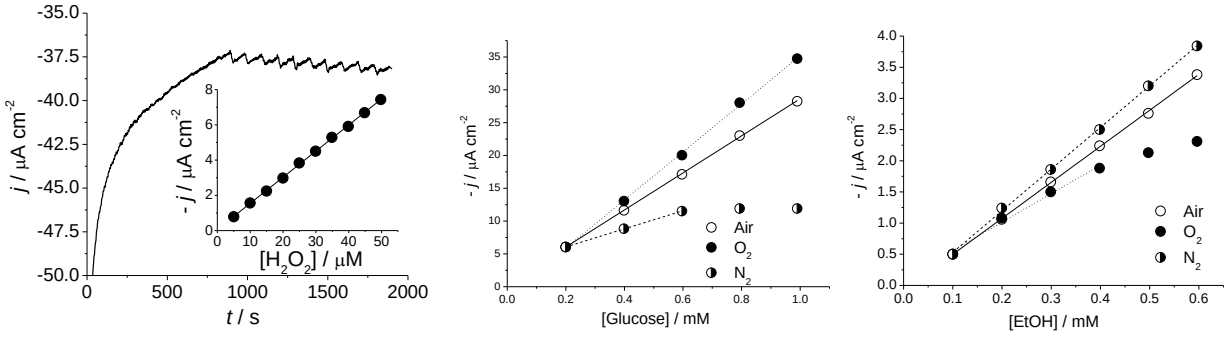

Figure 1.8. Amperometric detection of hydrogen peroxide (left) and calibration plots obtained for glucose (centre) and ethanol (right) in different atmospheres.

Proton conducting polymers show a cation/proton conductivity along the polymer backbone thanks to the presence of carboxylated or sulfonated groups with a cationic counter ion, whose mobility can be increased by water swelling. For this peculiarity, they present low electrical resistance (obtained increasing ion exchange capacity and water content and decreasing membrane thickness), high permeoselectivity for anions and non-ionized molecules, good mechanical and chemical stability over long periods. Their properties depend on many factors, such as the chemical nature of the polymer backbone, the polymer molecular weight and molecular weight distribution, the nature of the solvent used for casting and the possible presence of residual solvent in the polymeric film.

Poly(aryl ether sulfone) (PES) was studied as a new material for the production of modified electrodes in comparison with Nafion. For its characterization, different parameters have been studied: the quantity and the form of the polymer, its storage, its method of drying and the casting solvent. In particular, 1 % linear PES in the acidic form, dried at 25 °C in oven, dissolved in N-Methylpyrrolidone, showed the best performance, superior to Nafion. These polymers presented a very interesting behaviour, since without the redox probe, capacitance was comparable to glassy carbon, while when the redox probe was present, capacitance increased of two orders of magnitude and diffusion of the probe changed, probably due to variation of diffusion mechanism in the polymeric structure.

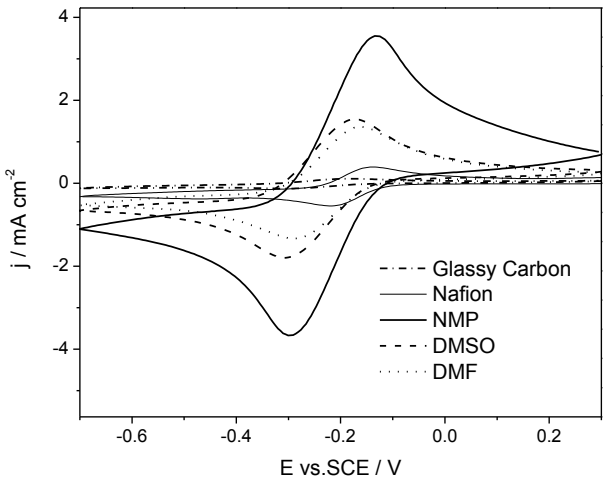

Figure 1.9. Cyclic voltammograms of linear 1 % PES in different solvents and comparison with Nafion and glassy carbon.

Future developments will consider the applications of these new interesting systems for the detection of various important analytes or pollutants. Furthermore, new types of sensors and biosensors based on different types of the advanced materials studied and their combination will be considered.

[1] D.T. Pierce, J.X. Zhao, *Trace Analysis with Nanomaterials*, Wiley-VCH, Weinheim (Germany), (2010)
[2] J. Zima, I. Svancara, J. Barek, K. Vytras, *Crit. Rev. Anal. Chem.* **2009**, 39, 204-227
[3] J. Barek, K. Peckova, V. Vyskocil, *Current Anal. Chem.* **2008**, 4, 242-249
[4] J. Barek, J. Cvacka, A. Muck, V. Quaiserovà, J. Zima, *Fres. J. Anal. Chem.* **2001**, 369, 556-562
[5] M. Alvarez-Icaza, U. Bilitewski, *Anal. Chem.* **1993**, 65, 525A-533A
[6] J. Wang, B. Tian, V.B. Nascimento, L. **2000**, 12, 1293-129
[7] J.A. Maga, CRC *Crit. Rev. Food Sci. and Nutrition* **1979,** 11, 355-400
[8] J. Vranová, Z. Ciesarová, *Czech J. Food Sci.* **2009,** 27, 1-10
[9] K.-T. Chung, S.-C. Chen, L. D. Claxton, *Mutation Research* **2006**, 612, 58–76
[10] T.J. Haley, *Clin. Toxicol.* **1975**, 8, 13–42
[11] J. Barek, A. Berka, Z. Tocksteinov, J. Zima, *Talanta* **1986**, 33, 811-815
[12] J. Barek, J. Cvacka, A. Muck, V. Quaiserovà, J. Zima, *Electroanalysis* **2001**, 13, 799-803
[13] V. Gomez, M.P. Callao, *TrAC, Trends Anal. Chem.* **2006,** 25, 1006–1015
[14] Directive 2008/51/EC
[15] I. Svancara, C. Prior, S.B. Hocévar, J. Wang, *Electroanalysis* **2010,** 22, 1405–1420
[16] J. Barek, K. Peckova, V. Vyskocil, *Curr. Anal. Chem.* **2008,** 42, 42–249
[17] V.K. Sharma, M. Sohn, *Environ. Int.* **2009**, 35, 743
[18] C.N.R. Rao, B.C. Satishkumar, A. Govindaraj, M. Nath, *ChemPhysChem*, **2001**, 2, 78-105
[19] J. J. Gooding, *Electrochimica Acta*, **2005**, 50, 3049-3060
[20] L. Rassaei, M. Amiri, C.M. Cirtiu, M. Sillanpaa, F. Marken, M. Sillanpaa, *Trends in Analytical Chemistry*, **2011**, 30 (11), 1705-1715 [21] M.E. Ghica, C.M.A. Brett, *Electroanalysis*, **2006**, 18, No. 8, 748-756
[22] M.M. Barsan, E.M. Pinto, C.M.A. Brett, *Electrochimica Acta*, **2008**, 53, 3973-3982
[23] M.E. Ghica, C.M.A. Brett, *Journal of Electroanalytical Chemistry*, **2009**, 629, 35-42
[24] X. Crispin, F.L.E. Jakobsson, A. Crispin, P.C.M. Grim, P. Andersson, A. Volodin, C. Van Haesendonck, M. Van der Auweraer, W.R. Salaneck, M. Berggren, *Chem. Mater.*, **2006**, 18, 4353-4360

2. Introduction

2.1. Trace analysis

Trace analysis (Pierce & Zhao, 2010) is the analysis of analytes in concentration low enough to cause difficulty, generally few ppm or even ppb. Trace analysis is a fundamental research field with important fallouts, from the environmental monitoring and national security, to food safety, clinical diagnosis and forensic investigation. In particular, it finds applications galore in water quality control for the determination of water pollutants, such as toxic metals, carcinogenic organic compounds, explosives, synthetic chemicals, pharmaceuticals, illicit drugs, cosmetics, personal care products and food supplements.

In this context, sensitive and robust analytical methodologies are essential, requiring the fundamental properties of high sensitivity, low detection limits, wide linear dynamic range, high selectivity, short response time, good reversibility and long-term stability. These characteristics can be obtained by using chemical sensors (Bănică, 2012), which are self-contained devices capable of providing real-time analytical information about a test sample containing the target species, the analytes. The chemical sensor integrates in the same device two important functions: recognition and transduction. The first function allows the analyte interacting in a more or less selective way with the recognition or sensing element; the second one consists on the sensor conversion of changes in physical or chemical properties of the sensing element into a measurable physical quantity. The first chemical sensor was the glass electrode for pH determination. A particular class of very selective and specific chemical sensors, which are

growing in importance, are the biosensors, characterized by a recognition system based on a biochemical/biological mechanisms.

Trace analysis based on the use of sensors and biosensors, has shown, in the last years, a tremendous growth, particularly prompted by the urgent need of many International Organizations (US Environmental Protection Agency EPA, U.S. Food and Drug Administration FDA, European Food Safety Authority EFSA, World Health Organization WHO) looking for new analytical techniques for the detection of different molecules in different and increasingly more complex matrixes and thanks to the development of new cross-disciplinary ideas among different fields, supported by the extensive research of novel high-tech materials and new methodologies.

2.2. Electroanalytical techniques

In the field of sensors and biosensors for trace analysis, electrochemical methodologies and techniques are really fundamental (Bănică, 2012). Electroanalysis (Lubert & Kalcher, 2010) is based on the measurement of electrical quantities, such as current, potential or charge, and allows the determination of different species in solution, expecially aqueous, both quantitatively and qualitatively.

Electroanalytical techniques (Bard & Faulkner, 2001; Bard, 2007; C. M. A. Brett & Oliveira Brett, 1993) can be divided into three classes, considering the measured electrical quantity: volt/amperometry, potentiometry and conductimetry (C. M. a. Brett, 2001; Hanrahan, Patil, & Wang, 2004). The first class is based on an applied potential between a reference and a working electrode, causing the oxidation or reduction of an electroactive species. The applied potential

is the driving force for the electron transfer reaction and the resulting current is the direct measure of the rate of electron transfer reaction, proportional to the target analyte concentration. The second class converts an ion-recognition event into a potential signal, calculated as the difference between the ion-selective electrode and the reference electrode, which is a function of species activity. The third class permits the determination of charge concentration through measurement of solution resistance. Clearly, all the three types of electroanalytical techniques can be influenced by the nature of the analyte, the type of electrode and the choice of the electrolyte.

For application in trace analysis, amperometry and voltammetry are the most employed techniques (Pierce & Zhao, 2010), since the possibility to choose and tune the applied potential together with the chance to vary the electrode material allows high selectivity, specificity and even speciation. Moreover, electrochemical instrumentation permits not only high sensitivity and low detection limits, but also the possibilities of real time data treatment, portability and sensor miniaturization (C. M. a. Brett, 2001). Furthermore, electrodes can show all the properties of an ideal sensor: high specificity for the target analyte, sensitivity to changes in target species concentration, fast response time, extended lifetime, small size with the possibility of low cost manufacture (Liza Rassaei et al., 2011). For all these reasons, electrochemical techniques can be used as alternative methodologies, possibly in combination with other detection methods (chromatography, luminescence, spectroscopy), showing low cost, easiness of use, accuracy and reliability. Furthermore, these techniques are no more confined to the detection of inorganic species and have been already and successfully employed for the determination of organic compounds and environmental carcinogens, as the

Jirí Barek UNESCO Laboratory of Environmental Electrochemistry and the Trace Element Satellite Centre has widely demonstrated in the last decades (Jiri Barek, Peckova, & Vyskocil, 2008; Jiří Zima, Švancara, Barek, & Vytřas, 2009).

2.3. Aim of the thesis

In this involving and challenging context, this PhD thesis has sought to provide a contribution for both the above correlated fields, trying to enhance the technological potentialities of electroanalytical methodologies for inorganic and organic trace analysis with the use of two quite recent technological developments, which showed the chances of progress and growth in this area:

- the screen-printing microfabrication technology, which offers the possibility of large-scale mass production of extremely inexpensive, disposable and reproducible electrochemical sensors. These devices increase the potentialities of the voltammetric techniques, since they allow to work with small amounts of samples, considerably reducing the analytical costs and facilitating on-line and on-site monitoring;

- the use of nanosized and/or nanostructured materials, possibly combined with the use of polymeric membranes for the modification of electrodes, with the aim of increasing the affinity for the analyte, improving sensitivity, lowering the limits of detection and minimizing or completely avoiding interferences.

3. Screen-Printed-Electrodes

3.1. Introduction

In the very last years, recent improvements in electroanalytical chemistry have been brought by the screen-printing microfabrication technology (Metters, Kadara, & Banks, 2011). This technique is based on the use of a screen, in particular a porous woven mesh, where a stencil is formed and a thixotropic fluid is forced on the mesh, which defines the shape and the size of the desired electrode. The thixotropic fluid is an ink with high viscosity and it is composed by graphite, carbon black, solvents and a polymeric binder. After this operation, the screen is pressed on the desired substrate, usually ceramic material, to obtain the desired device. The thickness of the layer can be modulated between 20 to 100 μm. This printing procedure has been commonly used for large-scale production of extremely inexpensive, disposable and yet highly reproducible electrochemical sensors, increasing the potentialities of the voltammetric methods (Joseph Wang, Tian, Nascimento, & Angnes, 1998).

Screen-printed electrodes are complete electrochemical cells (Figure 3.1), since they are usually composed by three electrodes: a working electrode of the desired material, a pseudo-reference electrode, usually of silver, and a counter electrode, normally of carbon. SPEs can be designed in different ways and configurations, according to specific aims; for example with two working electrodes or as array of electrodes.

These devices present several advantages with respect to conventional bulk electrodes: easiness of use, low cost, good precision and accuracy, high sensitivities and low detection

limits, portability, disposability, the possibility to work with small amounts of samples and the adaptability to specific target analytes (Metters et al., 2011). SPEs may also constitute an interesting, reliable and low-cost choice to be used as electrochemical detector for chromatography, particularly HPLC.

They can also be modified with various types of compounds, such as nanomaterials, metal nanoparticles, mediators and metal oxide, like bismuth oxide, paving the way for interesting potential applications in clinical and environmental fields, in aqueous or non-aqueous solvents. SPEs find application in routine water quality tests, for the monitoring of pH, dissolved oxygen, nitrite and phosphate, in environmental pollutant analysis (M. Li, Li, Li, & Long, 2012) of organic compounds, such as phenols, pesticides, herbicides and polyaromatic hydrocarbons, and of heavy metals, such as Pb(II), Cd(II), Hg(II) and As(III), in the determination of gas pollutants (CO, NOx and VOCs) and in the medical field (Alvarez-lcaza & Bilitewski, 1993; Serena Laschi, Fránek, & Mascini, 2000), for the detection of bacteria, drugs and antibiotic residues.

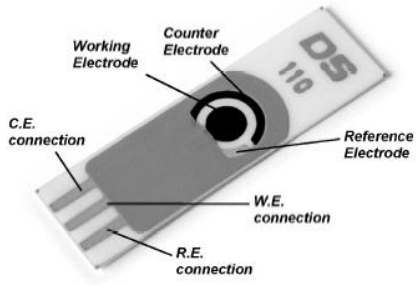

Figure 3.1. Screen-printed electrode scheme

In this chapter, different types of commercially available screen-printed electrodes were studied to find new electroanalytical methodologies for the determination of various pollutants, organic and inorganic, in food matrix or water:

- Platinum-based SPEs for the determination of furan in water and coffee;
- Carbon-based and Platinum-based SPEs for the determination of benzidine and its derivatives in water;
- Bismuth oxide-based SPEs for the determination of Chromium (VI) in water;
- Gold-based SPEs for the determination of Arsenic (III) in water.

3.2. Platinum-based electrodes: Furan determination

3.2.1. Furan

Furan (Figure 3.2) is a volatile oxygen eterocyclic compound which is unintentionally produced, together by dioxin, during different forms of combustion, such as municipal or medical wastes burning, backyard trash burning and industrial processes (Stockholm Convention on Organic Persistent Pollutants). It is also a trace contaminant in herbicides, in wood preservatives and in foods, where it is also responsible, together with its derivatives (furaldehyde, furfuryl alcohol), of their flavour. Furan is produced by commercial or domestic heat treatment, when thermal degradation of carbohydrates takes place, and for this reason it can be found in canned, jarred and roasted foods, like coffee or jarred baby foods.

The International Agency for Research on Cancer (IARC, 1995) has classified furan as possible human carcinogen, with the liver as primary target organ, after oral application. For this reason, a limit of 1×10^{-3} mg/kg a day is defined as the Reference Dose for Chronic Oral Exposure stated by the United States Environmental Protection Agency (US EPA). Moreover, several reports on the occurrence of furan in food were published by many healthcare international agencies (European Food and Safety Authority, US Food and Drug Administration (US FDA), Swiss Federal Office of Public Health), regarding also the available analytical methodologies for its determination. The scarce available data about its presence in food and about its reliable risk assessment has urged the need of new improved analytical methodologies.

Many analytical methods have been tested for furan determination in food and they can be resumed in two different approaches, the first based on head-space-GC/MS and the second on

solid-phase microextraction-GC/MS (Altaki, Santos, & Galceran, 2007; Goldmann, Périsset, Scanlan, & Stadler, 2005; La Pera et al., 2009). These methods are rapid and highly sensitive, but they require high-cost instrumentation and qualified personnel. Another problem is the possible generation of furan during analysis, due to the heating of the foodstuff required by the methodology, which can affect the final results.

In the Literature, only few examples on the electrochemical activity of furan are reported. Furan has been characterized in acetonitrile by electrochemical methods, particularly because of its use as starting monomer for the electrochemical polymerization of conducting films (Demirboğa & Önal, 1999). The determination of furanics (furaldehyde and furfuryl alcohol) in transformer oils with amperometric techniques is reported in two cases, but in this case furan was found to be non-electroactive (Bosworth, Setford, Heywood, & Saini, 2001).

In this context, electroanalytical techniques for the detection of furan could offer a good alternative to other analytical methods and, in particular, the use of screen-printed electrodes could allow a rapid, portable and low cost determination.

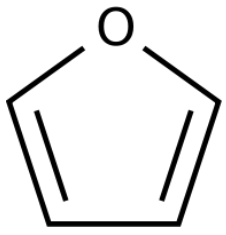

Figure 3.2. Chemical structure of furan

3.2.2. Materials and methods

Acetonitrile was chosen as solvent and 0.1 M tetrabuthylammonium perchlorate (TBAP) as supporting electrolyte, referring to (Demirboğa & Önal, 1999; Groenendaal, Zotti, Aubert, Waybright, & Reynolds, 2003).

Among different working materials tested, only Pt disk electrode presented an electrochemical response in acetonitrile, and was chosen to develop the new electroanalytical methodology for the determination of furan.

Two types of Pt-based electrodes were used:

- Pt disk electrode
- Platinum Screen-Printed Electrode (Pt-SPE) with or without Nafion membrane, used to prevent electrode fouling.

The voltammetric technique used was Square Wave Voltammetry (SWV).

3.2.3. Results and Discussion

Furan at Pt electrode shows a chemical and electrochemical irreversible oxidation peak at 1.945 V (SCE). Square Wave Voltammetry was chosen as electroanalytical technique among the other voltammetric or amperometric tested, because it provided the best performances: high intensity of the signal and high sensitivity.

SWV parameters were optimized, in particular the frequency value, that strongly affects the voltammetric response. The peak height and consequently the sensitivity increases by

increasing the frequency, but it is accompanied by an enhancement of the background noise. Different tests in the range 10-500 Hz were performed, concluding that the frequencies of 100 and 200 Hz appear to be the best choice. The optimized parameters are presented in Table 3.1.

Table 3.1. Square Wave Voltammetric parameters

Parameter	Value
Purging time (s)	60
Equilibration time (s)	10
Frequency (Hz)	100-200
Start potential (V)	1.50
End potential (V)	2.40
Step potential (V)	0.005
Amplitude (V)	0.05

Calibration plots were obtained under the optimized conditions with consecutive additions of 0.01 M furan. The peak at 1.945 V (SCE) increases linearly with furan concentration for both electrodes in the range 1-70 ppm, as shown in Figure 3.3 and Figure 3.4. Calibration plots show good linear correlation, better for peak height than for peak area. Saturation was reached at 70 ppm in the case of Pt bulk electrode.

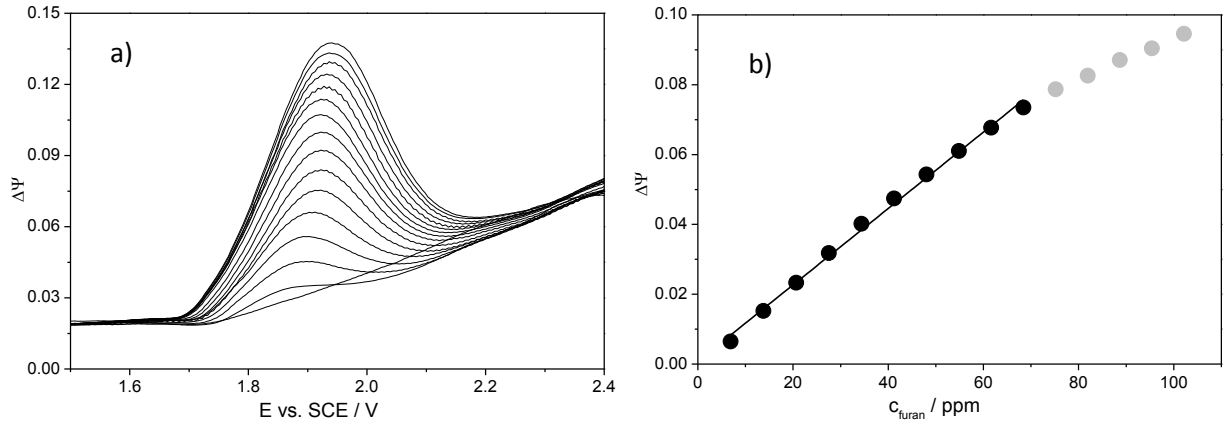

Figure 3.3. Square Wave Voltammetries of furan in acetonitrile with TBAP 0.1 M on Pt disk electrode (a) and linear relationship between peak height and furan concentration (b).

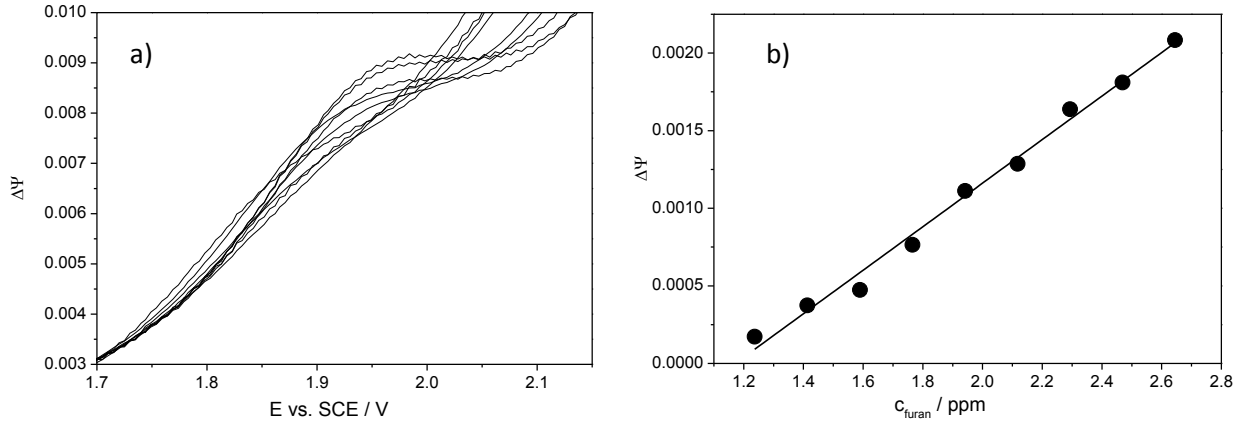

Figure 3.4. Square Wave Voltammetries of furan in acetonitrile with TBAP 0.1 M on Pt-SPE (a) and linear relationship between peak height and furan concentration (b).

Table 3.2-3.3-3.4-3.5 report the analytical parameters of the tested methodologies. In this context, the cross-validated correlation coefficients R^2_{CV} (Currie, 1995) are considered to evaluate the effective predictive power of the proposed method in comparison with the fitting power described by R^2. Both R^2 present values very close to 1. LoD and LoQ are good and better for Pt disk. Apparent recovery factors were calculated measuring three different concentrations and present values close to 100 %. Repeatability was also tested, reaching quite good values of

RSD %, particularly if compared with the results obtained with other non-electroanalytical methodologies (Altaki et al., 2007; Goldmann et al., 2005; La Pera et al., 2009).

The use of Nafion (Gouveia-caridade, Brett, & Liess, 2006) membrane to cover the electrodes had no-influence on the analytical parameters, as indicated by the very similar values, but it can prevent electrode fouling (Demirboğa & Önal, 1999).

Table 3.2. Analytical features of the proposed new method, using a Pt disk electrode, in the lower concentration range at a 100 Hz SW frequency.

c_{furan} / ppm	Peak	LoD / ppm	LoQ / ppm	R^2	R^2_{cv}	S / (A mol^{-1} dm^3)	RSD %	Apparent Recovery Factor %
2.05	Height	0.09	1.37	0.997	0.994	0.138 ± 0.003	4.4	102.1
4.08								101.2
5.43								99.1
2.05	Area	0.27	1.37	0.991	0.980	0.029 ± 0.001	5.1	102.3
4.08								101.7
5.43								97.5

Table 3.3. Analytical features of the method, using a Pt disk electrode, in the higher concentration range at a 100 Hz SW frequency.

c_{furan} / ppm	Peak	R^2	R^2_{cv}	S / (A mol^{-1} dm^3)	RSD%	Apparent Recovery Factor %
20.67	Height	0.997	0.993	0.074 ± 0.002	1.3	99.5
48.04					3.2	101.8
61.64					-	99.2
20.67	Area	0.995	0.992	0.0165 ± 0.0001	3.7	90.0
48.04					2.6	103.4
61.64					-	104.8

Table 3.4. Analytical features of the method, using peak heights of a Pt-SPE with or without Nafion, in the lower concentration range at two different SW frequencies.

c_{furan} / ppm	WE	Frequency / Hz	LoD / ppm	LoQ / ppm	R^2	R^2_{cv}	S / (A mol^{-1} dm^3)	RSD %	Apparent Recovery Factor %
1.24	SPE	100	0.95	1.06	0.992	0.987	0.064 ± 0.002	10.7	100.8
		200	0.94	1.06	0.995	0.991	0.070 ± 0.002	5.8	101.3
	SPE + Nafion	100	1.01	1.06	0.986	0.977	0.039 ± 0.002	9.0	102.5
		200	1.00	1.24	0.979	0.963	0.041 ± 0.002	5.9	105.3
1.94	SPE	100	0.78	1.41	0.987	0.972	0.039 ± 0.002	2.2	101.5
		200	0.54	1.41	0.965	0.931	0.043 ± 0.003	4.5	89.5
	SPE + Nafion	100	1.17	1.24	0.991	0.985	0.095 ± 0.003	5.6	101.5
		200	1.24	1.24	0.969	0.950	0.096 ± 0.006	4.8	109.0
2.47	SPE	100	1.45	1.59	0.974	0.960	0.085 ± 0.006	9.5	112.8
		200	1.54	1.59	0.975	0.944	0.099 ± 0.007	2.2	124.8
	SPE + Nafion	100	1.24	1.41	0.982	0.974	0.090 ± 0.005	7.1	97.5
		200	1.28	1.41	0.978	0.966	0.093 ± 0.006	5.3	104.6

Table 3.5. Analytical features of the method, using peak areas of a Pt-SPE with or without Nafion, in the lower concentration range at two different SW frequencies.

c_{furan} / ppm	WE	Frequency / Hz	LoD / ppm	LoQ / ppm	R^2	R^2_{cv}	S / (A mol^{-1} dm^3)	RSD %	Apparent Recovery Factor %
1.24	SPE	100	1.01	1.06	0.982	0.965	0.0109 ± 0.0005	11.8	97.9
		200	1.02	1.06	0.989	0.983	0.0122 ± 0.0004	5.2	99.5
	SPE + Nafion	100	1.10	1.06	0.980	0.964	0.0065 ± 0.0003	17.5	104.5
		200	1.09	1.24	0.979	0.964	0.0062 ± 0.0003	15.0	108.1
1.94	SPE	100	0.52	1.41	0.975	0.951	0.0045 ± 0.0003	2.5	101.0
		200	0.78	1.41	0.972	0.944	0.0070 ± 0.0005	9.9	94.3
	SPE + Nafion	100	1.23	1.24	0.986	0.971	0.0173 ± 0.0008	7.0	99.5
		200	1.32	1.24	0.969	0.952	0.017 ± 0.001	6.7	106.8
2.47	SPE	100	1.47	1.59	0.931	0.884	0.014 ± 0.002	12.0	116.1
		200	1.64	1.59	0.983	0.962	0.016 ± 0.001	3.7	133.2
	SPE + Nafion	100	1.28	1.41	0.977	0.967	0.0148 ± 0.0009	8.5	100.7
		200	1.31	1.41	0.975	0.961	0.015 ± 0.001	7.4	108.0

The new method for the detection of furan was applied to a complex matrix to verify the efficiency of the electroanalytical procedure in a real case. Coffee was chosen as matrix, since

furan can be present in this beverage. Coffee samples, obtained by capsules with the following composition: 40 % Arabic Brazilian and 60 % Robusta Asian ground coffee, were spiked with 0.01 M furan. Pt-SPEs covered with 0.01 % Nafion were used as electroanalytical cells and calibration plots were carried out under the same conditions of the previous experiments, with addition of 0.01 M furan in acetonitrile. Using the analyte addition method (Figure 3.5a), after the calibration plot, an apparent recovery factor of 106 % was obtained. Moreover, a calibration plot (Figure 3.5b) was obtained for consecutive additions of coffee spiked with furan, showing a very good linear correlation.

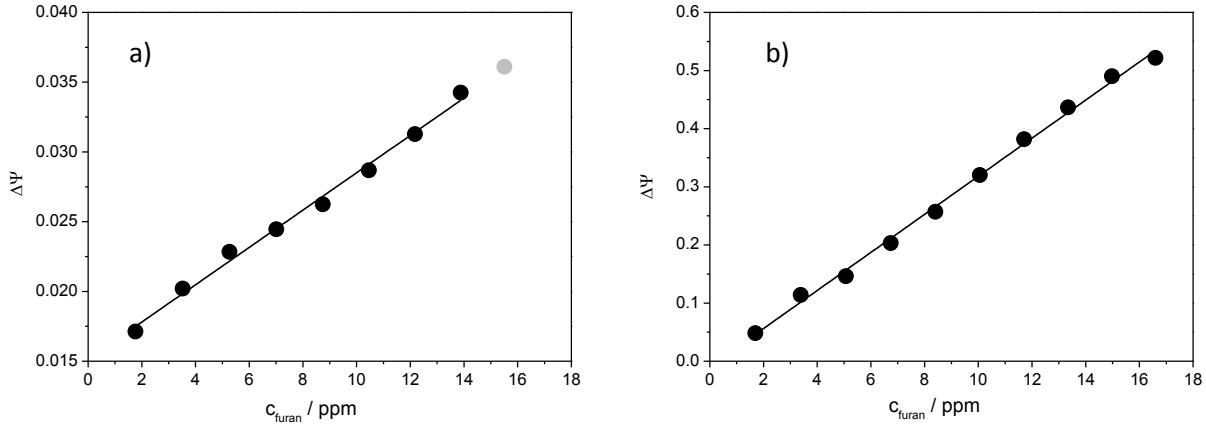

Figure 3.5. Analyte addition technique applied to a coffee sample 0.01 M in furan (a) and calibration plot obtained with subsequent additions of coffee spiked with furan 0.01 M (b).

3.2.4. Conclusions

A new electroanalytical methodology based on Pt disk electrode and Pt Screen Printed Electrode was optimized for the determination of furan by using Square Wave Voltammetry. Peak height and peak area are proportional to furan concentration in the dynamic linearity range 1-70 ppm, with limits of detection of 0.27 ppm and 0.536 ppm for Pt disk and Pt-SPE, respectively. The new method offers best RSD % values (around 5 % and in general lower than

10 %), and in particular best apparent recovery factors (very close to 100 %), in comparison with the Literature (RSD = 5-16 % and RF = 87-102 %) ones (Goldmann et al., 2005; La Pera et al., 2009). No heating of the sample is contemplated during the procedure, avoiding the possible production of furan as in the case of chromatographic methods reported in the Literature.

Moreover, the use of screen-printed electrodes offers the advantages of simplicity and disposability, without a loss in precision and accuracy. The coverage of a thick layer of Nafion membrane also allows prevention of fouling and damaging of the electrodes.

Finally, the application of the electroanalytical procedure to a complex matrix (coffee) appears really promising, considering the possibility of using it as detection method after a chromatographic separation.

Future developments will concern the use of modified electrodes with nanomaterials to decrease the limits of detection, which are still too high, and the application of the method for HPLC detection.

3.3. Carbon-based and Platinum-based electrodes: benzidines determination

3.3.1. Benzidine and its derivatives

Benzidine, called also Fast Corinth Blue B, is an odourless, white or slightly reddish solid organic compound which evaporates slowly from water or soil. This compound is polar and can be protonated in acidic media, allowing its transport and dispersion in the aquatic environment.

Benzidine and its derivatives (Figure 3.6) are employed as reagents for the detection of blood, as rubber compounding agents, as stain in microscopy, in security printing and in lignifications measurement, as laboratory agents for detection of hydrogen cyanide and sulphate or for the quantitative determination of nicotine, as spray reagents for sugars or even as electrochemical substrates for immunoassays (Volpe, Draisci, Palleschi, & Compagnone, 1998). The main use is as intermediate in the synthesis of azo-dyes (Chung, Chen, & Claxton, 2006), by coupling benzidine with phenols and amines. For this use, benzidine-based compounds have application in textile, printing, leather, paper making, drug and food industries and constitute the 60-70 % of all produced dyestuffs (Yiğitoğlu & Temoçin, 2010). Considering their use, benzidines can be found in workplaces, in the effluents and wastewaters (Yiğitoğlu & Temoçin, 2010).

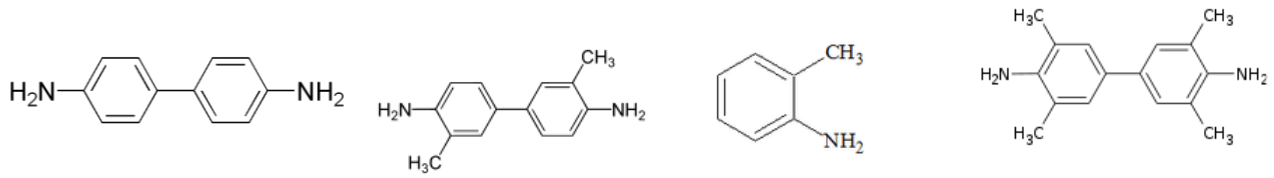

Figure 3.6. Chemical structures of benzidine, *o*-tolidine, *o*-toluidine and tetramethylbenzidine.

Benzidine was identified since 1975 (Makena & Chung, 2007) as carcinogenic agent for human urinary bladder, because human enzymes can oxidate it, allowing its binding with DNA, and its

presence together with its derivatives causes serious health problems. Intestinal and environmental microorganisms are able to reduce benzidine-based azo-dyes to benzidine and, for this reason, their production and use were forbidden in many countries since 1970s (Chung et al., 2006; Golka, Kopps, & Myslak, 2004; Makena & Chung, 2007). Nevertheless, the problem of benzidine pollution remains serious and current, since these types of azo-dyes are still employed in many research laboratories and industries of emerging countries, as demonstrated by very recent Literature. Today, the potential risk for exposure to azo-dyes and benzidine is evident and its prevention is very important (Harden, Donaldson, & Nyman, 2005; Yiğitoğlu & Temoçin, 2010; Yilmaz, Memon, & Yilmaz, 2010).

In this context, benzidine was added to the list of hazardous compounds (Priority Pollutants), drawn up by the Environmental Protection Agency of the United States (US EPA) and by the European Union 2006/11/CE Directive, and its carcinogenicity was again considered during the meeting of the International Agency for Research on Cancer (IARC) in 2008.

After discovering the toxicity of benzidine, also its derivatives, particularly *o*-toluidine, *o*-tolidine and tetramethylbenzidine have attracted attention. *o*-toluidine is a light yellow liquid slightly soluble in water. In 2009, *o*-toluidine was manufactured by 18 companies worldwide as intermediate in the production of azo-dyes (more than 90) in textile, printing, leather, paper making, drug and food industries, toy industry but also in the manufacture of rubber vulcanization accelerators, hypnotic and anesthetic pharmaceuticals, and pesticides. Moreover, *o*-toluidine is present in work environments, in tobacco smoke and in water and some foods: fresh kale, celery and carrots, and in shelled peas, red cabbage, and black tea aroma. *o*-

toluidine is highly toxic for human and it is classified by IARC as probable human carcinogen. *o*-tolidine is a yellow-brown powder, slightly soluble in water and it is used as colorant or as intermediate in textile, paper, food, leather industries. It is used for the vulcanization of the rubber and for the production of synthetic polymers, but also in analytical, clinical and forensic chemistry as indicator. *o*-tolidine can be found in food as contaminant, deriving from packaging and plastic materials, and it is classified by IARC as possible carcinogen, with the same target organs of benzidine. Tetramethylibenzidine is a white powder, slightly soluble in water and it is extensively used as colorimetric indicator in many areas, such as the combur-test, the determination of some hormones and for glucose detection. It is not mutagenic, but it is really toxic and it is classified as suspected carcinogenic by IARC.

Considering the hazardousness of benzidine and its derivatives, precise and accurate analytical techniques for their determination at trace level and for their regular monitoring in natural and wastewaters are needed. In the Literature, various methodologies are proposed, such as colorimetric, spectrophotometric and mainly chromatographic (LC, GC, HPLC, Supercritical Fluid) with different detectors (Bouzige, Legeay, Pichon, & Hennion, 1999; Hsu et al., 1996; S Lacorte, Guiffard, Fraisse, & Barcelo, 2000; Sílvia Lacorte, Perrot, Fraisse, & Barceló, 1999; Patel & Agrawal, 2003; Riggin & Howard, 1979; Shin & Ahn, 2006; Zhu et al., 2002). Colorimetric and spectrophotometric methods show high detection limits and low selectivity in the presence of other aromatic amines, while chromatographic techniques, frequently associated with mass spectrometry or with amperometric detection on a glassy carbon electrode, are the most used techniques for their low detection limits, high accuracy and precision. Nevertheless, high equipment and running costs, necessity of qualified personnel, elaborated and time-consuming

procedures, problems of column fouling and in particular limited possibility of on-line and on-site detection are the major drawbacks of these techniques.

For these reasons, voltammetric methods are very interesting as valid and independent alternative to the other standardized ones. In particular, Barek's Group of the UNESCO Lab of Environmental Electrochemistry already demonstrated the determination of polycyclic aromatic hydrocarbons and aminobiphenyls (Jiri Barek, Jandová, Pecková, & Zima, 2007; Jiří Barek, Pumera, Muck, Kadeřábková, & Zima, 1999; Jiri Zima, Dejmkova, & Barek, 2007), but also benzidine and its derivatives (J Barek, Cvacka, Muck, Quaiserová, & Zima, 2001) on Platinum and Glassy Carbon electrodes. Furthermore, Screen-Printed Electrodes (SPE) may also constitute an interesting, reliable and low-cost choice to be used for the detection of benzidine and its derivatives.

3.3.2. Materials and Methods

0.1 M HCl was used as supporting electrolyte.

Initially, many different conventional electrodes were tested. Pt disk and Glassy Carbon electrodes gave better responses, so they were chosen to optimize the new electroanalytical procedure for the detection of benzidine.

Four types of electrodes were used:

- Pt disk electrode;
- Platinum Screen-Printed Electrode (Pt-SPE) with or without Nafion membrane, used to prevent electrode fouling;

- Glassy Carbon electrode (GC);

- Carbon Screen-Printed Electrode (C-SPE).

Considering the results on benzidine, only carbon-based electrodes were used for the determination of benzidine derivatives.

The voltammetric technique used was Differential Pulse Voltammetry (DPV), previously optimized.

3.3.3. Results and Discussion

Benzidine has different reactive behaviour considering the active media and pH. In this case 0.1 M HCl was chosen as supporting electrolyte, since it is considered the most suitable for this analytical scope. In particular, benzidine presents in this acidic media at GC electrode a chemically and electrochemically reversible bi-electronic oxidation peak at 0.630 V (SCE). The electrochemical reversibility disappears for scan rates > 500 mV s^{-1}, while the bi-electronic character derives from the bi-electronic oxidation to quinonediimine, which predominates in acidic media.

Different types of voltammetric techniques were tested, but DPV showed the best results. In Figure 3.7 DPV is compared with SWV using the same experimental conditions. SWV presents a slightly usable peak, while in the case of DPV the peak is sharp and well defined. Probably, this behaviour can be ascribed to the fouling of electrode surface caused by polymers formed as products. In the case of SWV, the high scan rates impede the dissolution of products before the following analysis. In fact, CV experiments demonstrate that for high scan rates the chemical

and electrochemical reversibility of the system is lost, which is an important requirement in SWV experiments.

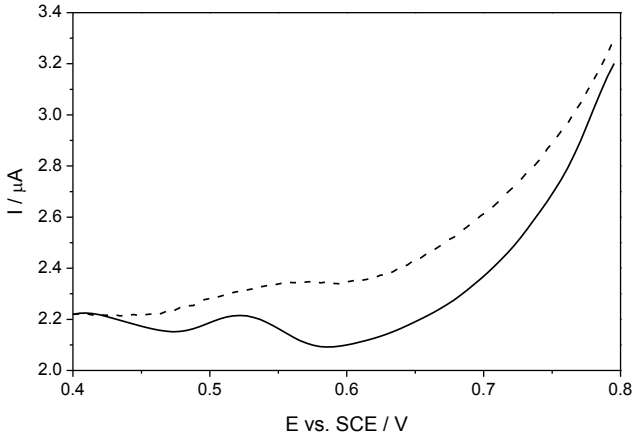

Figure 3.7. SWV (dashed line) and DPV (continuous line) patterns for benzidine 47 ppb on C-SPE.

The optimized parameters for DPV are shown in Table 3.6 and were applied for all the electrodes tested.

Table 3.6. Differential Pulse Voltammetric parameters.

Parameter	Value
Equilibration time (s)	10
Modulation time (s)	0.002
Interval time (s)	0.5
Start potential (V)	+ 0.4
End potential (V)	+ 0.8
Step potential (V)	0.005
Modulation amplitude (V)	0.05

Pt wire electrode was tested for the determination of benzidine, but presented a strong passivation of the surface with fouling phenomena. For this reason, experimental data about Pt wire electrode are not here shown. Pt-SPE showed also this effect of fouling, reaching very

rapidly saturation. This problem is probably due to the adsorption of the products of benzidine polymerization, which occurs in such experimental conditions. In this context, the use of Nafion, widely described in the Literature (Falciola, Pifferi, Possenti, & Carrara, 2012; Gouveia-caridade et al., 2006), appears to be a possible solution, avoiding the adsorption of products and protecting the electrodes. Different percentages of Nafion (0, 0.01, 0.05, 0.1 %) were tested and the best results were obtained for 0.05 %, which showed the best defined and highest current peak, as shown in Figure 3.8.

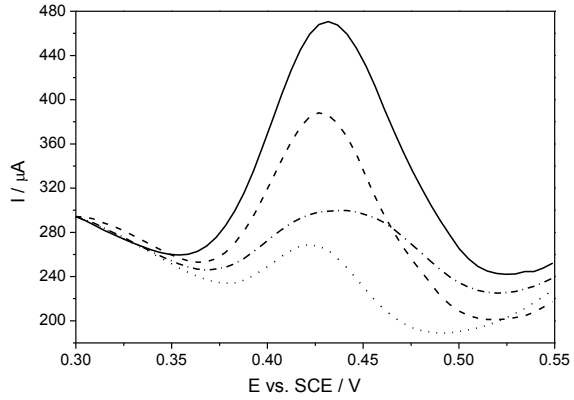

Figure 3.8. DPV patterns for benzidine 47 ppb on Pt-SPEs covered by layers of different percentage of NAFION: 0% (dotted line); 0.01% (dashed line); 0.05% (continuous line); 0.1% (dash-dotted line).

Benzidine presents a DPV peak at 0.52 V (*vs* pseudo Ag) for C-SPE and at 0.43 V (*vs* pseudo Ag) for Pt-SPE, which increases with concentration (Figure 3.9).

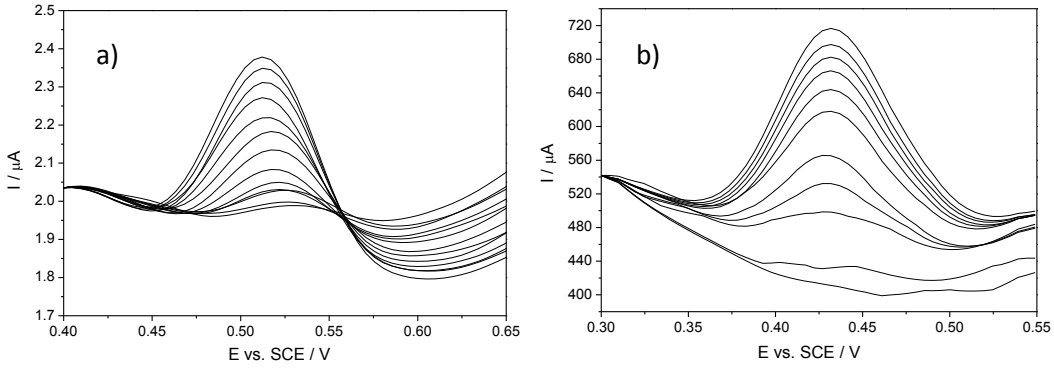

Figure 3.9. DPV patterns on C-SPE (a) and on Pt-SPE (b) for different concentrations of benzidine.

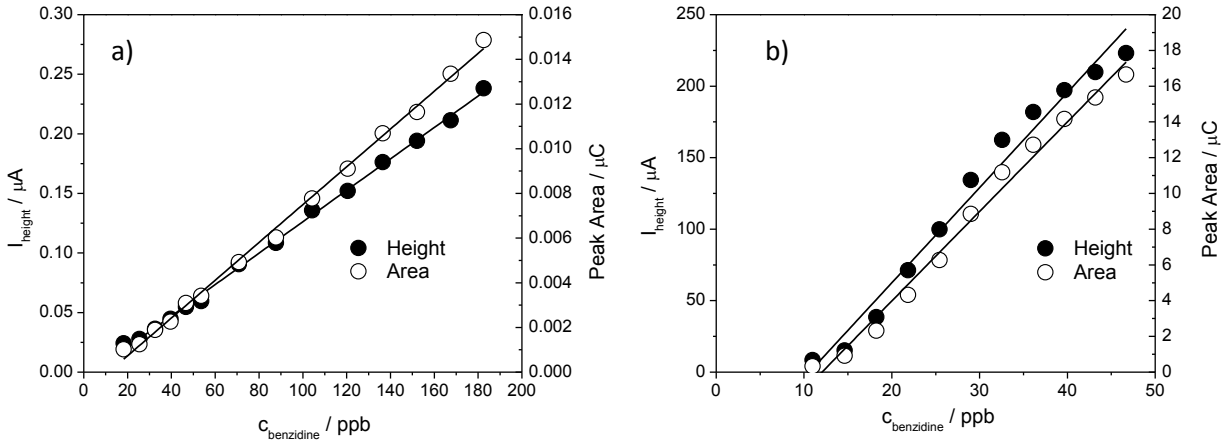

Figure 3.10. Calibration Plots (peak height and area) for the detection of benzidine on C-SPE (a) and on Pt-SPE (b).

Calibration plots (Figure 3.10) were carried out for consecutive additions of benzidine, showing a very good relationship between the oxidation peak current and benzidine concentration, as demonstrated by good correlation. Analytical parameters are shown in Table 3.7. The cross-validated correlation coefficients R^2_{CV} were also evaluated, to consider the effective predictive power of the proposed method in comparison with the fitting power. The best LoD and LoQ (Currie, 1995)were obtained with C-SPE considering peak area and these values are lower than those obtained by previous voltammetric methods in the Literature (J Barek et al., 2001).

Table 3.7. Low concentration linearity ranges, linear correlation and cross-validated linear correlation coefficients, LODs and LOQs evaluated using peak height and area in the DPV detection of benzidine on C-SPE, Pt-SPE and GC as comparison.

Electrode type	Concentration range in cell	Peak height			
	ppb	R^2	R^2_{CV}	LoD / ppb	LoQ / ppb
C-SPE	20 – 180	0.998	0.998	1.88	5.73
Pt-SPE	10 – 50	0.980	0.970	0.22	0.68
GC	80 - 180	0.998	0.997	22	67
Electrode type	**Concentration range in cell**	**Peak area**			
	ppb	**R^2**	**R^2_{CV}**	**LoD / ppb**	**LoQ / ppb**
C-SPE	20 – 180	0.997	0.996	0.33	1.00
Pt-SPE	10 – 50	0.989	0.980	1.66	5.07
GC	80 - 180	0.994	0.993	4.14	13

Repeatability and the best achievable internal precision of the method (Currie, 1995; Thompson, Ellison, & Wood, 2002) were also tested and the relative standard deviations are presented in Table 3.8. RSD % are good and they are always better for SPEs, in particular for Pt-SPE, than for GC. Also the intermediate repeatability was evaluated, repeating the procedure in different days, by different analysts and using different equipments and the obtained parameters are very similar to those reported in Table 3.8.

Three different methodologies were adopted to calculate the apparent recovery factors: calibration plot, standard addition technique and analyte addition method. The better results were obtained with the last procedure and the values are shown in Table 3.8. Apparent recovery factors are > 93 % for all three electrodes and very close to 100 % in the case of C-SPE, while are lower for Pt-SPE, probably due to electrode fouling, as already discussed.

Table 3.8. Relative standard deviations and apparent recovery factors evaluated using peak height and area for three concentrations of benzidine in the low concentration range, on C-SPE, Pt-SPE and GC for comparison.

Electrode type	Concentration	RSD %		Apparent Recovery Factors	
	ppm	Height	Area	Height	Area
C-SPE	0.15	0.9	1.5	97.6	97.9
	0.17	5.1	8.0	95.5	100.4
	0.18	2.1	7.2	97.7	101.1
Pt-SPE	0.04	2.6	4.0	95.5	98.8
	0.04	2.3	3.2	91.5	95.8
	0.05	0.5	0.8	88.2	93.6
GC	0.17	8.2	8.1	99.7	97.9
	0.18	8.8	11.5	100.0	99.2
	0.20	4.9	4.9	99.2	99.0

In general, this study demonstrates that SPEs, besides their advantages of low cost, disposability and easiness of use, show better analytical performances than conventional electrodes. This aspect could be probably related to the different physical state of carbon and/or to their higher real surface area. This last parameter was evaluated according to the in-situ voltammetric method (Trasatti & Petrii, 1991) and C-SPE real area results 23 % higher than GC electrode. Moreover, the roughness of the electrode area is visible in SEM images of C-SPE and Pt-SPE (Figure 3.11).

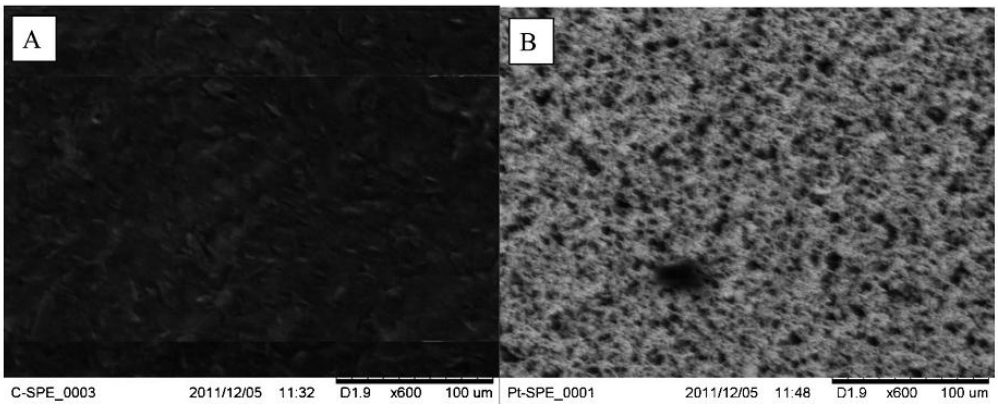

Figure 3.11. SEM images of C-SPE (A) and Pt-SPE (B).

The evaluation of the analytical performances of this new methodology was also conducted in a real sample, since the main application is focused on environmental analysis. The water of a river canal in an industrial area (Canale Villoresi, Milano north suburbs, Italy) was chosen as real sample and characterized, showing 10.37 ppm of Total Organic Carbon, 53.37 ppm of Inorganic Carbon and 0.864 mS cm^{-1} of conductivity. For comparison, Milli Q water values, used for the previous characterization, are 2 ppb of TOC and 0.935 µS cm^{-1}, three orders of magnitude lower. The real water sample was used to prepare 0.1 M HCl for analyte addition and 0.1 mM benzidine for the determination of the calibration plot and for the analyte addition method. All the analytical parameters are reported in Table 3.9-3.10. The results show a slight worsening of the method validation parameters, but remaining very good, demonstrating the applicability of the new electroanalytical method to real samples. Furthermore, they confirm the best performances for C-SPE using peak area.

Table 3.9. Concentration linearity ranges, linear correlation and cross-validated linear correlation coefficients, LODs and LOQs evaluated using peak height and area in the DPV detection of benzidine on C-SPE and Pt-SPE in a real sample.

Electrode type	Concentration range in cell	Peak height			
	ppb	R^2	R^2_{cv}	LoD / ppb	LoQ / ppb
C-SPE	10 – 120	0.98	0.96	29	89
Pt-SPE	20 – 130	0.95	0.92	30	92
Electrode type	**Concentration range in cell**	**Peak area**			
	ppb	**R^2**	**R^2_{cv}**	**LoD / ppb**	**LoQ / ppb**
C-SPE	10 – 120	0.94	0.91	15	46
Pt-SPE	20 – 130	0.96	0.94	38	117

Table 3.10. Relative standard deviations and apparent recovery factors evaluated using peak height and area for three concentrations of benzidine in a real sample, on C-SPE and Pt-SPE.

Electrode type	Concentration	RSD %		Apparent Recovery Factors	
	ppm	Height	Area	Height	Area
C-SPE	0.10	9.5	7.4	107.9	119.8
	0.11			99.5	101.4
	0.12			94.5	99.2
GC	0.11	7.0	9.1	110.4	108.2
	0.12			107.8	104.7
	0.13			97.5	99.3

Considering the results obtained for the determination of benzidine, carbon based-electrodes were chosen for the detection of three benzidine derivatives: *o*-toluidine, *o*-tolidine and tetramethylbenzidine. In fact, carbon-electrodes gave very good results and were less affected by fouling problems. The use of Nafion in these cases was not necessary and in the case of real application, LoDs and RFs were slightly better in comparison with Pt based electrodes.

Initially, all derivatives were studied with GC electrode using cyclic voltammetry, to identify the peak potential positions, the chemical and electrochemical reversibility and the reaction mechanism for each compound. As shown in Figure 3.12, peak potential shifts to less positive potential in the case of *o*-tolidine and tetramethylbenzidine for the electrodonating effect of the methyl groups, while *o*-toluidine potential shifts to more positive values, for the presence of only one carbon ring. Moreover, for *o*-tolidine and tetramethylbenzidine the reaction is chemical and electrochemical reversible and the mechanism is bielectronic as in the case of benzidine, while for *o*-toluidine the reaction is irreversible and monoelectronic. Scan rate studies in the range 10-1000 mV s^{-1} demonstrate that the rate determining step of the reaction at the electrode is the diffusion.

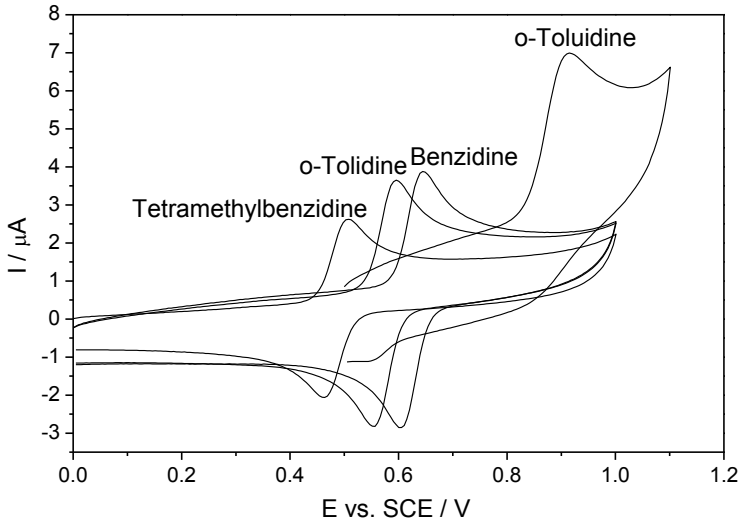

Figure 3.12. Cyclic Voltammograms of benzidines at C-SPE.

Calibration plots for consecutive additions of the analyte were carried out with Differential Pulse Voltammetry at GC and at C-SPE, showing a proportional increase of peak height and area with concentration. Figure 3.13 shows the calibration plots considering peak height and peak area for each compound at C-SPE as example. In general, good correlations were obtained both with peak height and peak area, slightly worse in the case of *o*-toluidine.

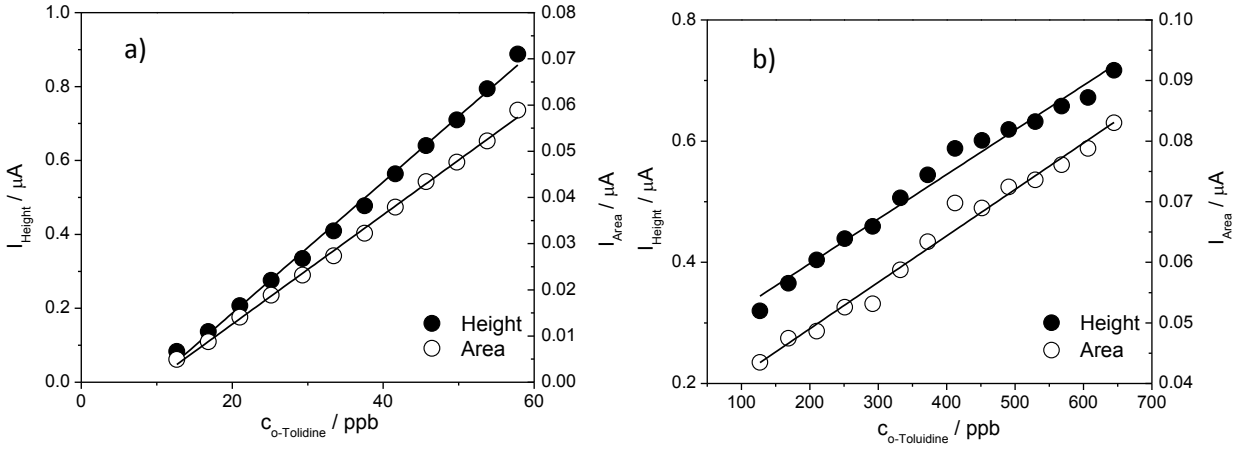

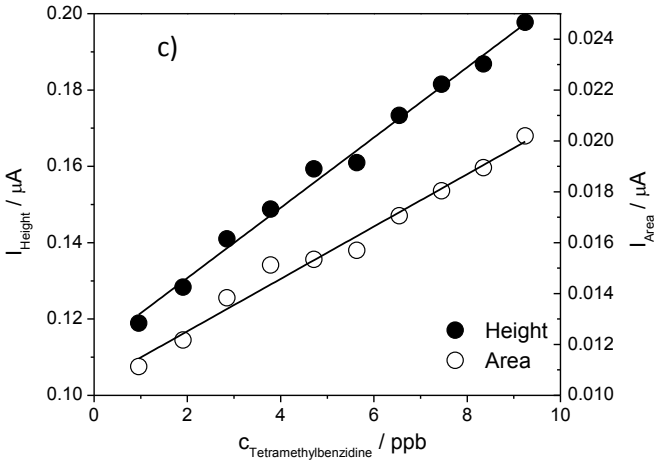

Figure 3.13. Calibration Plots (peak height and area) for the detection of o-Tolidine (a), o-Toluidine (b) and Tetramethylbenzidine (c) on C-SPE.

In Table 3.11 all the analytical parameters were reported for each analyte and also for benzidine considering both the carbon based electrodes. The analytical parameters are worse in the case of *o*-toluidine, as expected, considering the high potential of oxidation in comparison with the other molecules and the irreversibility of the reaction, which causes electrode fouling. In general, correlation is very good, with RSD % below 10 %, LoD and LoQ in the range of ppb and apparent recovery factors, calculated with the method of analyte addition, very close to 100 %. In particular, all the parameters are better in the case of C-SPE, showing the very good performances of this type of electrode in trace analysis application.

Table 3.11. Analytical parameters evaluated for all the benzidines at GC and C-SPE.

Molecule	Glassy Carbon				
	R^2	RSD %	LoD / ppb	LoQ / ppb	Apparent Recovery Factors
Benzidine	0.994	4.9	4.15	12.60	98-99
o-Tolidine	0.993	9.0	6.19	18.82	103-105
o-Toluidine	0.90	10.6	532.37	1618.16	91-99
Tetramethylbenzidine	0.990	8.6	1.35	4.10	98-100
Molecule	**Carbon-based Screen-Printed Electrode**				
	R^2	RSD %	LoD / ppb	LoQ / ppb	Apparent Recovery Factors
Benzidine	0.997	2.1	0.33	1.66	98-101
o-Tolidine	0.998	3.2	0.43	1.32	100-103
o-Toluidine	0.98	6.0	123.01	373.88	94-96
Tetramethylbenzidine	0.98	4.1	1.45	4.40	99-102

Moreover, experiments were performed using the same water of the canal river tested for benzidine. Also in this case, results remain very good, though a slight worsening of analytical parameters is evident, as already seen in the case of benzidine.

Preliminary studies about the potential interference of benzidine derivatives during the determination of benzidine were carried out, using CV at GC electrode. A quantity of the interferent compound was firstly added and then, consecutive additions of benzidine were performed. As shown in Figure 3.14, good calibration plots can be obtained for benzidine, also in the presence of the interfering species, demonstrating the applicability of the electroanalytical method.

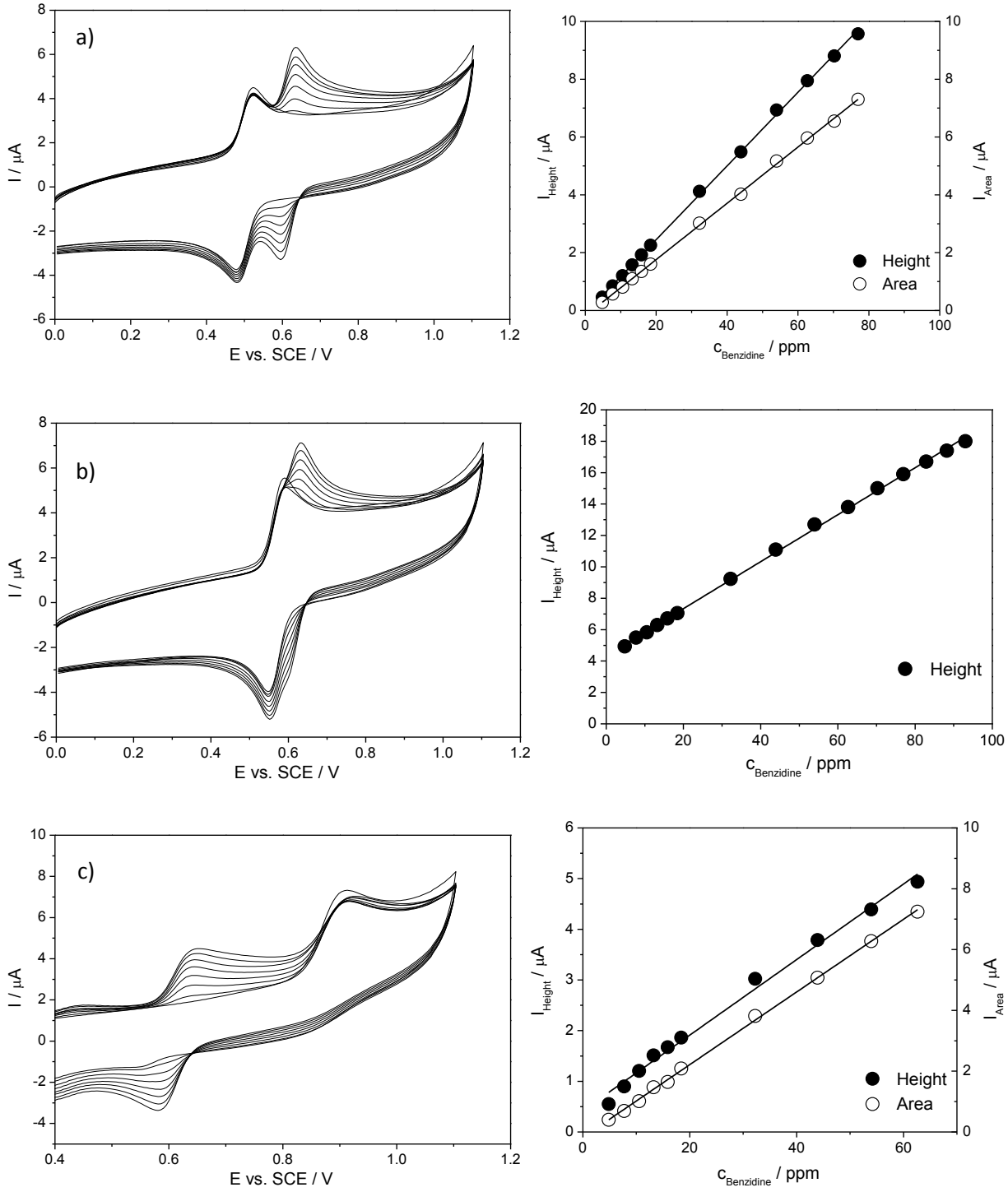

Figure 3.14. Cyclic voltammograms obtained for consecutive additions of benzidine in the presence of tetramethylbenzidine (a), *o*-tolidine (b) and *o*-toluidine (c) as interferences and corresponding calibration plots.

Finally, the simultaneous detection of all four compounds was preliminarly considered, performing CV and DPV with the species present in the same quantity. The possibility to

distinguish among the various compounds thanks to different peak potentials, as shown in Figure 3.15, is promising for application of this electroanalytical procedure as alternative to chromatographic separation or more probably as detector after a chromatographic separation.

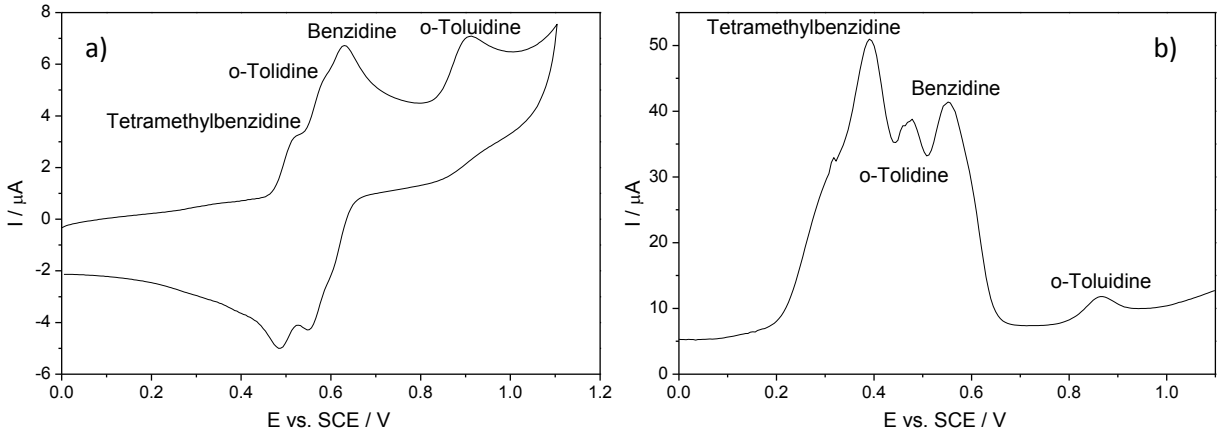

Figure 3.15. Cyclic (a) and differential pulse (b) voltammograms of all benzidines.

3.3.4. Conclusions

Carbon-based and Platinum-based screen printed electrodes have shown very good performances for the determination of benzidine in acidic media using Differential Pulse Voltammetry. The new electroanalytical method is characterized by extreme sensitivity with very low LoD (0.33 ppb) and LoQ (1.66 ppb), very good RSD % and apparent recovery factors, offering a valid and independent alternative to other techniques reported in the Literature. SPEs results are better than those obtained on conventional electrodes, GC and Pt wire electrodes, and the best performances are reached using peak area and the analyte addition technique. The real surface area of SPE in comparison with that of conventional electrodes could be probably the cause of this better behaviour.

The problem of fouling, probably due to the formation of benzidine polymers on the surface, is evident on Pt-based electrodes, but the use of Nafion membrane for SPE protection, helped to obtaine optimum results.

Considering all these results about benzidine, carbon-based electrodes were chosen for the determination of benzidine derivatives. *o*-toluidine, *o*-tolidine and tetramethylbenzidine were characterized by cyclic voltammetry and calibration plots were carried out using DPV at both electrodes (SPEs and GC), showing very good results. In general, C-SPE gave the best performance, when compared with GC. *o*-toluidine showed slightly worse electroanalytical parameters, probably due to the higher potential of peak determination.

The new procedure can also be used for detection in real environmental samples, as analysis in a river canal water in an industrial area demonstrated.

Preliminary results about interference of derivatives during the determination of benzidine and in simultaneous detection were evaluated, showing promising results.

The method could be conveniently applied as detection method after a chromatographic separation, in particular to separate benzidine and its derivatives.

The use of nanomaterials, in particular carbon-based nanomaterials as carbon nanotubes, to modify electrode surface, appears to be a promising pursuance of this methodology for the determination of benzidine and its derivatives (Chapter 4).

3.4. Bismuth oxide-based electrodes: Chromium determination

3.4.1. Chromium

Chromium is a metallic element that exists primarily in the mineral chromite, which is present in soils, waters, rocks, fauna and flora, and volcanic dust and gases. Chromium exists in three oxidation forms with different properties. Metallic chromium can be found principally in alloys, because it is resistant to corrosion, temperature, wear and decay. Trivalent chromium can be found in natural waters in its hydrolyzed form and it is an essential micronutrient for human body, since it combines with various enzymes. In industrial field, it is used during the production of dyes, paint pigments and salts for leather tanning. Hexavalent chromium exists principally as chromate and it is a dangerous, carcinogenic and mutagenic compound, present in the Priority Pollutants List. It has high mobility in water and, since it is widely used in several industrial processes (metal plating, leather tanning, paint making, *etc*.), it can be found in wastewaters, causing great environmental damages and human health problems. For all these reasons Cr(VI) is one of the highly harmful, hazardous and toxic pollutants.

In this context, determination of Cr(VI) at trace level is very important and in recent years several efforts have been made for the development of efficient and accurate techniques for this purpose (Gómez & Callao, 2006). Traditionally, chromium species are determined by spectroscopic measurements (FAAS, GF-AAS, ET-AAS and ICP-tandem), chromatographic systems (HPLC, GC and IC), chemiluminescence methods and mass spectrometry. These techniques provide low detection limits (at the ng/L or μg/L level), but they are time consuming, need expensive equipments and laborious sample pre-treatments. Another very

common procedure is based on the absorbance of diphenylcarbazide, but with great analytical problems, low sensitivities and high detection limits. Also in this area, electroanalytical methods can find application, due to their several advantages and different voltammetric techniques (Differential Pulse Voltammetry, Square Wave Voltammetry and Linear Sweep Voltammetry), which can be preceded by cathodic or anodic preconcentration steps , giving excellent results with various types of conventional electrodes.

Mercury electrodes were the first ones employed and the most studied in association with these techniques, especially in the presence of chromium complexing agents, such as Diethylenetriaminepentaacetic acid (DTPA) (Grabarczyk, Baś, & Korolczuk, 2008; Grabarczyk, Kaczmarek, & Korolczuk, 2004; Grabarczyk, 2008; Sander, Navrátil, & Novotný, 2003), N-(2-Hydroxyethyl)-ethylenediamine-N,N',N'-triacetic acid (HEDTA) (Domínguez, Sanllorente, Alonso, & Arcos, 2001), Ammonium 1-pyrrolidinedithiocarbamate (APDC) (Domínguez, Asunción Alonso, & Arcos, 2002), cupferron, pyrocetechol violet (PCV) (Domínguez & Arcos, 2000; Domínguez & Julia Arcos, 2002; Vukomanovic, Vanloon, Nakatsu, & Zoutman, 1997) and pyridine (Korolczuk, 1999). Recently, despite its good performances (LOD in the range of ng/L), mercury electrodes tend to be replaced because of their important drawbacks. The first problem concerns mercury toxicity: mercury is present in the Priority Pollutants List and the Directive 2008/51/EC of the European Union planned the abolition of the use of mercury in glass thermometers and other devices. Other relevant issues are related to the difficulties in the management and handling of mercury electrodes. In this context, other types of electrodes represent possible alternatives to the mercury. These devices can be used as bare or modified with other metals or organic compounds. Glassy Carbon (GC), gold and Boron-Doped Diamond

(BDD) unmodified (Manova, Humenikova, Strelec, & Beinrohr, 2007; Christine M Welch, Nekrassova, & Compton, 2005) or functionalized (Carrington, Yong, & Xue, 2006; B. Liu, Lu, Wang, & Zi, 2008; Svancara, Foret, & Vytras, 2004; S. Xing, Xu, Chen, Shi, & Jin, 2011) with Au and Ag nanoparticles, pyridine and surfactants show good results for Cr determination, but bismuth (Švancara, Prior, Hočevar, & Wang, 2010) seems to be the most promising alternative. First of all, bismuth has physicochemical properties and electrochemical behaviour relatively similar to mercury, permitting analysis in a wide range of potentials also with stripping. Moreover, it shows an excellent mechanical stability and its toxicity is negligible. As for chromium determination with complexing agents and stripping techniques, GC electrodes with electrodeposited Bi film (Chatzitheodorou, Economou, & Voulgaropoulos, 2004; Jorge, Rocha, Fonseca, & Neto, 2010; Lin, Lawrence, Thongngamdee, Wang, & Lin, 2005) exhibit very good results comparable to the mercury ones, for simplicity of analysis and low detection limits (ng/L).

Screen-Printed electrodes can be useful for the detection of chromium, particularly for their property of disposability, permitting on-site analysis. In fact, in the Literature, different types of home-made SPEs, modified with poly-L-histidine, Au, Ag and Hg films (Bergamini, dos Santos, & Zanoni, 2007; Calvo-Pérez, Domínguez-Renedo, Alonso-Lomillo, & Arcos-Martínez, 2010; Domínguez-Renedo, Ruiz-Espelt, García-Astorgano, & Arcos-Martínez, 2008; Hallam, Kampouris, Kadara, & Banks, 2010; G. Liu, Lin, Wu, & Lin, 2007), were successfully employed for Cr(VI) determination with Adsorptive Stripping (AdSV) voltammetry. The use of these disposable devices, together with bismuth, could be very interesting, but only few examples of

preliminary results on home-made SPEs functionalized with electrodeposited bismuth can be found in the Literature (Lin et al., 2005).

In this context, the investigation of the behaviour of commercial Bi-SPE towards Cr(VI) determination and the comparison with HDME is a topic of interest.

3.4.2. Materials and Methods

Electroanalytical determination of Cr(VI) was performed using two different methodologies and two different working electrodes:

- Hanging Mercury Drop Electrode (HMDE);
- Commercially available bismuth screen-printed electrodes (Bi-SPEs), by DROPSENS (Spain).

Acetate buffer and potassium nitrate were employed as supporting electrolytes for HDME, while only potassium nitrate was used in the case of Bi-SPE. Pyrocatechol violet was the chelating agent for both procedures and all the analysis were performed under nitrogen bubbling.

The voltammetric technique used was the Differential Pulse Adsorptive Stripping Voltammetry (DPAdSV) for HDME and the Square Wave Voltammetry (SWV) for Bi-SPE.

3.4.3. Results and Discussion

Previous literature works (Domínguez & Arcos, 2000; Domínguez & Julia Arcos, 2002; Vukomanovic et al., 1997) reported the determination of Cr(VI) with PCV (used as an

electroactive probe) by DPAdSV at the HMDE. The operative parameters used in that papers, have been optimized for our experimental conditions adopting the ones reported in Table 3.12.

Table 3.12. Operative parameters used in Differential Pulse Adsorptive Stripping Voltammetry measurements at HMDE.

Parameter	Value
Purge time (s)	120
Deposition potential (V)	-0.5
Duration (s)	60
Equilibration time (s)	10
Modulation time (s)	0.002
Interval time (s)	0.4
Initial potential (V)	-0.5
End potential (V)	-1
Step potential (V)	0.005
Modulation amplitude (V)	0.05

As general rule, deposition potential was fixed at -0.5 V (SCE) for HMDE and voltammograms were recorded between -0.5 and -0.8 V (SCE). In this potential window, PCV shows an intense reductive peak at -0.65 V, which decreases when Cr(VI) is added, because of the complexation of Cr(VI) by PCV. In fact, Cr(VI)-PCV complex is not electroactive: complex formation lowers PCV concentration in the solution and its electroanalytical signal decreases.

A good calibration plot, in the 0-0.65 µM concentration range, was obtained for consecutive additions of Cr(VI) solution, as shown in Figure 3.16, yielding a detection limit of 0.01 µM.

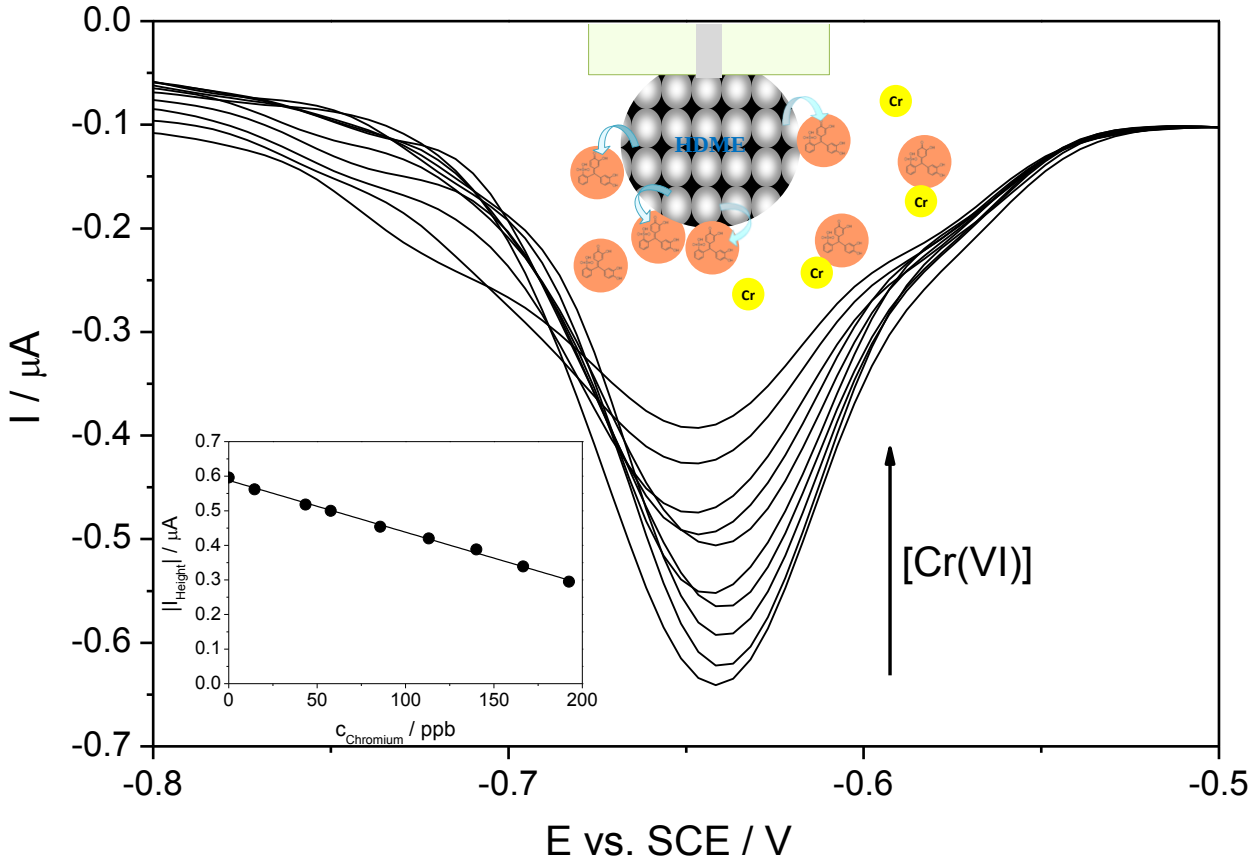

Figure 3.16. DPAdS voltammograms and relative calibration plot (inset) at HMDE for consecutive additions of Cr(VI) solution. Schematic representation of PCV behaviour at the electrode surface.

Since HMDE presents several disadvantages, particularly due to its toxicity, despite its good performances, we decided to replace it by using a Bi-SPE in a Square-Wave Voltammetric determination (voltammetric parameters shown in Table 3.13). This method offers several advantages: first of all, it is a mercury-free analytical technique performed without stripping, thus lowering analysis time. Moreover, Bi-SPEs are portable, permitting on-site analysis, and disposable, avoiding surface contamination and the difficult polishing steps.

Table 3.13. Operative parameters used in Square Wave Voltammetry measurements at Bi-SPE.

Parameter	Value
Equilibration time (s)	10
Frequency (Hz)	100
Initial potential (V)	-0.4
End potential (V)	-1.4
Step potential (V)	0.005
Modulation amplitude (V)	0.05

By using this technique, the reduction peak of PCV appears at -1.18 V (*vs* pseudo Ag) and the addition of Cr(VI) solution causes an increase in peak height. By contrast with the previous method, in this case, the complex Cr(VI)-PCV is electroactive and it reacts at the electrode surface, inducing a signal increase, as in the case of other Cr complexes (Chatzitheodorou et al., 2004; Jorge et al., 2010; Lin et al., 2005; Sander et al., 2003).

In order to be sure that Cr(VI)-PCV is the only responsible of the signal increase, several other experiments were performed trying to monitor Cr(VI) without PCV, and Cr(III) with and without PCV. From these analysis neither a peak in the absence of PCV, nor a peak increase in the presence of PCV with Cr(III) was detected. Moreover, possible little interferences of Cr(III) were completely suppressed by adding an appropriate quantity of HEDTA as Cr(III) chelating agent, yielding better analytical results, as the calibration plots with and without HEDTA show in Figure 3.17. In fact, the sensitivity is higher for the method with HEDTA + PCV than PCV alone.

A good calibration plot in the 0-0.4 µM concentration range, was obtained with consecutive additions of Cr(VI) solution, as shown in Figure 3.17, yielding a detection limit of 0.001 µM, one

order of magnitude lower than that obtained with HMDE. The accuracy of the new method was tested spiking three times with a standard solution after a calibration plot (analyte addition technique) performed with 8 standard additions, obtaining an apparent recovery factor of 102 %.

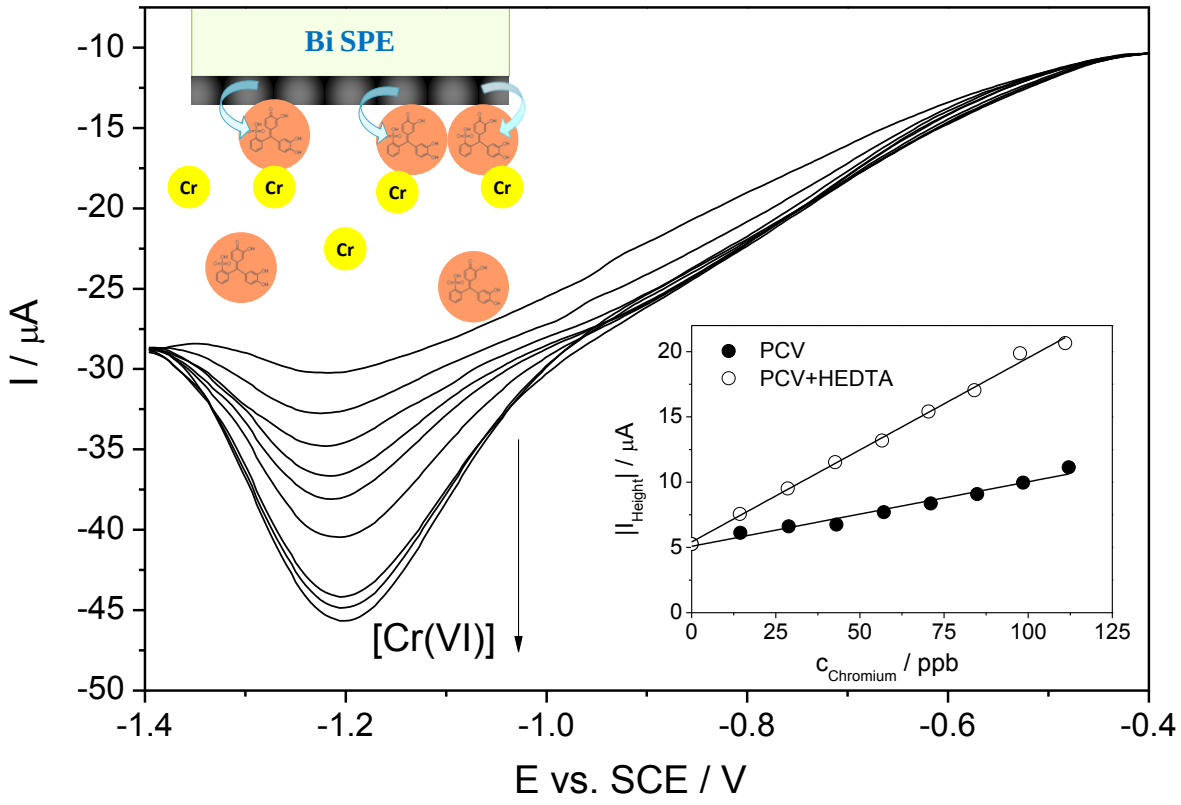

Figure 3.17. SW voltammograms at Bi-SPE for consecutive additions of Cr(VI) solution. Inset: calibration plots with (open circles) and without (full circles) HEDTA. Schematic representation of PCV behaviour at the electrode surface.

In order to test its reliability and to show possible real applications, the new optimized method was used in collaboration with Prof. Ardizzone and Dr. Cappelletti group to follow the photocatalytic reduction of Cr(VI) (Cappelletti, Bianchi, & Ardizzone, 2008; Cho, Kyung, & Choi, 2004; Ku & Jung, 2001), collecting samples during the photocatalysis. The samples were

analyzed using analyte addition technique (three additions for each sample) after a calibration plot performed with 8 standard additions.

The reduction of Cr(VI) was performed in liquid phase (pH 4, instead of pH 2 (Cappelletti et al., 2008; Qing Wang, Shang, Zhu, & Zhao, 2011; Xiaoling Wang, Pehkonen, & Ray, 2004), to meet environmental conditions), under UV illumination using electrodeposited titania nanopowder as photocatalyst and isopropyl alcohol as scavenger (Cappelletti et al., 2008). The choice of titania nanopowder electrodeposited on a Ti grid, using a procedure published in (Paoli, Cappelletti, & Falciola, 2010), was justified since the photoreduction in the case of immobilized titania particles is markedly greater than that of slurry, reaching the total removal of Cr(VI) in 60 minutes, as shown in Figure 3.18. The best degradation in the case of titania thin films can be explained on the grounds of the total absence of turbidity, a typical disadvantage of the slurries; in these conditions the irradiation power of the lamp is preserved.

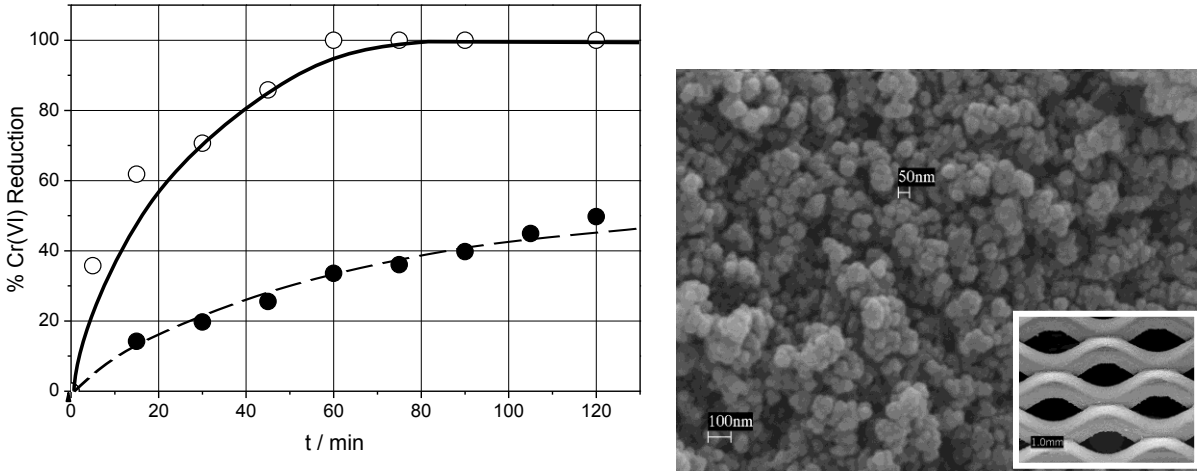

Figure 3.18. Comparison between the Cr(VI) reduction performances of Hombikat powders in slurry or electrodeposited on Ti grids. Inset: SEM image of the titania layer.

Three different titania photocatalysts, two commercial and one home-made, were tested for the Cr(VI) reduction and their physico-chemical characteristics are reported in Table 3.14.

Table 3.14. Structural and morphological features of three different types of titania (Spadavecchia et al., 2010) **used in the photocatalytic tests.**

Sample	% Anatase	% Brookite	% Rutile	$<D_{anat}>$ (nm)	S_{BET} (m^2g^{-1})	V_{pore} ($mL\ g^{-1}$)
P25	75	-	25	30.0 ± 0.3	50	0.256
T_400	66	37	-	4.8 ± 0.1	150	0.44
Hombikat	100	-	-	10.0 ± 0.3	354	0.35

Figure 3.19 shows the comparison of the three titania photocatalysts toward Cr(VI) disappearance as function of reaction time. Also the adsorption (90 minutes) was considered and reported in the inset. All the photocatalysts show excellent performances with a sequence in correlation with the surface area. In fact, Hombikat reaches the best performance, while P25, characterized by the lowest surface area is the worst. Moreover, as shown in Figure 3.19, not only adsorption follows the values of surface area, but also the rate constants are influenced, following the same sequence of adsorption. For this reason, the adsorption of Cr(VI) at the surface of titania was considered the rate determining step and all the reaction kinetics can be described by a pseudo-first order rate equation (Kajitvichyanukul, Ananpattarachai, & Pongpom, 2005).

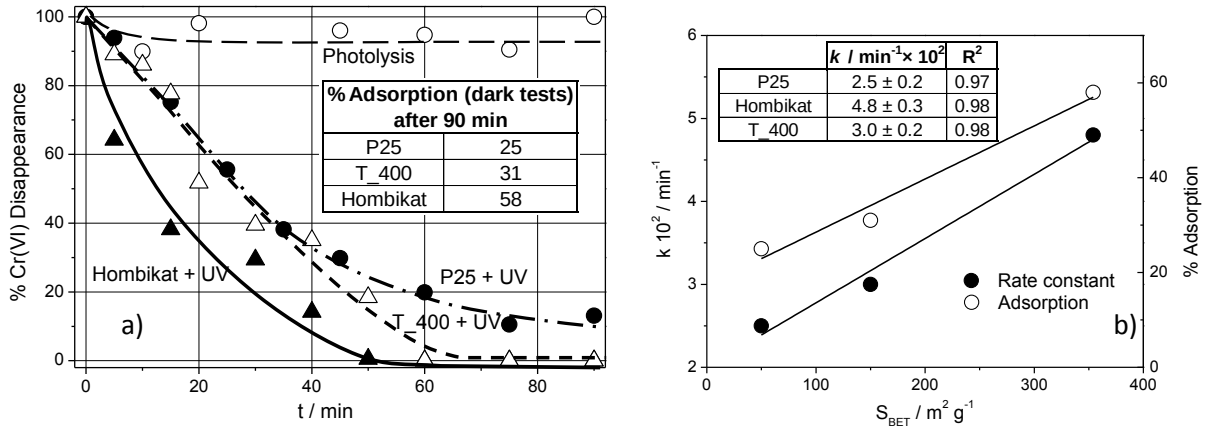

Figure 3.19. (a) Results of the photocatalytic tests for photolysis, adsorption (table in inset) and photocatalysis of Hombikat, P25 and T 400. (b) Linear trends of pseudo-first order kinetic constants and adsorption in the dark after 90 min as a function of surface area of the different TiO2 samples. Inset: rate constants for P25, T_400 and Hombikat.

To evaluate the speciation of chromium at the end of the photocatalysis, titania powders were removed from the substrate and submitted to XPS analysis. Figure 3.20 shows the high resolution scan of Cr 2p multipeaks for P25, as representative sample, while in Table 3.15 binding energies and ratios of chromium species are presented. The presence, for all three powders, of a considerable amount of Cr(III) confirms the efficient photoreduction process. In the case of the two commercial samples the quantity of Cr(0) is appreciable, probably due to a redox reaction between the scavenger and Cr(III).

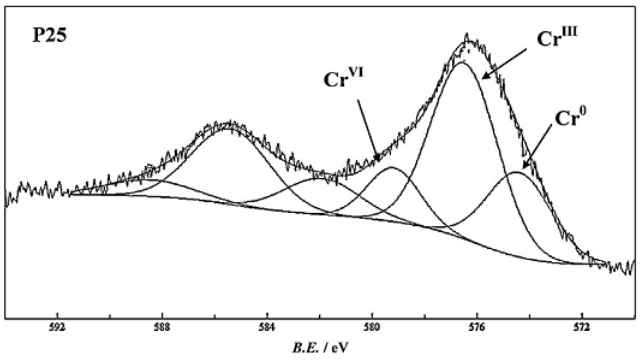

Figure 3.20. Cr 2p1/2 (BE > 580 eV) and Cr 2p3/2 (BE < 580 eV) XPS components in the case of P25 used sample at the end of the photocatalytic test (90 min).

Table 3.15. Binding energies and ratios of Cr(VI), Cr(III) and Cr(0) on Cr $2p_{3/2}$ fitting.

Sample	B.E. Cr $2p_{3/2}$ (eV)			Cr(VI)/Cr	Cr(III)/Cr	Cr(0)/Cr
	Cr(VI)	Cr(III)	Cr(0)			
P25	579.2	576.8	574.6	0.27	0.59	0.14
T_400	580.1	577.1	-	0.31	0.69	-
Hombikat	579.4	576.5	574.2	0.28	0.55	0.17

For all the photocatalytic tests and adsorption kinetics, the new electroanalytical method based on Bi-SPE and pyrocathecol violet, using SWV, was employed for each collected sample. This demonstrates the applicability of the technique, which allowed discriminating the performances of the three different photocatalysts during photocatalysis and also adsorption. Furthermore, it is important evidencing how the presence of Cr(III) and Cr(0) during the photoreduction does not interfere with the analysis, as also the presence of nitric acid and isopropyl alcohol.

Finally, for comparison with the Literature methodology (Domínguez & Arcos, 2000; Domínguez & Julia Arcos, 2002; Vukomanovic et al., 1997), the conventional HMDE method was also employed on the same sample during T_400 photocatalysis showing that the new method offers similar or even better results, being less affected by interferences of the complex matrix, which causes scattered values in the case of HDME (Figure 3.21).

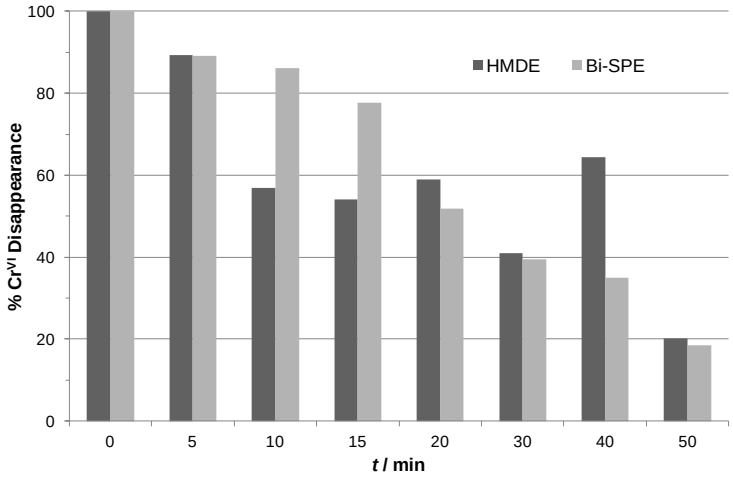

Figure 3.21. Cr(VI) disappearance in T_400 photocatalytic test monitored by HDME and Bi-SPE.

3.4.4. Conclusions

A new electroanalytical methodology using commercially available Bi-SPEs and pyrocatechol violet was studied and optimized for the determination of Cr(VI). Bismuth was chosen as eco-friendly alternative to HDME and the new technique was compared with the conventional method, that uses HDME and pyrocathecol violet.

In the case of HDME, a Differential Pulse Adsorptive Stripping Voltammetry (DPAdSV) was employed and the peak of pyrocathecol violet decreases for consecutive addition of Cr(VI), since this compound forms a non-electroactive complex with chromium. However, in the case of Bi-SPE, a Square-Wave Voltammetry was performed without stripping and pyrocatechol violet shows a peak, which increses with the concentration of Cr(VI), probably because the complex is in this case electroactive. Moreover, the presence of HEDTA helps in enhancing sensitivity, since it decreases the influence of possible interferences.

The reliability and applicability of the new method were tested following the photocatalytic reduction of Cr(VI) by three titania nanopowders photocatalysts, electrodeposited on Ti grids.

The electroanalytical technique: allowed discriminating the different photocatalytic performances, demonstrated the best performances for titania immobilized in comparison with slurry, permitted the kinetic study of the photoreduction and had no problems of interferences with other chromium species and other compounds (nitric acid and isopropyl alcohol).

Finally, the performance of the new procedure was compared with HDME technique on a representative photocatalytic test, showing very similar results and lower interferences of the matrix.

Future developments will concern the use of bismuth nanoparticles modified electrodes to further improve the sensitivity and to lower the LODs.

3.5. Gold-based electrodes: Arsenic determination

3.5.1. Arsenic

Arsenic is a hazardous, dangerous and toxic compound and its contamination is widely recognized as a global health problem (Amini et al., 2008; Nordstrom, 2002; Sharma & Sohn, 2009). For this reason As is at the first place of the Priority Pollutants List. High levels of As can be found in soil, groundwater and drinking water, since arsenic derivatives are largely used in agricultural poisons, such as fungicides, insecticides and pesticides. Restricted geographical areas (especially in Asian countries) are arsenic rich and have the arsenic level which exceeds even more than one order of magnitude with respect to other countries, resulting in a massive environmental exposition (Berg et al., 2001). Chronic arsenic exposure can cause a lot of health diseases, such as skin lesions, cancers, cardio-vascular system problems (Hopenhayn-Rich, Biggs, & Smith, 1998; Xia & Liu, 2004).

Arsenic is present in nature in different oxidation states, from which its toxicity is dependent. In fact, arsenite or As(III) is the predominant form in the environment and it is also more toxic and mobile than arsenate or As(V) (Pichler, Veizer, & Hall, 1999). For these reasons, in 2006 the Environmental Protection Agency decreased from 50 to 10 $\mu g\ L^{-1}$ the maximum contaminant level for arsenic in drinking water (Smith, Lopipero, Bates, & Steinmaus, 2002) and this value became the guideline of the World Health Organization (WHO).

Many analytical methods for As detection and speciation can be found in the Literature (Hung, Nekrassova, & Compton, 2004; Leermakers et al., 2006; Melamed, 2005), as inductively coupled plasma mass spectrometry (Y. L. Feng, Chen, Tian, & Narasaki, 1998; Thomas & Sniatecki, 1995),

graphite furnace atomic absorption spectrometry (Anezaki, Nukatsuka, & Ohzeki, 1999), neutron activation analysis (Melamed, 2005) and biosensors (Diesel, Schreiber, & van der Meer, 2009). In particular, electroanalytical techniques are extensively employed in As determination for their advantages and they usually need a preconcentration step followed by stripping (Giacomino, Abollino, Lazzara, Malandrino, & Mentasti, 2011; S Laschi, Bagni, Palchetti, & Mascini, 2007; Mardegan et al., 2012; Pal, Sarkar, Bhattacharyay, & Pal, 2010; A O Simm et al., 2005). Among all types of voltammetric techniques, Linear Sweep Adsorptive Stripping Voltammetry (LSAdSV) with HCl as supporting electrolyte (Giacomino et al., 2011; Khairy, Kampouris, Kadara, & Banks, 2010; S Laschi et al., 2007; Mardegan et al., 2012) is one of the most used and gold (S Laschi et al., 2007; Song & Swain, 2007) is the preferred choice as working electrode, since it provides the best electrocatalytic response towards As. Moreover, in recent years the use of gold nanoparticles (Campbell & Compton, 2010; Liza Rassaei et al., 2011) showed its potentialities in electroanalysis and in particular in stripping analysis for arsenic determination. Finally, the use of disposable screen-printed electrodes in this field of environmental trace analysis is very helpful and its combination with nanoparticles could be really promising.

3.5.2. Materials and Methods

Electroanalytical determination of As(III) was performed using three different working electrodes:

- Gold electrode
- Gold Screen-Printed Electrode (Au-SPE)

- Gold nanoparticle-modified Screen-Printed Electrode (AuNP-SPE)

Hydrochloric acid or citric acid was employed as supporting electrolytes.

The voltammetric techniques used was Linear Sweep Adsorptive Stripping Voltammetry (LSAdSV) with a surface pretreatment, which allows the cleaning of the gold surface (cleaning step).

3.5.3. Results and Discussion

The optimized analytical conditions for the use of SPEs devices were investigated, considering firstly the supporting electrolyte. 1 M HCl is usually employed (Giacomino et al., 2011; Khairy et al., 2010; S Laschi et al., 2007; Mardegan et al., 2012) as stripping medium for As detection to avoid hydrolized species formation and was selected for the preliminary tests. However, Au-SPE in the presence of hydrochloric acid suffered from a simultaneous delamination and damage of the working electrode from the ceramic support and damaging of both counter and reference electrodes, as shown in Figure 3.22.

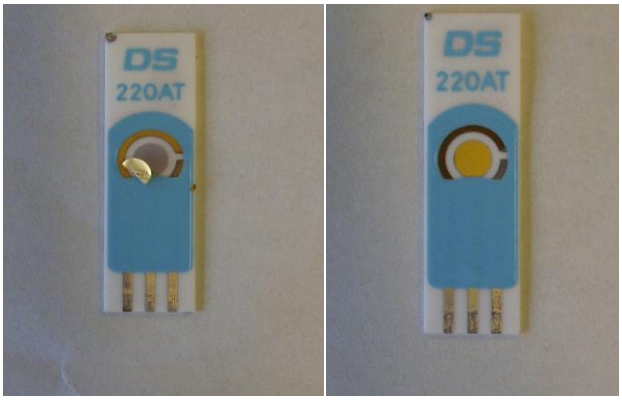

Figure 3.22. Delamination or degradation of gold-based screen printed electrode used in HCl as supporting electrolyte.

In order to avoid this problem, another acidic media, citric acid, was chosen, already used as HCl substitute in the Literature (Huang & Dasgupta, 1999). Initially, the procedure was optimized (resulting analysis parameters are shown in Table 3.16) using the bare gold electrode and compared with the results obtained with HCl as supporting electrolyte.

Table 3.16. Linear Sweep Adsorptive Stripping Voltammetric parameters.

Parameter	Value
Conditioning (CV)	
Purge time (s)	300
Potential range (V)	-0.1/+0.8
Step potential (V)	0.005
Scan rate (V s^{-1})	0.2
Analysis (LSAdSV)	
Deposition potential (V)	-0.6
Deposition time (s)	30
Equilibration time (s)	5
Stripping potential range (V)	-0.4/+0.6
Step potential (V)	0.005
Scan rate (V s^{-1})	0.2

Figure 3.23 reports the voltammetric peaks and the calibration plots in the range 0.002 – 1.97 ppm for HCl and citric acid, showing the good linear correlation and the fully comparability of the analysis performed in citric acid.

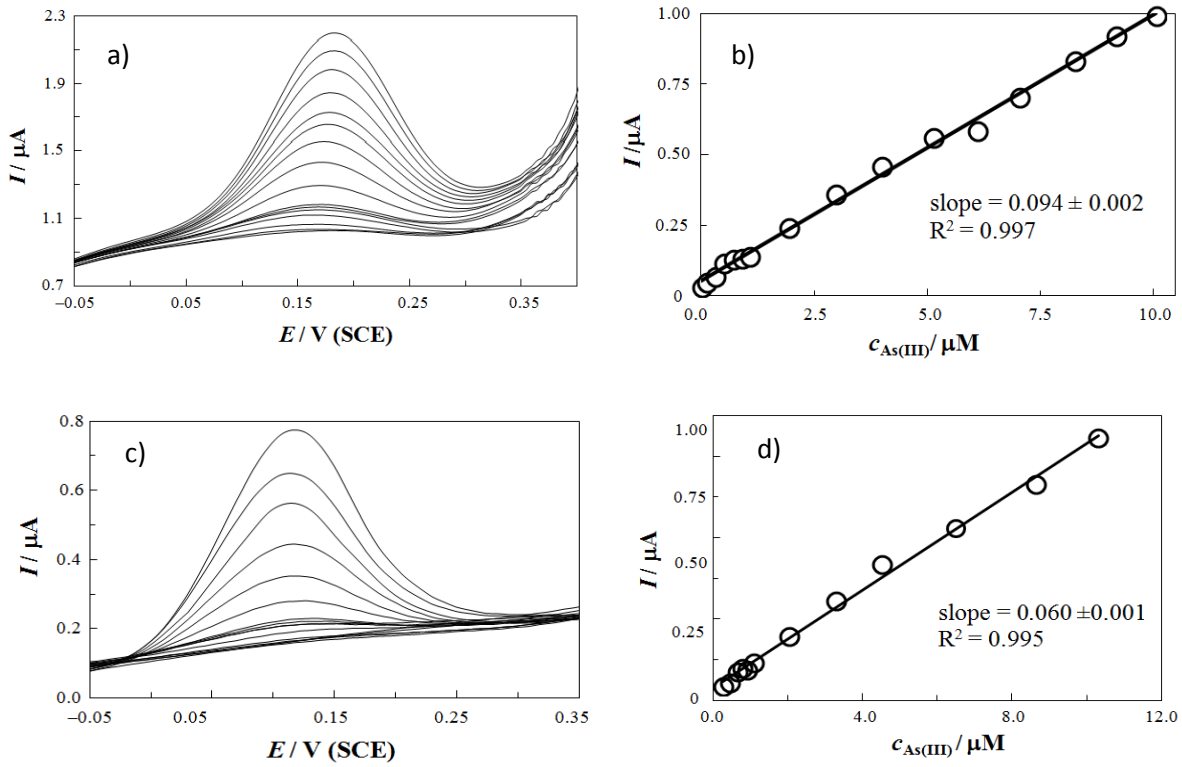

Figure 3.23. LSAdS voltammograms recorded at bare gold electrode in 1 M HCl (a) and 1 M citric acid (c) and corresponding calibration plots (b, d) for consecutive additions of As(III) solution.

The optimized methodology was applied to gold-based SPEs and in Figure 3.24 the calibration plots obtained for Au-SPE and AuNP-SPE in the presence of citric acid are shown. Au nanoparticles on carbon SPE support were detected by SEM analysis, equipped with EDS, directly on the electrode and images showed single isolated Au aggregates. In citric acid no damage of the electrodes was observed. Therefore, this type of electrolyte can be proposed as a valid alternative to hydrochloric acid. For both the electrodes a good calibration plot was obtained, with a broader concentration range for AuNP-SPE. The presence of nanoparticles also allows the increase of one order of magnitude in the current signal in comparison with Au-SPE, since probably a random nanoparticles array on the three-dimensional carbon substrate with intermediate diffusional behaviour between planar and convergent is formed (Campbell &

Compton, 2010; Andrew O Simm, Ward-Jones, Banks, & Compton, 2005; C M Welch, Banks, Simm, & Compton, 2005; S. J. Xing, Xu, Chen, Shi, & Jin, 2011). In this context, higher sensitivities and lower detection limits for the target analyte could be achieved.

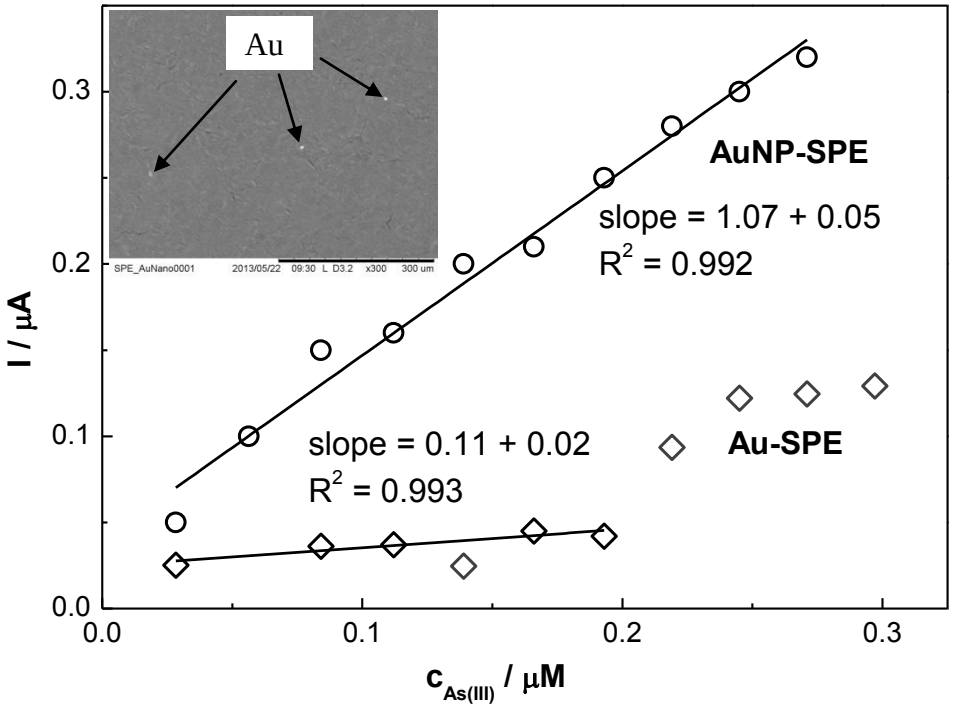

Figure 3.24. Calibration plots of Au-SPE and AuNP-SPE obtained for consecutive additions of As(III) solution. Inset SEM image of the AuNP-SPE working electrode.

This optimized procedure based on citric acid and AuNP-SPE was applied to follow the photocatalytic oxidation of As(III), testing the applicability of the method, in collaboration with Prof. Ardizzone and Dr. Cappelletti group. Samples were collected during the photocatalysis and analyzed with the proposed method using the analyte addition technique, in which each sample was added three times after a calibration plot.

The photocatalysis was performed using three different titania photocatalysts, two commercial and one home-made (Meroni et al., 2011; Spadavecchia et al., 2012), whose surface area and relative phase composition are reported in Table 3.17.

Table 3.17. Structural and morphological features (V Pifferi et al., 2013) **of three different types of titania electrodeposited onto Ti grids, used in the photocatalytic tests.**

Sample	% Anatase	% Brookite	% Rutile	$<D_{anat}>$ (nm)	S_{BET} (m^2g^{-1})	V_{pore} ($mL\ g^{-1}$)
P25	75	-	25	30.0 ± 0.3	50	0.256
T_400	66	37	-	4.8 ± 0.1	150	0.44
Hombikat	100	-	-	10.0 ± 0.3	354	0.35

Before photocatalysis, titania thin layers were electrodeposited on Ti grids, following a procedure reported in previous works (Paoli et al., 2010; V Pifferi et al., 2013), and they were used in photoxidation of As(III) at pH 5, to meet environmental conditions. In particular, the oxidation of As(III) to As(V) is thermodynamically favoured on titania in these conditions, since the valence band of anatase (the principal phase for all the photocatalysts) at pH 5 in an aqueous electrolyte is much more positive than the As(V)/As(III) couple (D. Chen & K. Ray, 2001; Sharma, Dutta, & Ray, 2007) (Figure 3.25).

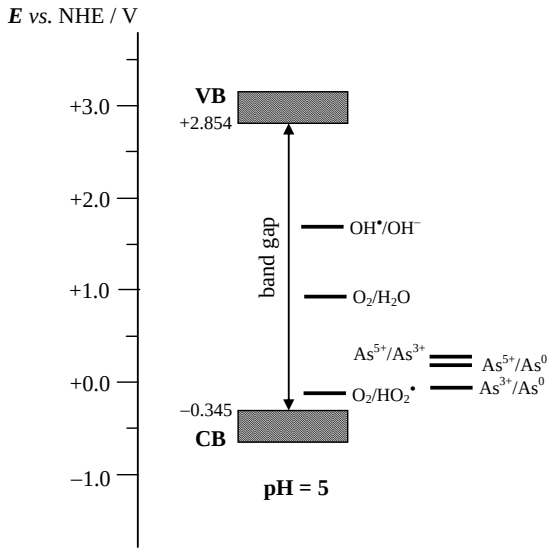

Figure 3.25. Sketch of the positions of the valence and conduction band of anatase together with the redox potentials of arsenic and other relevant oxidant couples at pH 5.

Figure 3.26 reports the removal of As(III) performed by the three different titania films as a function of time, showing excellent activity for all the samples in the order P25 < T_400 < UV 100. In particular, UV 100 shows the best photocatalytic performance, since after only 75 minutes the As(III) concentration drops below the limit of detection of the present electroanalytical technique, which is an order of magnitude lower than the WHO allowed contaminant As(III) level. Moreover, the order of activity follows closely the surface area sequence and the rate determining step of the photocatalysis can be considered the adsorption of the pollutants on titania (Pena, Korfiatis, Patel, Lippincott, & Meng, 2005; Z. Xu & Meng, 2009). Finally, the direct photoxidation of As(III) under UV illumination in the absence of the photocatalyst was considered and ranged around 30 % after 90 minutes.

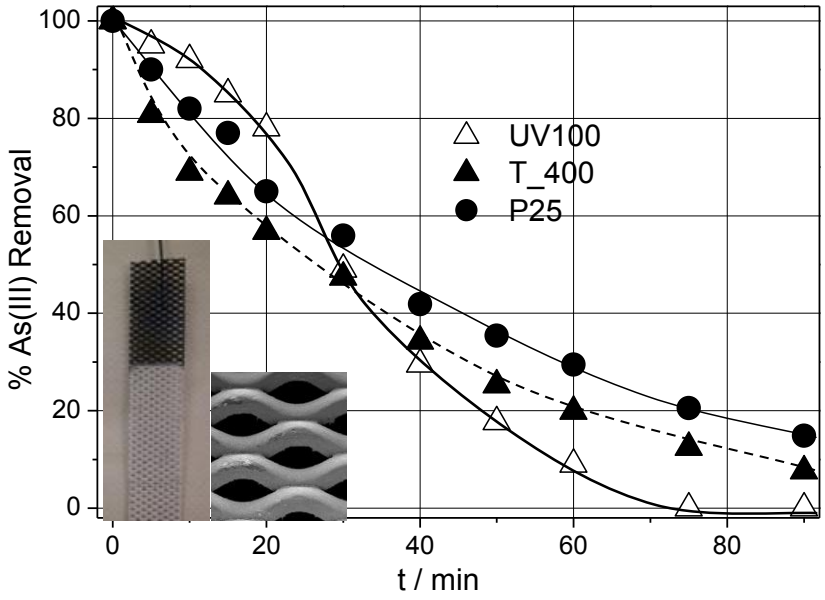

Figure 3.26. Photocatalytic results concerning the As(III) photooxidation in the presence of Hombikat UV100, P25, and T_400-deposited layers. Inset images of the titania layers EPD onto the Ti grid.

For all the collected samples the electroanalytical methodology based on AuNP-SPE and citric acid was used to evaluate the concentration of As(III), showing its applicability also in the presence of interferents.

3.5.4. Conclusions

A simple electroanalytical technique based on the use of gold-based Screen-Printed Electrodes was optimized. Hydrochloric acid was conveniently substituted by citric acid avoiding the damaging of the gold electrodes. The procedure with citric acid was initially tested using bare gold electrode to verify its equivalence with the conventional technique based on HCl. Finally, calibration plots were performed using both Au-SPE and AuNP-SPE. The detection limit of the proposed methodology is one order of magnitude lower than the WHO tolerance level. Sensitivities are higher for SPE with nanoparticles, probably due to intermediate diffusional

behaviour between planar and convergent of the electrode caused by the presence of Au nanoparticles.

This procedure was also tested measuring samples collected during the photoxidation of As(III) to less toxic arsenate by electrodeposited titania nanopowders. The methodology allows discriminating different performances of the three photocatalysts, showing that the activity is influenced by titania surface area.

The electroanalytical procedure together with the remediation method could be proposed as a starting point for the scaling-up of an As(III) remediation process. Future developments will concern the deposition of pre-synthetized or electrodeposited Au nanoparticles to form a more uniform distribution of nanoparticles, together with the use of other types of nanomaterials.

4. Nanomaterials

On 18th October 2011, the European Commission gave the following definition of nanomaterial: "a natural, incidental or manufactured material containing particles, in an unbound state or as an aggregate or as an agglomerate and where, for 50% or more of the particles in the number size distribution, one or more external dimensions is in the size range 1 nm – 100 nm". Considering this definition, nanomaterials can present different sizes and shapes (sphere, rod, tube, etc.) and can have different nature, such as metallic, metal oxide, carbonaceous, polymeric, dendrimeric, composites. Nanomaterials find application in many areas of research and their development is growing in importance, showing employment also in industrial processes (Pierce & Zhao, 2010; C. N. R. Rao, Müller, & Cheetham, 2004; Schmid, 2003). The number of applications is continuing to increase exponentially and the scientific community is also considering their potential effects in the environment, due to their aggregation and toxicity for their size, composition and surface chemistry. Despite the limited number of studies about this topic, the best approach is considered the evaluation of each type of nanomaterial as a distinct entity, but the most important problem remains the method of nanomaterials detection in the environment for their low concentrations and for the number of interferences (Klaine et al., 2008; Pierce & Zhao, 2010).

Nanomaterials possess peculiar properties very different from the corresponding bulk materials and this fact gives them their uniqueness. They can be synthesized by using two different approaches, top-down, where a macroscopic block of the desired material is processed to etching or layering, and bottom-up, where assembly of atoms, ions, molecules are driven by

specific physical or chemical interactions (gas-phase or solution-phase processes), which can be adjusted to obtain the desired size, shape and composition.

Nanomaterials match the size of the majority of relevant chemical compounds and biomolecules (antibodies, enzymes, nucleic acids) and for this reason they are applied in trace analysis (Pierce & Zhao, 2010) for the detection and extraction of contaminants, separation membranes, biological and chemical analysis. In particular, they find extensive application in combination with electrochemical techniques for the introduction of powerful, reliable electrochemical devices, with surface-dependent electron transport properties, correlated to physical/chemical sorption of analytes on nanomaterials (Campbell & Compton, 2010; Luo, Morrin, Killard, & Smyth, 2006; Pumera, Sánchez, Ichinose, & Tang, 2007; Liza Rassaei et al., 2011; Jing Wang, 2012). In comparison with bulk materials normally used in electroanalysis, they offer high active surface area, improved selectivity, catalytic activity, higher signal-to-noise ratio, unique optical properties and the possibility of biomolecules incorporation.

The modification of electrode surfaces (Bănică, 2012; Hodes, 2001) with nanomaterials allows an enhancement in the electron transfer rate, a favourable geometry (area-to-volume ratio) over bulk materials and a compatibility with design of nanoarray. Moreover, the influence of mass transport on the limiting current depends on the size and spacing of nanomaterials, since the diffusion can experiment deeply changes (Campbell & Compton, 2010). In fact, the diffusion layer is increasingly compressed at higher scan rates, causing an enhancement in the current, and, when diffusion layers interact, the current for nanomaterials is reduced from that predicted for isolated nanomaterial elements. In this context, three cases can be described

(Figure 4.1), depending on the nanomaterials coverage of the electrode: low coverage, where isolated elements experiment convergent diffusion and currents scale with particles radius, medium coverage, where diffusion layers of each element partially overlap and diffusion is between convergent and linear, high coverage, where diffusion layers heavy overlap and diffusion is modelled as one-dimensional and linear. Both the kinetic regimes governed by high and low coverages are characterized by higher signal-to background current ratios: in the first case because the faradaic current is proportional to the geometric area, while the capacitive current is proportional to the active surface area; in the second case since the current is proportional not only to the geometric area, but also to the radius of nanomaterials, being independent to the diffusion coefficient. Furthermore, the first case presents a peak-shaped cyclic voltammogram, the second one a steady-state cyclic voltammogram.

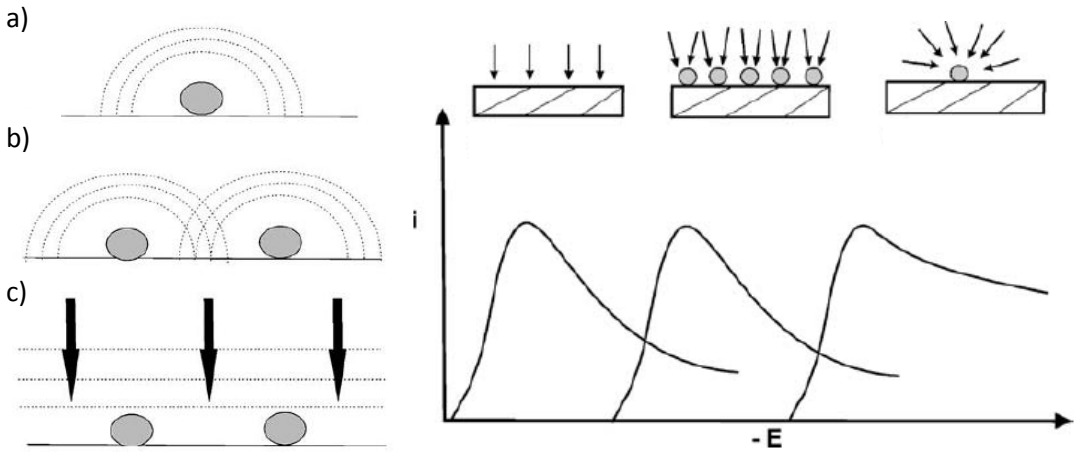

Figure 4.1. Radial diffusion at diffusionally independent spherical particles (a), overlap of diffusion zones of neighbouring particles (b) and heavy overlap of neighbouring diffusion zones leading to overall linear diffusion (c). The effect of mass transport on the voltammetric behaviour reported as a function of electrode type.

In this context, in this PhD Thesis, nanomaterials-modified electrodes were studied and characterized for application in electroanalysis. In particular, two different families of

nanomaterials, carbon nanotubes and metal/semiconductor nanoparticles, were taken into consideration.

4.1. Carbon-based Nanomaterials

4.1.1. Introduction

Carbon in its miscellaneous forms has been used in technology and art since prehistoric times. It is present in nature in two allotropic forms (Noked, Soffer, & Aurbach, 2011; Qureshi, Kang, Davidson, & Gurbuz, 2009), diamond and graphite, the first showing the typical sp^3 structure of carbon atoms and the second presenting a honeycomb sp^2 configuration. Carbon possesses the ability to hybridize into sp, sp^2 and sp^3 configurations, depending on the bonding with neighbouring atoms. This possibility is due to the narrow band gap between 2s and 2p electron shells. These hybrid states are responsible for the different characteristics of various organic species, which open the possibility to fabricate a wide range of different carbon-based materials (Leary & Westwood, 2011; Mauter & Elimelech, 2008; Wanekaya, 2011).

By the early 1980s, carbon science was widely considered to be a mature discipline without possible other surprises, due to the vast knowledge in this field. Today the situation is different thanks to the discover of the first all-carbon molecule, the Buckminsterfullerene (Harris, 2009). From this moment, the union between the properties of sp^2 carbon and the unique behaviour of nanoscale compounds allows the production of carbon-based nanomaterials with distinct characteristics in terms of size, surface area, strength, optical and electrical properties (Mauter & Elimelech, 2008; Wanekaya, 2011). These types of materials can be produced with various microtextures, tunable surface area and porosity, different degree of graphitization, rich variety of dimensionality from 0 to 3D and many synthetic procedures. Moreover, they are well

polarisable, chemically and thermally stable, amphoteric, acting in both donor and acceptor forms, accessible, easily processable and inexpensive (Wanekaya, 2011).

All these advantages make them suitable for the production of modified electrodes (Noked et al., 2011; Švancara, Vytřas, Kalcher, Walcarius, & Wang, 2009). In particular, two processes are used for this purpose, casting and direct growth on the surface of the electrode (Wanekaya, 2011). The principal carbon-based nanomaterials used for the modification of electrodes are fullerenes, graphene, nanofibers and nanotubes (Gooding, 2005; Kochmann, Hirsch, & Wolfbeis, 2012; Ratinac, Yang, Gooding, Thordarson, & Braet, 2011; Tessonnier et al., 2009).

Fullerenes are composed only by carbon atoms in different structures, as hollow spheres, ellipsoids and tubes and they are applied in the electrochemical field particularly in amperometric enzymatic sensors. Graphene is a single layer of graphite and it is classified as a zero-gap semiconductor with ballistic transport of charge carriers, electrons or holes. It can be easily functionalized and it presents very good thermal conductivity and stability, high surface-to-volume ratio and high electron transfer rate. Nanofibers are usually synthesized by vapour-growth and are composed by graphene sheets hold together by Van der Waals forces, arranged as stacked cones, cups or plates around the fiber axis, presenting more reactive sites. They have an average diameter between 5 and 500 nm and their structure depends on the nature of the catalyst metal. Nanotubes represent the most famous, but also the most debated carbon-based nanomaterial in electroanalysis. Their electrochemical properties and applications to the sensoristic field will be discussed later in this chapter.

4.1.2. Carbon Nanotubes

4.1.2.1. Introduction

Carbon nanotubes (Harris, 2009) were discovered in October 1991 by Sumio Iijima, while he was studying the cylindrical deposit on a cathode during the arc-evaporation of graphite. They are based on sp^2 atoms of carbon, π-type chemical bonds, and they are arranged in graphene sheets, which have been rolled up to form a seamless hollow tube. They are usually capped at the end by a fullerene type hemisphere and their dimensions range from 10 nanometers to several micrometers (Gooding, 2005).

The synthetic procedure usually follows two ways, arc or laser evaporation, which allows to obtain small quantities of pure carbon nanotubes, and chemical vapour deposition, that produce big amount of carbon nanotubes, but characterized by larger quantity of amorphous carbon and metal nanoparticles (used as catalysts for their production) impurities (Gooding, 2005; D. Zhang, Shi, Fang, Li, & Dai, 2005).

Carbon nanotubes can be divided into two classes (Figure 4.2): single-walled carbon nanotubes (SWCNTs) and multi-walled carbon nanotubes (MWCNTs). The first ones are composed by only one sheet of graphene rolled up in a tube with the diameter in the range 0.4-2 nm, while the second type is formed by concentric graphene tubes with a distance of 0.34 nm and a total diameter between 2 and 100 nm (Gooding, 2005).

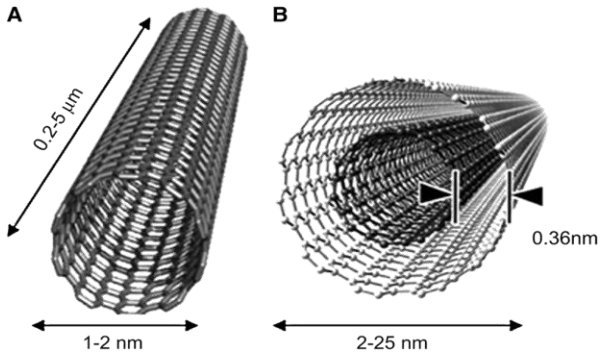

Figure 4.2. Single-walled carbon nanotubes (A) and multi-walled carbon nanotubes (B).

Since their discovery, carbon nanotubes show impressive structural, mechanical, and electronic properties, such as high chemical and thermal stability, high elasticity, high tensile strength, metallic conductivity, allowing their application in many fields, in particular, nanotechnology, pharmaceuticals, gas storage, catalysis, solar cells and transistors. Moreover, their small size and metallic conductivity make them suitable for the production of small electrodes with interesting properties from an electrochemical and electroanalytical point of view (Agüí, Yáñez-Sedeño, & Pingarrón, 2008; Bănică, 2012; Gooding, 2005; Pierce & Zhao, 2010; Pumera, 2009; Yáñez-Sedeño, Pingarrón, Riu, & Rius, 2010). The first application in electrochemistry was the design of a MWCNTs paste electrode for the detection of dopamine, showing really promising results in comparison with traditional electrodes. In fact, carbon nanotubes electrodes are characterized by larger surface area, higher electrocatalytic activity and faster electron transfer rate. MWCNTs and SWCNTs behave differently, since MWCNTs generally present a metallic behaviour, while SWCNTs can behave like metals or semiconductors and, for this last reason, are usually less suitable for electroanalysis.

The preparation of carbon nanotubes modified electrodes (Gooding, 2005; Valentini, Amine, Orlanducci, Terranova, & Palleschi, 2003) plays an important role in the subsequent electrode

electrochemical performances, since these properties depend on nanotubes pre-treatment and purification (Cañete-Rosales et al., 2012; Chiang, Brinson, Smalley, Margrave, & Hauge, 2001; Curulli, Cesaro, Coppe, Silvestri, & Palleschi, 2005; Datsyuk et al., 2008; Dumitrescu, Wilson, & Macpherson, 2007; Fang et al., 2004; Heras et al., 2009; Hou, Liu, & Cheng, 2008; Mazov et al., 2012; Moraes, Cabral, Mascaro, & Machado, 2011; T. Park, Banerjee, Hemraj-Benny, & Wong, 2006; Scheibe, Borowiak-Palen, & Kalenczuk, 2010). In fact, carbon nanotubes are normally purified by acidic treatment (Pumera, Šmíd, & Veltruská, 2009; Rosca, Watari, Uo, & Akasaka, 2005) which is able to remove fullerenic hemispherical caps and produces oxygenated functional groups localized at the ends of the tube (Banks, Moore, Davies, & Compton, 2004). The functionalization confers a hydrophilic character to CNTs ends and a hydrophobic behaviour to walls, making their dispersion in water or polar solvents difficult. For this reason, dimethylformamide is usually employed as suspending agent prior deposition. Furthermore, the presence of oxygenated species (Chou, Bocking, Singh, & Gooding, 2005; LI & LI, 2011) allows the easy functionalization of carbon nanotubes with an infinite number of materials, for example redox mediators, conducting polymers and nanoparticles (Ates & Sarac, 2009; Carvalho, Gouveia-Caridade, & Brett, 2010; Tamburri et al., 2005; Valentini, Biagiotti, Lete, Palleschi, & Wang, 2007). Another important aspect to take in consideration is the presence of amorphous carbon (Ambrosi & Pumera, 2011; Scott & Pumera, 2011; L. Wang, Ambrosi, & Pumera, 2013) and metal nanoparticles (Jones et al., 2007) derived from the synthetic process, which can distort the electrochemical behaviour. In fact, in the Literature, many examples of electrode activity attributed to CNTs, but actually deriving from the presence of carbonaceous

materials or metal nanoparticles, are reported. For all the above reasons, the choice of the correct purification and functionalization method is a fundamental key point.

Finally, in the last years an intense debate about the effective utility of carbon nanotubes in electroanalysisis is in evolution (Banks, Ji, Crossley, & Compton, 2006; Pumera, 2012), since similar performances can be obtained with other carbon-based materials (Banks & Compton, 2006).

In this context, the total removal of amorphous carbon and metal nanoparticles, together with the maintenance of CNTs structure and properties are essential to avoid misunderstanding when they are employed in the sensoristic field.

4.1.2.2. Materials and Methods

Different types of MWCNTs functionalization were chosen, according to the Literature, to study their influence in electroanalytical performances:

- No functionalization;
- 3 M HNO_3 for 24 h;
- 3:1 H_2SO_4/HNO_3 mixture for 24 h;
- 3:1 H_2SO_4/HNO_3 mixture for 24 h with removal of amorphous carbon;
- 3:1 H_2SO_4/HNO_3 mixture for 48 h.

A known quantity of MWCNTs was stirred in the chosen acid for 24 or 48 h. After that time, CNT were filtered on a polyvinyldienfluoride (PVDF) membrane (Ø 47 mm and 0.22 µm pore size),

washed with Milli-Q water until neutral pH and dried in an oven for 24 h at 80°C. In the case of removal of amorphous carbon, CNTs were successively treated in 0.1 M NaOH and sonicated for 15 minutes. After 24 h, CNTs were filtered as explained before and treated newly in NaOH, until filtered water was transparent. Then, CNTs were acidified in 0.1 M HCl for 24 h, filtered and dried in an oven for 24 h at 80°C.

The chosen volume of a dispersion of CNT (volume, solvent and concentration will be discussed) were dropped on the surface of a GC electrode.

Two kinds of MWCNTs have been used: MWCNTs from Sigma Aldrich (SA, purity > 98%, 6-13 nm diameter and 2.5-20 μm length) and MWCNTs from Politecnico di Milano (POLI, no specifications were given), both produced by chemical vapour deposition.

4.1.2.3. Results and Discussion

Optimization of experimental conditions

First, optimization of the deposition variables was carried out and, in particular, the volume of deposition, the solvent and CNTs concentration were considered. The volume of deposition was varied between 5 and 20 μL, because the drop of 20 μL covers the entire area of GC (also the Teflon part) while 5 μL drop covers only the GC electrode area. In the case of the solvent, DMF is usually employed for CNT drop casting, as the Literature reports (Pumera, 2009), while water was chosen to solve toxicity problems of DMF. In Figure 4.3 the study of deposition volume and solvent are both reported, showing higher values of the oxidation peak of the model probe molecule ($K_4[Fe(CN)_6]$) in the case of DMF and for 20 μL deposition volume. These results can

be interpreted considering the better interactions of DMF with acidic groups on the surface of CNTs, as reported in the Literature, and the better coverage of the conductive part of the electrode. The use of a water-DMF mixed solvent also causes a decrease in the signal, so DMF was chosen as solvent and 20 µL as deposition volume. Finally, CNTs deposition solution concentration was evaluated, varying the concentration between 0.5 mg mL^{-1} and 4.0 mg mL^{-1}. Figure 4.3 presents cyclic voltammograms and the variation of probe oxidation peak. The highest oxidation current is obtained for 4 mg mL^{-1}, but values are very similar for all the concentrations. Moreover, observing the cyclic voltammograms, capacitance values generally increase with the highest value for 4 mg mL^{-1} concentration. Since for electroanalytical purposes, high capacitance values are detrimental and cause a lowering of the sensitivity, 0.5 mg mL^{-1} concentration was at last chosen.

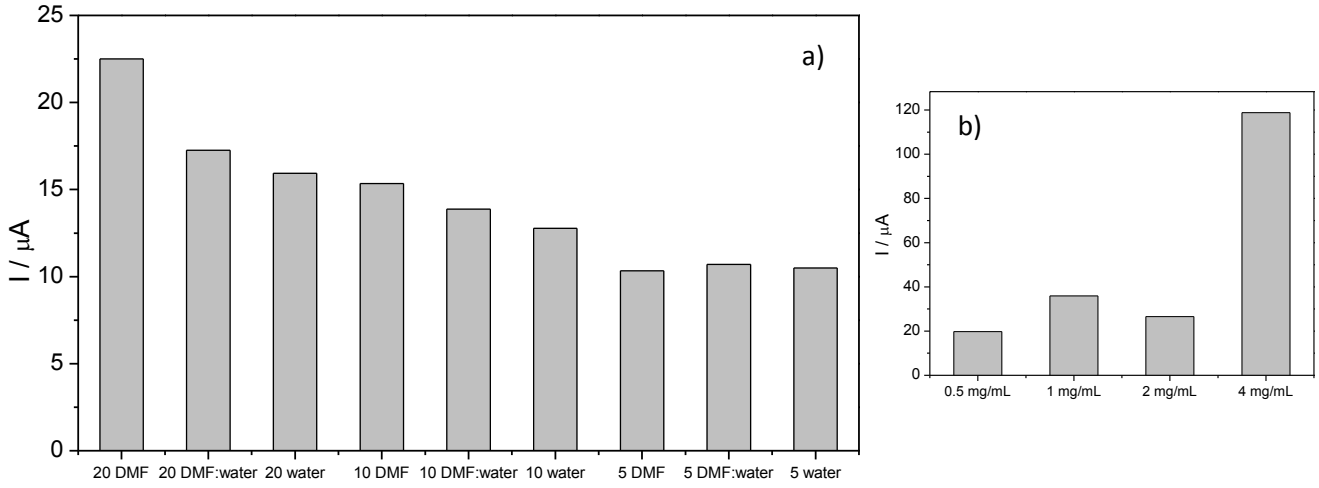

Figure 4.3. Casting solvent study (a) and concentration deposition study (b).

The optimized parameters are thus:

- Solvent: DMF

- Deposition volume: 20 µL

- CNT concentration: 0.5 mg mL^{-1}

Characterization of carbon nanotubes

All the types of functionalized CNTs were tested in the optimized conditions and cyclic voltammograms in 0.1 M KCl with $K_4[Fe(CN)_6]$ as model probe molecule are shown in Figure 4.4. CNTs used as received show an electroanalytical signal very similar to GC electrode, while all the functionalized ones present higher peak currents. In particular, the best results are obtained for CNTs treated in the sulphonitric mixture for 24 h. In the case of nitric acid, the signal is less intense, while for 48 h treatment the shape of voltammogram changes. In fact, the peak becomes a step, showing a change in the kinetic diffusion mechanism. The further removal of amorphous carbon, allows a further increment of the peak current. In order to shed light upon these results, an extended characterization of CNTs was performed.

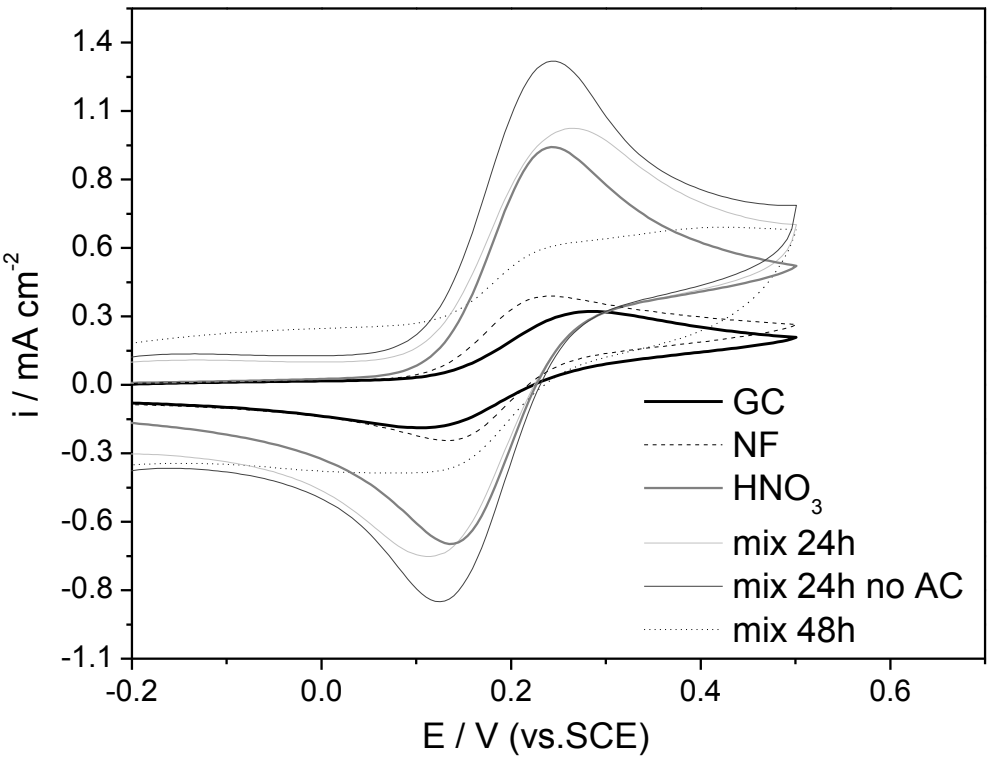

Figure 4.4. Cyclic voltammograms of CNTs after different purification methods.

First of all, functionalized CNTs were studied with Transmission Electron Microscopy (TEM), to evaluate their morphology and the eventual impurities derived from the synthetic process. TEM images are presented in Figure 4.5. CNTs without functionalization and purified in nitric acid show the presence of catalytic metal nanoparticles used for their synthesis. The sulphonitric treatment is capable of eliminating these metal impurities. Moreover, the prolonged treatment (48 h), causes a cutting of CNTs and an increase of the amorphous carbon. These results can explicate the different voltammetric behaviour of CNTs, in particular considering the behaviour of CNTs treated for 48 h or without amorphous carbon. In the first case, the current signal is step-shaped because probably the diffusion mechanism changes from planar to radial-convergent, due to the CNTs cutting in small nano-subunities; in the second case, the current

increase is probably caused by the amorphous carbon removal after its production during the sulphonitric treatment.

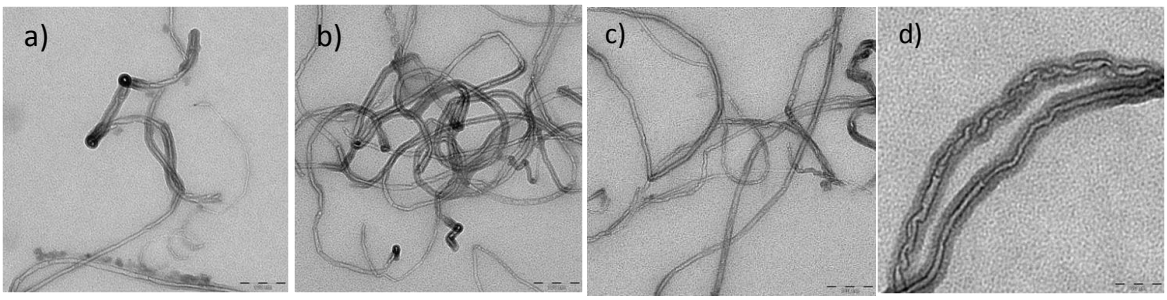

Figure 4.5. TEM images on CNTs non-functionalized (a), treated in nitric acid (b), treated in sulphonitric mixture for 24 h (c) and for 48 h (d).

Considering the morphologic differences evinced by TEM, complementary BET analysis were also performed to evaluate the CNTs surface area and porosity. In Figure 4.6 a typical BET graph is presented. The hysteresis loop evidences the presence of slit-shaped pores for all the samples. BET parameters are reported In Table 4.1. A surface area and pore volume increase can be noticed for all treated CNTs. Moreover, the percentage of microporosity (< 2 nm) is reduced, accompanied by an increase of the percentage of mesopores (10-80 nm) (Figure 4.7-4.8). All these effects can be considered as responsible for the current increase. Mesoporosity is more suitable for analyte diffusion in the modified electrode structure.

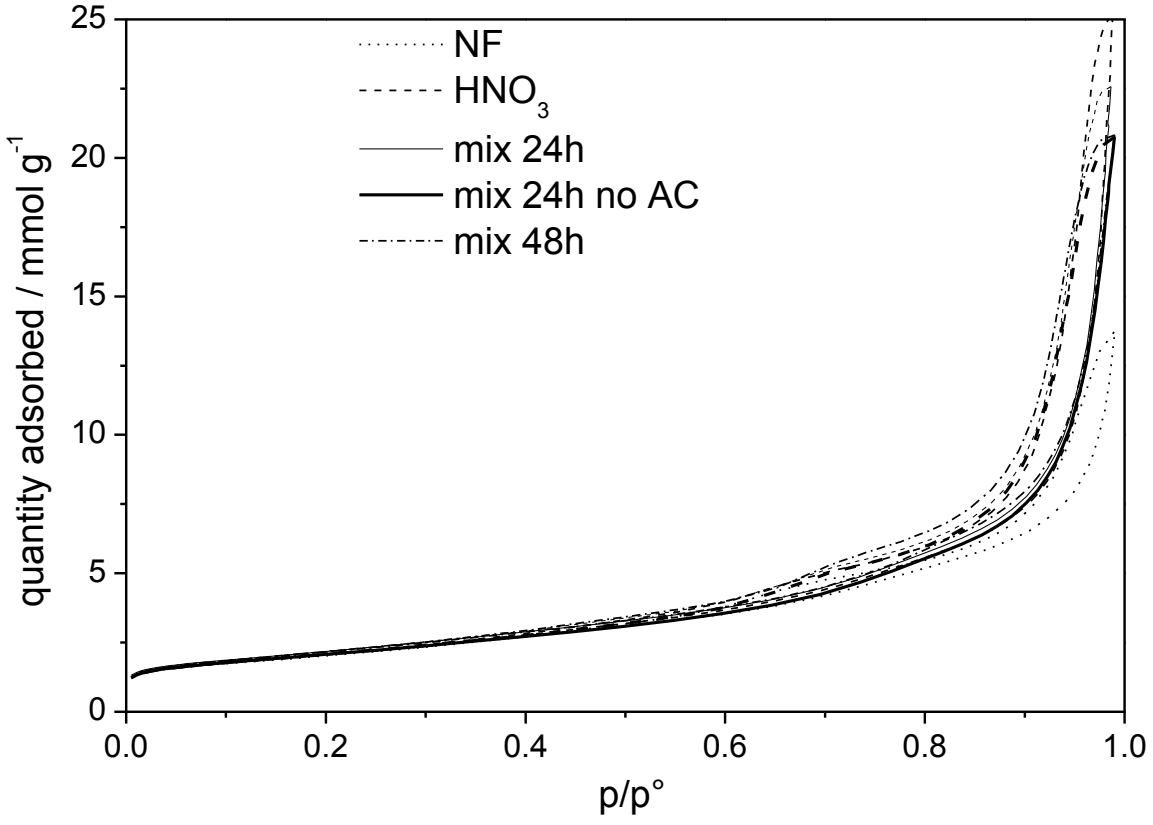

Figure 4.6. BET isotherms for CNTs with different purification treatments.

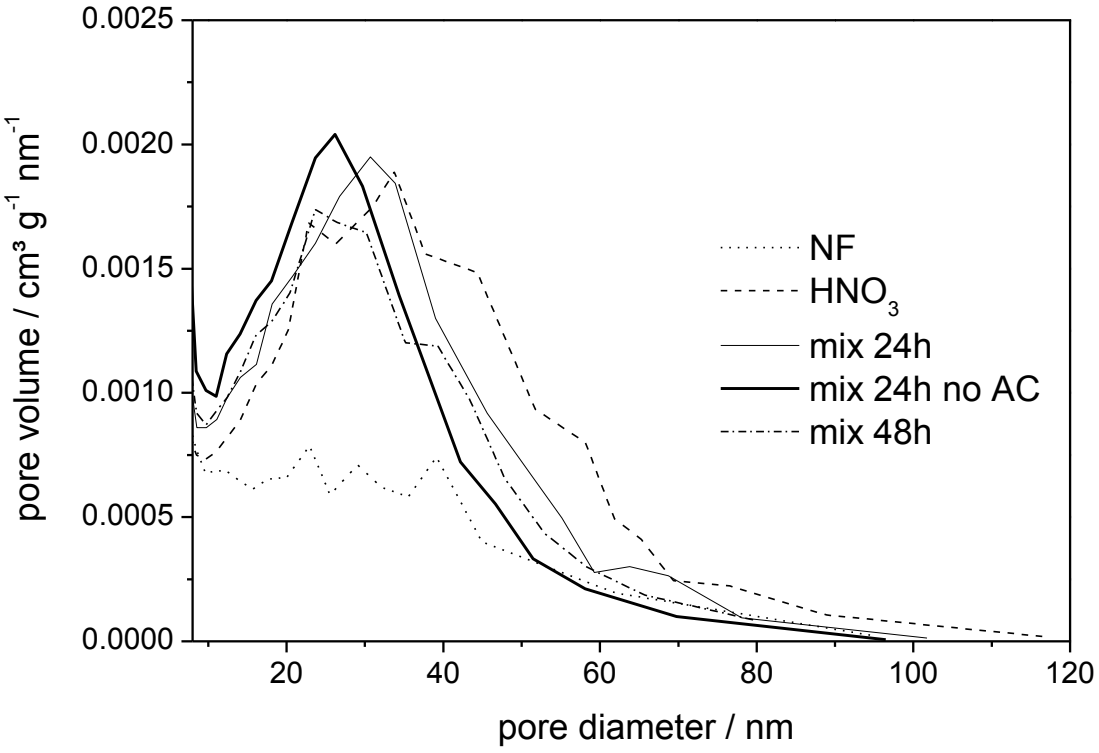

Figure 4.7. Distribution of the pore volume on pore diameters for different purification treatments.

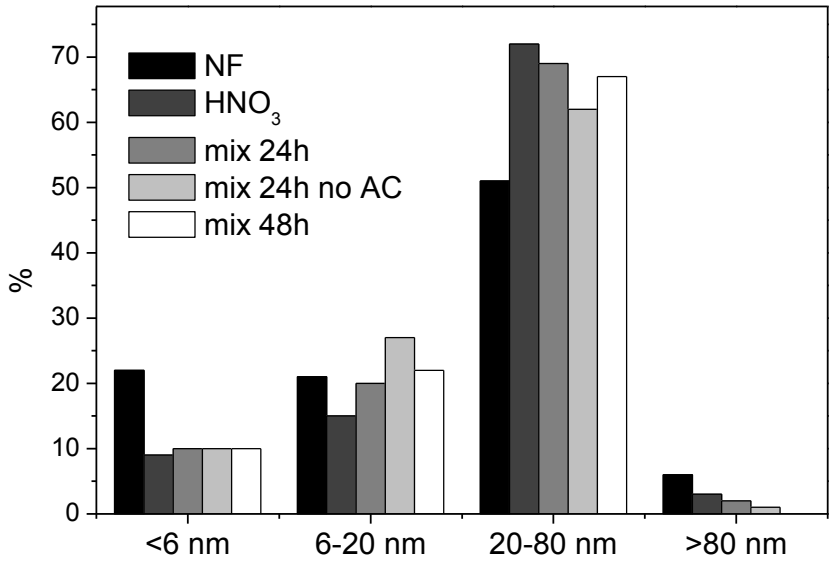

Figure 4.8. Pore distribution representation for different purification treatments.

Table 4.1. Parameters obtained from BET analysis for CNTs with different purification treatments.

CNTs	S_{BET} / $m^2 g^{-1}$	V_{pores} / $cm^3 g^{-1}$	$A_{micropores}$ / $m^2 g^{-1}$	% micropores
NF	150.8 ± 0.8	0.47	51.4	10.2
HNO3	161 ± 1	0.87	10.7	6.6
Mix 24h	172 ± 1	0.78	13.2	7.7
Mix 24h no AC	170 ± 1	0.72	5.8	3.4
Mix 48h	164 ± 1	0.71	12.8	7.8

The electroanalytical properties can be influenced also by the presence of different catalytic groups on the CNTs surface. In particular, the Literature (LI & LI, 2011) reports the covalent acidity as responsible for higher performances of functionalized CNTs. CNTs were characterized from this point of view by titration, in order to quantify the total acidity, the desorptive acidity, the covalent acidity and the CO_2 presence (Hanelt, Orts-Gil, Friedrich, & Meyer-Plath, 2011). An example of titration curve is shown in Figure 4.9. The curve presents three equivalent points: the first correlated with the residual NaOH derived from the neutralization of total acidity, the second representing the quantity of desorptive acids, formed on the CNTs surface during the synthetic process and released in solution after neutralization, and the third related to CO_2 in solution, which causes an acidification of water for reaction with NaOH. Figure 4.10 reports the quantity of the different types of acidity for each type of functionalization. The quantity of desorptive acids and CO_2 in solution remain the same in all cases, confirming that desorptive acids derive from the synthetic process, while CO_2 derives from the environment, both having no influence on voltammetric performances. The difference is in the covalent acidity, which is higher for the sulphonitric treatment. The higher quantity of acidic groups on the surface can be considered as another key feature capable of causing more intense current signals.

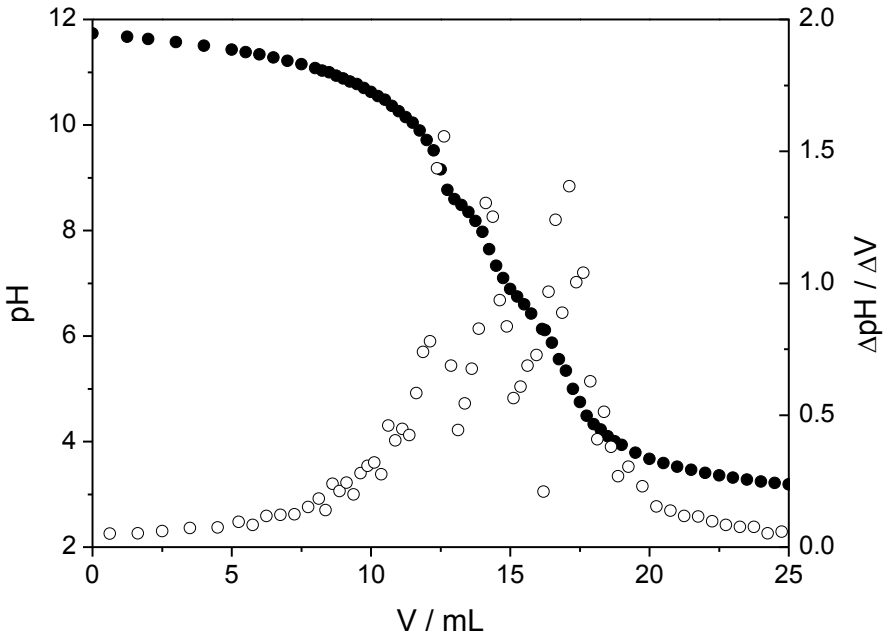

Figure 4.9. Example of CNTs acid functionalities titration.

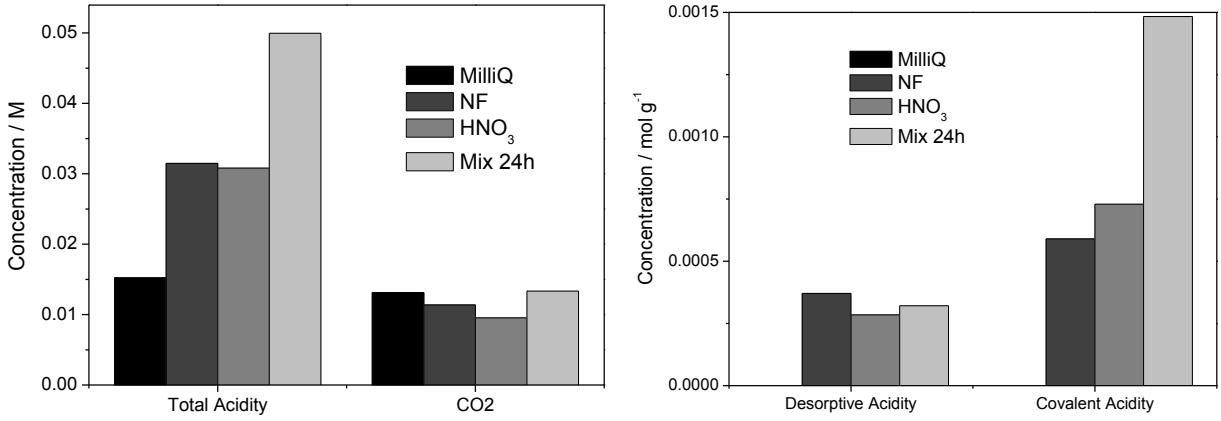

Figure 4.10. Representation of different acid functionalities obtained from titrations of CNTs with different purification treatments.

As reported in the Literature (Ambrosi & Pumera, 2011; Scott & Pumera, 2011; L. Wang et al., 2013), the oxidative treatment can produce oxidated brown fragments, known as amorphous carbon. These compounds were found in NaOH solution during titration, since they dissolve in the presence of NaOH, confering a brownish colour to the solution. This colour is evident in the case of sulphonitric treatment, while for the other cases the solution remains transparent.

Amorphous carbon presents an intense UV-vis absorption peak at 200-220 nm, with a shoulder at 280 nm, visible only in the cases of sulphonitric mixture, the highest absorbance registered for 48 h treatment, confirming the strong erosion of the CNTs and the damaging of the structure observed by TEM.

The presence of amorphous carbon can alter the properties of CNTs and for this reason it was removed by consecutive treatments in NaOH. An increase in the voltammetric signal consequent to the amorphous carbon removal is evinced in Figure 4.4.

Finally, electrochemical characterization was performed by Cyclic Voltammetry varying the scan rate between 0.01 and 1 V s^{-1} and Electrochemical Impedance Spectroscopy with and without the redox probe molecule: ($K_4[Fe(CN)_6]$).

The obtained parameters are reported in Table 4.2. In general, capacitance values follow the sequence of surface area obtained by BET analysis. The electrochemical reversibility is improved or maintained in comparison with GC, as can be observed from the values of E_p-$E_{p/2}$ and ΔE_p, but in the case of sulphonitric mixture treatment the values are higher than those obtained for non-functionalized and nitric acid treated CNTs. The kinetic mechanism remains generally under diffusion control with slopes of the linear ln *i* vs ln *v* close to 0.5. In the case of sulphonitric mixture the diffusive behaviour is partially lost. The removal of carbonaceous amorphous material increases the reversibility and the diffusion character of the process. Moreover, this electrode reaches the highest capacity values, probably due to the presence of a major quantity of covalent acids on the CNT surface. On the other hand, an increase in the cathodic and anodic slopes is evidenced. This behaviour can be attributed not only to the

increase in the surface area (which is not so drastic), but also to the model probe molecule diffusion coefficient change through the CNT network. For all the above reasons, CNTs without amorphous carbon appear to be the most promising materials for electroanalytical applications.

Table 4.2. Voltammetric parameters obtained from cyclic voltammograms of glassy carbon and of CNTs-modified electrodes.

Parameters	GC	NF	HNO_3	Mix 24h	Mix 48h	Mix 24h no AC
C_{CV} / mF cm^{-2}	0.080	0.18	0.28	2.11	1.44	2.36
S_{BET} / m^2 g^{-1}	-	150.8 + 0.8	161 + 1	172 + 1	164 + 1	170 + 1
E_p-$E_{p/2}$ / mV	96	74	74	94	Step shaped	80
ΔE_p / mV	171	102	107	147	Step shaped	117
Slope i_p *vs* $v^{0.5}$ / µA $mV^{-0.5}$ cm^{-2} $s^{0.5}$	31	35	107	63	35	129
Slope Ln i_p *vs* ln *v*	0.44	0.42	0.44	0.34	0.28	0.45

Electrochemical Impedance Spectroscopy was carried out with or without model probe molecule at – 0.10, + 0.10 and + 0.25 V (SCE). Operative potentials were chosen considering the cyclic voltammogram of the model probe molecule: + 0.10 and + 0.25 V are the peak potentials of the cathodic and anodic scan, respectively, while – 0.10 V is a potential value chosen in the capacitive area.

In the absence of the model probe molecule, complex plane spectra in Figure 4.11 are very similar for all the considered potentials and present a semicircle for high frequencies followed in some cases by a straight line with the slope close to 90°. Bode plots have the typical shape of a time-dependent process, correlated to the formation of the double layer. In the case of non-functionalization and treatment with nitric acid, only a big semicircle is present and values of

impedance are higher, indicating the electron transfer difficulty and the low double layer capacitance. On the other hand, in the case of sulphonitric mixture the semicircle is smaller and characterized by lower impedance, demonstrating the formation of a more capacitive double layer with a faster electron transfer. In particular, in terms of semicircle size, a better situation is obtained with the 24 h treatment in comparison with the 48 h one. The removal of amorphous carbon allows the best performance, also considering the straight line closer to 90°, behaviour typical of a pure-like capacitor. Equivalent circuits used to fit impedance data are presented in Figure 4.12. Non-functionalized or nitric acid treated CNTs present equivalent circuits formed by the solution resistance in series with a CPE_{DL} and a R_{CT} in parallel, while for sulphonitric mixture treated CNT a CPE_{POL} has to be added.

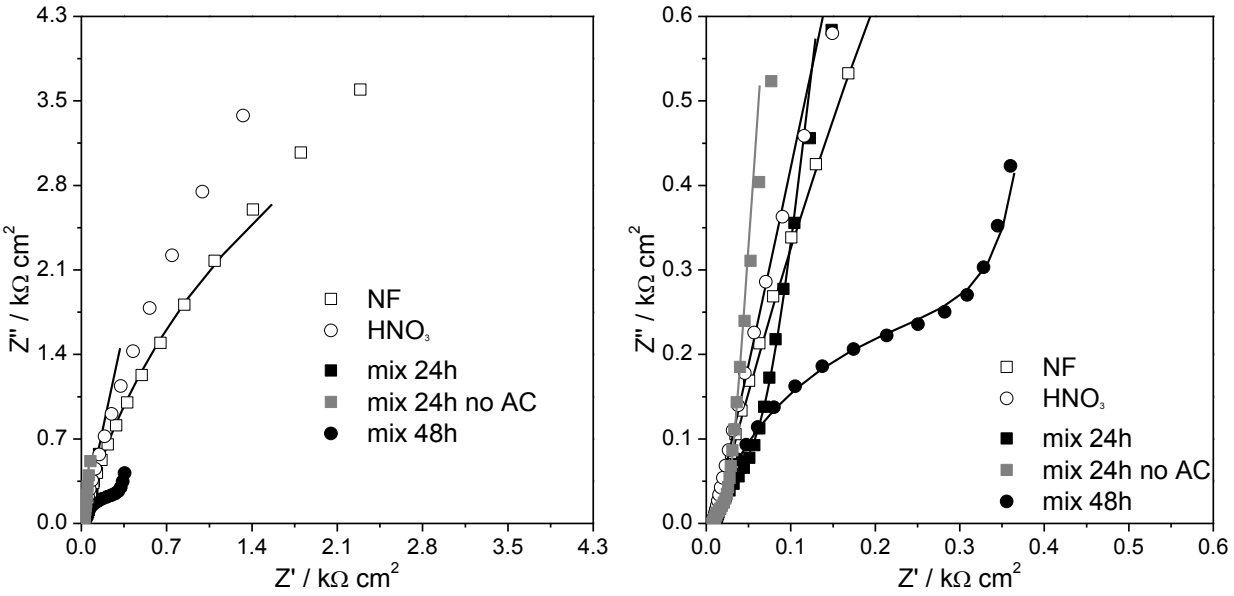

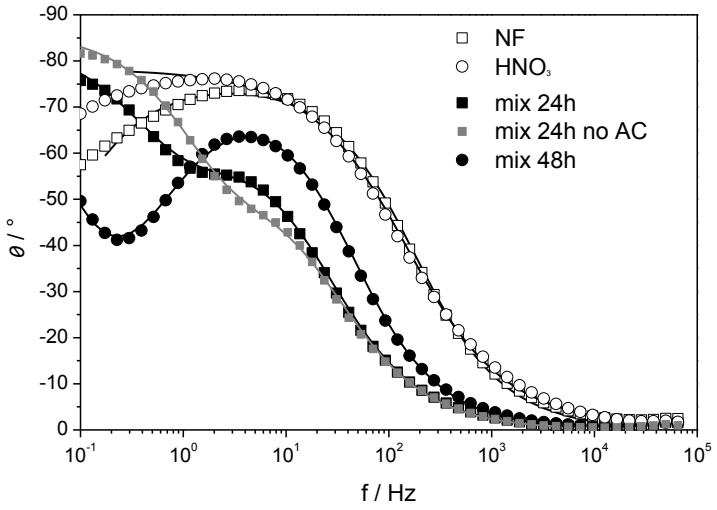

Figure 4.11. Complex plane plot and Bode plot at – 0.1 V in the absence of redox probe.

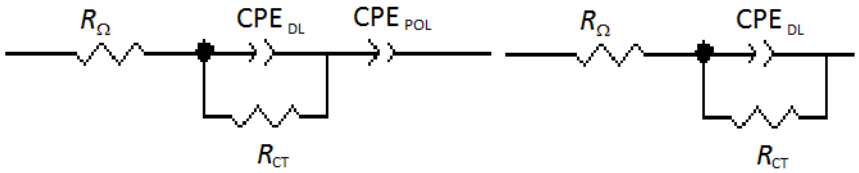

Figure 4.12. Equivalent circuits used to fit impedance data.

Table 4.3 reports the values of equivalent circuit parameters obtained by the fitting procedure. The values of the three potentials for each electrode are very similar, demonstrating that the electrodes are very stable. As expected, higher capacitances of the double layer and lower charge transfer resistances are obtained for the sulphonitric mixture samples, while values of CPE_{POL} and α_{POL} are higher when amorphous carbon is removed, indicating a pure-like capacitor behaviour. Double layer capacitances obtained by EIS were compared with capacitances derived from CV and reported in Table 4.4, showing an excellent results agreement.

Table 4.3. Impedance parameters obtained by impedance fitting in the absence of redox probe.

Electrode	E_{ap}vs SCE / V	R_Ω / Ω cm^2	CPE_{DL} / mF cm^{-2} s$^{\alpha-1}$	α_{DL}	R_{CT} / Ω cm^2	CPE / mF cm^{-2} s$^{\alpha-1}$	α
NF	-0.10	9.8	0.266	0.85	10489	-	-
	0.10	9.8	0.243	0.86	11173	-	-
	0.25	9.8	0.253	0.86	10499	-	-
HNO_3	-0.10	7.4	0.384	0.86	23872	-	-
	0.10	7.4	0.302	0.88	28168	-	-
	0.25	7.3	0.265	0.89	22156	-	-
Mix 24 h	-0.10	10.1	3.11	0.78	61	2.70	0.93
	0.10	10.0	2.18	0.81	53	1.95	0.93
	0.25	9.9	2.23	0.82	41	1.82	0.93
Mix 48 h	-0.10	9.7	0.919	0.86	392	4.72	1
	0.10	9.6	0.617	0.88	351	3.19	1
	0.25	9.6	0.595	0.89	292	2.92	1
Mix 24 h no AC	-0.10	7.8	3.75	0.79	20	3.01	0.96
	0.10	7.8	2.88	0.82	17	2.22	0.97
	0.25	7.6	3.20	0.82	13	2.26	0.97

Table 4.4. Comparison between capacitance values obtained from CV and EIS study.

Electrode type	C / mF cm^{-2}	
	CV	EIS
GC	0.0803	0.116
Mix 24h	2.109	2.157
Mix 24h no AC	2.362	2.5
Mix 48h	1.437	3.61
HNO_3	0.284	0.318
NF	0.179	0.254

In the presence of the model probe molecule, impedance spectra at – 0.10 V are similar to those obtained previously, since at this potential the Fe^{3+}/Fe^{2+} couple is not electroactive (Figure 4.13). At the other two potentials (Figure 4.14-4.15) impedance values strongly

decrease, because the probe reacts at the electrode, and the trend of the spectra changes. The complex plane plots show in general: a semicircle for high frequencies, which is larger for non-functionalized and nitric acid treated CNTs, and a straight line for low frequencies, with higher slope in the case of sulphonitric treatment. Higher impedance values are reached, as in the previous case, when CNTs are treated in nitric acid or are not functionalized. Equivalent circuits used to fit impedance data are shown in Figure 4.16 and parameters obtained from the fitting are presented in Table 4.5.

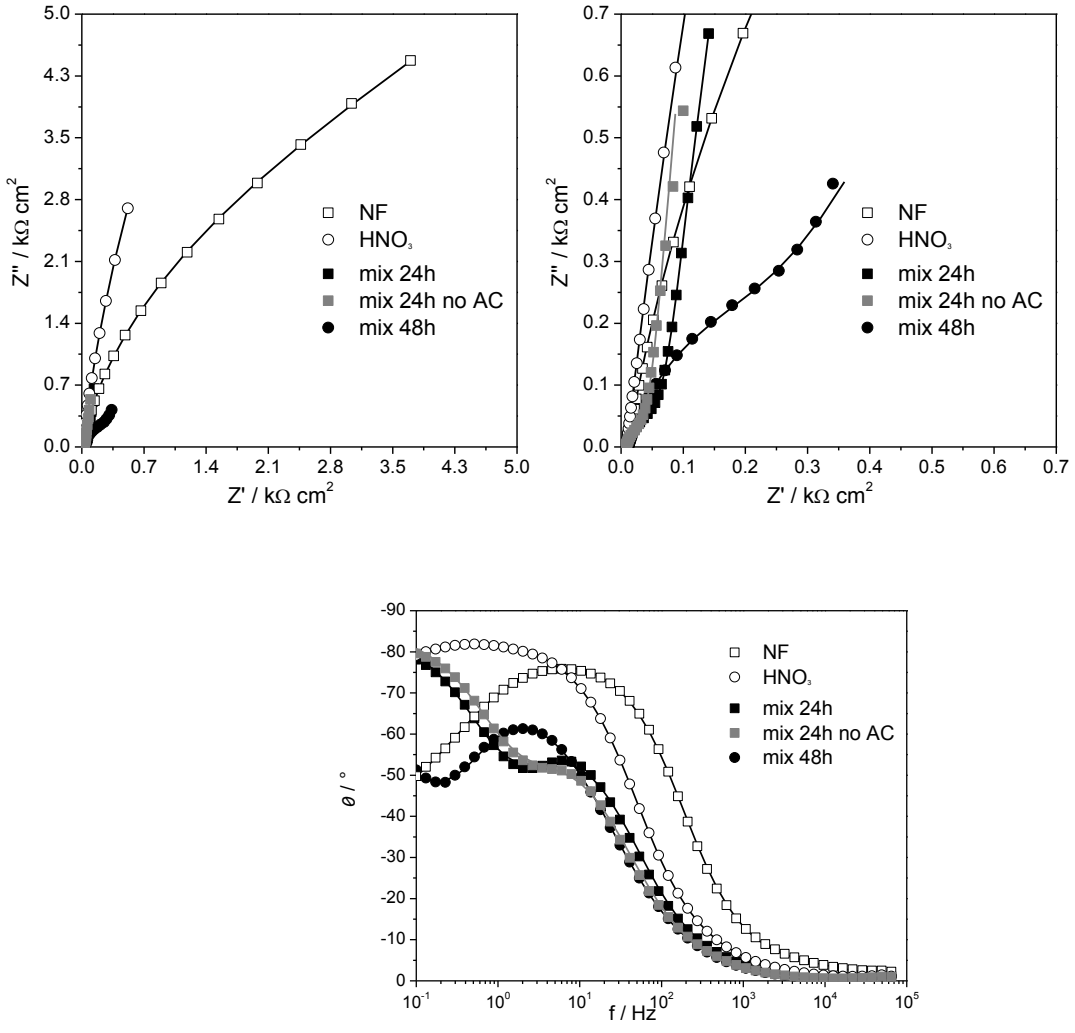

Figure 4.13. Complex plane plot and Bode plot at – 0.1 V in the presence of redox probe.

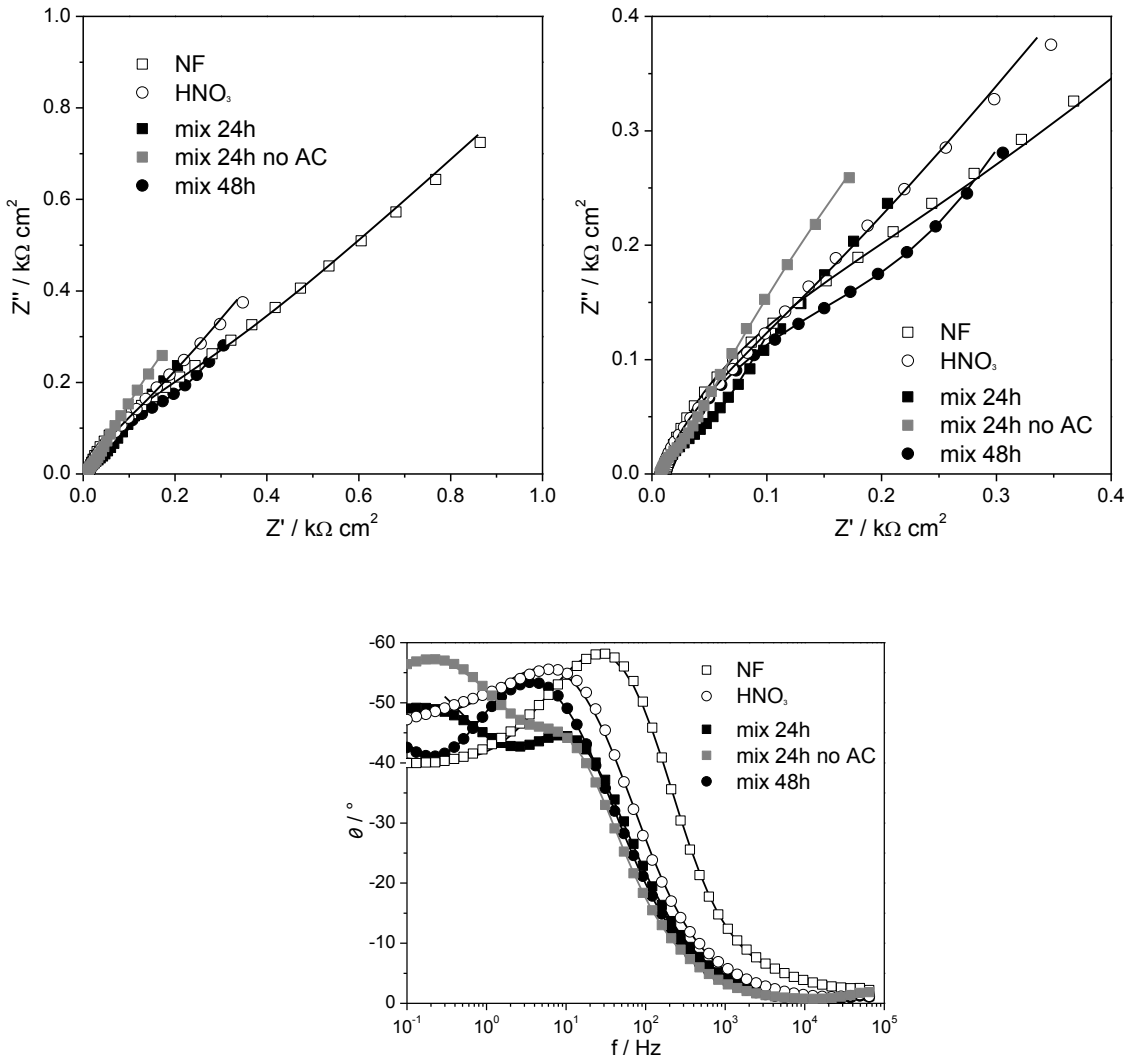

Figure 4.14. Complex plane plot and Bode plot at + 0.1 V in the presence of redox probe.

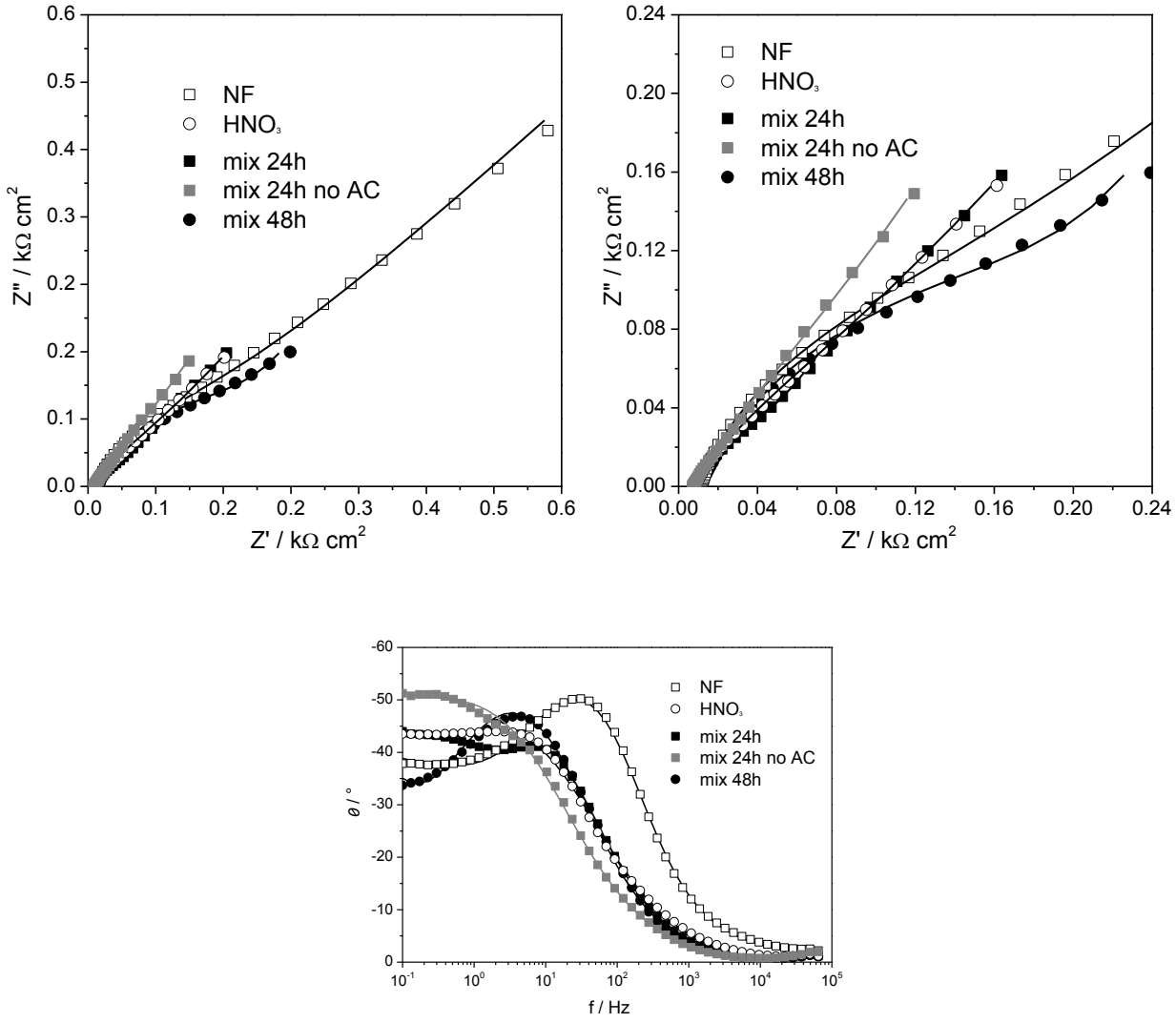

Figure 4.15. Complex plane plot and Bode plot at + 0.25 V in the presence of redox probe.

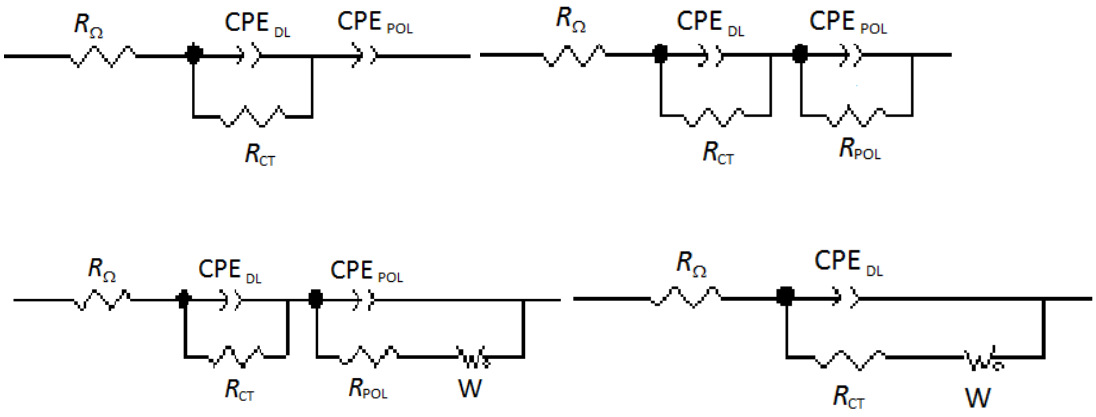

Figure 4.16. Equivalent circuits used to fit impedance data.

Equivalent circuits used for the fitting are the same of the no-probe analysis when the sulphonitric functionalization is performed, while in the case of non-functionalized CNTs an additional RC has to be added, correlated with the reaction of the redox couple at the electrode. In the case of nitric acid treatment, increasing the potential the situation becomes similar to that of sulphonitric treatment, probably due to easier redox reaction at higher potential. In general higher capacitances are obtained increasing the potential and CNTs after removal of amorphous carbon show the best performances.

Table 4.5. Impedance parameters obtained by impedance fitting in the presence of redox probe.

Electrode	E_{ap}vs SCE / V	R_Ω / Ω cm^2	CPE_{DL} / mF cm^{-2} s$^{\alpha-1}$	α_{DL}	R_{CT} / Ω cm^2	CPE_{POL} / mF cm^{-2} s$^{\alpha-1}$	α_{POL}	R_{POL} / Ω cm^2	R_w / Ω cm^2	τ / s	α	CPE / mF cm^{-2} s$^{\alpha-1}$	α
NF	-0.10	10.5	0.23	0.77	1.29	0.13	0.91	2031	8294	4.07	0.24	-	-
	0.10	10.3	2.84	0.50	1.81	0.16	0.89	123	283	0.1	0.24	-	-
	0.25	10.4	2.76	0.53	1.26	0.27	0.83	93	173	0.1	0.24	-	-
HNO_3	-0.10	7.5	7.95	0.62	1.35	0.54	0.93	39496	-	-	-	-	-
	0.10	7.7	1.09	0.80	187	-	-	-	125	0.1	0.28	-	-
	0.25	7.5	3.45	0.66	194	-	-	-	-	-	-	4.51	0.55
Mix 24 h	-0.10	8.6	1.71	0.82	64	-	-	-	-	-	-	2.34	0.94
	0.10	8.5	1.98	0.88	28	-	-	-	-	-	-	4.50	0.68
	0.25	8.5	3.08	0.79	32	-	-	-	-	-	-	6.28	0.68
Mix 48 h	-0.10	11.2	2.18	0.96	166	-	-	-	-	-	-	3.17	0.71
	0.10	11.1	1.82	0.79	200	-	-	-	-	-	-	5.26	0.73
	0.25	11.2	2.12	0.72	218	-	-	-	-	-	-	12.5	0.80
Mix 24 h no AC	-0.10	7.4	2.84	0.80	37	-	-	-	-	-	-	2.89	0.95
	0.10	7.3	3.26	1.00	90	-	-	-	-	-	-	4.57	0.70
	0.25	7.2	10.9	0.63	106	-	-	-	-	-	-	11.0	0.74

In conclusion, the different purification and functionalization treatments produce CNTs with different electrochemical behaviours, as the extensive characterization has showed. Metal nanoparticles derived from the synthetic process are still present after nitric acid treatment and only a slight increase in surface area, peak current and capacitance can be observed. Better results can be obtained with the sulphonitric treatment, with the complete removal of metal nanoparticles, higher increase of the surface area and mesoporosity, higher current intensities and capacitance values, formation of a relevant quantity of surface covalent acidity. When this treatment is performed for longer time (48 h), the result is a cutting of CNTs, which changes capacitance, charge transfer resistance, current intensity and the kinetic mechanism from planar to convergent, causing the formation of a step-shaped cyclovoltammogram. At last, the removal of amorphous carbon is beneficial for the electrochemical response, yielding to more sensible electrodes, more capacitive and less resistant to electron transfer, without losing the diffusion control and reversibility. For all these reasons, CNTs treated in sulphonitric mixture for 24 h and purified by amorphous carbon were chosen for the following electroanalytical applications.

*o-Toluidine determinatio*n

CNTs without amorphous carbon were chosen for the electroanalitycal detection of o-toluidine, considering the promising results obtained previously with carbon-based electrodes (Chapter 3).

Consecutive cyclic voltammograms on the same analyte concentration (Figure 4.17) show the o-toluidine peak at about + 0.9 V (SCE), but also the formation of a polymer, with satellite peaks

between + 0.3 to + 0.7 V and 0 to + 0.5 V. This behaviour, probably already present also when using other carbon-based electrodes, is in this case amplified, due to their higher surface area and higher density of active sites of CNTs electrodes. Firstly, considering the previous results, Differential Pulse Voltammetry was performed for consecutive analyte addition, but no good results were obtained, as shown in Figure 4.17, possibly due to the formation of a fouling polymer during the pulse. Square Wave Voltammetry was not considered, since the electrochemical reaction is irreversible. Chronoamperometry was carried out, as shown in Figure 4.17, but also in this case the fixed potential causes the quick saturation of the electrode caused by the production of the polymer.

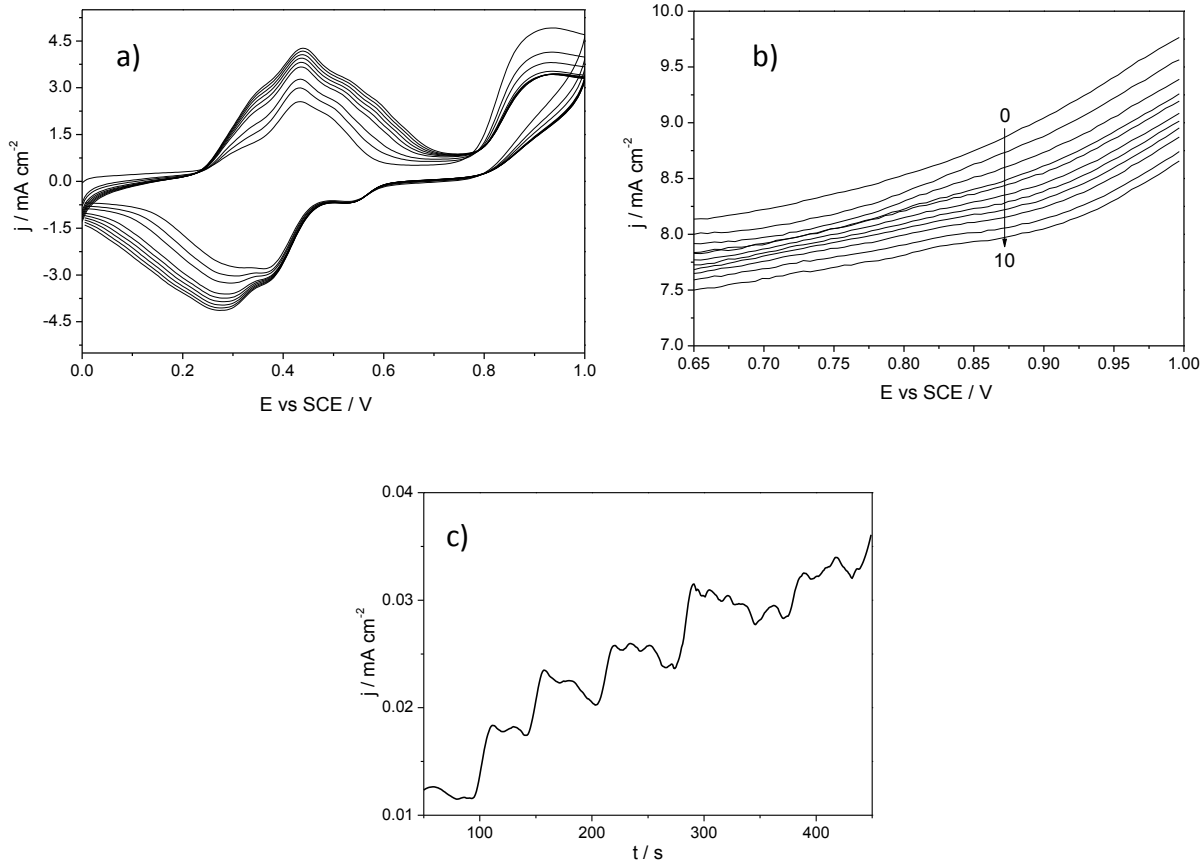

Figure 4.17. Polymerization (a) of *o*-toluidine on CNTs modified electrode and detection of *o*-toluidine using DPV (b) and chronoamperometry at + 1.0 V (c).

To avoid the formation of the polymer, Linear Sweep Voltammetry was employed between 0.65 V and 1.00 V, potentials out of the range of polymerization. Indeed, excellent results are obtained, characterized by *o*-toluidine peaks linearly increasing for consecutive analyte additions. A good calibration plot was obtained (Figure 4.18). All the analytical parameters evaluated are reported in Table 4.6: LoD are in the range of ppb and excellent RSD % and Apparent Recovery Factors were obtained, better than those obtained with previously tested electrodes and with better reproducibility.

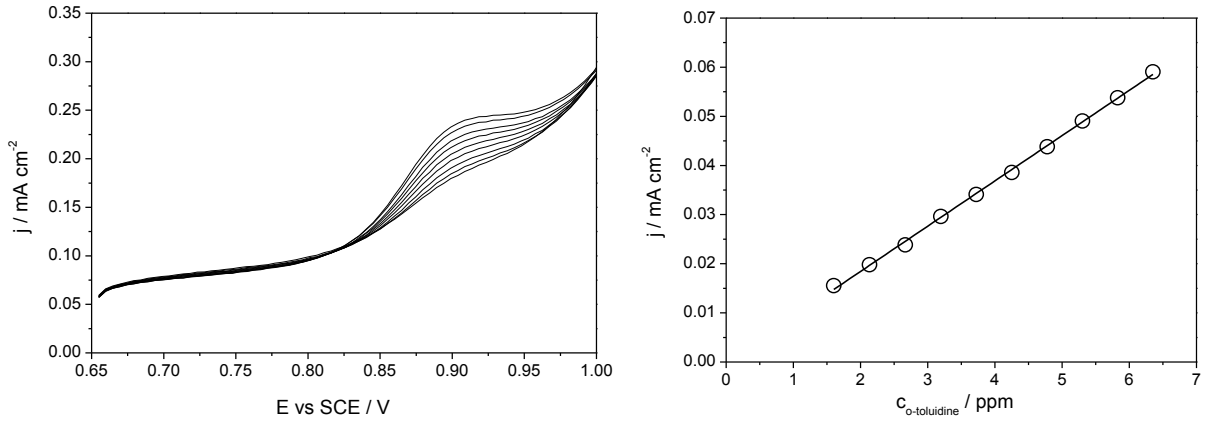

Figure 4.18. Linear Sweep voltammograms for consecutive additions of *o*-toluidine and corresponding calibration plot.

Table 4.6. Analytical parameters evaluated using peak height in the LSV detection of *o*-toluidine.

Parameter	Value
LoD / ppm	0.161
LoQ / ppm	0.563
R^2	0.9998
RSD %	5 %
Apparent Recovery Factor 1	102 %
Apparent Recovery Factor 2	102 %
Apparent Recovery Factor 3	102 %

The optimized electroanalytical method was used in two real applications: the detection of *o*-toluidine during its photo-oxidation by ZnO and *o*-toluidine absorption by cyclodextrines.

In the first real application, nanocristalline ZnO synthetized via microemulsion technique by Prof. Ardizzone and Dr. Cappelletti group was used for the photoremoval under UV light of *o*-toluidine in water. Zinc oxide is a photocatalyst, which under UV light can remove pollutants in water, mineralizing them or converting them in safer products. Figure 4.19 presents the cell used for the analysis, a scheme of microemulsion technique and the HR-TEM image of the obtained ZnO powder, showing the formation of hexagonal nanoparticles. The photoreaction was followed contemporaneously by HPLC with UV detector, DPV at C-SPE (Chapter 3) and LSV at CNTs without amorphous carbon. Figure 4.20 reports the comparison of the three analytical methods for the same photochemical reaction, showing the comparable results for the standard HPLC technique and that based on CNTs, while no good performances are obtained for C-SPE.

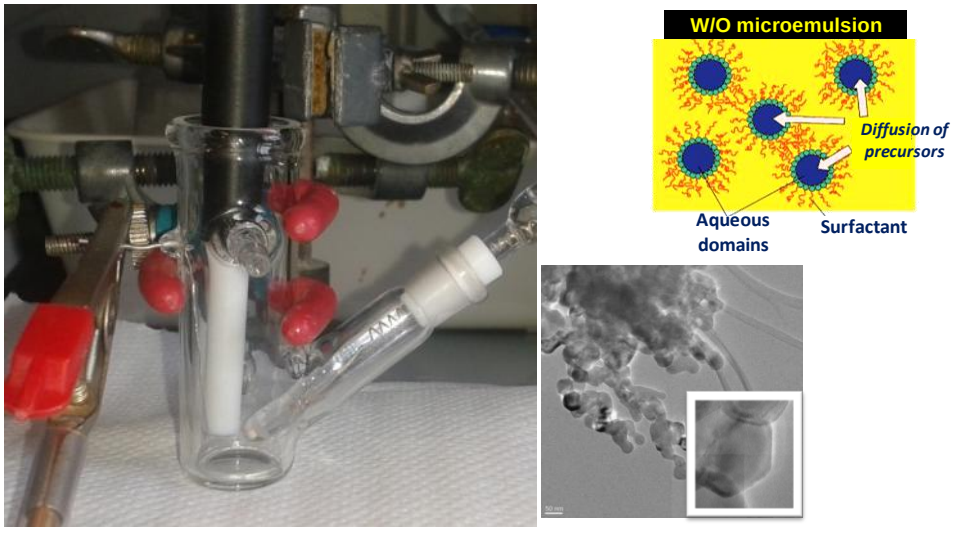

Figure 4.19. Cell setup for electroanalytical experiments; HRTEM image of ZnO photocatalyst and schematic representation of microemulsion synthesis.

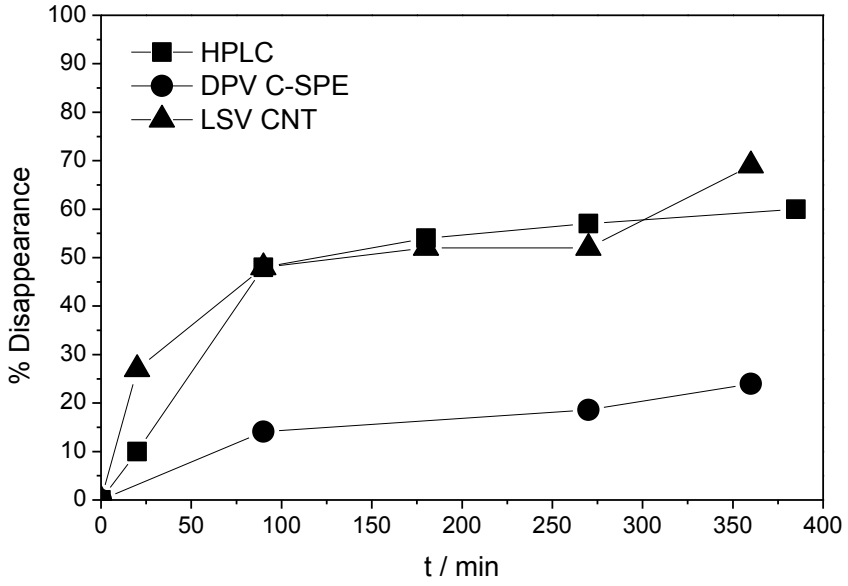

Figure 4.20. Comparison of three different analytical procedures used to evaluate *o*-toluidine photoremoval by ZnO.

In the second real application, *o*-toluidine absorption by cyclodextrines or by their combination with polyamido-aminic resins (PAA) (Ferruti et al., 2013), produced by Prof. Ranucci and Prof. Ferruti group, was followed using the CNTs based electrode. Cyclodextrines are cyclic oligosaccharide macrocycles with different sizes of the internal cavity. According to the number of glucose monomeric unit, they are classified in three groups: α (6-membered sugar ring); β (7-membered sugar ring) and γ (7-membered sugar ring), as shown in Fig. These macromolecules are widely used for the absorption of various types of pollutants, since they can enter into the the cavity of the correct size, allowing the remediation of water. In particular, β-cyclodextrines are suitable for absorption of aromatic compounds. In this context, they appear to be the most favourable for *o*-toluidine removal.

In the first part of the study, the three types of cyclodextrines were dissolved in water and used in solution. The results are presented in Figure 4.21. As expected, β-cyclodextrines absorb the major quantity of *o*-toluidine.

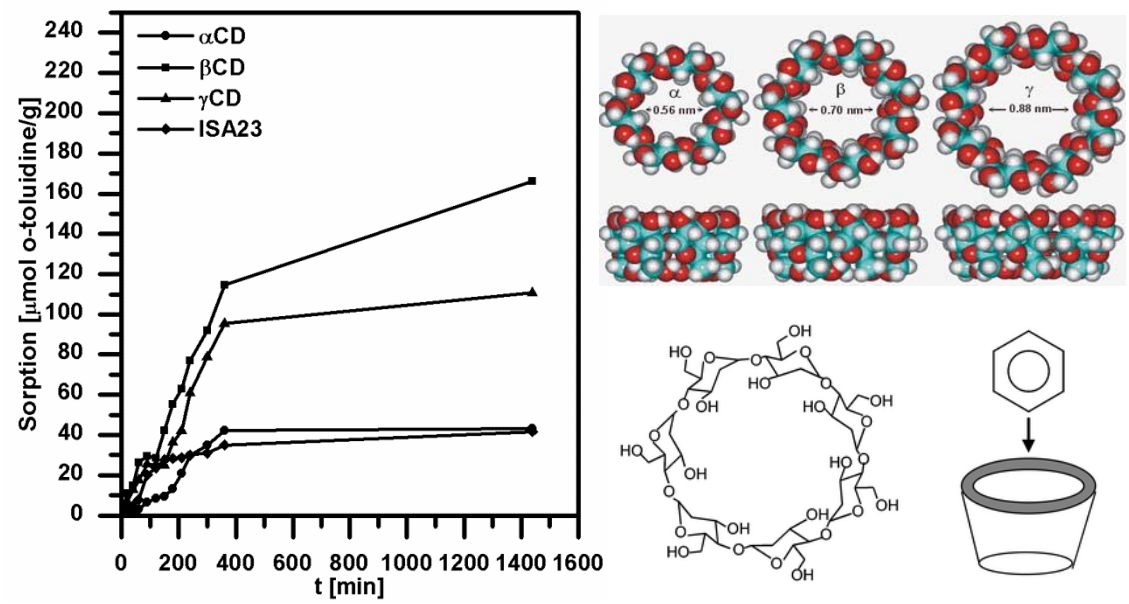

Figure 4.21. Comparison of absorption behaviour of α, β, γ cyclodextrines and ISA 23 hydrogel. Schematic representation of α, β, γ cyclodextrines.

Since after the absorption of the pollutants, the solubilised complexes can be removed from the water with difficult separation steps, cyclodextrines were used in combination with polyamidoamine resins (Figure 4.22), which act as a solid support in a hydrogel form, that can be easily inserted in a filter and finally easily removed after the remediation.

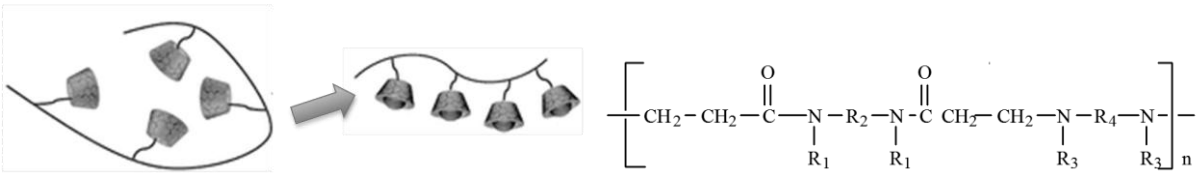

Figure 4.22. Schematic representation of resin with cyclodextrine and poly(amido amine).

Three PAA types were used as support material for cyclodextrine. The results are shown in Figure 4.23. All the PAA-cyclodextrine resins absorb better than the corresponding cyclodextrine. This fact can be explained considering some favourable interactions between the PAA and the cyclodextrines. Moreover, better results in terms of highest sorption values and less scattered points are obtained in the case of the absorption by β-cyclodextrines, as expected by Literature evidences. The larger cavities of γ-CD allows the entering of the aromatic molecule, but also its exiting, causing a scattering of the results and a final lower absorption value.

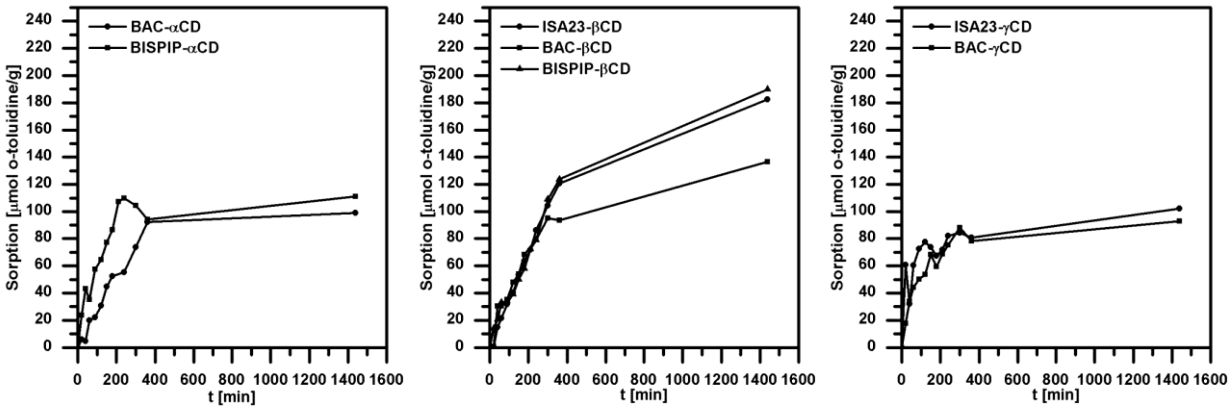

Figure 4.23. Sorption performance of soluble CDs and CD-containing nanosponges in µmol of o-toluidine per µmol of CD in the sorbent.

The electroanalytical method used has also permitted to calculate kinetic parameters, reported in Table 4.7, from absorption curves.

The absorption kinetic curves were fitted according to a mono exponential kinetic model, indicating the presence of only one type of absorption site. The relative equation is: $q_t = q_e - (D/m_{abs})(\exp(-k_D t)$, where m_{abs} is the weight of the sample of the sorbing material, k_D is the relevant sorption rate, q_e is the metal-pollutant sorption capacity at equilibrium and D is a

further parameter modulating the sorption rate. As expected, the sorption capacity at equilibrium and the factor D are higher, while the rate constant is lower, for samples containing β-cyclodextrines, confirming their best absorption. The best performances are obtained for BISPIP-βCD and ISA23- βCD with very similar results, followed by BAC-βCD.

Table 4.7. Kinetic parameters of sorption performance of soluble CDs and CD-containing nanosponges obtained using the mono-exponential kinetic model.

Sample	*o*-toluidine			
	q_e (μmol g^{-1})	D (μmol dm^{-3})	$k_D \times 10^{-3}$ (min-1)	$t_{1/2}$ (min)
αCD	47 ± 6	1.6 ± 0.2	3.6 ± 0.9	223
βCD	174 ± 9	5.3 ± 0.3	2.4 ± 0.3	294
γCD	117 ± 11	3.6 ± 0.3	3.0 ± 0.6	243
ISA23	40 ± 2	1.2 ± 0.1	6.6 ± 0.9	111
BAC-αCD	104 ± 7	3.5 ± 0.2	4.1 ± 0.6	183
BISPIP-αCD	112 ± 7	3.0 ± 0.2	8 ± 2	80
BAC-βCD	137 ± 5	4.2 ± 0.2	3.4 ± 0.3	192
BISPIP-βCD	199 ± 10	6.3 ± 0.3	2.3 ± 0.2	306
ISA23-βCD	188 ± 6	5.7 ± 0.2	2.6 ± 0.2	277
BAC-γCD	88 ± 4	2.7 ± 0.2	8 ± 1	78
ISA23-γCD	82 ± 6	2.1 ± 0.4	19 ± 8	29

Finally, after a first use, the best β-cyclodextrine-based composites were submitted to a regeneration step, which consisted in methanol extraction and thus re-used other two times, showing maintenance or even improvement of absorption performances, as shown in Figure 4.24.

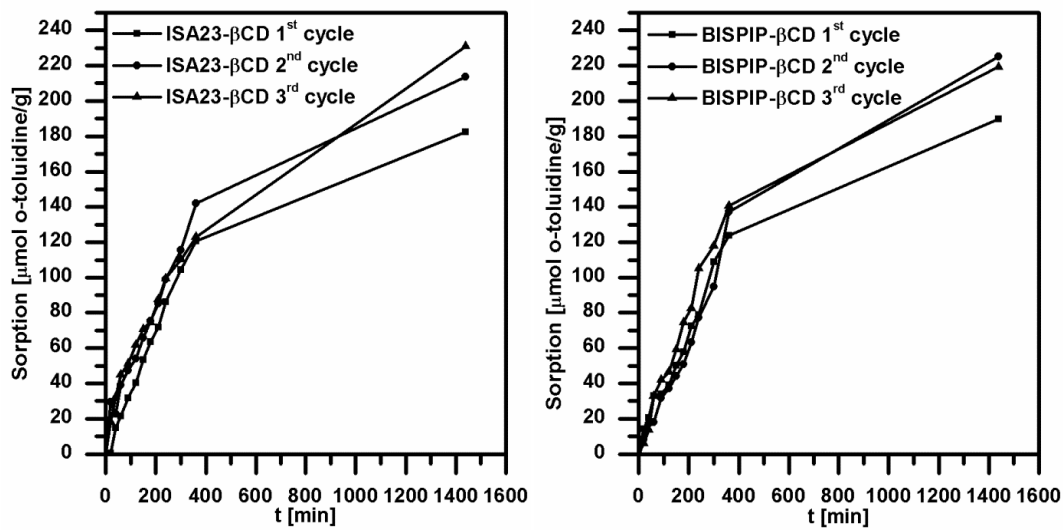

Figure 4.24. Absorption capacities of o-toluidine for ISA23-βCD and BISPIP-βCD nanosponges before (1st cycle) and after recycling (2nd and 3rd cycles).

In conclusion, the applicability of the optimized electroanalytical method based on CNTs without amorphous carbon electrodes was demonstrated, following *o*-toluidine disappearance during photoremoval mediated by ZnO and *o*-toluidine absorption by cyclodextrine-based resins.

Benzidine determination

CNTs without amorphous carbon were also employed for the detection of benzidine, considering the promising results obtained previously for carbon-based electrodes (Chapter 3).

Initially, CV and EIS were carried out to evaluate the behaviour of the electrode toward benzidine. Figure 4.25 shows cyclic voltammograms obtained for consecutive additions of benzidine and study of the scan rate. Benzidine presents also in this case two intense peaks at + 0.57 V and + 0.65 V (SCE). Varying the scan rate, each peak splits into two peaks, probably due to a small difference between the two aromatic units constituting the molecule.

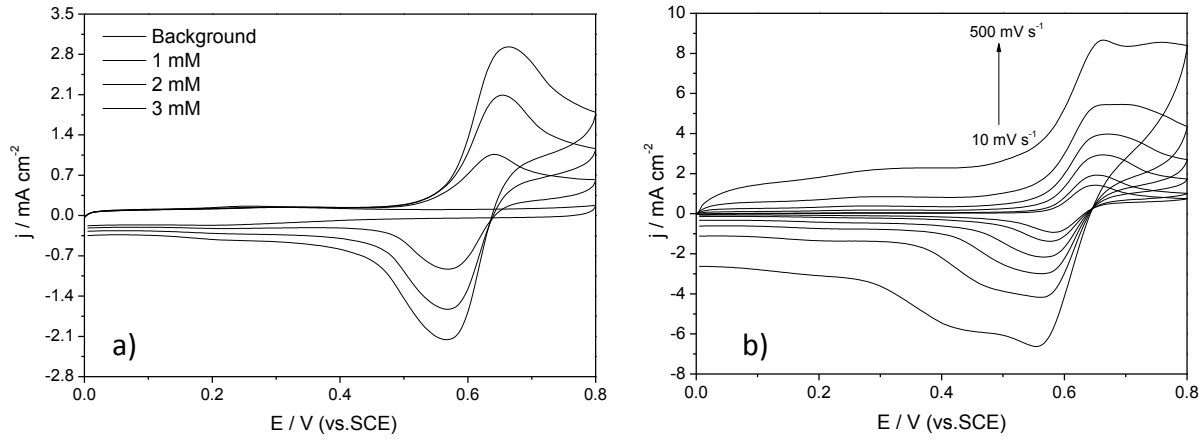

Figure 4.25. Cyclic voltammograms for consecutive additions of benzidine (a) and scan rate study (b).

Figure 4.26 reports complex plane spectra and Bode plots, while the relative equivalent circuits are reported in Figure 4.27.

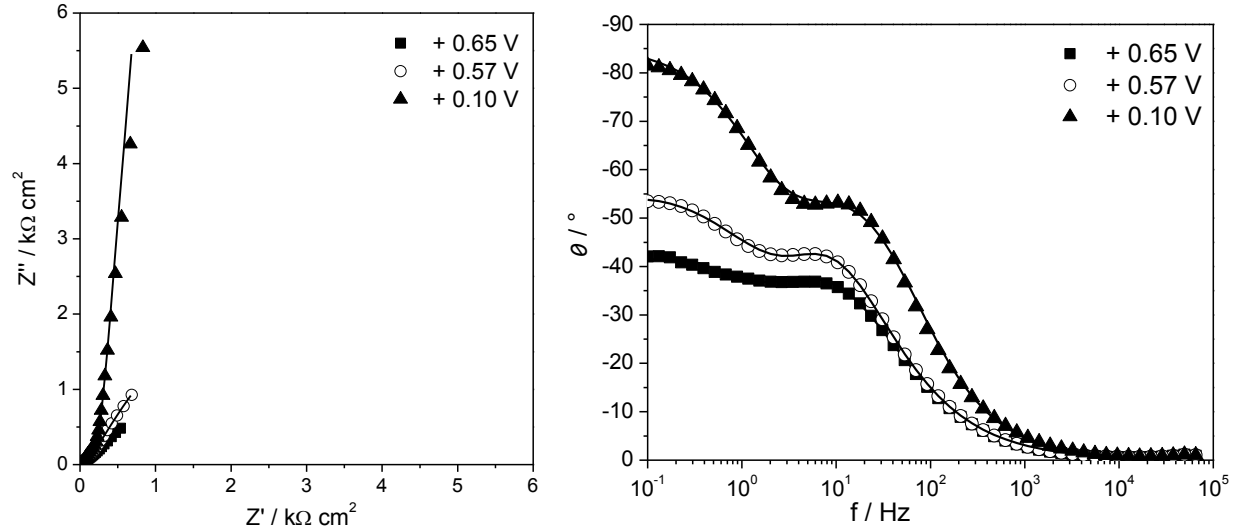

Figure 4.26. Complex plane plot and Bode plot in the presence of benzidine.

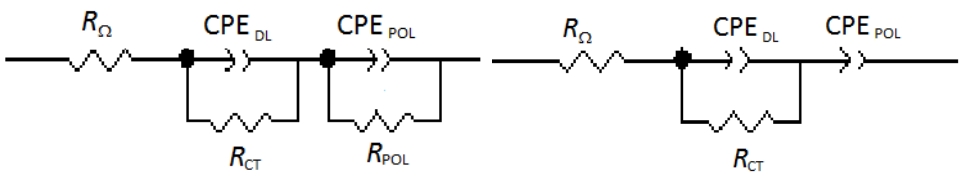

Figure 4.27. Equivalent circuits used to fit impedance data.

Table 4.8 shows the impedance parameters obtained from the fitting. Impedance potentials were chosen from cyclic voltammograms, considering the peak potentials, + 0.57 V and + 0.65 V, and the capacitive potential, + 0.10 V. The trend of the spectrum at + 0.10 V shows a semicircle for high frequencies, representedby a RC circuit, and a straight line for low frequencies, indicating a CPE in series. The Bode plot is in accordance with this trend. Values of capacitances and resistance are in agreement with previous values obtained in the characterization of CNTs. At + 0.57 V and + 0.65 V, the straight line becomes a second semicircle and a resistance in parallel with the CPE has to be added to the equivalent circuit. In the Bode plots, the initial phase angle changes for the presence of the new resistance and also the frequency of the peak attributed to the first RC shifts, indicating the reaction of the molecule. Also the values of capacitances and resistances change due to the presence of another process.

Table 4.8. Impedance parameters obtained by impedance fitting in the presence of benzidine.

$E_p$vs SCE / V	R_Ω / Ω cm^2	CPE_{DL} / mF cm^{-2} $s^{\alpha-1}$	α_{DL}	R_{CT} / Ω cm^2	CPE_{POL} / mF cm^{-2} $s^{\alpha-1}$	α_{POL}	R_{POL} / Ω cm^2
0.10	2.8	3.7	0.83	15	4	0.94	
0.57	2.8	8.45	0.98	4.3	17.3	0.68	1221
0.65	2.8	11.86	0.83	6.2	26.3	0.66	198

After electrode characterization in the presence of benzidine, different electroanalytical techniques were used to optimize the detection method. Table 4.9 shows the analytical parameters for SWV, LSV, DPV and Chronoamperometry .

Table 4.9. Analytical parameters of different electroanalytical techniques for the determination of benzidine at CNT-modified electrode.

Method		R^2	LoD / ppm	LoQ / ppm	RSD %	Apparent Recovery Factor %
SWV	Height	0.992	0.201	0.611	3	102
	Area	0.991	0.227	0.691	5	108
DPV	Height	0.991	0.231	0.703	7	95
	Area	0.990	0.244	0.742	10	96
LSV 100 mV s^{-1}	Height	0.990	0.224	0.682	7	118
	Area	0.977	0.348	1.057	9	126
LSV 200 mV s^{-1}	Height	0.990	0.194	0.589	5	96
	Area	0.991	0.183	0.558	6	96
Chronoamperometry	Step	0.995	0.176	0.535	7	95

Figure 4.28 presents SWV plots for consecutive additions of benzidine with the corresponding calibration plots, considering peak height and area. LoD and LoQ are very similar for all the electroanalytical procedures, but considering RSD % and Apparent Recovery Factors, SWV appears to be the best technique.

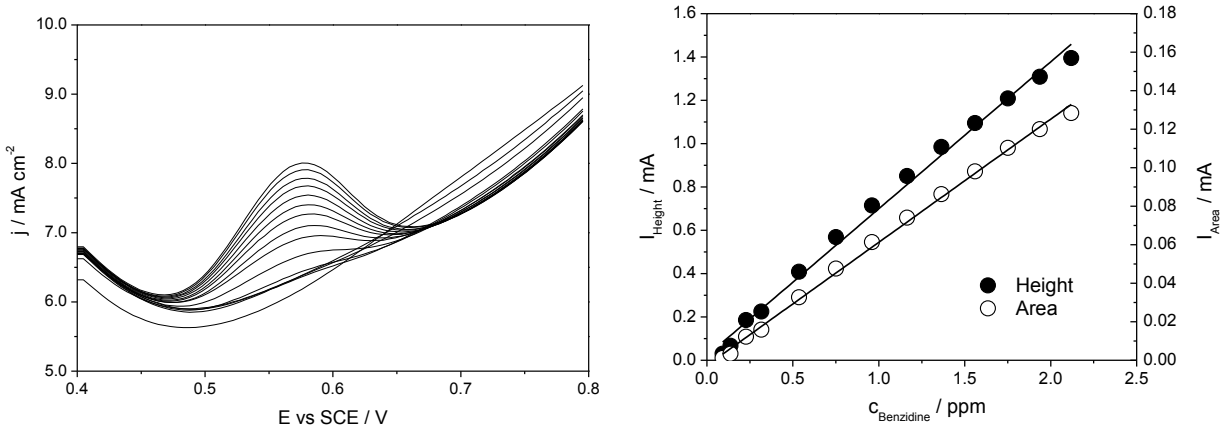

Figure 4.28. Square wave voltammograms and corresponding calibration plots for consecutive additions of benzidine.

Future developments will consider the applications of this optimized methodology to real applicative cases, to test the possibility to use it in online and onsite environmental analysis.

Furan determination

In the case of furan determination, Pt electrodes showed good performances, but not sufficiently low detection limits (Chapter 3). For this reason, we decided to use Pt nanoparticles electrodeposited on CNTs, to combine the properties of nanoparticles with those of CNTs.

Before the production of this type of electrodes, the behaviour of furan was studied at GC electrode, to evaluate also the possible activity of carbon materials toward furan. Figure 4.29 presents SW voltammograms and the corresponding calibration plots obtained for consecutive additions of furan; in Table 4.10 the analytical parameters are reported. GC shows a very good activity for furan determination with lower limits of detection with respect to Pt-based electrodes and good apparent recovery factors.

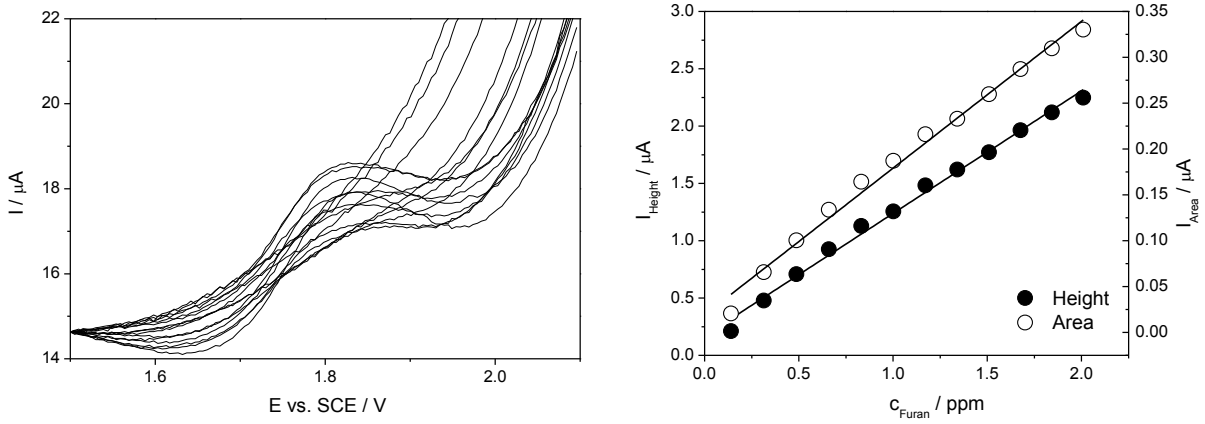

Figure 4.29. Square wave voltammograms and corresponding calibration plots for consecutive additions of furan.

Table 4.10. Analytical parameters for the determination of furan at glassy carbon electrode.

c_{Furan} / ppm	Peak	S / A mol^{-1} L	R^2	LoD / ppm	LoQ / ppm	RSD %	Apparent Recovery Factor %
0.14	Height	0.073 ± 0.002	0.994	0.23	0.70	35	97
0.45		0.070 ± 0.002	0.996	0.17	0.52	11	95
0.49		0.069 ± 0.001	0.997	0.14	0.42	6	93
0.14	Area	0.0109 ± 0.0003	0.991	0.19	0.57	45	96
0.45		0.0104 ± 0.0002	0.995	0.18	0.55	13	94
0.49		0.0101 ± 0.0002	0.997	0.19	0.59	9	92

Composite electrodes were produced in two steps (Figure 4.30): a dip coating of the electrode with a solution of CNTs dispersed in Nafion and the successive electrodeposition of Pt nanoparticles. The time of deposition influences the quantity of Pt deposited. In particular, small deposition time favoured a better growth of Pt nanoparticles, as shown in Figure 4.30. The electrode was tested toward the detection of furan, first using cyclic voltammetry. The voltammograms and the corresponding calibration plots are shown in Figure 4.31. Furan presents a peak at about + 1.8 V (SCE), which increases for consecutive additions, yielding to good calibration plots.

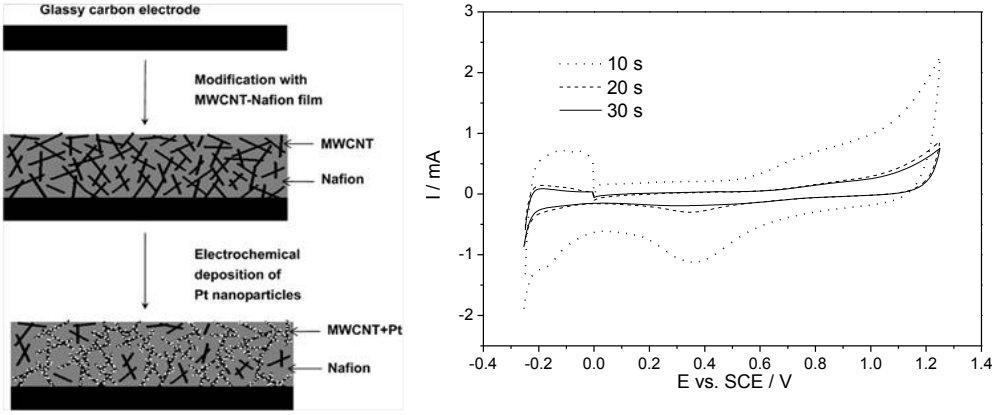

Figure 4.30. Schematic representation of modified-electrode preparation and cyclic voltammograms after different times of Pt deposition.

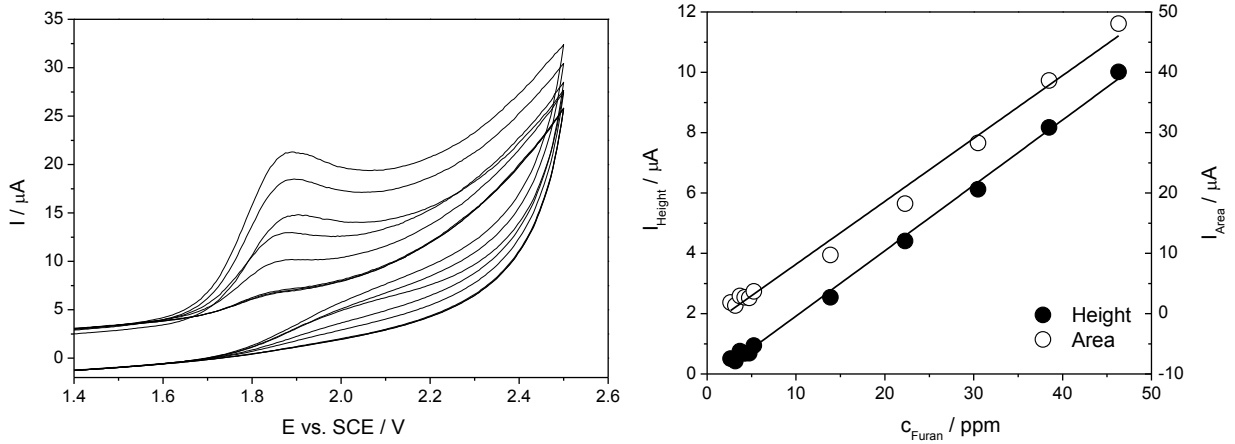

Figure 4.31. Cyclic voltammograms and calibration plots for consecutive additions of furan at CNT/PtNPs-modified electrode.

These are only preliminary results and future developments will consider: the effects of deposition potential and Pt solution concentration; the study of the behaviour of CNTs combined with Nafion ; the morphological and electrochemical characterization of modified electrodes; the use of more sensible electroanalytical techniques for furan detection.

4.1.2.4. Conclusions

In recent years, the application of CNTs in electroanalysis is growing in importance, due to CNTs unique properties. However, the type of CNTs and their functionalization are key points which need to be taken into consideration before their application.

The deposition parameters, such as solvent, deposition volume and CNTs concentration, strongly influence electroanalytical performances. In our study, DMF has proved to be the best solvent. The type of functionalization is very important: the treatment in different acidic media can produce CNTs with very different performances. Sulphonitric mixture yields to CNTs without metal nanoparticles and characterized by higher surface area and pore volume, in the

range of mesoporosity, higher covalent acidity, allowing higher peak currents in the presence of the model probe molecule, higher capacitance and lower resistance. Furthermore, also the time of treatment and the presence of amorphous carbon proved to be key parameters. Indeed, the treatment of CNTs for longer time causes the cutting of CNTs, changing the diffusion mechanism from planar to radial convergent, with a consequence in the shape of the voltammogram which becomes step-like, and yielding to worse values of the double layer capacitance and the electron transfer resistance. On the other hand, the removal of amorphous carbon, produced during sulphonitric functionalization, is beneficial for the electrochemical activity, giving CNTs with higher currents and capacitance, more reversible and diffusive behaviour and lower resistance to the electron transfer.

Finally, after having optimized the synthetic and purification procedures the resulting best electrodes were used for real applications: the detection of *o*-toluidine, benzidine and furan, already studied in previous determinations (Chapter 3).

In the case of *o*-toluidine, excellent results in terms of limits of detection (ppb range) and reproducibility (apparent recovery factors very close to 100 %) were obtained and applications to real cases were performed. The photoremoval of *o*-toluidine by ZnO was successfully followed with the optimized technique and the comparison with the standard method (HPLC) shows excellent results. The new electroanalytical method was also employed to the study of *o*-toluidine absorption by β-cyclodextrine-based resins, allowing evaluating the best absorption performance and absorption kinetic parameters.

In the case of benzidine, the optimized method was based on SWV, which reached LoD in the order of magnitude of SPE results, but permitting better reproducibility. At last, the electrodeposition of Pt nanoparticles on CNTs and Nafion was demonstrated to be promising for the determination of furan, but parameters optimization and systematic characterization have to be performed in order to project the best electrode design to obtain lower detection limits.

Future developments will regard the study of electrochemical performances and applications of other carbon-based nanomaterials, in particular graphene and nanofibers, for the production of new electroanalytical sensors.

4.2. Metallic and Semiconductor Nanoparticles

4.2.1. Introduction

Nanoparticles (NPs) present a unique electronic nature, since they follow quantum mechanical rules instead of the laws of classical physics, which governs bulk materials. Nanoparticles colloid science has begun in the middle of the 19th century with experiments of Michael Faraday on gold sols, when a chloroaurate solution was reduced using phosphorus producing a red sol. After that moment, the invention of new characterization techniques and further synthetic experiments signed the rapid growth of this new area of research (Hodes, 2001; Pierce & Zhao, 2010; C. N. R. Rao et al., 2004; Schmid, 2003).

Nanoparticles have peculiar properties, usually dependent on their size and shape and which are not typical of the corresponding bulk materials. These properties make NPs very attractive for many applications. In particular, considering their application in the electrochemical field (Campbell & Compton, 2010; Luo et al., 2006; Liza Rassaei et al., 2011), they can change the diffusion mechanism, depending on the size of NPs and voltammetric scan rate, they have high active surface area and high surface-to-volume ratio, they show improved selectivity and electron transfer rates, catalytic activity, higher signal-to-noise ratio, control over the local microenvironment, compatibility with nanoarray design and low costs.

Among all available compounds, two types of nanoparticles seem to be very promising from the electrochemical point of view: metal and semiconductor nanoparticles (Liza Rassaei et al., 2011). The first class allows unique characteristics for stripping voltammetry, confers conductivity changes of the electrochemical systems and electrocatalysis, permits production of

stable modified electrodes very active towards specific analytes. Modified electrodes with metal nanoparticles are produced by grafting, *i.e.* deposition of nanoparticles on the electrode after their synthesis usually performed via colloidal way, or by electrodeposition, *i.e.* direct *in situ* generation on the electrode. Gold, silver, platinum, palladium, nickel, copper, ruthenium, bismuth and iridium are the most employed metal nanoparticles for electrode modification (Hernández-Santos, González-García, & García, 2002; Jing Wang, 2012).

The second class (semiconductor NPs) is widely used in electrochemical gas sensors for their high detection ability and stability, but their application in modified electrodes is still at the beginning. This type of nanoparticles can be produced by colloidal suspension, sol-gel synthesis, deposition from vapour phase, chemical bath deposition and electrodeposition. WO_3, TiO_2, ZnO, SnO_2 and SiO_2 are the usual semiconductor nanoparticles employed for electrochemical purpose. To further increase electrochemical performances, nanoparticles can be used in combination with carbon nanotubes, improving the conductivity and availability of active sites.

Metal and semiconductor nanoparticles can be used to monitor inorganic and organic analytes, in particular pesticides, heavy metals and air pollutants. Research in this field is still in rapid growth to understand nanoparticles chemistry, reactivity and possible mechanisms involved in their interaction with the analyte (Campbell & Compton, 2010; Liza Rassaei et al., 2011).

In this chapter, two types of metal nanoparticles, gold and silver, and one type of semiconductor nanoparticles, titanium dioxide, in combination with carbon nanotubes were studied and characterized, finally testing them in different applications in the electroanalytical field.

4.2.2. Gold Nanoparticles and Carbon Nanotubes

4.2.2.1. Gold

Gold is a material employed in various fields, thanks to its unique properties, such as efficient conductivity, malleability, ductility, softness, biocompatibility and chemical inertness. In particular, it was extensively used in electrochemistry as bulk electrode for a big number of applications, from the sensoristic to the electrocatalysis area. In the last 20 years, thanks to the discovery of gold nanoparticles, its employment in this fields is rapidly growing (Campbell & Compton, 2010).

Gold nanoparticles show a series of advantages in comparison with bulk gold (Hodes, 2001; Pierce & Zhao, 2010; C. N. R. Rao et al., 2004; Schmid, 2003). First of all, they are a less expensive material, which can be synthesized in many ways and presents high surface-to-volume ratio. Moreover, their properties can be tuned by varying size, shape and chemical environment, and for this reason, they can be functionalized with many types of compounds (inorganic and organic species, biomolecules). They can be produced in different shapes (spherical, cubic and rod), showing different redox, fluorescent, conductive, optical, catalytic, thermal and electronic properties. In electroanalysis, they are used for the detection of an infinite number of compounds, such as metal ions, small molecules, proteins, nucleic acids, malignant cells, environmental pollutants (Campbell & Compton, 2010; S Laschi et al., 2007; L Rassaei, Amiri, Cirtiu, Sillanpaa, & Marken, 2011; Song & Swain, 2007).

Among the innumerable types of gold nanoparticles synthesis, two are the most employed ones for the production of materials suitable for electroanalytical applications: colloidal synthesis

and electrodeposition (Campbell & Compton, 2010). The first consists in the reduction of a Au salt using a reducing agent ($NaBH_4$, citric acid, etc.) and the subsequent casting of the nanoparticles on the electrode, while the second generates *in situ* nanoparticles directly on the electrode. Colloidal synthesis has the disadvantages of more complex synthesis and aggregation phenomena, while, on the other hand, homogeneous deposits and controlled shape and size are difficult to obtain in electrodeposition. Moreover, gold nanoparticles obtained via colloidal synthesis can be deposited on a support, avoiding the critical problem of aggregation. Different types of support can be used, but carbon nanotubes seem to be very attractive, considering also the possibility of enhancement of the electrochemical activity of the nanoparticles.

In this context, the study of the electrochemical performance of gold nanoparticles syhntesized by colloidal procedure supported on carbon nanotubes is an interesting field of research.

4.2.2.2. Materials and Methods

Materials used in this work were produced by Prof. Prati and Dr. Villa group of the University of Milan. Gold nanoparticles were synthesized via colloidal method and supported on carbon nanotubes (MWCNTs), to improve conductivity and prevent agglomeration, in the presence or absence of polyvinylalcohol (PVA) (Tsai & Huang, 2006) as protective agent for the metal. In the first case, nanoparticles were formed in the presence of PVA and immobilized on the support, while in the second case, nanoparticles were produced directly on carbon nanotubes.

Glassy Carbon electrode was modified using 0.5 mg mL^{-1} suspension of the desired material, using DMF as suspending solvent. Different materials were used to study the influence of

CNTs and gold nanoparticles on the electrochemical response, bringing to the following modified electrodes:

- Glassy Carbon electrode without any modification (GC)
- GC/CNT electrode, modified with a suspension of Baytubes CNTs
- GC/CNT-PVA electrode, modified with a suspension of CNTs modified with PVA
- GC/CNT-1%AuNP electrode, modified with a suspension of CNTs decorated with 1 % gold nanoparticles, obtained by precipitation
- GC/CNT-1%AuNP-PVA electrode, modified with a suspension of CNTs decorated with 1 % gold nanoparticles, obtained by PVA mediated synthesis
- GC/CNT-5%AuNP electrode, modified with a suspension of CNTs decorated with 5 % gold nanoparticles, obtained by precipitation
- GC/CNT-5%AuNP-PVA electrode, modified with a suspension of CNTs decorated with 5 % gold nanoparticles, obtained by PVA mediated synthesis

0.1 M KCl aqueous solution was used as supporting electrolyte for all the characterizations.

4.2.2.3. Results and Discussion

First of all, different carbonaceous materials were tested to evaluate which was the most suitable support. Four types of carbonaceous compounds were considered (Tessonnier et al., 2009) in particular two types of nanofibers and two types of nanotubes:

- CNF-LMT: carbon nanofibers with a diameter around 20 nm, fishbone;
- CNF-HHT: carbon nanofibers with a diameter > 80 nm, with nitrogen residues and a higher graphitization degree;
- CNT-Baytube: carbon nanotubes produced by Bayer;
- CNT-Nanocyl: carbon nanotubes produced by Nanocyl.

Voltammetric analysis with $K_4[Fe(CN)_6]$ as model probe molecule were carried out and results are shown in Figure 4.32. Nanofibers show a small current signal increment in comparison with bare GC, with not well defined and very broad peaks, typical of a strongly electrochemical irreversible system. However, peak shapes and currents are better in the case of CNF-HHT, characterized by the higher graphitization degree. The intensity of the peaks doubles for carbon nanotubes and also peak shape becomes less broad, demonstrating that carbon nanotubes are the better material to be used in this application. CNT-Nanocyl gives the highest peak current, with peak potentials very similar to GC, but CNT-Baytube present the best peak-to-peak separation and the sharpest peak, indicating a more reversible electrochemical system. For these reasons, CNT-Baytube were chosen as ideal material for modified electrodes, although it shows also the highest capacitance, which is sometimes detrimental for sensitivity.

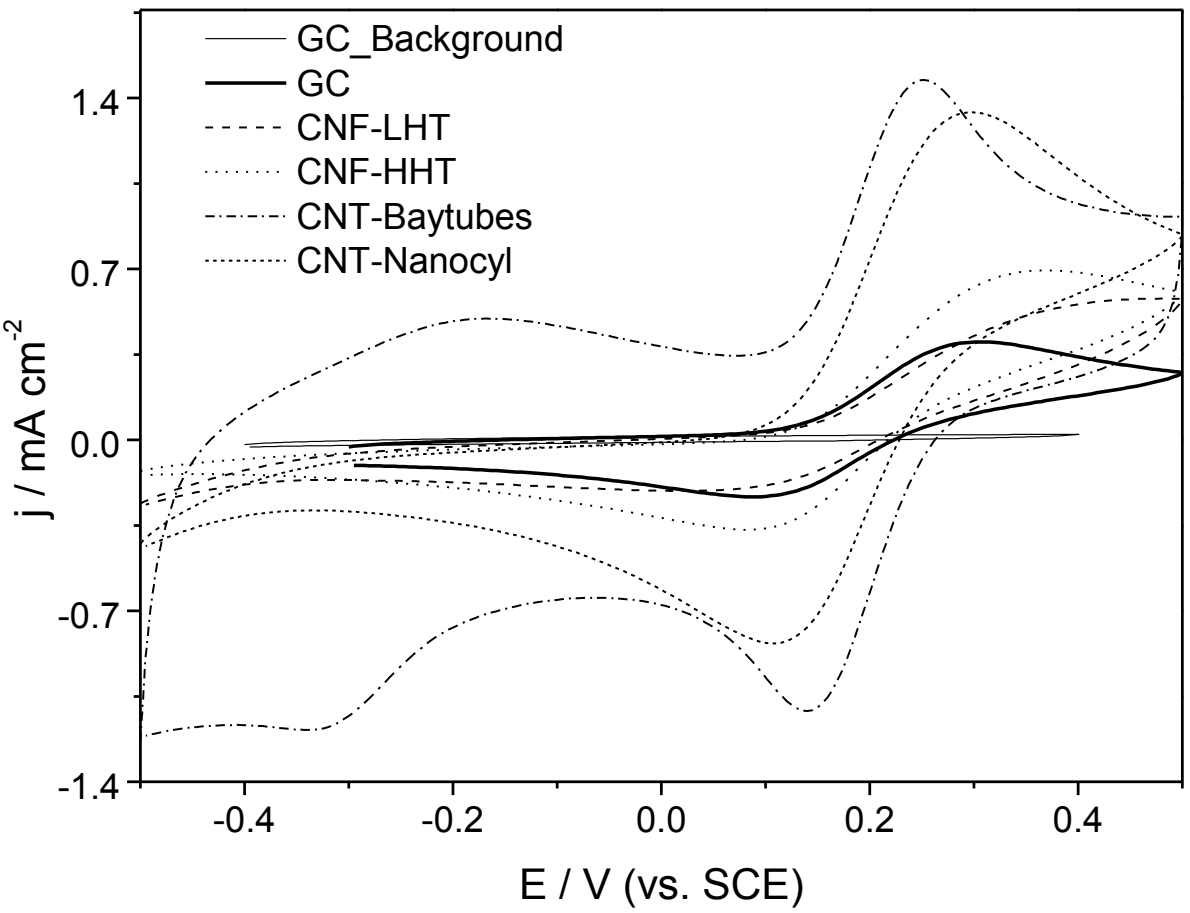

Figure 4.32. Cyclic voltammograms of different types of carbon nanofibers and carbon nanotubes modified electrodes.

Figure 4.33 shows cyclic voltammograms of Baytube carbon nanotubes with different gold nanoparticles percentages and with or without protective polymer. When protective polymer is present on the surface of carbon nanotubes, capacitance decreases and the current signal is lower and appears as step-shaped, indicating that the polymer probably generates a disordered surface changing the diffusion process. The addition of 1 % precipitated Au nanoparticles causes the increase of the signal intensity, maintaining the shape and peaks separation, while for 5 % Au, the current is lower. The detrimental effect of the polymer can be seen also in the case of GC/CNT-1%Au-PVA, with a decrease of peak current and capacitance and a broader

peak shape. The case of 5 % Au nanoparticles and PVA is completely different, since it gives the best electrochemical performances, probably due to a better ordered structure and cooperation among nanoparticles.

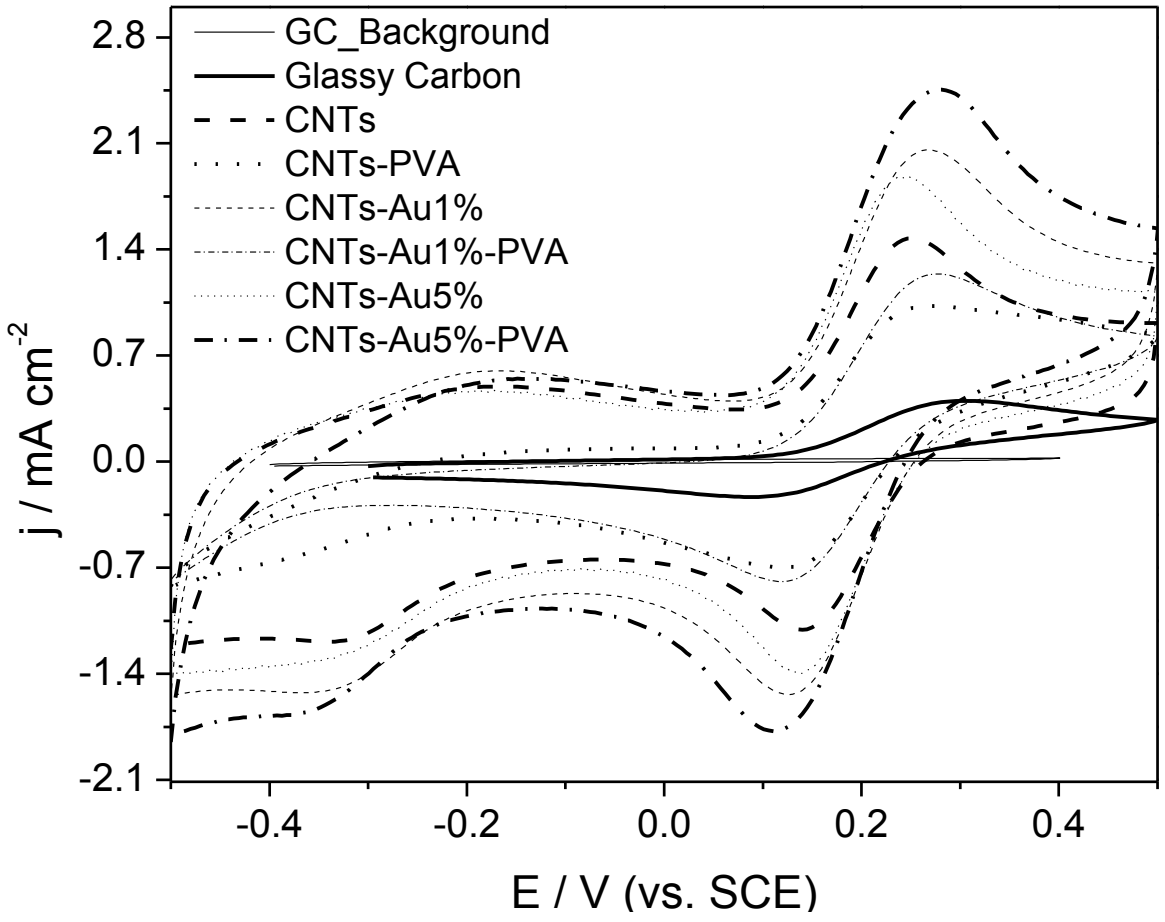

Figure 4.33. Cyclic voltammograms of Au nanoparticles and carbon nanotubes modified electrodes.

Table 4.11 presents the parameters obtained from cyclic voltammetry for the tested materials. For all the modified electrodes capacitance increases in comparison with GC, particularly for GC/CNT-1%AuNP and GC/CNT-5%AuNP-PVA. The reversibility of the system decreases with addition of Au nanoparticles and PVA , probably for the formation of a more disordered surface, but values remain acceptable in the case of 1 % Au with and without PVA and 5 % Au

with PVA. Considering the slope of the Randles-Sevcik plot, higher values can be obtained with the CNTs modification with Au nanoparticles, probably for an increase of surface area, but also for a change in the diffusion mechanism. The presence of PVA with only CNTs shows a completely different behaviour, since reversibility and diffusion control are lost, possibly due to the formation of a disordered inhomogeneous surface. This type of conformation is probably not the same when Au nanoparticles are present, because in this case PVA localizes around nanoparticles avoiding a chaotic assembly.

Table 4.11. Voltammetric parameters obtained from cyclic voltammograms of Au nanoparticles and carbon nanotubes modified electrodes.

CV parameters	GC	CNTs	CNTs-PVA	CNTs-Au1%	CNTs-Au1%-PVA	CNT-Au5%	CNTs-Au5%-PVA
C / mF cm^{-2}	0.08	2.88	2.06	4.26	0.54	1.41	3.64
E_p-$E_{p/2}$ / mV	96	68	92	82	80	95	79
ΔE_P / mV	171	103	146	129	122	171	127
Slope i_p *vs* $v^{0.5}$ / µA $mV^{-0.5}$ cm^{-2} $s^{0.5}$	31	106	62	129	123	154	161
Slope Ln i_p *vs* ln v	0.44	0.48	0.38	0.41	0.44	0.51	0.49

Electrochemical impedance spectroscopy was performed in the presence or absence of the model probe molecule at – 0.16 V (SCE), the capacitive area of cyclic voltammogram, and at + 0.11 V and + 0.27 (SCE), where the redox reaction takes place.

Figure 4.34 shows impedance spectra obtained in the absence of the redox probe. Complex plane plots present a semicircle for high frequencies, referring to the formation of the double layer, and a straight line with slope > 0.5, in some cases substituted by a semicircle, indicating the diffusive process. Bode spectra show very similar trend, with a time-dependent process for

medium frequencies, which is present only for the electrodes with the highest capacitance and for GC/CNT-PVA.

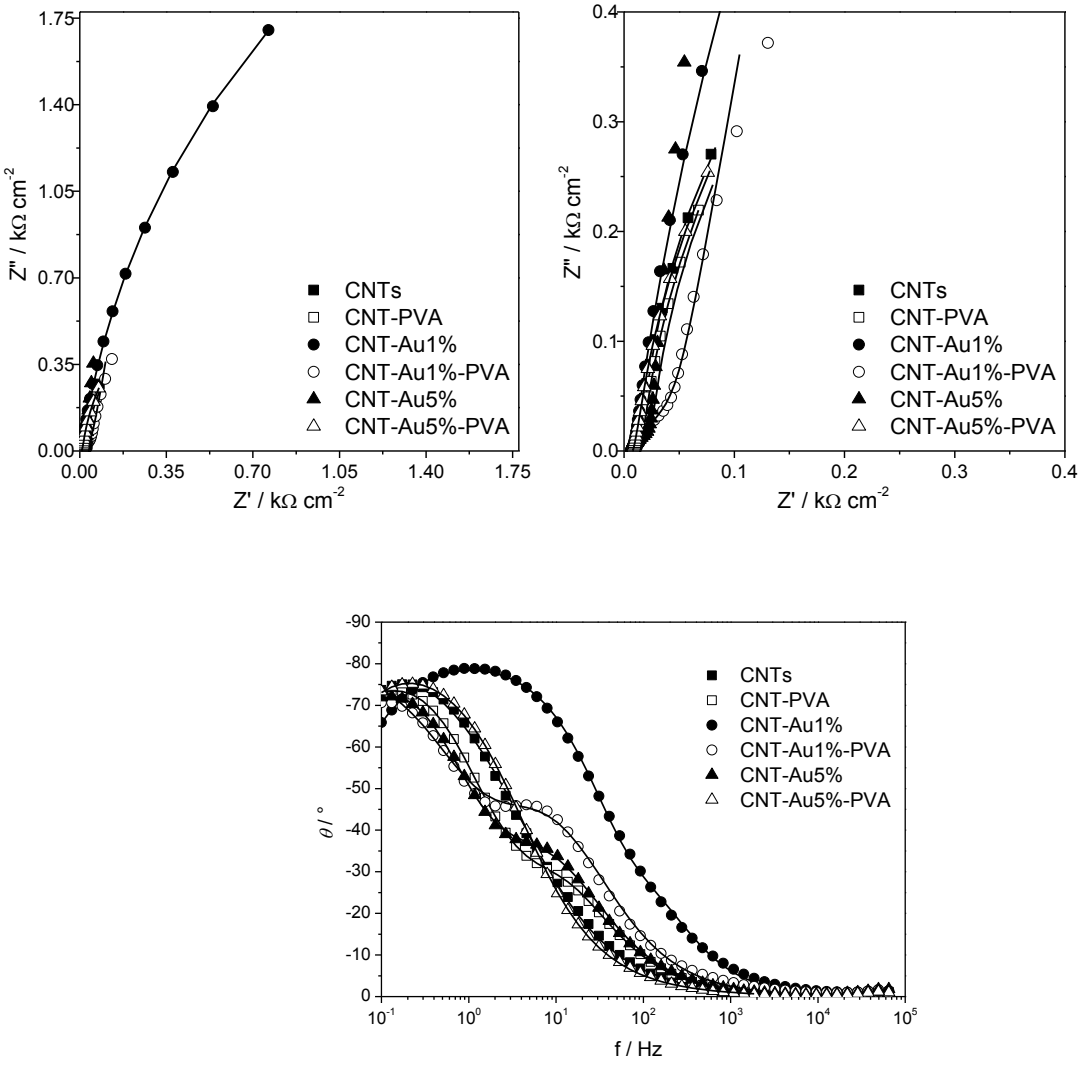

Figure 4.34. Complex plane plot and Bode plot at – 0.16 V in the absence of redox probe.

Equivalent circuits used to fit data are presented in Figure 4.35, while Table 4.12 reports impedance parameters obtained from the fitting. The presence of PVA together with CNTs causes the formation of a disordered and inhomogeneous structure, as already demonstrated by cyclic voltammetry, since in comparison with CNTs alone capacitance decreases and resistance increases. The addition of Au nanoparticles shows in general the decrease of charge

transfer resistance, which is beneficial for fast and easy electrode reactions. The highest capacitance values obtained for GC/CNT-1%AuNP and GC/CNT-5%AuNP-PVA confirm cyclic voltammetric results. Moreover, in the case of GC/CNT-1%AuNP-PVA the double layer capacitance and polarization capacitance decrease, while polarization resistance increases, probably due to the formation of isolated aggregates of nanoparticles and polymer, producing insulating and inhomogeneous surface.

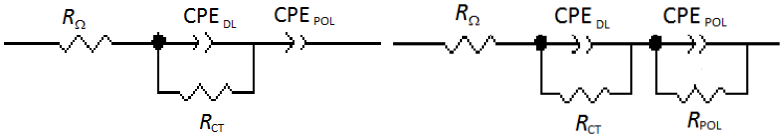

Figure 4.35. Equivalent circuits used to fit impedance data.

Table 4.12. Impedance parameters obtained by impedance fitting in the absence of redox probe.

Electrodes	E / V	R_Ω / Ω cm^2	CPE_{DL} / mF cm^{-2} s$^{\alpha-1}$	α_{DL}	R_{CT} / Ω cm^2	CPE_{POL} / mF cm^{-2} s$^{\alpha-1}$	α_{POL}	R_{POL} / Ω cm^2
CNTs	-0.16	7.98	19.80	0.63	32	5.76	1.02	1211
	0.11	7.92	25.70	0.57	631	4.36	1.00	-
	0.27	7.82	22.40	0.60	26	3.23	1.00	-
CNTs-PVA	-0.16	9.08	2.92	0.80	35	4.16	0.89	-
	0.11	8.97	1.86	0.82	42	2.87	0.96	-
	0.27	8.88	1.68	0.84	36	2.35	0.95	-
CNTs-Au1%	-0.16	7.29	4.06	0.85	7.60	6.98	0.90	-
	0.11	7.34	2.72	0.86	9.25	4.54	0.95	-
	0.27	7.26	2.66	0.86	8.35	3.83	0.96	-
CNTs-Au1%-PVA	-0.16	6.47	0.56	1.00	2.04	0.75	0.92	6521
	0.11	6.52	0.55	1.00	1.88	0.66	0.92	22744
	0.27	6.51	0.58	1.00	1.74	0.69	0.92	25280
CNTs-Au5%	-0.16	7.71	58.06	0.55	11	5.81	0.95	1530
	0.11	7.77	5.02	1.00	0.81	3.88	0.94	-
	0.27	7.65	4.14	1.00	0.75	3.79	0.94	-
CNTs-Au5%-PVA	-0.16	8.18	3.94	0.80	19	6.19	0.96	1453
	0.11	8.13	2.73	0.83	17	4.36	0.95	-
	0.27	8.11	2.38	0.85	15	3.53	0.95	-

The complex plane spectra and Bode plots in the presence of redox probe are shown in Figure 4.36-4.37-4.38. Complex plane spectra have a trend similar to the previous one, with a semicircle for high frequencies and a straight line with a slope > 0.5 or a second semicircle for low frequencies. The difference can be appreciated when the redox reaction takes place, since at these potentials impedance values strongly decrease together with the slope of the straight line, showing a less capacitive behaviour. Moreover, in Bode plots also GC/CNT-PVA and GC/CNT-1%AuNP-PVA present the time-dependent process at medium frequencies.

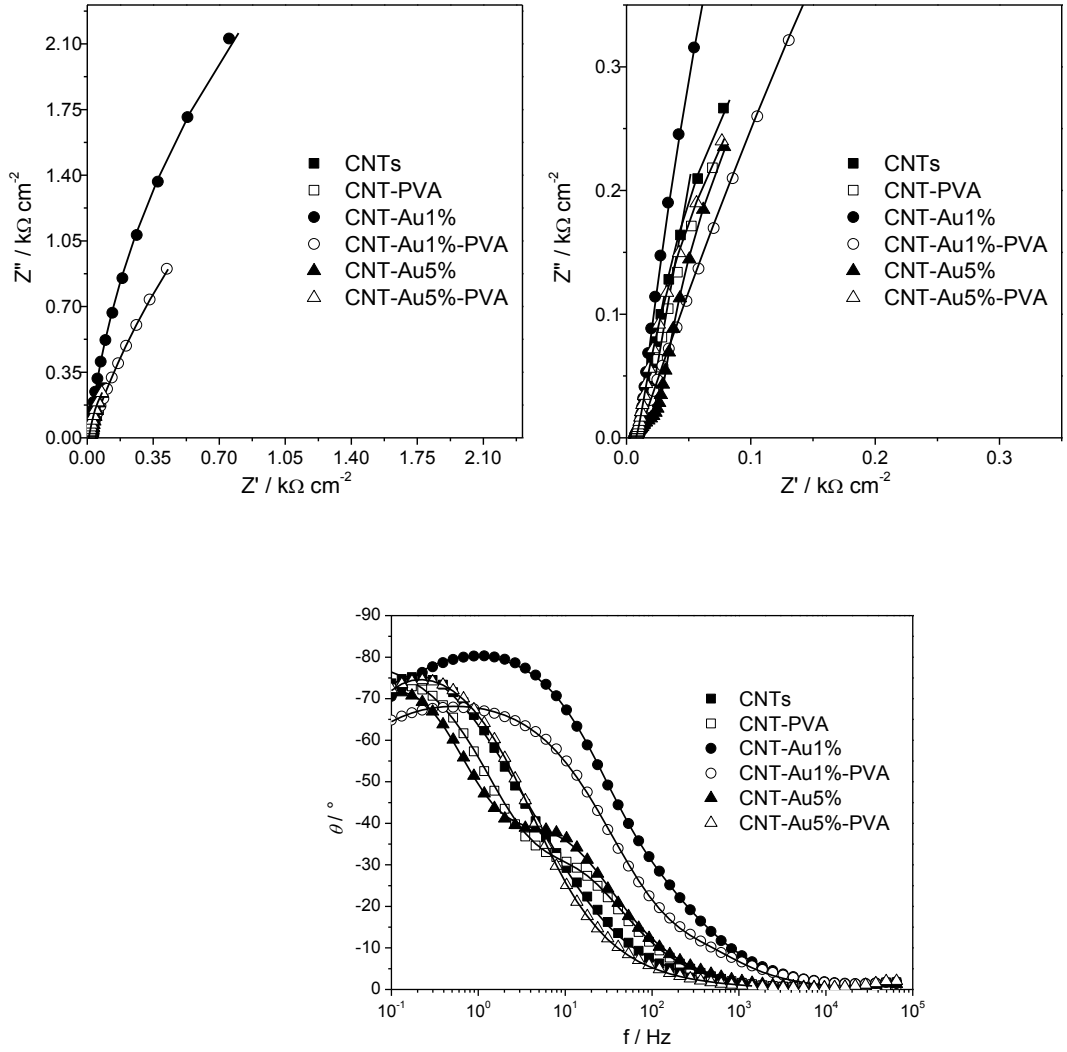

Figure 4.36. Complex plane plot and Bode plot at – 0.16 V in the presence of redox probe.

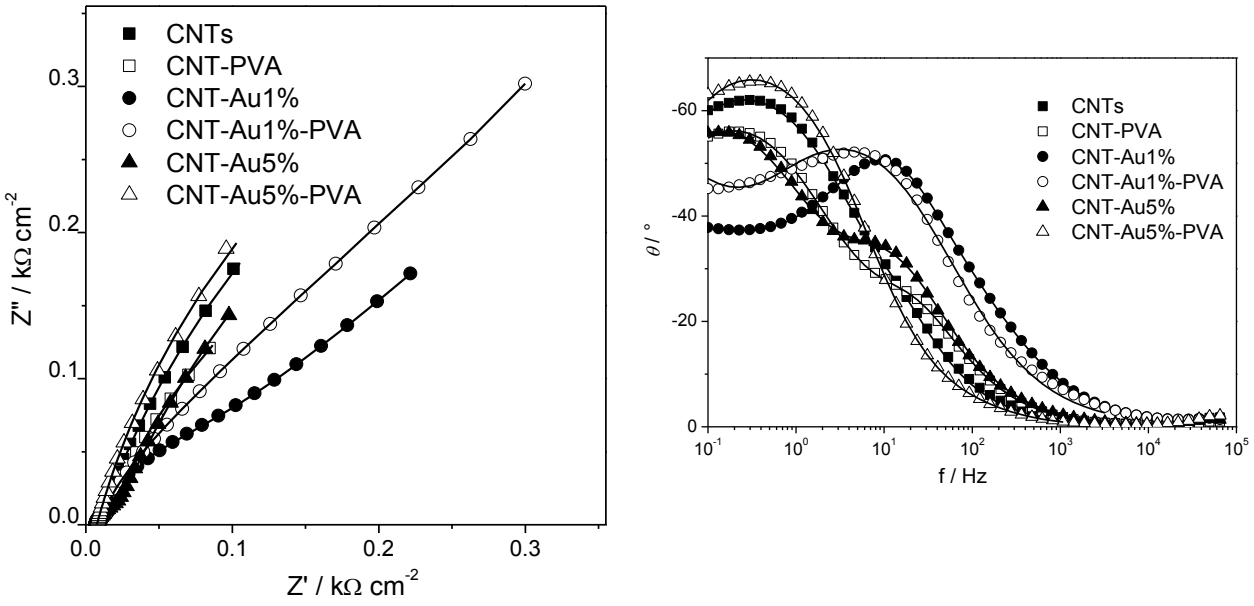

Figure 4.37. Complex plane plot and Bode plot at + 0.11 V in the presence of redox probe.

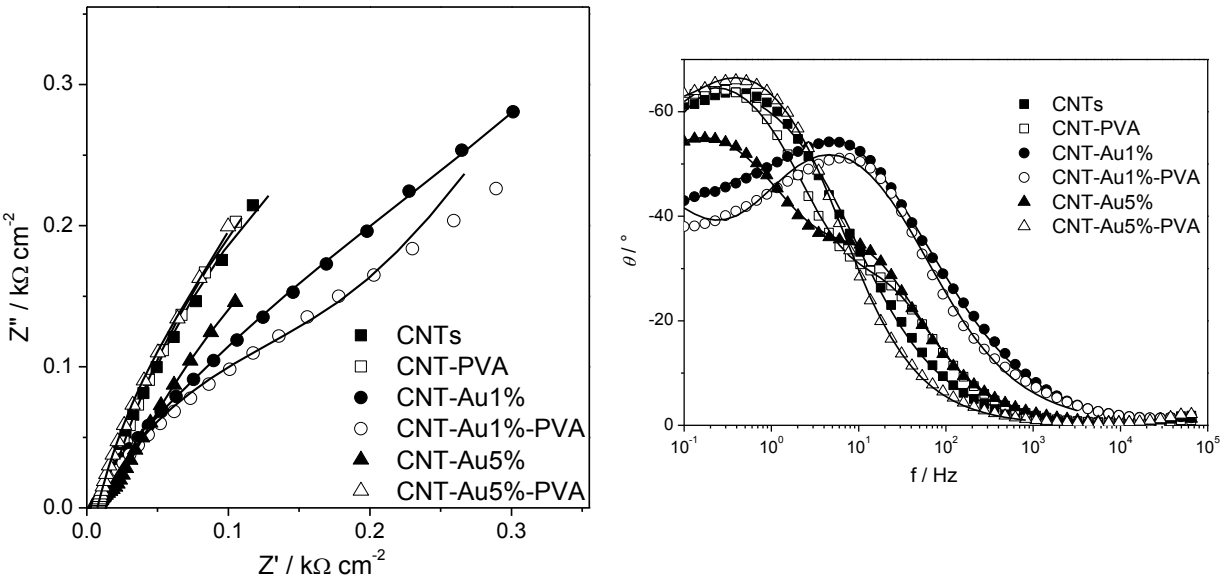

Figure 4.38. Complex plane plot and Bode plot at + 0.27 V in the presence of redox probe.

Figure 4.39 shows equivalent circuits used to fit impedance spectra and Table 4.13 reports the values obtained from the fitting. Also in the presence of redox probe, the presence of PVA on CNTs is detrimental for the electrochemical activity, because capacitance decreases and

resistance increases. Gold nanoparticles contribute to lower electron transfer resistance and GC/CNT-1%AuNP and GC/CNT-5%AuNP-PVA show the highest capacitance. Once again, GC/CNT-1%AuNP-PVA has the worst performance, adding a resistance to the diffusion process, which confirms the formation of an insulating and resistive surface.

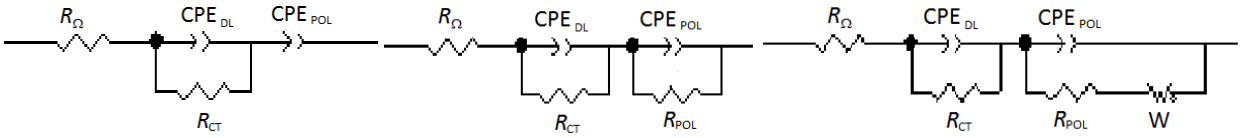

Figure 4.39. Equivalent circuits used to fit impedance data.

Table 4.13. Impedance parameters obtained by impedance fitting in the presence of redox probe.

Electrodes	E / V	R_Ω / Ω cm^2	CPE_{DL} / mF cm^{-2} s$^{\alpha-1}$	α_{DL}	R_{CT} / Ω cm^2	CPE_{POL} / mF cm^{-2} s$^{\alpha-1}$	α_{POL}	R_{POL} / Ω cm^2	R_w / Ω cm^2	τ / s	α
CNTs	-0.16	7.25	18.26	0.63	25	5.73	1.00	1170	-	-	-
	0.11	7.43	7.64	1.00	1.64	6.62	0.79	1160	-	-	-
	0.27	7.16	10.82	0.69	84	7.21	1.00	643	-	-	-
CNTs-PVA	-0.16	8.30	0.34	1.00	1.03	1.39	0.80	7837	-	-	-
	0.11	8.38	2.72	0.74	170	4.66	0.70	-	-	-	-
	0.27	8.39	2.05	0.79	142	5.43	0.65	-	-	-	-
CNTs-Au1%	-0.16	6.81	3.77	0.85	8.16	6.99	0.89	-	-	-	-
	0.11	6.82	3.35	0.89	5.01	9.08	0.76	766	-	-	-
	0.27	6.76	2.78	0.89	6.08	6.08	0.84	1143	-	-	-
CNTs-Au1%-PVA	-0.16	6.32	2.02	0.74	4.14	0.63	0.93	9367	-	-	-
	0.11	6.23	2.66	0.70	4.83	0.67	0.93	44	66	0.1	0.44
	0.27	6.18	2.84	0.65	469	1.64	1.00	19	19	0.1	0.40
CNTs-Au5%	-0.16	7.33	46.00	0.57	46	6.43	0.97	1233	-	-	-
	0.11	7.30	7.68	1.00	0.17	6.35	0.83	1070	-	-	-
	0.27	7.36	17.96	0.93	83	8.84	0.81	-	-	-	-
CNTs-Au5%-PVA	-0.16	7.46	3.64	0.80	22	6.34	0.97	1465	-	-	-
	0.11	7.42	3.78	0.82	13	8.11	0.78	1011	-	-	-
	0.27	7.36	3.57	0.86	9.73	7.60	0.75	1046	-	-	-

The most promising material (CNTs-Au1%) was tested for the determination of glycerol. Glycerol is an important intermediate in the production of biodiesel and numerous efforts are made to find the best way of transformation in industrial advantageous products. For these reasons its determination using simple and cheap techniques is important. In the Literature (Pop et al., 2012), only few examples of electroanalytical determination of glycerol are reported, using Boron Doped Diamond electrode or bare gold electrode, but no example of nanomaterials can be found. Considering the results obtained by bare gold electrodes employed for the amperometric detection of glycerol, gold nanoparticles modified electrodes seem to be a more promising device. GC/CNT-1%AuNP working electrode was used and preliminary results are shown in Figure 4.40, using NaOH 0.1 M as supporting electrolyte. Glycerol has an intense oxidation peak at + 0.10 V (SCE), which increases for consecutive additions of the analyte, allowing to obtain a calibration plot. Future developments will consider also GC/CNT-5%AuNP-PVA and the use of more appropriate electroanalytical methods for a quantitative analysis.

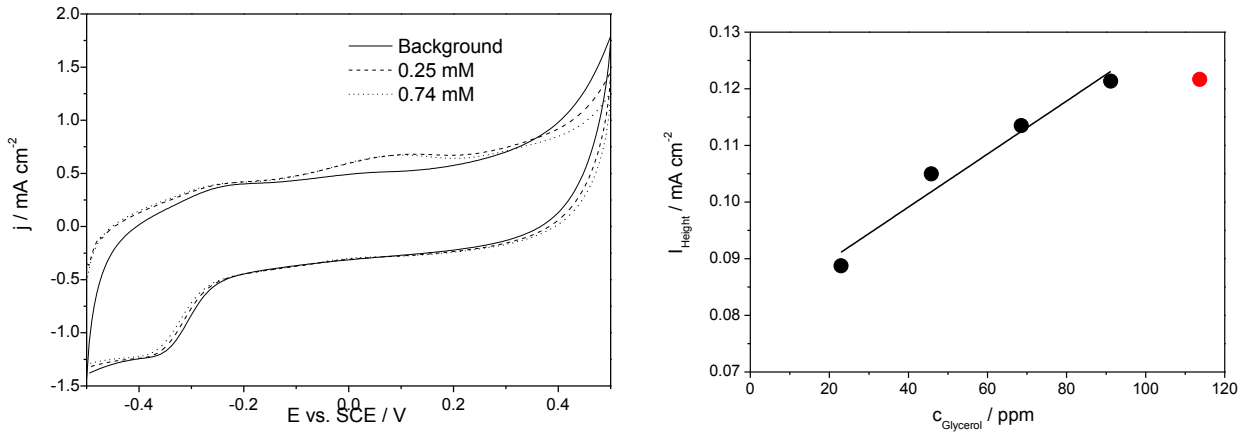

Figure 4.40. Cyclic voltammograms and corresponding calibration plots for consecutive additions of glycerol.

4.2.2.4. Conclusions

Baytube carbon nanotubes seem to be the most suitable material for electrochemistry in terms of intensity and shape of the peak of the model probe molecule. For these reasons they are chosen

as matrix for immobilization of gold nanoparticles, prepared by precipitation method or by mediated-polymer synthesis.

Cyclic voltammetric and electrochemical impedance spectroscopic characterization show that the presence of the polymer on CNTs has a detrimental effect on the electrochemical performance of the electrode also when Au 1 % is present, probably due to the formation of an inhomogeneous and disordered surface. The addition of gold nanoparticles improves the properties of the electrodes, reaching higher peak current and capacitance values and lower charge transfer resistance in comparison with CNTs and allowing the maintenance of diffusion control and reversibility. The presence of gold nanoparticles at 1 % without PVA and at 5 % with PVA on CNTs show the best performences in terms of peak current, high capacitance and lower resistance. The first type of material is used for a glycerol preliminary determination by cyclic voltammetry, giving promising results.

Future developments will consider the determination of glycerol using also CNTs with 5 % Au nanoparticles with PVA and the employment of different electroanalytical techniques more suitable for quantitative analysis. Moreover, the determination of other types of analytes, active on gold electrodes (*e.g*. As), will be taken into consideration.

4.2.3. Synthetic Silver Nanoparticles

4.2.3.1. Silver

Silver is an ideal metal for the design of electrodes, due to its unique properties: the highest electrical conductivity of all metals (Chun et al., 2010) and the good stability at different potential and pH. For these reasons and for silver catalytic properties towards particular analytes, silver nanoparticles modified electrodes are employed in the determination of various compounds of chemical and biological interest (Hodes, 2001; Pierce & Zhao, 2010; C. N. R. Rao et al., 2004; Schmid, 2003). In the Literature, many examples of silver nanoparticles modified electrodes for the catalysis of hydrogen peroxide reduction can be found (Han, Zheng, & Dong, 2013; Lu, Liao, Luo, Chang, & Sun, 2011; Qin et al., 2012; Qi Wang & Yun, 2012), followed by the detection of a variety of analytes, such as halides (Bellomunno et al., 2005; Abdirisak A Isse, Falciola, Mussini, & Gennaro, 2006; Abdirisak Ahmed Isse et al., 2009)(in particular chlorinated compounds (Chu & Zhang, 2012; Q. Li et al., 2013)), toxic compounds (pesticides (Kumaravel & Chandrasekaran, 2010), chromium (Domínguez-Renedo et al., 2008; S. Xing et al., 2011), nitrates (Atmeh & Alcock-Earley, 2011; Fajerwerg et al., 2010), nitrobenzene (Devi et al., 2012; Manivannan & Ramaraj, 2013), polyphenols (Rawal, Chawla, & Pundir, 2011), arsenic (Prakash, Chakrabarty, Singh, & Shahi, 2012), antimony (Renedo & Julia Arcos Martínez, 2007), metronidazole (Sadeghi, Hemmati, & Garmroodi, 2013), mercury (Manivannan & Ramaraj, 2013)) and other organic compounds (glucose (Jia, Wang, Liang, & Hu, 2012; Quan, Park, & Park, 2010; Ren, Meng, Chen, Tang, & Jiao, 2005), adriamycin (K. Zhang & Zhang, 2010; Yuzhong Zhang, Zhang, & Ma, 2009), glutathione (Narang, Chauhan, Jain, & Pundir, 2012), tryptophane (J. Li et al., 2013)).

The principal silver nanoparticles production methods are electrodeposition and colloidal synthesis by reduction of a silver salt in the presence of a protecting or stabilizing agent. Using

electrodeposition homogeneous deposits and controlled shape and size are difficult to obtain, while colloidal synthesis allows the formation of nanoparticles with various controlled shapes and sizes, with different electroanalytical performances (Campbell & Compton, 2010).

Another critical point to obtain good modified electrodes is the homogeneous distribution of nanoparticles, because pre-synthetized nanoparticles can aggregate in solution, giving agglomerates in the order of micrometers. In this context, polymeric membranes used as dispersive agents find applications and particularly Nafion, which is extensively used as a host ionomer membrane for nanoparticles. Nafion presents many advantages: chemical stability, it prevents agglomeration and corrosion of guest species, it is easy to handle and it could help in avoiding anionic interferences (C. M. A. Brett, Alves, & Fungaro, 2001; Dura, Murthi, Hartman, Satija, & Majkrzak, 2009; Mardegan et al., 2012; Liza Rassaei et al., 2011; Wood, Chlistunoff, Majewski, & Borup, 2009). In the case of silver nanoparticles, some examples can be found in the Literature about electrodeposited Ag nanoparticles in Nafion (Kumaravel & Chandrasekaran, 2010; S. Xing et al., 2011) or other polymers (B. Liu, Deng, Hu, Gao, & Sun, 2012), but according to our knowledge only one paper (Ghilane, Fan, Bard, & Dunwoody, 2007) deals with pre-synthetized Ag nanoparticles in Nafion suspension, but without any application as electroanalytical sensor. Another possible way to prevent the aggregation of nanoparticles is their dispersion on carbon nanotubes, allowing at the same time the enhancement of conductivity and the increase of active sites availability.

In this context, the study of the electrochemical performances of silver nanoparticles produced by colloidal synthesis and supported on Nafion and on carbon nanotubes is an interesting and promising research field.

4.2.4. Silver Nanoparticles on Nafion

4.2.4.1. Materials and Methods

Preparation of spherical Ag-Nanoparticles

The synthesis was modified from (Shervani et al., 2007). 250 mL of 1% wt aqueous solution of corn waxy starch were filtered on a 0.45 m Durapore® Millipore filter. d(+)-Glucose was added to 200 mL of the previous solution in order to obtain a solution 1% wt (solution A). 100 mL of 10^{-3}M $AgNO_3$ solution were prepared using solution A. This solution was divided into two pyrex vials equipped with screw cap, and inserted in an oven (T = 70°C, 24 h). It was noticed that at the end of the reaction time, reaction solution turned from transparent to yellowish. Nanoparticles were washed in three steps: reaction solution was centrifuged for 60 min, water was removed and silver nanoparticles were dispersed in water. The three steps were repeated 4 times, but finally silver nanoparticles were re-dispersed in 2 mL of ethanol, instead of water.

Preparation of modified-electrodes

The Glassy Carbon electrode was modified using a silver nanoparticle suspension in Nafion® prepared diluting (1:5) a Nafion® 5% wt solution with ethanol containing silver NPs. Three electrodes were used to study the influence of Nafion® and silver nanoparticles in the electrochemical response:

- Glassy Carbon electrode without any modification
- Glassy Carbon/NAFION® electrode, modified with a solution containing only Nafion®

- Glassy Carbon/NAFION®/AgNPs electrode, modified with a solution containing Nafion® and silver nanoparticles

A silver nanoparticles modified electrode without Nafion® was prepared but not considered in this work, since not stable.

0.1 M $NaClO_4$ aqueous solution was used as supporting electrolyte for all the characterizations.

4.2.4.2. Results and Discussion

Pre-synthetized Ag nanoparticles were chosen instead of electrodeposition in order to obtain homogeneous nanoparticles shape and distribution on the electrode, as recent study in Literature explains (Campbell & Compton, 2010; Du, Ding, Cai, & Zhang, 2007; Liza Rassaei et al., 2011). The procedure of synthesis was modified from (Shervani et al., 2007), in particular changing the duration of the thermal step (24 h instead of 30 minutes) and performing starch filtration before use. In fact, no nanoparticles were formed without these variations and particularly reaction time is fundamental, as shown in Figure 4.41, where UV-spectra show the presence of the typical plasmonic resonance band of Ag NPs at 420 nm after 6 h, with the complete nanoparticles formation only after 24 h. Also TEM image confirms the formation of spherical nanoparticles with the diameter of 10-30 nm. Moreover, this modified synthetic route was repeated 5 times, obtaining the same voltammetric pattern, and Ag NPs are very stable, since they can be stored for months in ethanol. In fact, Ag NPs produced and stored were tested every week for 6 months, giving the same voltammetric pattern.

Furthermore, the dispersion in Nafion is very simple and stable, as the UV-spectra in the inset of Figure 4.41 shows. In fact, the plasmonic band of Ag NPs is still present when they are dispersed in Nafion, with a shift of the maximum to higher values than AgNPs during synthesis, probably for

the formation of small aggregates or for changes in the refractive index (Moores & Goettmann, 2006).

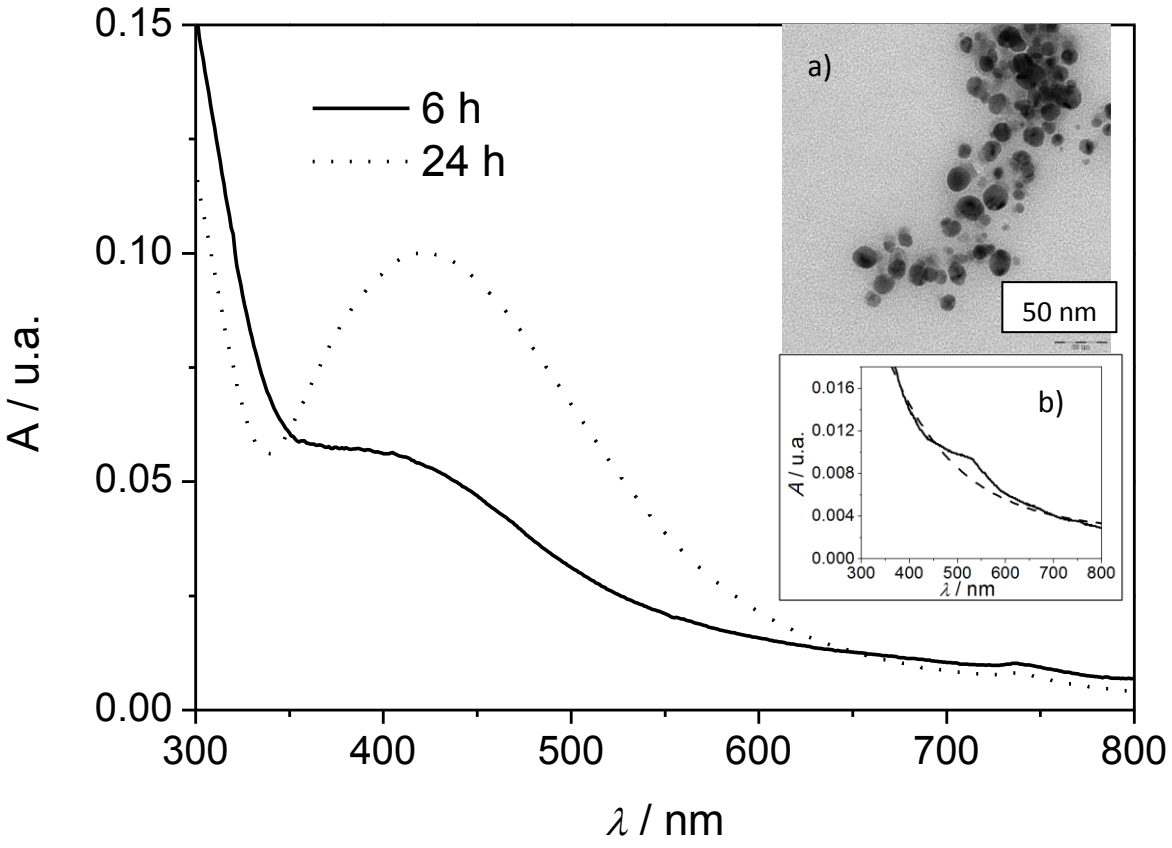

Figure 4.41. UV-vis spectrum of Ag nanoparticles during synthesis. Inset: a) TEM image of Ag nanoparticles after synthesis and b) UV-vis spectrum of Nafion-AgNPs suspension.

For the modification of GC electrode, a deposition of 20 µL of a dispersion of Ag NPs in Nafion was performed, leaving successively the electrode to dry in air for 15 minutes. The volume of deposition was chosen after experiments with different volumes: 45 µL causes a decrease in voltammetric signal, probably due to a too thick film of Nafion which prevents diffusion or to Ag oxidation, and 30 µL has very similar results to 20 µL, but the need of two depositions can cause problems of repeatability.

Figure 4.42 shows the presence of a quite uniform dispersion of Ag NPs on GC with very similar dimensions. EDS analysis also indicates the presence of metallic Ag, showing the classical peaks at

2.98, 3.15 and 3.35 keV. Nafion spectrum was performed for comparison, demonstrating that the presence of the peaks of F and S can be attributed to the polymeric membrane. The reproducibility of the observed Cl peak could be ascribed to impurities from reagents.

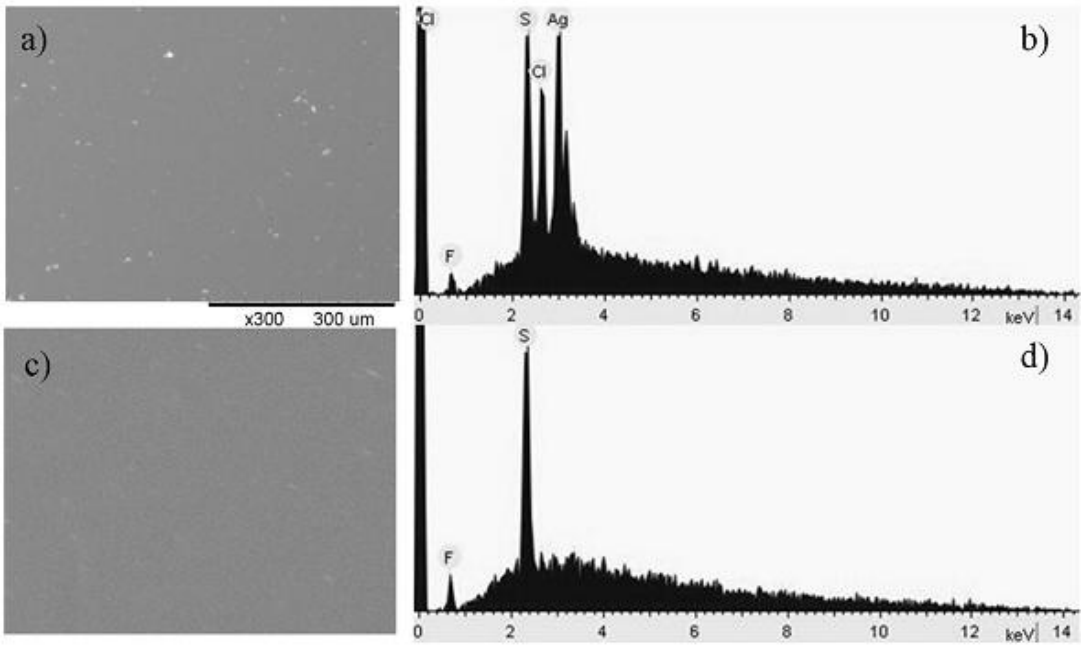

Figure 4.42. SEM image (a) and EDS (b) analysis of Glassy Carbon/NAFION®/AgNPs electrode; SEM image (c) and EDS analysis (c) of Glassy Carbon/NAFION® electrode, forcomparison.

Cyclic voltammograms were performed on the three types of electrodes using 1 mM $[Ru(NH_3)_6]Cl_3$ as model probe. The potential window was chosen considering the stability region of metallic silver in the Pourbaix diagram.

Figure 4.43 shows cyclic voltammograms of the three tested electrodes. The presence of the only Nafion causes an increase in the peak current, probably ascribable to the affinity of the membrane for the probe, but with the presence of Ag nanoparticles the signal is 10 times higher in comparison with GC. This behaviour is probably due to the increase of the effective surface area and/or to a formation of a random array of nanoparticles on a three-dimensional substrate, which can cause a diffusion between planar and convergent (Campbell & Compton, 2010; Kumaravel & Chandrasekaran, 2010; Andrew O Simm et al., 2005; C M Welch et al., 2005). In fact, when

nanoparticles are widely spaced in the Nafion membrane and can be considered isolated, they are possibly characterized by convergent diffusion, with the current intensity proportional to the particles radius. When the concentration of nanoparticles increases, each nanoparticle diffusion layer partially overlaps with the others, resulting in a more planar and less convergent diffusional process. The final result is an increase in the current in comparison with the macroelectrode, but without reaching the values for isolated nanoparticles. Moreover, the reduction peak of the Ag NPs electrode shifts towards more negative potentials, confirming the change in mass-transport regime, from planar to partially convergent (Campbell & Compton, 2010).

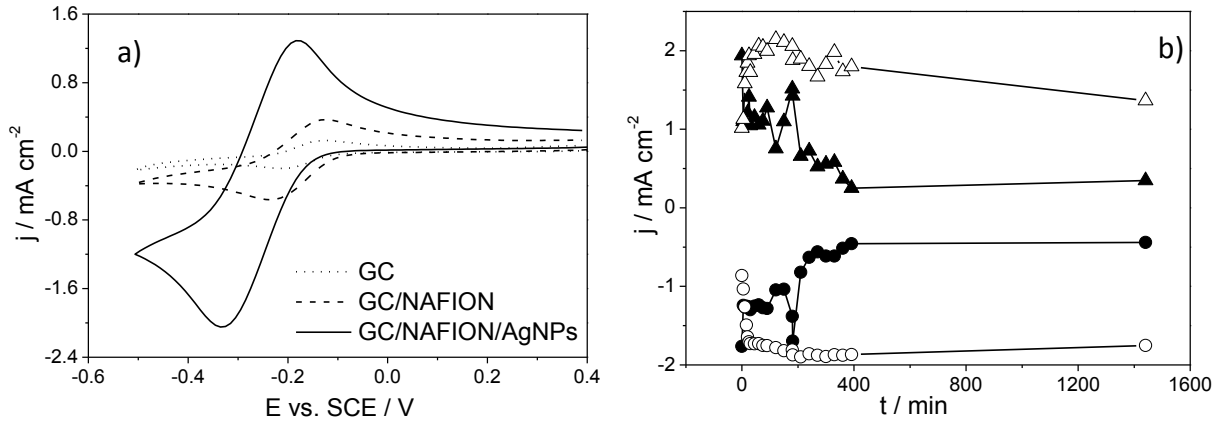

Figure 4.43. (a) Cyclic voltammograms of Glassy Carbon, Glassy Carbon/NAFION®and Glassy Carbon/NAFION®/AgNPs electrodes recorded in a solution of 0.1 M $NaClO_4$ containing 1 mM $[Ru(NH_3)_6]Cl_3$; (b) Stability of Glassy Carbon/NAFION®/AgNPs electrode: trend of the cathodic and anodic peak heights in air (full symbols) and in solution (empty symbols).

This result was also confirmed by scan rate studies, which were performed varying the scan rate in the range 10-500 mV s^{-1}. The trend of the Randles-Sevcik plot is linear, evidencing a process governed principally by diffusion. The values of the slope of the anodic and cathodic peaks are reported in Table 4.14, showing an increase for Ag NPs modified-electrode of 10 times and 6 times with respect to GC and GC with Nafion, respectively. Slope values for the electrode without Ag are very similar, while higher values in the presence of Ag NPs confirm a change in surface area and/or a partial change towards a convergent diffusional regime.

Table 4.14. Slopes of plots of j_p *vs.* $v^{1/2}$ (cyclic voltammograms recorded in 0.1 M $NaClO_4$ containing 1 mM $[Ru(NH_3)_6]Cl_3$), from v = 10 to v = 500 mV s^{-1}.

Electrode	*anodic slope* $\mu A\ cm^{-2}\ mV^{0.5}\ s^{-0.5}$	*cathodic slope* $\mu A\ cm^{-2}\ mV^{0.5}\ s^{-0.5}$
GC	19.2 ± 0.4	4.8 ± 0.1
GC/NAFION	21 ± 1	6.2 ± 0.3
GC/NAFION/AgNPs	186 ± 5	32 ± 4

Stability of Ag was also considered (Campbell & Compton, 2010), performing cycling voltammetric tests with the model probe cation at different intervals of time in air or in solution. When the electrode was left in air and reconditioned in solution before analysis, a rapid decrease in the reduction and oxidation currents occurred with some discontinuities, probably due to degradation of the electrode. On the other hand, if the electrode was left in solution with the supporting electrolyte, after a short equilibration time where current increases, peaks intensity stabilizes to a plateau value and Ag is stable.

Finally, repeatability was tested, comparing voltammograms obtained from three different electrodes prepared with Ag NPs Nafion dispersion. The registered spectra were reproducible, with 5 % maximum standard deviation on the cathodic peak.

Electrochemical Impedance Spectroscopy was carried out to evaluate physical and interface properties of the electrodes at + 0.150 V, - 0.130 V and – 0.230 V (SCE) in the presence of the probe molecule. The potentials were chosen considering cyclic voltammograms in the presence of the probe molecule: + 0.150 V is in the capacitive area of the spectrum, while – 0.130 V and -0.230 V are in the faradaic zone where oxidation and reduction of the redox probe take place.

Figure 4.44 shows complex plane plots and Bode plots with the corresponding fitting for all the electrodes at different potentials, while equivalent circuits used for the fitting are presented in Figure 4.45 and the correspondent obtained fitting values are reported in Table 4.15.

In the case of GC, spectra present for all the potentials a semicircle in the high frequency region, corresponding to the formation of the double layer, and a straight line for lower frequencies, correlated to the diffusional process. Single peak in the Bode plots represent a time-dependent process, usually the formation of the double layer. These spectra were fitted with an equivalent circuit composed by R_{Ω} in series with CPE_{dl} in parallel with a series of R_{ct} and CPE_{pol}. Capacitance of the double layer increases from positive to negative potentials, while resistance to charge transfer decreases, since at the potential of probe reaction, transfer of electrons is easier. The capacitance of polarization increases for the same reasons, while α_{pol} remains constant (0.56), indicating an irregular surface.

Impedance values for GC covered with Nafion are lower than only GC, demonstrating an improvement of the performances of the electrode only in the presence of Nafion. Trends of the complex plane plot and of Bode plot were very similar to those of GC and spectra were fitted with the same equivalent circuit. Also in this case, CPE_{pol} and CPE_{dl} increase and R_{ct} decreases from positive to negative potentials for the faster electron transfer, but values are in general higher for capacitances and lower for resistance in comparison with GC. This fact confirms better electrochemical properties for GC with Nafion, already observed in cyclic voltammetry.

Important differences were observed for the faradaic and capacitive area in the presence of Ag with Nafion on GC. At + 0.150 V, in capacitive area, the spectra profile is very similar to the precedent electrodes, with the same equivalent circuit and values very close to those obtained for GC with Nafion. When the applied potential is in the faradaic area, the trend of the complex

spectrum changes, showing a straight line with lower slope for high frequencies instead of the semicircle and a straight line with higher slope for low frequencies. Considering Bode plots, no peaks are present since no time-dependent processes , as the formation of double layer, were involved. Probably the double layer is very thin and only a diffusional process takes place. The values of diffusional resistance are low and decrease to more negative potentials, showing a fast and easy process of diffusion of the model probe cation, while CPE_{pol} increases, reporting the highest values in comparison with GC (20 times lower) and with GC with Nafion (4 times lower). These results confirm that Ag nanoparticles effectively improved the electroanalytical performances of the electrodes.

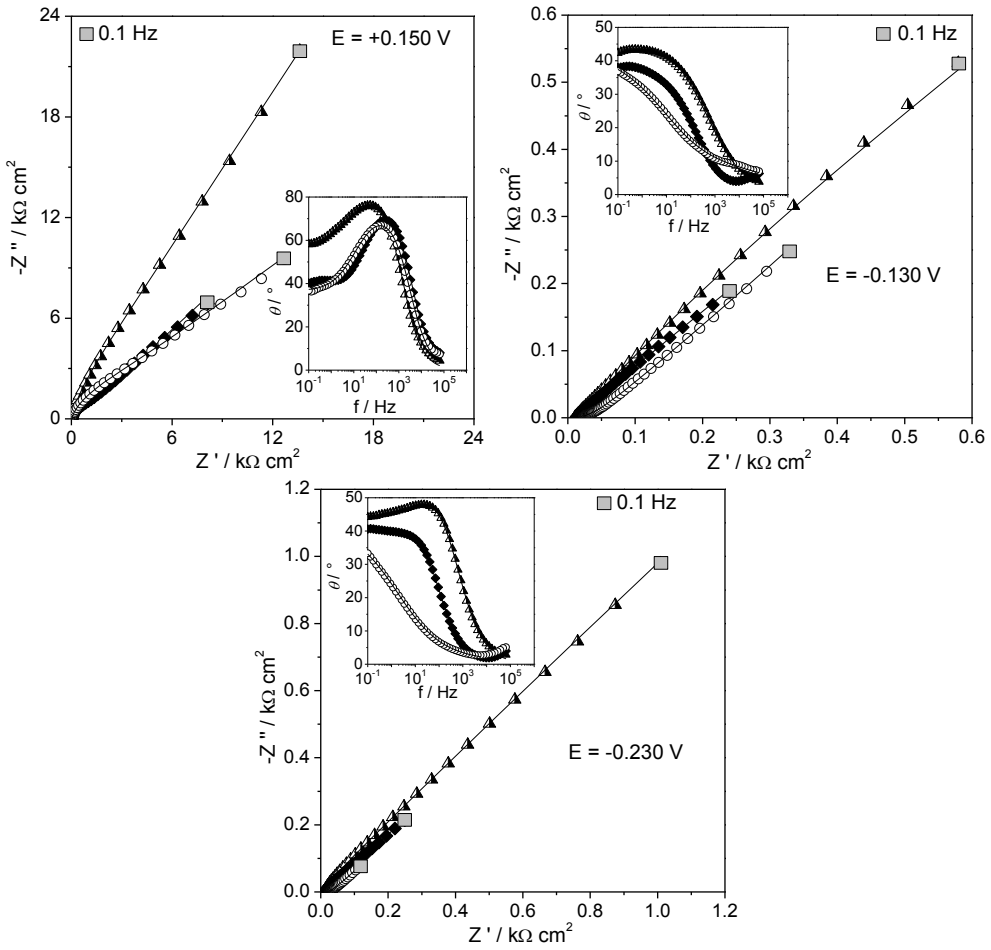

Figure 4.44. Complex plane impedance and relative Bode plots (inset) at different potentials [(a) E = +0.150 V; (b) E = −0.130 V; (c) E = −0.230 V] recorded in 0.1 M $NaClO_4$ containing 1 mM $[Ru(NH_3)_6]Cl_3$ for the electrodes Glassy Carbon (triangle), Glassy Carbon/NAFION® (full diamond), Glassy Carbon/NAFION®/AgNPs (empty circles); the lines represent equivalent circuit fitting.

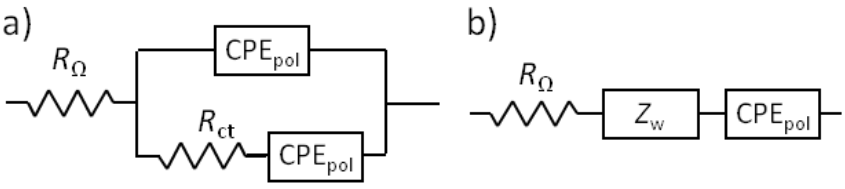

Figure 4.45. Equivalent circuits used to fit impedance spectra.

Table 4.15. Values of the parameters obtained by fitting impedance spectra with the equivalent circuits for Glassy Carbon, Glassy Carbon/NAFION®, Glassy Carbon/NAFION®/AgNPs.

Electrode	E_{ap}vs SCE / V	CPE$_{dl}$ / mF cm^{-2} s$^{\alpha-1}$	α_{dl}	R_{ct} / Ω cm^2	R_w / Ω cm^2	τ / s	α	CPE$_{pol}$ / mF cm^{-2} s$^{\alpha-1}$	α_{pol}
GC	0.15	0.02	0.90	5441	-	-	-	0.04	0.56
	-0.13	0.15	0.54	1562	-	-	-	0.43	0.60
	-0.23	0.29	0.71	176	-	-	-	0.70	0.56
GC/NAFION	0.15	0.01	0.88	1193	-	-	-	0.12	0.59
	-0.13	1.82	0.60	67	-	-	-	2.79	0.50
	-0.23	1.03	0.74	55	-	-	-	3.43	0.56
GC/NAFION /AgNPs	0.15	0.01	0.85	2158	-	-	-	0.08	0.52
	-0.13	-	-	-	61	0.1	0.18	5.65	0.52
	-0.23	-	-	-	11	0.1	0.16	14.23	0.60

The new modified electrode was used for the determination of chlorine containing species, a field where Ag is widely employed for its very pronounced electrocatalytic activity towards this atom (Bellomunno et al., 2005; Dai, Wildgoose, & Compton, 2006; Rondinini & Vertova, 2004; Andrew O Simm et al., 2005; Vertova et al., 2008). Their determination is very important for their high toxicity and in particular halothane and dichloromethane were chosen for this study using GC with Nafion and Ag nanoparticles electrode.

Halothane is an example of organic chlorinated molecule characterized by a complex structure; it is a typical anaesthetic and its determination is essential. Dichloromethane is a representative example of simple chlorinated compounds, very toxic and widely used as common solvent and as

component of paint strippers. Due to its toxicicty, the use of dichloromethane was recently regulated by an European Commission Regulation No 276/2010 and a Recommendation of the Scientific Committee on Occupational Exposure Limits for methylene chloride.

Figure 4.46 reports some preliminary results obtained by cyclic voltammetry. Halothane shows an intense and clear peak at – 0.69 V (SCE) at 2 and 4 mM concentrations, with current densities comparable or even better than those reported in the Literature (Andrew O Simm et al., 2005). For higher concentrations, the peak potential shifts to more negative values, probably because of the adsorption of halothane at the electrode, causing fouling. In the case of dichloromethane, a peak at – 0.71 V (SCE) was detected for 3 mM concentration, which doubles in intensity for 6 mM.

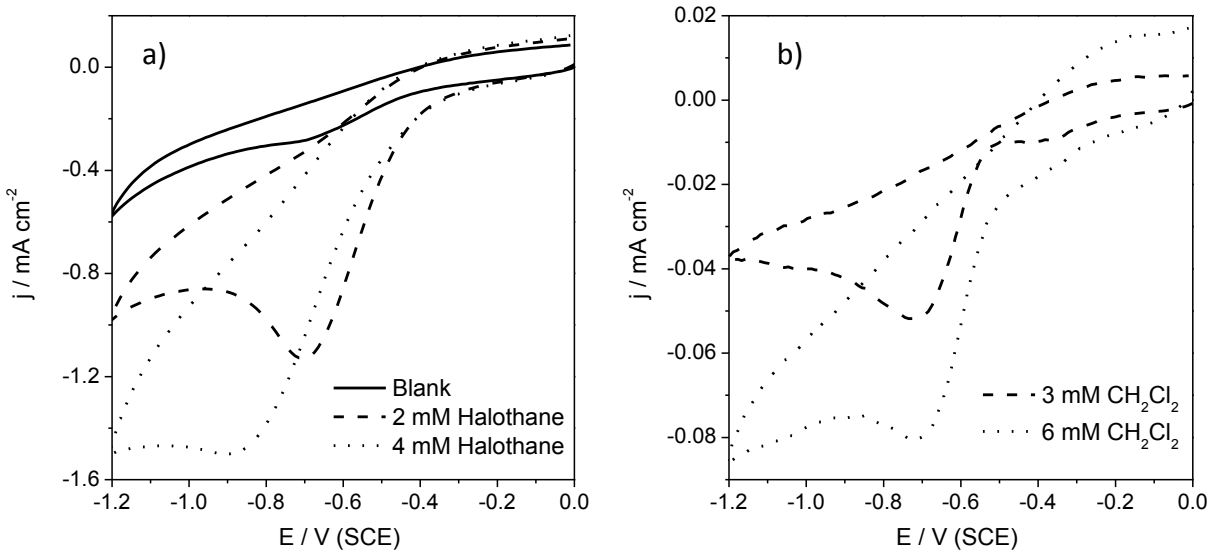

Figure 4.46. Cyclic voltammograms recorded in a solution containing $NaClO_4$ 0.1 M after addition of halothane (a) and CH_2Cl_2 (b). Blank subtraction was applied for CH_2Cl_2.

4.2.4.3. Conclusions

Spherical silver nanoparticles of 10-30 nm were successfully synthesized, optimizing a synthesis reported in the Literature, and completely characterized. A suspension of Ag nanoparticles in Nafion was used to modify a Glassy Carbon electrode and the modified electrode was studied using cyclic voltammetry and electrochemical impedance spectroscopy, comparing the results with

bare Glassy Carbon and Glassy Carbon with Nafion. $[Ru(NH_3)_6]Cl_3$ was used as redox probe molecule.

The Ag-modified electrode shows higher current intensity and anodic/cathodic slopes than the other two electrodes, probably due to the increase of effective surface area, to a formation of a nanoparticles random array in the Nafion three-dimensional substrate with intermediate diffusional behaviour between planar and convergent and to a very small double layer capacitance.

The modified electrode was also tested, exploiting the electrocatalytic properties of silver, for two hazardous chlorinated compounds, halothane and dichloromethane, showing promising performances.

Even though these results about the detection of chlorinated compounds are preliminary, they show the applicability of the modified electrode. Future developments will consider the optimization of the electroanalytical method for the determination of halothane and dichloromethane, applying also more appropriate techniques, such as pulsed and stripping analysis, and the design of new modified electrodes with composite with others nanomaterials (carbon nanotubes, titanium dioxide, polymers).

4.2.5. Silver Nanoparticles on Carbon Nanotubes

4.2.5.1. Materials and Methods

Materials used for this work were produced by Prof. Prati and Dr. Villa group of the University of Milano. Silver nanoparticles were synthesized via colloidal method and supported on carbon nanotubes (MWCNTs), to improve conductivity and prevent agglomeration, in the presence or absence of polyvinylalcohol (PVA) (Tsai & Huang, 2006) as metal protective agent. In the first case, nanoparticles were formed in the presence of PVA and immobilized on the support, while in the second case, nanoparticles were produced directly on carbon nanotubes.

Glassy Carbon electrode was modified using 0.5 mg mL^{-1} suspension of the desired material, with DMF as solvent. Different electrodes, built with the above synthesized materials, were used to study the influence of CNTs and silver nanoparticles on the electrochemical response:

- Glassy Carbon electrode without any modification (GC);
- GC/CNT electrode, modified with a suspension of CNTs Baytubes;
- GC/CNT-PVA electrode, modified with a suspension of CNTs modified with PVA;
- GC/CNT-AgNP electrode, modified with a suspension of CNTs decorated with 1 % silver nanoparticles, obtained by precipitation;
- GC/CNT-AgNP-PVA electrode, modified with a suspension of CNTs decorated with 1 % silver nanoparticles, obtained by PVA mediated synthesis.

0.1 M KNO_3 aqueous solution was used as supporting electrolyte for all the characterizations.

4.2.5.2. Results and Discussion

First of all, operative conditions were studied and optimized, considering the role of supporting electrolyte and the presence of oxygen dissolved in solution. The results are presented in Figure 4.47. In the case of KCl as supporting electrolyte, the presence of two sharp peaks at + 0.1 V and – 0.1 V (SCE) indicates the oxidation and reduction of silver, due to the presence of Cl^- in solution. Using $NaClO_4$, the two peaks disappear, with only the presence of a small shoulder around + 0.1 V, while in the case of KNO_3 the phenomenon is practically absent. For these reasons the last electrolyte was chosen and used for all the subsequent analysis. Moreover, the influence of oxygen was studied in aerated and deaereted solutions (the last one obtained by inert gas bubbling). The analysis demonstrated that the removal of oxygen was beneficial, giving a wider and more regular potential window.

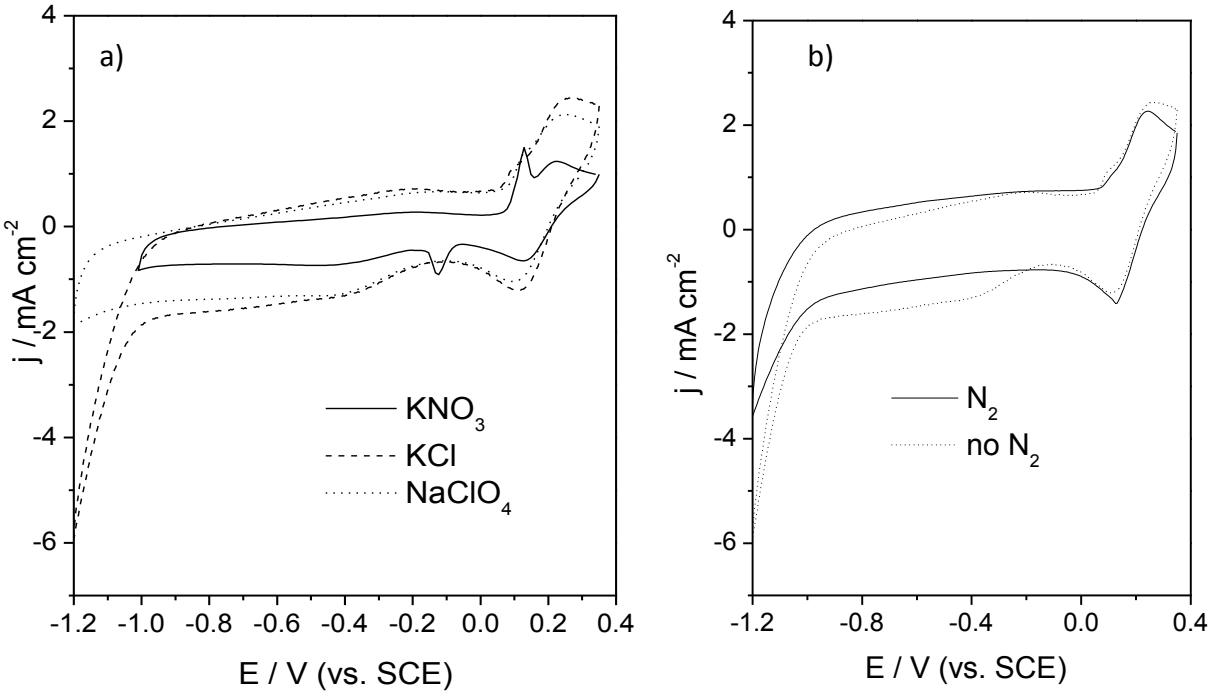

Figure 4.47. Cyclic voltammograms of CNTs-Ag1% electrode in different electrolytes (a) and under different atmosphere (b).

Figure 4.48 shows the voltammetric behaviour of the five types of electrodes in the presence of $K_4[Fe(CN)_6]$ as model probe molecule. The most important difference is the potential window, since the presence of silver nanoparticles allows extending the potential range in the cathodic region, maintaining the intensity of the peak of the redox probe.

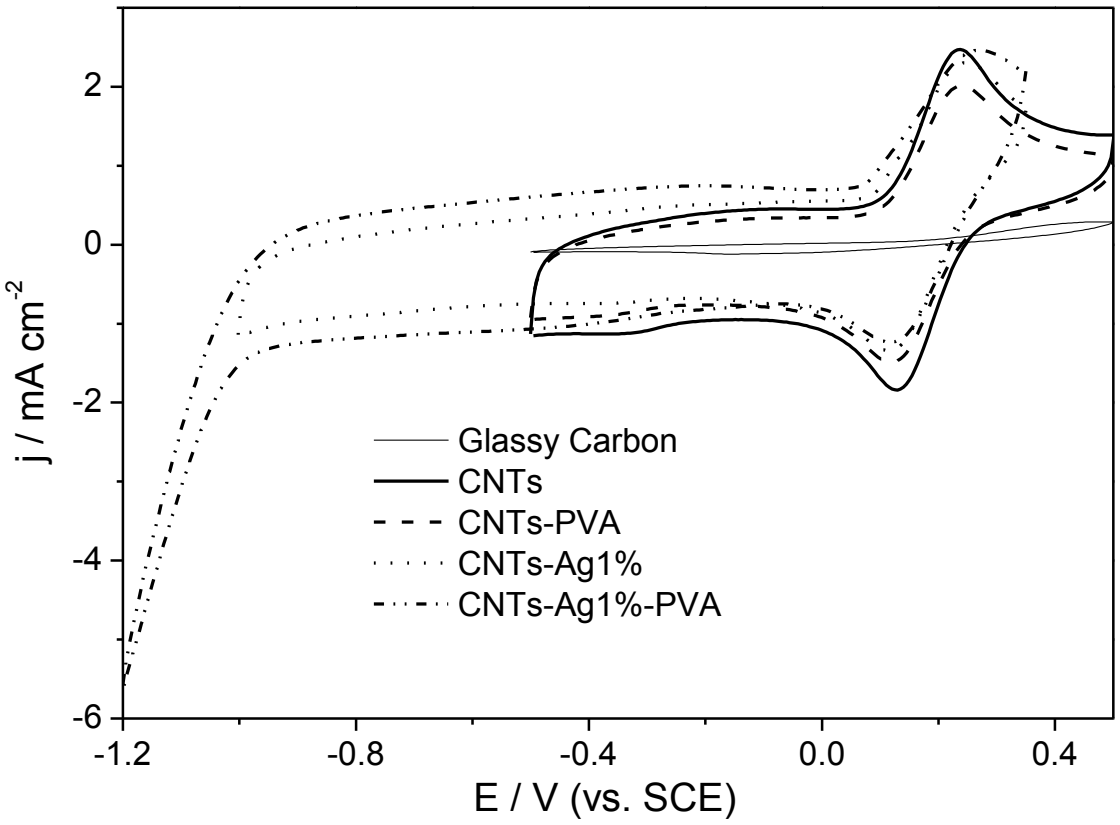

Figure 4.48. Cyclic voltammograms of Ag nanoparticles and carbon nanotubes modified electrodes.

Table 4.16 presents the voltammetric parameters, showing in general a diffusive mechanism and improving properties for all the electrodes in comparison with GC. The addition of Ag nanoparticles causes an increase in capacitance and a decrease of the Randles-Sevcik plot slope, probably due to a smaller surface area and to a different diffusive behaviour in comparison with CNTs alone.

Table 4.16. Voltammetric parameters obtained from cyclic voltammograms of Ag nanoparticles and carbon nanotubes modified electrodes.

CV parameters	GC	CNTs	CNTs-PVA	CNTs-Ag1%	CNTs-Ag1%-PVA
C / mF cm^{-2}	0.05	3.49	3.08	4.40	6.15
E_p-$E_{p/2}$ / mV	164	68	76	78	129
ΔE_P / mV	157	65	70	43	50
Slope i_p *vs* $v^{0.5}$ / µA mV$^{-0.5}$ cm^{-2} s$^{0.5}$	692	102	117	136	156
Slope Ln i_p *vs* ln v	17	182	125	115	119
C / mF cm^{-2}	0.44	0.46	0.41	0.40	0.43

Electrodes were characterized by electrochemical impedance spectroscopy in the absence and in the presence of the redox probe. Potentials were chosen from the cyclic voltammogram, at – 0.16 V (SCE) in the capacitive area and at + 0.11 V and + 0.27 V (SCE), where the redox reaction takes place.

In the absence of the redox probe, complex plane spectra (Figure 4.49) can be in general divided into two parts, a semicircle for higher frequencies and a straight line with the slope close to 90° for lower frequencies, which becomes a second semicircle in the case of GC/CNT-PVA. Only for GC/CNT the first semicircle is not present, indicating the absence of the double layer, probably due to a uniform and highly conductive surface. Bode plots (Figure 4.49) are generally very similar, except for GC/CNT-AgNP-PVA, which shows a time-dependent process for medium frequencies.

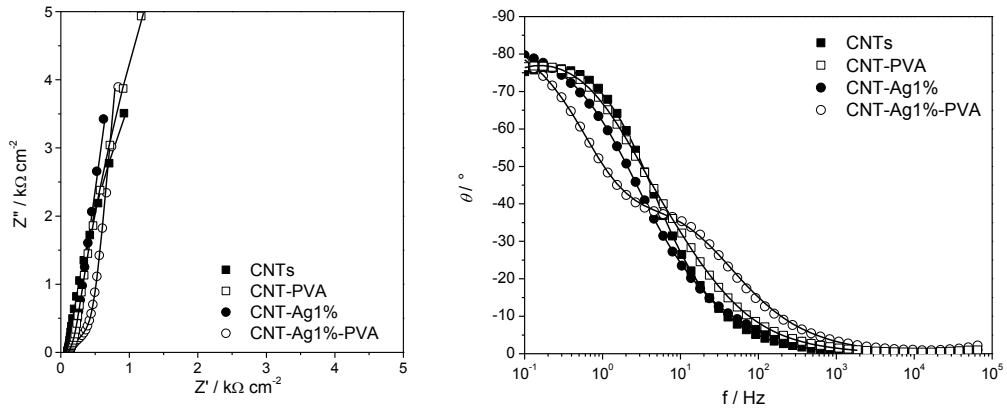

Figure 4.49. Complex plane plot and Bode plot at – 0.16 V in the absence of redox probe.

The equivalent circuits used to fit the data are presented in Figure 4.50, while the values obtained from the fitting are reported in Table 4.17. CNTs alone show a capacitive behaviour, in particular for positive potentials, while in the other cases the formation of the double layer takes place. When PVA is present together with CNTs but without Ag, the presence of a second semicircle with high resistance is an evidence of a highly resistive material, probably for the formation of a disordered surface of PVA and CNTs. The presence of Ag nanoparticles contributes to increase the capacitance of the double layer and also allows maintaining the capacitive behaviour of CNTs, while the addition of PVA causes a decrease in the capacitance of the double layer and an increase of charge transfer resistance. Nevertheless, the capacitive behaviour of the electrode is maintained, probably because the polymer has not a disordered distribution on the surface, as when Ag is absent, but it is localized on Ag nanoparticles. Moreover, capacitance values are in accordance to those obtained from cyclic voltammetric studies.

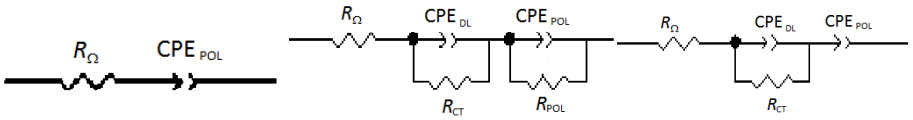

Figure 4.50. Equivalent circuits used to fit impedance data.

Table 4.17. Impedance parameters obtained by impedance fitting in the absence of redox probe.

Electrodes	E / V	R_Ω / Ω cm^2	CPE_{DL} / mF cm^{-2} s$^{\alpha-1}$	α_{DL}	R_{CT} / Ω cm^2	CPE_{POL} / mF cm^{-2} s$^{\alpha-1}$	α_{POL}	R_{POL} / Ω cm^2
CNTs	-0.16	6.99	16.26	1	0.56	5.78	0.92	2256
	0.11	6.96	-	-	-	4.87	0.89	-
	0.27	6.89	-	-	-	4.21	0.89	-
CNTs-PVA	-0.16	8.06	13.14	0.70	6.70	4.22	0.93	4081
	0.11	8.06	9.97	0.75	4.69	3.25	0.90	6217
	0.27	8.44	4.64	1	2.12	2.95	0.88	10654
CNTs-Ag1%	-0.16	8.28	28.37	0.58	5.33	6.30	0.92	-
	0.11	8.21	25.24	0.56	7.11	4.70	0.93	-
	0.27	8.25	21.21	0.60	3.94	4.15	0.92	-
CNTs-Ag1%-PVA	-0.16	7.65	4.12	0.72	2.42	5.65	0.95	-
	0.11	7.09	2.99	0.74	26.27	4.23	0.94	-
	0.27	7.00	2.98	0.75	20.93	3.83	0.92	-

In the presence of model probe molecule, impedance values decrease when the redox reaction takes place. The impedance spectra are shown in Figure 4.51-4.52-4.53. The complex plane spectra present a semicircle for higher frequencies for all the electrodes, indicating the formation of the double layer, while for lower frequencies the behaviour is really different. For CNTs a straight line with slope under 0.5 shows a resistance of the diffusion process of the redox probe; for GC/CNT-PVA the formation of a second semicircle represents a non-homogeneous material; the presence of a straight line with slope value > 0.5 at – 0.16 V (SCE), which becomes a semicircle at + 0.11 V and + 0.27 V, indicates a general capacitive behaviour with the addition of an electron transfer resistance when the redox probe reacts. Bode plots show a change for low frequencies when the probe is present or absent, reflecting the different behaviour of the second part of the complex plane spectra. For GC/CNT-Ag1%-PVA a time dependent process at medium frequencies is still present, probably due to a particular interaction between Ag nanoparticles and the polymer.

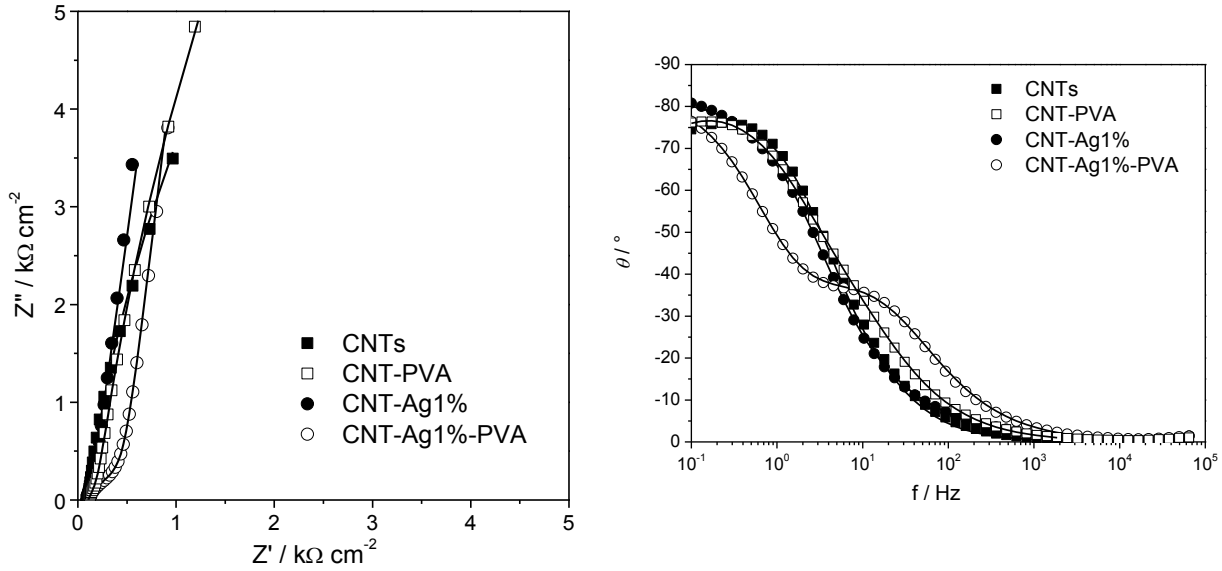

Figure 4.51. Complex plane plot and Bode plot at – 0.16 V in the presence of redox probe.

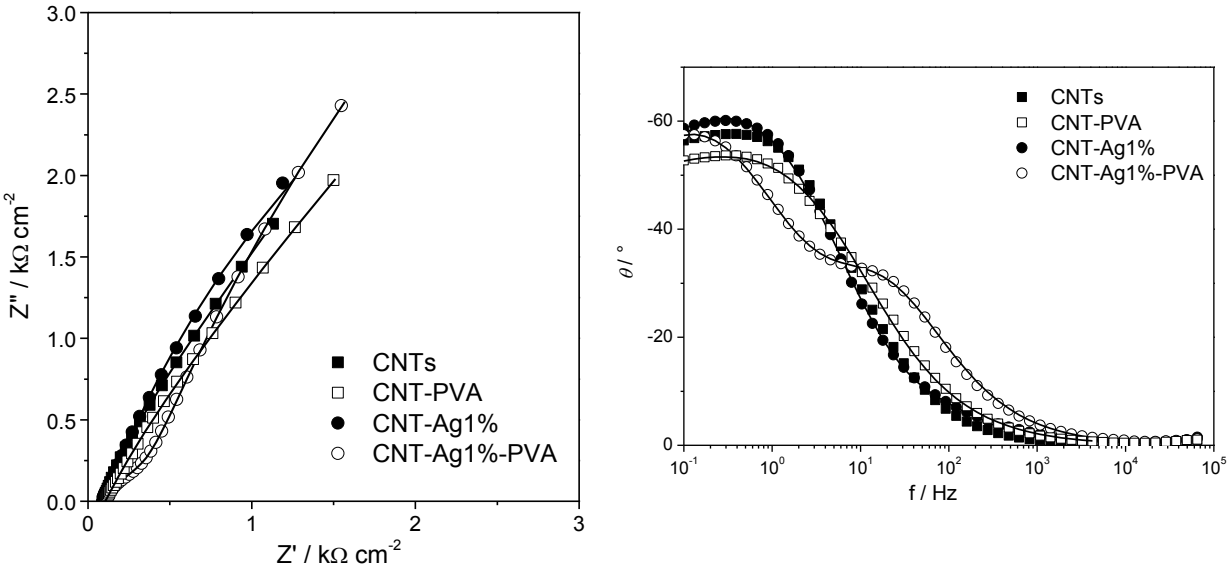

Figure 4.52. Complex plane plot and Bode plot at + 0.11 V in the presence of redox probe.

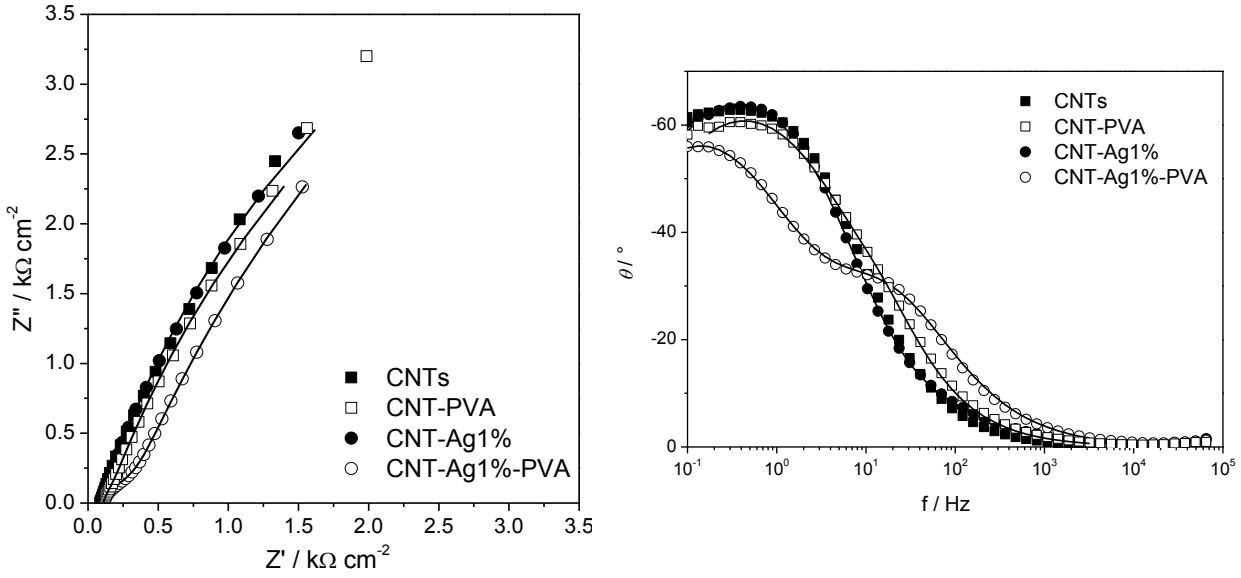

Figure 4.53. Complex plane plot and Bode plot at + 0.27 V in the presence of redox probe.

Figure 4.54 reports the equivalent circuits used to fit impedance data, while the values obtained from the fitting are shown in Table 4.18. In general, working at more positive potentials contributes to increase capacitance and to decrease resistance, since for positive potential the reaction of the probe is favoured. When only CNTs are present, a diffusive behaviour dominates the reaction of the redox molecule, due to a more ordered structure. For CNTs and PVA the use of the same circuit for all the potentials shows a more disordered structure with an intrinsic resistance to charge. When Ag nanoparticles are present, the electrodes have a capacitive behaviour with a small resistance to electron transfer only during redox reaction. Moreover, when Ag nanoparticles are covered with polymer, the capacitance decreases and the resistance increases, indicating that polymer partially blocks the beneficial role of Ag as reaction centre.

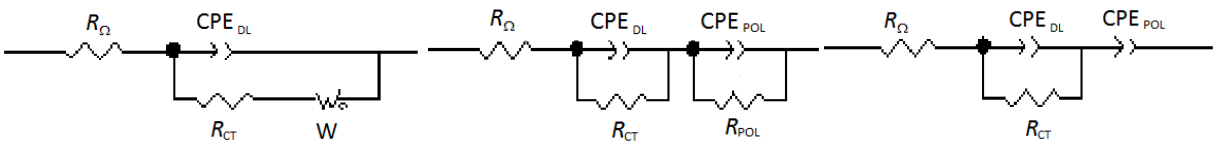

Figure 4.54. Equivalent circuits used to fit impedance data.

Table 4.18. Impedance parameters obtained by impedance fitting in the presence of redox probe.

Electrodes	E / V	R_Ω / Ω cm^2	CPE_{DL} / mF cm^{-2} s$^{\alpha-1}$	α_{DL}	R_{CT} / Ω cm^2	CPE_{POL} / mF cm^{-2} s$^{\alpha-1}$	α_{POL}	R_{POL} / Ω cm^2	R_w / Ω cm^2	τ / s	α
CNTs	-0.16	6.46	25.71	0.77	1.20	5.76	0.92	1929	-	-	-
	0.11	6.39	7.92	0.78	290.11	-	-	-	43.66	0.1	0.41
	0.27	6.38	6.07	0.83	389	-	-	-	76.47	0.1	0.40
CNTs-PVA	-0.16	7.55	12.20	0.70	7.39	4.27	0.93	3876	-	-	-
	0.11	7.51	15.79	0.65	80.08	10.43	0.77	1229	-	-	-
	0.27	7.72	7.87	1	1.78	4.70	0.79	1002	-	-	-
CNTs-Ag1%	-0.16	6.86	27.92	0.57	2.83	6.28	0.91	-	-	-	-
	0.11	6.84	2.87	1	0.48	8.08	0.78	831	-	-	-
	0.27	6.99	2.67	1	0.49	6.08	0.82	938	-	-	-
CNTs-Ag1%-PVA	-0.16	7.42	3.33	0.74	25.54	5.73	0.93	-	-	-	-
	0.11	7.37	3.23	0.75	16.68	7.01	0.79	1340	-	-	-
	0.27	7.35	3.58	0.74	14.97	7.28	0.78	1120	-	-	-

4.2.5.3. Conclusions

The electrochemical behaviour of silver nanoparticles precipitated on carbon nanotubes was deeply investigated and the influence of PVA as protective polymer was evaluated.

First of all, a chlorine-free environment is important to preserve the purity of nanoparticles and a free-oxygen analysis is essential to avoid oxygen undesirable reactions.

The presence of silver nanoparticles allows the extension of the potential range in the cathodic region, and maintains the diffusive control of the system, probably changing the type of diffusion with an intermediate mechanism between planar and convergent and improving the capacitance of the system. Furthermore, the protective polymer localizes on Ag nanoparticles, giving a more disordered and resistive structure, preventing Ag to be available as reaction centre.

In all cases capacitance values are higher than pre-synthetized silver nanoparticles/Nafion modified electrodes, discussed in the previous paragraph (4.2.4), highlighting the important contributes of CNTs to the system.

Future developments will consider the comparison between pre-synthetized and electrodeposited Ag nanoparticles on carbon nanotubes and the development of new electroanalytical methods for the determination of chlorinated compounds, which can take advantage of the wide potential window of these materials.

4.2.6. Titanium Dioxide and Carbon Nanotubes

4.2.6.1. Titanium dioxide

Nanosized titania is a material employed in many research areas thanks to its innumerable properties (CARP, 2004; Fujishima, Rao, & Tryk, 2000). First of all, it is a photoactive compound, since the irradiation by UV light causes its oxidation to Ti^{III}, the injection of electrons in the conduction band and the formation of holes in the valence band, completely changing the behaviour of the material (increase in conductance and redshift of the absorption band) and allowing different applications. Moreover, titanium dioxide shows an amphiprotic nature, permitting the alteration of surface charges by simply controlling the pH, and a quantum confinement effect together with a different movement of holes and electrons, only varying the size and shape of nanoparticles. The surface hydroxyl groups can be easily functionalized with other groups and molecules and hybridization with others materials is very simple. Titanium dioxide conductance varies depending on crystalline phase, in the order amorphous > anatase > rutile, and its resistance can change with adsorption of other species. Titania shows a wide range of properties, such as high thermal and chemical stability, optical transparency in visible and near-IR ranges, photovoltaic properties, photo-cleaning capabilities and strong adsorption characteristics (Maino et al., 2013; Meroni et al., 2012; V Pifferi et al., 2013; Valentina Pifferi, Ardizzone, Cappelletti, Falciola, & Meroni, 2013).

It can be synthesized by different types of procedures, in particular sol-gel method, hydrothermal (Meroni et al., 2012), solvothermal, microwave, microemulsion, direct oxidation and electrochemical techniques, allowing the control and design of specific parameters dependent on application (CARP, 2004; Y. Chen, Lunsford, & Dionysiou, 2008; Rani et al., 2010).

In the field of trace analysis (Hodes, 2001; Pierce & Zhao, 2010; C. N. R. Rao et al., 2004; Schmid, 2003), titania is employed in gas sensors, ion detectors, metal ions and organic compounds extractors, voltammetric and optical biosensors. In particular, its use in electroanalytical field shows wide margins of development (Maino et al., 2013), with the exploitation of not only its sensing properties, but also its self-cleaning characteristics (Benvenuto, Kafi, & Chen, 2009; Y. Chen et al., 2008; Daniele, Battistel, Gerbasi, Benetollo, & Battiston, 2007; J.-A. Park, Kim, Choi, & Lee, 2010; Rani et al., 2010; Satheesh Babu, Suneesh, Ramachandran, & Nair, 2010; Xie, Zhou, & Huang, 2007). The idea is to develop sensing platforms based on titania or hybrid systems with auto-cleaning features, allowing the removal of analytes, which cause fouling problems, simply irradiating the electrode with UV light.

In this context, the evaluation of electrochemical performances of titanium dioxide modified electrodes and of hybrid composites based on titania and single-walled carbon nanotubes is an interesting research topic.

4.2.6.2. Materials and Methods

Glassy Carbon electrode was modified using 0.5 mg mL^{-1} suspension of the desired material, with DMF as solvent. Different modified electrodes, prepared using materials synthesized by Prof. Agostiano group of University of Bari and Dr. Comparelli group of CNR-Bari, were used to study the influence of single walled carbon nanotubes and titanium dioxide nanorods in the electrochemical response:

- Glassy Carbon electrode without any modification (GC);
- GC/SWCNT electrode, modified with a suspension of single walled carbon nanotubes;
- GC/TiO_2NR electrode, modified with a suspension of titania nanorods;

- GC/SWCNT-TiO_2NR electrode, modified with a suspension of CNTs decorated with titanium dioxide nanorods.

0.1 M KCl aqueous solution was used as supporting electrolyte for all the analysis.

4.2.6.3. Results and Discussion

The new materials were electrochemically characterized by cyclic voltammetry and electrochemical impedance spectroscopy in the presence or absence of a model probe molecule, to understand the effect of UV light and single walled carbon nanotubes on titanium dioxide.

Figure 4.55 shows cyclic voltammograms of the different materials and voltammetric parameters are reported in Table 4.19. SWCNTs have the highest peak current, while when titania is present, the current decreases below the level of GC. This is due to the semiconductive nature of titania, which influences also the behaviour of CNTs. Under UV light only materials containing titanium dioxide show different voltammetric behaviour with the total disappearance of redox probe peaks. Capacitance values are higher for SWCNTs as expected, followed by TiO_2-NR, while the composite presents lower value than GC, probably due to disordered and inhomogeneous character of the material. Capacitance values remain the same for all materials under UV irradiation. The presence of SWCNTs produces a more reversible signal, considering peak-to-peak separation and full width at half maximum. The highest slope of the Randles-Sevcik plot is reached in the case of SWCNTs, due to carbon nanotubes higher surface area. The diffusive control is maintained. In the case of titania, for both materials, the slope decreases when UV irradiation is applied, probably since diffusion of model probe molecule changes due to interaction with excited titanium dioxide. Also diffusion control is lost, confirming the hypothesis that other mechanisms take place.

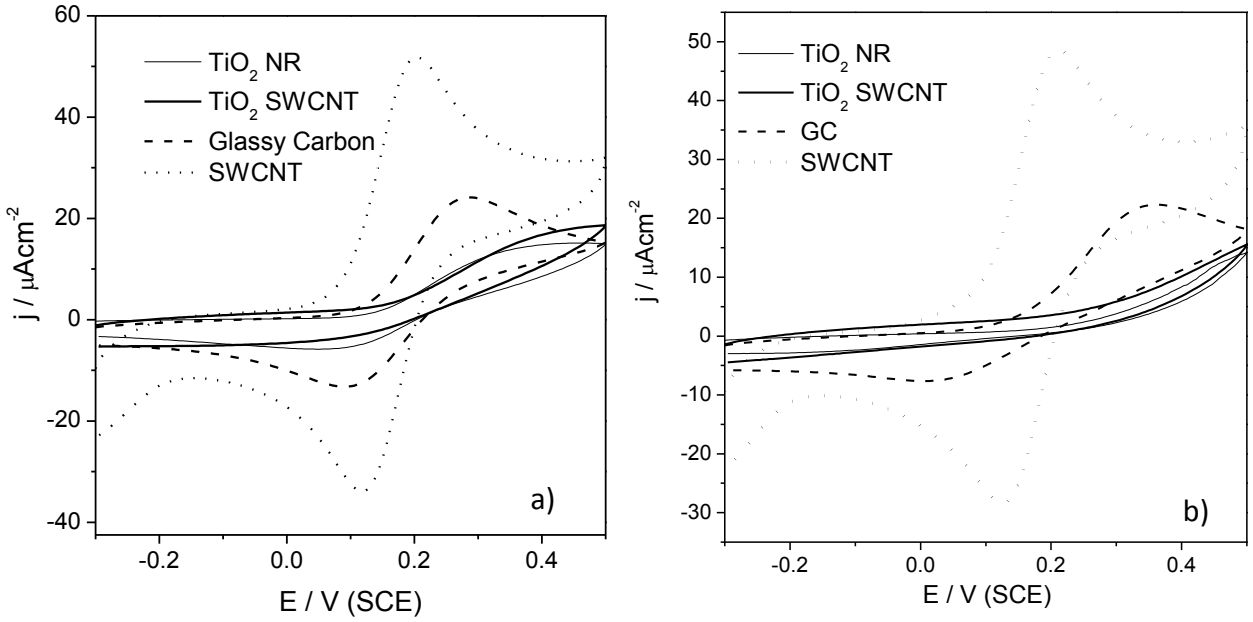

Figure 4.55. Cyclic voltammograms of titania and carbon nanotubes modified electrodes in the dark (a) and under UV illumination (b).

Table 4.19. Voltammetric parameters obtained from cyclic voltammograms of titania and carbon nanotubes modified electrodes.

CV parameters		GC	TiO_2	SWCNT	TiO_2-SWCNT
C / mF cm^{-2}	Dark	0.08	0.41	1.80	0.03
	UV	0.08	0.52	1.72	0.03
E_p-$E_{p/2}$ / mV	Dark	96	/	73	/
	UV	96	/	78	/
ΔE_P / mV	Dark	171	/	102	/
	UV	171	/	122	/
Slope i_p *vs* $v^{0.5}$ / µA $mV^{-0.5}$ cm^{-2} $s^{0.5}$	Dark	31	53	77	23
	UV	31	42	75	17
Slope Ln i_p *vs* ln v	Dark	0.44	0.50	0.45	0.31
	UV	0.44	0.33	0.49	0.22

Electrochemical impedance spectroscopy was performed at – 0.15 V (SCE), in the capacitive area of cyclic voltammogram, and at + 0.10 V and + 0.25 V (SCE), where redox peaks are present.

Figure 4.56 shows impedance spectra for all the electrodes in the absence of model probe molecule. Complex plane spectra present a semicircle for higher frequencies, corresponding to the formation of double layer, and a second semicircle for lower frequencies, which becomes a

straight line with slope < 0.5 only in the case of GC/TiO_2NR-SWCNT under UV light. Bode plots show that when titania is present the frequency of the time dependent process shifts to higher values than in the case of CNTs. In the case of TiO2-NR two different processes take place.

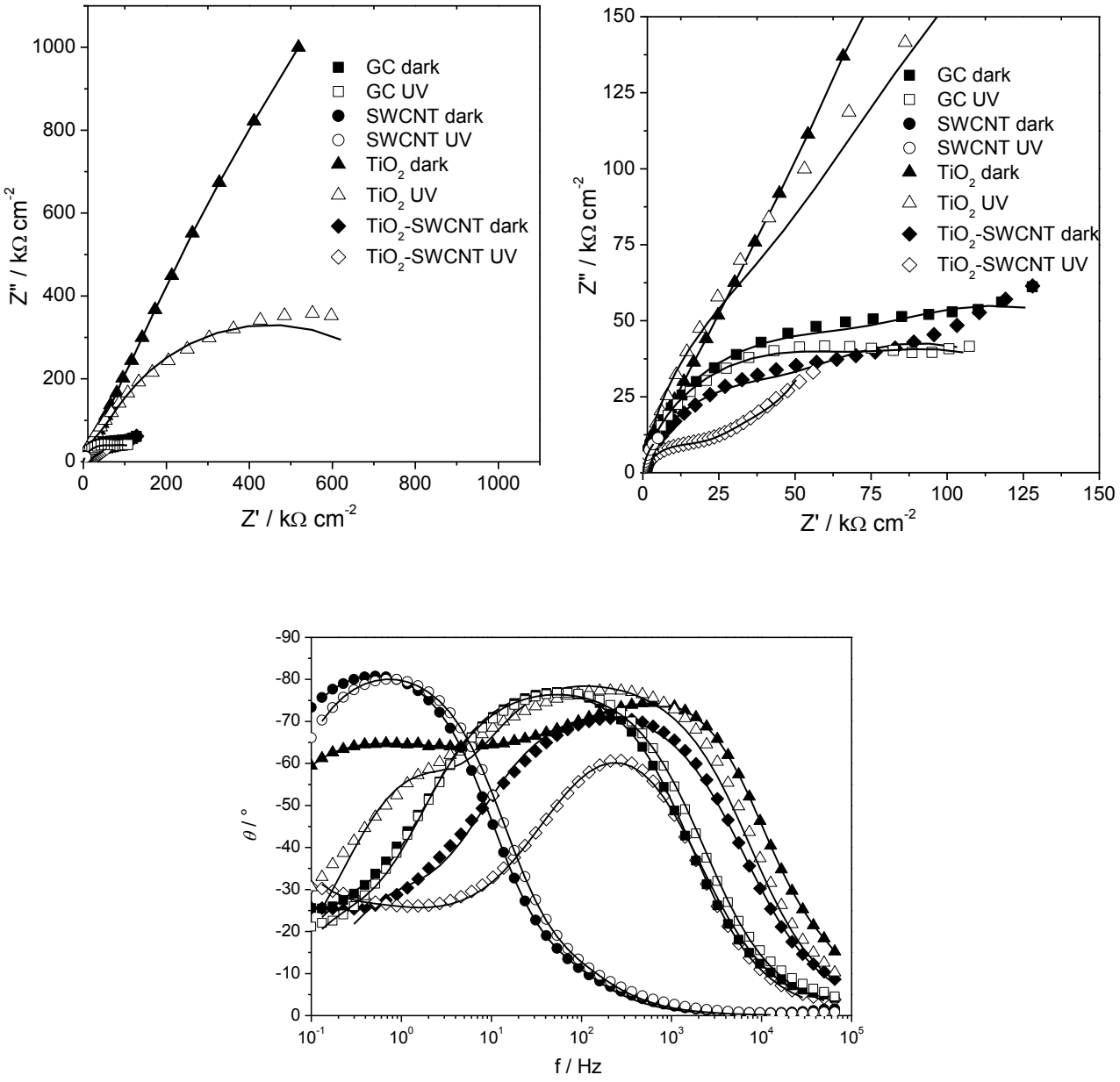

Figure 4.56. Complex plane plot and Bode plot at – 0.15 V in the absence of redox probe.

Figure 4.57 presents equivalent circuits used to fit impedance spectra, while Table 4.20-4.21 reports the corresponding fitting values. SWCNTs show, as expected, higher double layer and polarization capacitance with lower charge transfer resistance. When titania is present, the resistance to electron transfer increases, in particular for the composite of titania with CNTs,

probably because of both the semiconductive nature of titanium dioxide and the material non homogeneousity. Under UV irradiation no significant changes can be observed for GC and SWCNTs, as already demonstrated by cyclic voltammetry, but for TiO_2 samples a decrease in charge transfer and polarization resistance is registered and GC/TiO_2NR-SWCNT changes the equivalent circuit from a semicircle to a Warburg resistance. This fact could be explained with the formation of excited electrons from titania under UV irradiation, which contribute to a better conductivity of the material.

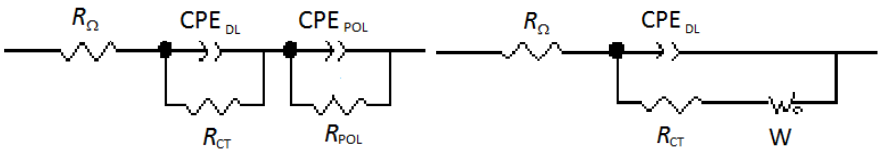

Figure 4.57. Equivalent circuits used to fit impedance data.

Table 4.20. Impedance parameters obtained by impedance fitting in the absence of redox probe in the dark.

Electrodes	E / V	R_Ω / Ω cm^2	CPE_{DL} / μF cm^{-2} s$^{α-1}$	α_{DL}	R_{CT} / Ω cm^2	CPE_{POL} / μF cm^{-2} s$^{α-1}$	α_{POL}	R_{POL} / kΩ cm^2
GC	-0.15	11.3	22.20	0.91	5898	133	0.89	9.40
	0.10	11.2	25.00	0.91	5083	150	0.88	8.08
	0.25	11.3	119.00	0.91	9440	19.8	0.92	6.06
SWCNT	-0.15	9.27	1570	1	1.28	1590	0.96	4.13
	0.10	8.89	1500	1	1.36	1600	0.97	10.90
	0.25	8.83	1680	1	1.41	1660	0.97	9.30
TiO2	-0.15	10.6	9.25	0.90	2046	10.40	0.84	355
	0.10	11.0	2.96	0.90	1634	8.01	0.84	781
	0.25	11.0	5.53	0.93	1231	8.81	0.83	781
TiO2-SWCNT	-0.15	11.3	13.10	0.85	3453	72.10	0.83	7.05
	0.10	11.3	13.00	0.85	4080	109.00	0.81	9.12
	0.25	11.3	8.14	0.89	4381	82.90	0.83	8.94

Table 4.21. Impedance parameters obtained by impedance fitting in the absence of redox probe under UV.

Electrodes	E / V	R_Ω / Ω cm^2	CPE_{DL} / μF cm^{-2} s$^{\alpha-1}$	α_{DL}	R_{CT} / Ω cm^2	CPE_{POL} / μF cm^{-2} s$^{\alpha-1}$	α_{POL}	R_{POL} / kΩ cm^2	R_w / kΩ cm^2	τ / s	α
GC	-0.15	7.83	225	0.91	5846	28.10	0.92	4.98	-	-	-
	0.10	8.18	150	0.90	6990	22.40	0.91	5.71	-	-	-
	0.25	8.59	23.70	0.90	102	108.00	0.97	0.32	-	-	-
SWCNT	-0.15	7.11	1680	1	0.88	1600	0.96	2.63	-	-	-
	0.10	6.71	1920	1	0.83	1600	0.97	8.54	-	-	-
	0.25	6.65	1920	1	0.89	1670	0.97	6.70	-	-	-
TiO2	-0.15	11.16	8.54	1	2469	11.70	0.85	59	-	-	-
	0.10	11.25	7.44	1	4744	7.06	0.88	155	-	-	-
	0.25	11.64	7.30	1	4340	6.01	0.89	218	-	-	-
TiO2-SWCNT	-0.15	36.96	12.50	0.82	1668	-	-	-	9.51	0.10	0.40
	0.10	34.00	8.30	0.85	2529	-	-	-	12.22	0.10	0.40
	0.25	23.40	5.97	0.89	1821	-	-	-	1.82	0.10	0.40

In the presence of redox probe, complex plane spectra (Figure 4.58-4.59-4.60) remain very similar to that obtained in the absence of the molecule, with a semicircle for higher frequencies, indicating the formation of the double layer, and a second semicircle for lower frequencies, corresponding to the diffusion process, which transforms in a straight line with slope < 0.5 when titania is present. In general, values of impedance decrease strongly at the potentials where redox reaction takes place. In Bode plots, frequency associated to SWCNTs time dependent process is in general lower than the others. Moreover, at – 0.15 V (SCE) under UV light, frequencies of titania based materials shift to higher frequencies, while for the others potentials the frequencies remain fixed.

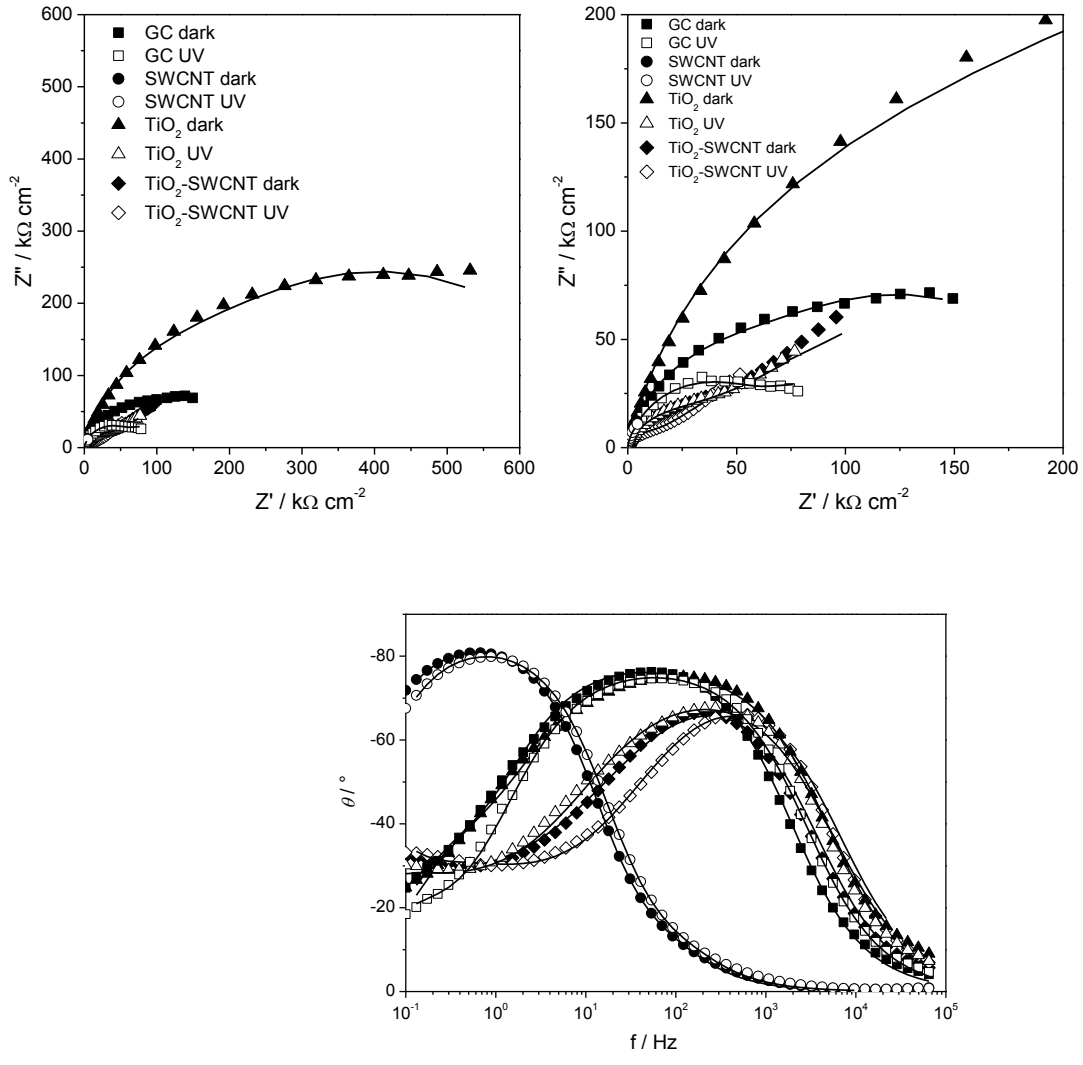

Figure 4.58. Complex plane plot and Bode plot at – 0.15 V in the presence of redox probe.

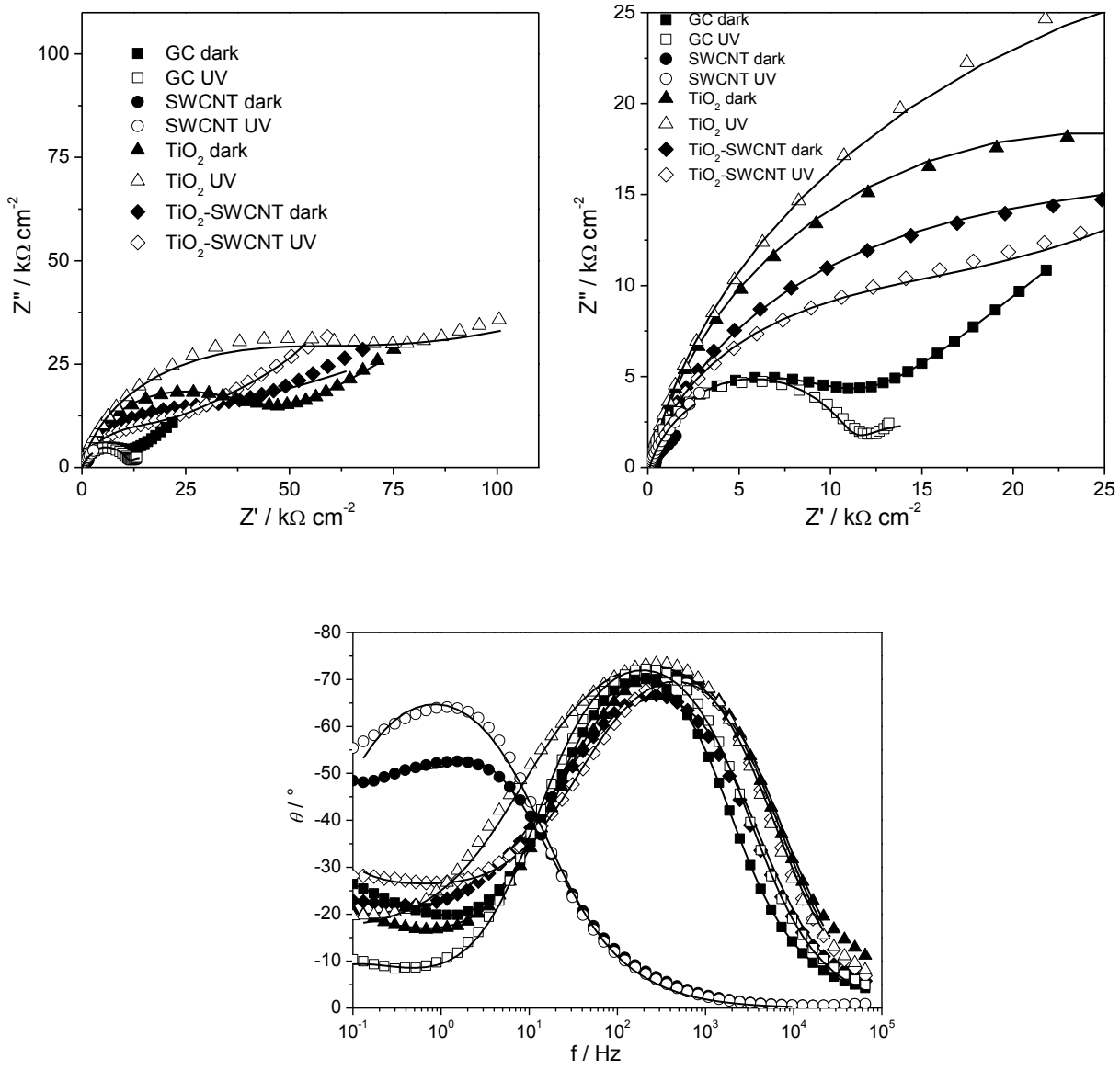

Figure 4.59. Complex plane plot and Bode plot at + 0.10 V in the presence of redox probe.

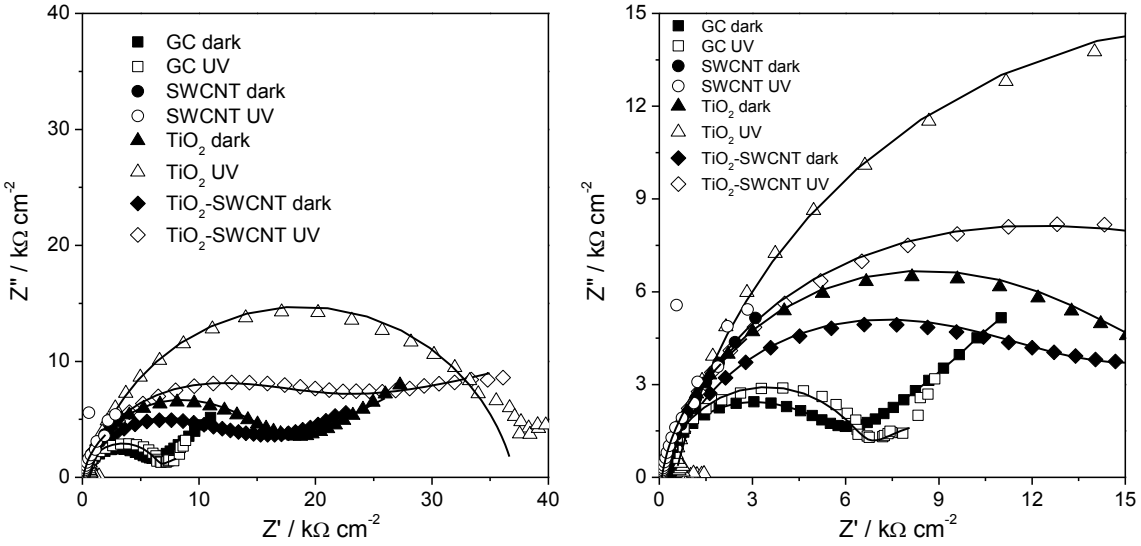

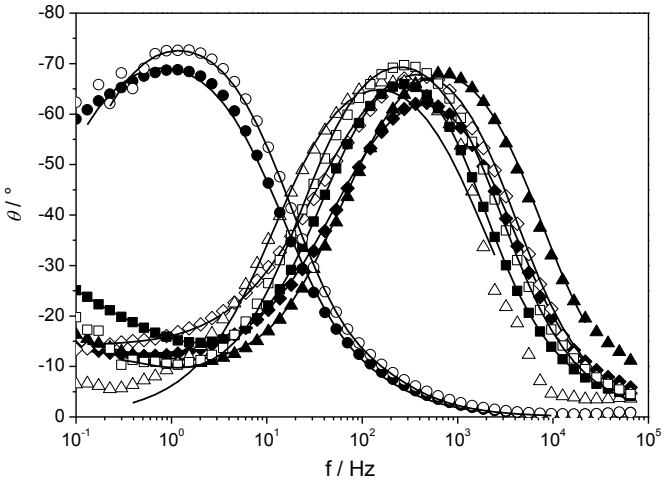

Figure 4.60. Complex plane plot and Bode plot at + 0.25 V in the presence of redox probe.

Equivalent circuits used to fit impedance spectra are presented in Figure 4.61, while Table 4.22-4.23 reports the corresponding parameters obtained from the fitting. Also in this case, charge transfer resistance is high for materials containing titanium dioxide, while when only SWCNTs are present, the lowest resistance and the highest capacitance are obtained. When UV light is used, no changes for GC and SWCNTs are registered, while in the case of titania resistances become higher, probably due to interference in the charge transfer of the redox probe caused by titania excited electrons.

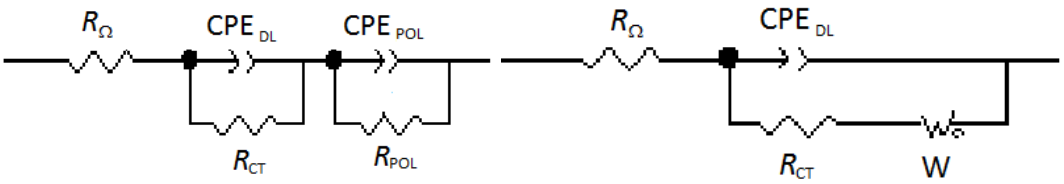

Figure 4.61. Equivalent circuits used to fit impedance data.

Table 4.22. Impedance parameters obtained by impedance fitting in the presence of redox probe in the dark.

Electrodes	E / V	R_Ω / Ω cm^2	CPE_{DL} / μF cm^{-2} $s^{\alpha-1}$	α_{DL}	R_{CT} / Ω cm^2	CPE_{POL} / μF cm^{-2} $s^{\alpha-1}$	α_{POL}	R_{POL} / kΩ cm^2	R_w / kΩ cm^2	τ / s	α
GC	-0.15	9.23	33.50	0.89	4894	104	0.89	10.10	-	-	-
	0.10	9.07	19.50	0.91	715	-	-	-	3.58	0.18	0.47
	0.25	9.18	18.50	0.92	371	-	-	-	1.77	0.21	0.46
SWCNT	-0.15	7.31	1800	1	0.94	1610	0.96	3.60	-	-	-
	0.10	7.09	8240	1	0.09	3220	0.83	0.85	-	-	-
	0.25	6.78	4310	1	0.23	2770	0.86	1.12	-	-	-
TiO2	-0.15	18.30	6.80	0.87	17530	-	-	-	151	0.10	0.47
	0.10	14.70	5.33	0.88	2253	-	-	-	1.18	0.10	0.49
	0.25	14.88	4.44	0.90	846	-	-	-	0.43	0.10	0.46
TiO2-SWCNT	-0.15	18.73	9.10	0.87	1450	-	-	-	2.97	0.10	0.46
	0.10	18.92	7.88	0.88	891	-	-	-	2.29	0.10	0.42
	0.25	19.87	7.18	0.88	364	-	-	-	0.61	0.10	0.41

Table 4.23. Impedance parameters obtained by impedance fitting in the presence of redox probe under UV.

Electrodes	E / V	R_Ω / Ω cm^2	CPE_{DL} / μF cm^{-2} $s^{\alpha-1}$	α_{DL}	R_{CT} / Ω cm^2	CPE_{POL} / μF cm^{-2} $s^{\alpha-1}$	α_{POL}	R_{POL} / kΩ cm^2	R_w / kΩ cm^2	τ / s	α
GC	-0.15	5.45	38.30	0.87	4391	487	0.88	4.03	-	-	-
	0.10	5.32	25.30	0.90	780	3730	0.72	0.49	-	-	-
	0.25	5.95	3220	0.73	379	23	0.91	0.46	-	-	-
SWCNT	-0.15	5.80	1820	1	0.67	1680	0.95	2.64	-	-	-
	0.10	5.55	1110	1	10.11	7340	0.74	0.49	-	-	-
	0.25	5.58	2370	1	0.41	2220	0.91	0.88	-	-	-
TiO2	-0.15	9.89	16.90	0.83	1287	-	-	-	18.30	0.10	0.49
	0.10	10.86	7.99	0.89	1965	-	-	-	3.90	0.10	0.40
	0.25	10.54	9.53	0.85	2577	-	-	-	-	-	-
TiO2-SWCNT	-0.15	9.80	11.10	0.86	367	-	-	-	17.03	0.10	0.41
	0.10	11.13	6.39	0.91	689	-	-	-	113	0.10	0.43
	0.25	10.56	6.10	0.92	851	-	-	-	1.36	0.10	0.49

4.2.6.4. Conclusions

The new materials have been extensively characterized to understand the behaviour of single walled carbon nanotubes and titanium dioxide nanorods from an electrochemical point of view. The characterization was performed in the dark or under UV light, considering the photoreactivity of titania.

Cyclic voltammetry showed that the highest peak current, capacitance and reversibility can be obtained with SWCNTs, while titanium dioxide with or without SWCNTs had worse performances than GC. Moreover, sample containing titania showed differences under UV irradiation, with the total disappearance of the peak, the loss of diffusional control and a decrease in the slope of the Randles-Sevcik plot, ascribable only to the change of diffusion of the redox probe caused by the production of titania excited electrons. These differences between dark and UV and SWCNTs and TiO_2 can be observed also in impedance results. Resistance to charge transfer was higher when titanium dioxide is present, in particular together with SWCNTs, but when UV light was on, this resistance decreased, probably for the contribution of excited electrons. As expected, no changes between dark and light can be seen in the case of bare electrode and SWCNTs alone.

These results showed that the use of combined compounds with different characteristic caused deep changes in the properties of the materials. In fact, the use of highly conductive material in combination with semiconductive material with activity under UV light produced a more resistive and less capacitive composite, whose properties can be changed by UV irradiation.

Future developments will consider the use of multi-walled carbon nanotubes to improve conductivity and different types and shapes of titanium dioxide to find the best material for electrochemical purposes. The idea is to develop electrodes with at the same time good electroanalytical performances towards different types of pollutants and self-cleaning properties due to photoactivity of titanium dioxide.

5. Conducting Polymers

5.1. Introduction

The characteristic of conduction is a key property essential for many applications, particularly in the field of sensors and electroanalytical chemistry. For this reason, research in this area is always in rapid growth. The large number of organic compounds which effectively are able to transport charges can be divided in three classes: charge transfer complexes, organometallic species and conducting polymers (Gerard, Chaubey, & Malhotra, 2002). This chapter is focused on the work done during this PhD thesis on the last class of compounds.

Traditionally, polymers were designed as insulators and any electrical conduction was generally regarded as an undesirable phenomenon caused by loosely bound protons. In the last decades, an opposite trend has started, which consider the utilization of ionic conductivity of polymeric systems. The active research on thermodynamic and kinetic properties of ion conducting polymers has found applications in electrochemical systems, such as in power sources, sensors, and the development of all-solid-state electrochemical devices (Inzelt, Pineri, Schultze, & Vorotyntsev, 2000).

Research about preparation, characterization and application of electrochemically active, electronically conducting polymeric systems is still growing in importance for two major reasons. Firstly, the mechanism of charge transfer and charge transport processes occurring in the course of redox reactions of conducting polymeric materials is still partially unknown. Secondly, these polymers have a wide range of promising applications in the field of energy

storage, electrocatalysis, organic electrochemistry, bioelectrochemistry, photoelectrochemistry, electroanalysis, sensors, electrochromic displays, microsystem technologies, electronic devices, microwave screening and corrosion protection (Inzelt et al., 2000).

The fundamental nature of charge propagation is completely understood, considering that the transport of electrons can occur by electron exchange reaction between redox sites in redox polymers and by motion of delocalized electrons through conjugated systems in the case of conjugated polymers. Moreover, the charge is also carried by the motion of non-electroactive ions during electrolysis. Nevertheless, considering the diversity and complexity of these systems, much research is still needed to obtain a detailed knowledge of all static and dynamic processes of interacting molecules in the polymeric network (Inzelt et al., 2000).

Conductive polymers show interesting electrical and optical properties (Bănică, 2012), previously found only in inorganic systems, and for this reason they are called “synthetic metals” (Ates, 2013; Gerard et al., 2002). They can be divided into two classes, characterized by two types of conduction: electron conducting polymers and proton conducting polymers (Inzelt et al., 2000).

The first class of compounds have a conjugated chain structure, which presents an extended π-bond system, leading to the formation of broad valence and conduction bands. Typical examples are polyacetylene, polypyrrole, polythiophene and polyaniline and they can be generated by chemical or electrochemical synthesis (Gerard et al., 2002; C. Li, Bai, & Shi, 2009). The chemical method is based on oxidative coupling and allows larger-scale production and

post-covalent modification, but has the disadvantages of complicated synthesis and impossibility to produce thin films (Gerard et al., 2002; X. Li et al., 2012). The electrochemical procedure considers the electropolymerization via galvanostatic, potentiostatic and dynamic procedure, showing the advantages of thin film formation, easy synthesis, entrapment of molecules and simultaneous doping, but causes difficulties in removal of the film and post-covalent modification (Gerard et al., 2002; X. Li et al., 2012). After synthesis, the neutral conjugated polymer can be converted into semi-conductive or conductive through chemical or electrochemical reactions, producing doped polymers or composites (Ahuja & Kumar, 2009; Janáky & Visy, 2013; C. Li et al., 2009). This type of compounds find application as fuel cells, electrochemical capacitors, batteries, memory devices, electrochromic devices, electrochemical actuators, field emission devices, superhydrophobic coatings and (bio)sensors (Ravichandran, Sundarrajan, Venugopal, Mukherjee, & Ramakrishna, 2012; Xiao et al., 2012). In particular, their use in the field of electrochemical sensors seems to be very promising, since they allow the enhancement of speed, sensitivity and versatility. Among all types of conjugated polymers, electroactive polymers seem to have the best qualities for sensor construction (Yang, 2012). Besides the high conductivity, they can act as electron donors/acceptors, exhibiting electrocatalytic effects and the possibility of redox-mediation. Polyphenazines (Pauliukaite, Ghica, Barsan, & Brett, 2010) are a class of electroactive polymers introduced successfully in the 1990s to build new and very sensitive modified electrodes. These types of sensor can detect a wide range of organic and inorganic compounds, such as NADH, nitrites, cysteine, haemoglobin, carboxylic acids, vitamin B6 and epinephrine, using different techniques, such as cyclic

voltammetry, pulsed methods and amperometry, also being used for the construction of biosensors for alcohol, acetaldehyde, glucose, glycerol and pyruvate.

The second class of conducting polymers shows a cation/proton conductivity along the polymer backbone thanks to the presence of carboxylated or sulfonated groups with a cationic counter ion, whose mobility can be increased by water swelling. For this peculiarity, they present low electrical resistance (obtained increasing ion exchange capacity and water content and decreasing membrane thickness), high permeoselectivity for anions and nonionized molecules, good mechanical and chemical stability over long periods (Inzelt et al., 2000). Properties depend on many factors, such as the chemical nature of the polymer backbone, the polymer molecular weight and molecular weight distribution, the nature of the solvent used for casting and the possible presence of residual solvent in the polymeric film (GUAN, DAI, LI, LIU, & XU, 2006). They find application in cell separators, chloro-alkali electrocatalysis, effluent treatment, recycling and energy production in fuel cells (Inzelt et al., 2000; Jannasch, 2003; Litster & McLean, 2004), but their use in electroanalysis is not extensively explored, except for Nafion membrane (Desimoni & Brunetti, 2012; Inzelt et al., 2000).

Both types of conducting polymers can provide several advantages in electroanalytical field, as electrocatalytic activity, easily diffusion of small ions and molecules into the polymer, increase of active surface area, anti-fouling capability and sample preconcentration (X. Li et al., 2012).

Results presented in this chapter consider both classes of conducting polymers and, in particular, two specific compounds, showing through their electrochemical characterization their applicability to electroanalysis. Polymer employed are:

- Poly(Brilliant Green), belonging to electron conducting polymer class;
- Poly(Aryl Ether Sulfone), belonging to proton conducting polymer class.

5.2. Electron Conducting Polymers

5.2.1. Poly(Brilliant Green)

Polytriphenylmethane dyes (Hu, Jiao, Sun, & You, 2006; Yi, Qu, & Huang, 2007) are a new class of electroactive conjugated polymers, which are very similar to polyphenazines, with the only difference of an open and ionized structure. This property can further improve electrode performances, for fast charge transfer and for catalytic ability in ionic transport.

Their use in the field of sensors is up to now very limited, concerning only one dye, Malachite Green (MG), successfully electropolymerized on glassy carbon electrodes (Wan, Wang, Wang, & Yang, 2006) and tested for the detection of dopamine (Xiaoxia Wang, Yang, Wan, & Wang, 2007), NADH and ascorbic acid (S.-M. Chen, Chen, & Thangamuthu, 2007).

In this paragraph another dye, Brilliant Green (BG) (Figure 5.1), was considered for application in electroanalysis. It belongs to the triphenylmethane family, the same as MG, and has been used as a biological stain and bacteriostatic agent in culture media and veterinary medicine (Mittal, Kaur, & Mittal, 2008; Nandi, Goswami, & Purkait, 2009); however, it has never been used previously in the field of sensors, excepting for ascorbate (M. Emilia Ghica, Wintersteller, & Brett, 2013).

To further improve electrode performances, electroactive polymers can be associated with other conductive polymers, such as poly(3,4-ethylenedioxythiophene) (PEDOT), or with carbon nanotubes.

In particular, PEDOT shows high conductivity, moderate band gap, low oxidation potential, high chemical stability in aqueous solutions and a good biocompatibility with biological media (Breiby, Samuelsen, Groenendaal, & Struth, 2002; Crispin et al., 2006), which permits its application in the field of supercapacitors and more recently in electrochemistry. PEDOT can be used alone (Pigani et al., 2011; L. Zhang et al., 2012), in combination with electroactive polymers to obtain composites with improved properties (Gonçalves, Ghica, & Brett, 2011; Kakhki, Barsan, Shams, & Brett, 2012), or in combination with nanoparticles (Thiagarajan, Rajkumar, & Chen, 2012), to improve the performance of different types of sensors.

The electrode architecture developed in this part of Thesis contains, beside PEDOT, carbon nanotube (CNTs) (Gooding, 2005; C. N. Rao, Satishkumar, Govindaraj, & Nath, 2001), since the association of CNTs and conducting polymers, initially used for energy conversion and storage purposes (Lota, Fic, & Frackowiak, 2011), is very attractive, due to the combination of the complementary properties of polymers and CNTs (Valcárcel, Simonet, Cárdenas, & Suárez, 2005), already discussed. In the recent Literature, very sensitive electrodes based on CNTs and conducting polymers were reported for the detection of hydrogen peroxide (Peña, Bertotti, & Brett, 2011), glucose (Chiu, Yu, Yen, & Chen, 2009; Mariana Emilia Ghica & Brett, 2010) and organochlorine pesticides (Abirama Sundari & Manisankar, 2010). However, only one example

of electrodes with CNTs in combination with polytriphenylmethanes was found, poly(malachite green) for the detection of catechol and quinol (Umasankar, Periasamy, & Chen, 2011).

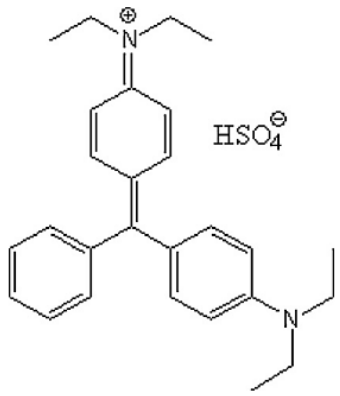

Figure 5.1. Chemical structure of brilliant green monomer

5.2.2. Materials and Methods

Commercially available carbon film electrodes (CFEs) were pre-treated in 0.2 M NaCl by cycling the potential 10 times between -1.0 and +1.0 V (SCE) at a scan rate of 100 mV s^{-1} in order to obtain a reproducible surface.

Brilliant Green electropolymerisation

Before electropolymerisation the electrodes were pre-treated in 0.1 M sulphuric acid for 10 cycles from -1.0 V up to +1.2 V (SCE) at a scan rate of 100 mV s^{-1}.

For electropolymerisation, 1 mM monomer solution was prepared by dissolving the appropriate quantity of BG in 0.1 M Mc Ilvaine buffer pH 4.0. Then, BG was electropolymerised by cycling the potential for 10 times from -1.0 V up to +1.2 V (SCE) with 100 mV s^{-1} scan rate.

EDOT electropolymerisation

EDOT was electropolymerised as reported in (Kakhki et al., 2012). The appropriate amount of monomer was dissolved in 0.1 M 4-styrenesulfonic acid sodium salt hydrate (NaSS) to obtain a concentration of 0.01 M and the solution was heated and stirred for 30 min until complete dissolution of the monomer. EDOT was then electropolymerised by cycling the potential (10 cycles) between -0.6 V and +1.2 V (SCE) at 50 mV s^{-1}.

Carbon nanotubes functionalization

Carbon nanotubes were purified and functionalised by stirring them in 5 M nitric acid for one night, filtered on a filter of paper and washed with water until neutral pH. The powder was dried in the oven at 80ºC for one night and collected. This procedure allowed to remove metal catalysts and amorphous carbon, derived from the synthetic process, and to functionalize the end of CNTs with –COOH groups.

A solution containing 1% chitosan and 1% acetic acid was prepared and used to form a 1% CNT suspension and sonicated in an ultrasound bath for 3 h. 10 µL were placed on the electrode by drop-casting and left to dry for one hour, before dropping another 10 µL. Afterwards, electrodes were left to dry in air, for at least 24 h.

Biosensor preparation

GOx and AlOx were immobilised using cross-linking with glutaraldehyde (GA) after electrode modifications. A solution was prepared by mixing the enzyme together with BSA in 0.1M phosphate buffer saline (NaPBS) pH 7.0 in concentration 1% w/v GOx + 4% w/v BSA or 5% w/v AlcOx + 10% w/v BSA, as reported in precedent works (Barsan & Brett, 2008, 2009). A volume of

10 µl of enzyme solution was then mixed with 5 µl GA (2.5%, v/v diluted in water). 10 µl of this mixture was dropped on the electrode surface and left to dry at room temperature for 4 h before the use.

The electrodes were left at 4 °C in their electrolyte after the first measurement.

Types of electrodes

Different architectures were studied in order to understand the role of each compound (PBG, PEDOT, CNT) and to find the best structure for sensing purposes. The carbon resistor electrodes were modified as follows:

- PBG/CFE, PEDOT/CFE, CNT/CFE: each compound was deposited or electropolymerised alone on the CFE, without other modification;
- PEDOT/PBG/CFE and CNT/PBG/CFE: PBG was deposited on the CFE and covered with PEDOT or CNT;
- PBG/PEDOT/CFE and PBG/CNT/CFE: PBG was electropolymerised on the top of the electrode after PEDOT or CNT deposition;
- PEDOT/CNT/CFE and CNT/PEDOT/CFE: electrodes without PBG, for comparison.

All the electrodes were left in air at least for 24 h at ambient temperature before use.

Two types of electrodes were chosen for the production of biosensors, since they gave better results in the determination of hydrogen peroxide:

- CNT/PBG/CFE: PBG was deposited on the CFE and covered with CNT;

- CNT/PEDOT/CFE: PEDOT was deposited on the CFE and covered with CNT.

5.2.3. Results and Discussion

Firstly, BG was electropolymerised on CFE and the relative cyclic voltammograms are shown in Figure 5.2. At high positive potentials around 1.0 V during the first four cycles, the formation of cation radicals can be observed. From the 4^{th} to the 10^{th} cycle, the oxidation current at 1.0 V begins to decrease, probably due to the polymer formed that impedes the monomer to reach the electrode surface. When BG is electropolymerised on CNT/CFE, a continuous increase of the corresponding polymer peaks at + 0.3, + 0.5, - 0.5 and -0.7 V is evident, indicating that PBG is electropolymerised until the last cycle, since the more open structure of CNT allows the passage of the monomer. The electropolymerisation of BG on PEDOT is demonstrated by the decrease in the capacitive currents for PEDOT with each cycle, since PBG enters in the structure of PEDOT, covering the polymer. For comparison, EDOT was also electropolymerised on CNT/CFE and on PBG/CFE. In the first case, the traditional increase of the capacitive current due to PEDOT formation is not so evident, since CNT are already very capacitive, while in the second case the profiles of CV are very similar to those recorded at the bare electrode, but with low current, probably for the diffusion barrier exhibited by PBG.

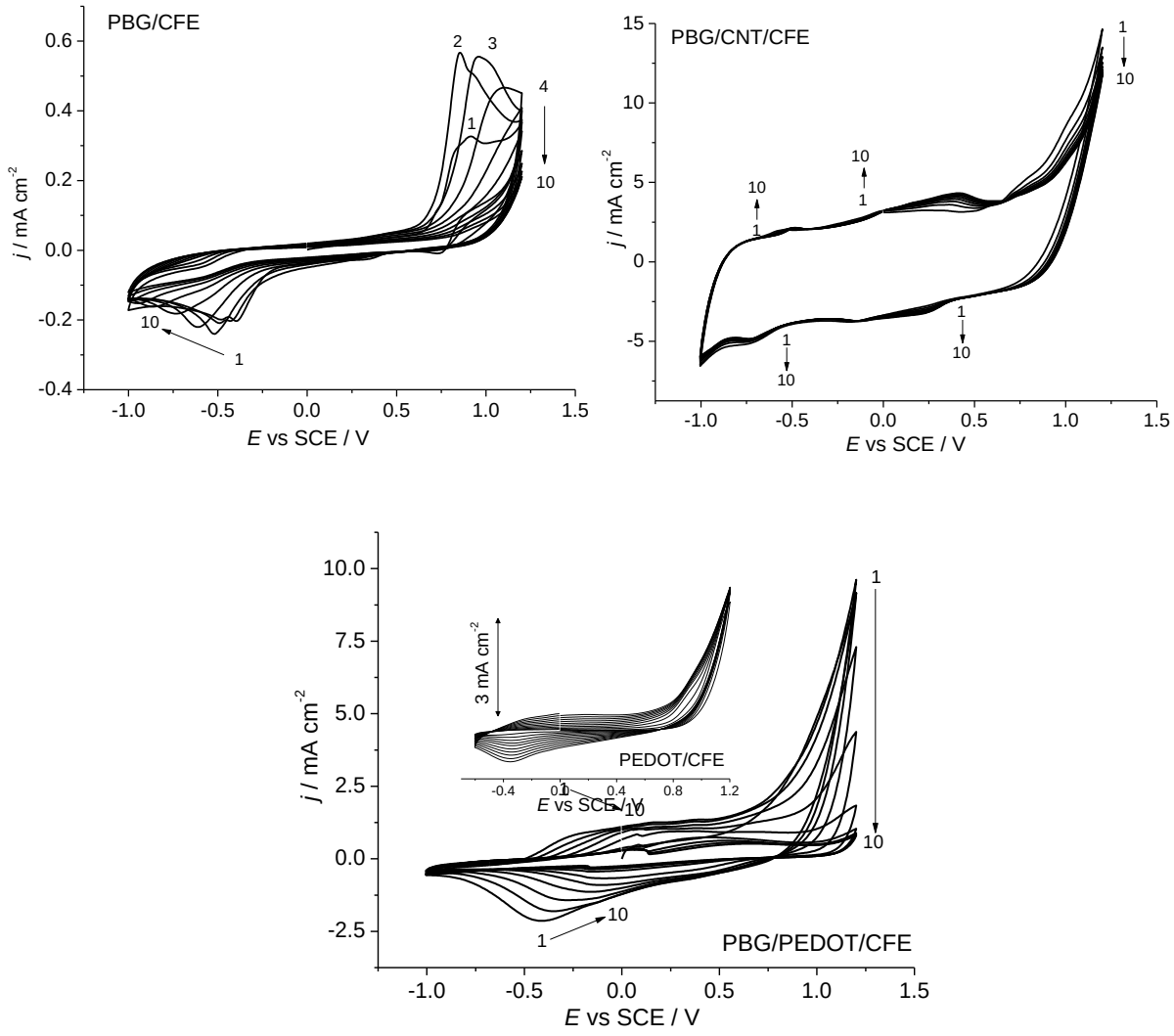

Figure 5.2. Electropolymerisation of BG at CFE (a), CNT/CFE (b) and PEDOT/CFE (c) from a solution containing 1 mM monomer in McIlvaine buffer pH 4.0; 10 scans at 100 mV s^{-1}. The inset shows the electropolymerisation of PEDOT at CFE in 0.1 M NaPSS; 10 scans at 50 mV s^{-1}.

Cyclic voltammagrams were recorded in 0.1 M KCl for all the electrodes at different scan rates (10-200 mV s^{-1}) and they show a linear dependence of the peak current with the square root of the scan rate, indicating an electrochemical process controlled by diffusion of the counterion. Table 5.1 reports the slope of these linear plots, allowing a comparison about how diffusion occurs at different electrodes. For PBG/CFE, the slope is two or three orders of magnitude lower than PEDOT/CFE and CNT/CFE, respectively, demonstrating difficult diffusion through PBG. The same behaviour can be observed when PBG is on the top of the electrodes

(PBG/CNT/CFE and PBG/PEDOT/CFE), since the slopes are lower than those for CNT and PEDOT alone, also in this case due to the compact structure of PBG film. Moreover, comparison of the slopes allows to evaluate the architecture, containing CNT in different positions, with better diffusion. Indeed, CNT on the top have higher values than CNT covered with polymers, since in the opposite case polymers can fill the porous structure of CNT, slowing diffusion.

Table 5.1 presents also capacitance values, showing an increase for electrodes with CNT, including that with PBG, which is two orders of magnitude higher than PBG alone. The presence of PEDOT together with CNT leads to the highest values of capacitance, due to the capacitive contribution of both.

Table 5.1. Slopes of plots of j_p vs. $v^{1/2}$ and capacitance values calculated from the slope of the plot of j vs. v (cyclic voltammograms recorded in 0.1 M KCl).

Electrode	*anodic slope* $\mu A\ cm^{-2}\ mV\ s^{-1}$	*cathodic slope* $\mu A\ cm^{-2}\ mV\ s^{-1}$	C / $mF\ cm^{-2}$
PBG/CFE	0.03	0.02	0.1
CNT/CFE	21.0	16.1	14.4
PEDOT/CFE	3.0	-	4.2
CNT/PEDOT/CFE	25.0	-	22.8
PEDOT/CNT/CFE	14.1	12.2	20.5
PBG/CNT/CFE	18.2	16.0	15.4
CNT/PBG/CFE	23.3	18.3	15.7
PEDOT/PBG/CFE	4.6	-	2.9
PBG/PEDOT/CFE	2.7	-	4.0

The influence of oxygen was considered, showing no influence for electrodes without PBG, while in the presence of PBG a significant decrease of the current takes place in the absence of O_2.

Operational stability experiments were undertaken by cycling the potential 100 times between – 0.7 and + 0.5 V with the scan rate of 50 mV s^{-1}. All the electrodes show a good stability, decreasing by only 7 % the cathodic and anodic initial peak current values after 100 cycles.

Electrochemical impedance spectroscopy was used to understand the physical and interface properties of the electrodes. Spectra were recorded in 0.1 M KCl at + 0.15, 0.0, - 0.2, -0.4 V (SCE), potentials chosen considering cyclic voltammograms to be in the electroactive regions of the modified electrode. Figure 5.3 shows complex plane plots, while Figure 5.4 presents the equivalent circuit used to fit impedance spectra. The values for equivalent circuit obtained from the fitting are presented in Table 5.2.

In the case of PBG/CFE, spectra present a semicircle in the higher frequency region and a straight line for lower frequencies at the first three potential, while at – 0.4 V a semicircle with large diameter substitutes the straight line. The corresponding equivalent circuits are the same for all the potentials with only an addition of resistance (R_{pol}) at – 0.4 V for the presence of the second semicircle. Decreasing the potential, the high frequency semicircle becomes bigger with a corresponding increase of R_{ct} and a decrease of CPE_{dl}, since the double layer becomes more resistive and less capacitive. The values of CPE_{pol} are higher at + 0.15 and – 0.4 V, the potentials where the polymer is electroactive, as shown by the cyclic voltammetric study.

The spectra recorded for PEDOT/CFE have very similar trend, with the only difference of a straight very capacitive line for low frequencies. Impedance values are much lower if compared with PBG/CFE, indicating a more conductive character for PEDOT. From positive to negative potentials, CPE_{dl} decreases and R_{ct} increases, since the polymer is less capacitive and more resistive in the negative potential region. α_{dl} values are very close to 0.5, illustrating the high porosity and non-uniformity of PEDOT/CFE interface. CPE_{pol} has values of three orders of magnitude higher than that for PBG/CFE and α_{pol} reaches values very close to 1, indicating a pure like capacitive behaviour of PEDOT.

CNT/CFE has a very different behaviour, since it shows a very capacitive straight line with a slope very close to 90° at low frequencies, in agreement with the high capacitive currents obtained by CV. In the high frequency region, spectra reported a straight line with slope lower than 45°, correlated to diffusional processes through the porous CNT structure. The equivalent circuit changes completely with the addition of a first Warburg element in substitution to RC circuit and of a pure capacitor as second element. For negative potentials the diffusional resistance increases and capacitance values are in agreement with cyclic voltammetric data.

In the case of PBG and CNT, the profile of the complex plane spectra is very similar to CNT/CFE and the same equivalent circuit was used for the fitting, giving very close R_W and C values. This fact shows that the overall electrical properties of the electrodes are more influenced by CNT than by the presence of the redox polymer.

Carbon nanotubes have also a dominant influence in the presence of PEDOT and in particular for PEDOT/CNT/CFE the profile and fitting values are very similar to those of CNT/CFE. On the

other hand, for CNT/PEDOT/CFE, the region at high frequencies is broader than in the case of CNT/CFE and for – 0.4 V the diffusional line becomes a very depressed semicircle. The values of R_{ct} increase for negative potentials and are higher than those of CNT/CFE and PEDOT/CNT/CFE. This different behaviour can be explained considering that probably CNT deposited on the porous structure of PEDOT are more disordered than on the bare CFE, causing a more chaotic and difficult diffusion. On the contrary, deposition of CNT on CFE and polymerisation of PEDOT on CNT give a more ordered architecture. Nevertheless, CNT/PEDOT/CFE gives the highest capacitance values, higher than CNT/CFE and PEDOT/CNT/CFE, in accordance with cyclic voltammetry.

Impedance spectra were also recorded at PEDOT/PBG/CFE and PBG/PEDOT/CFE for comparison. The profile of the complex plane plots and the equivalent circuits remain the same as for PEDOT/CFE, demonstrating the main influence of PEDOT on electrode characteristics. However, R_{ct} is higher while CPE_{dl}, α_{dl} and CPE_{pol} are lower than the values for electrode with PEDOT alone, so the association of PEDOT and PBG is worse for application in electroanalysis.

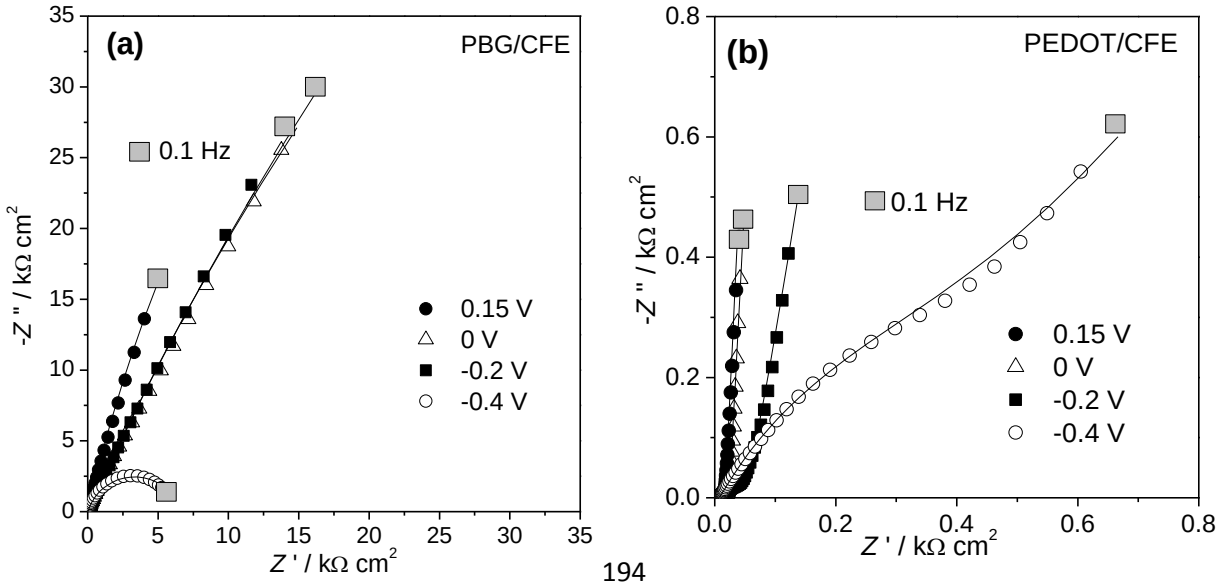

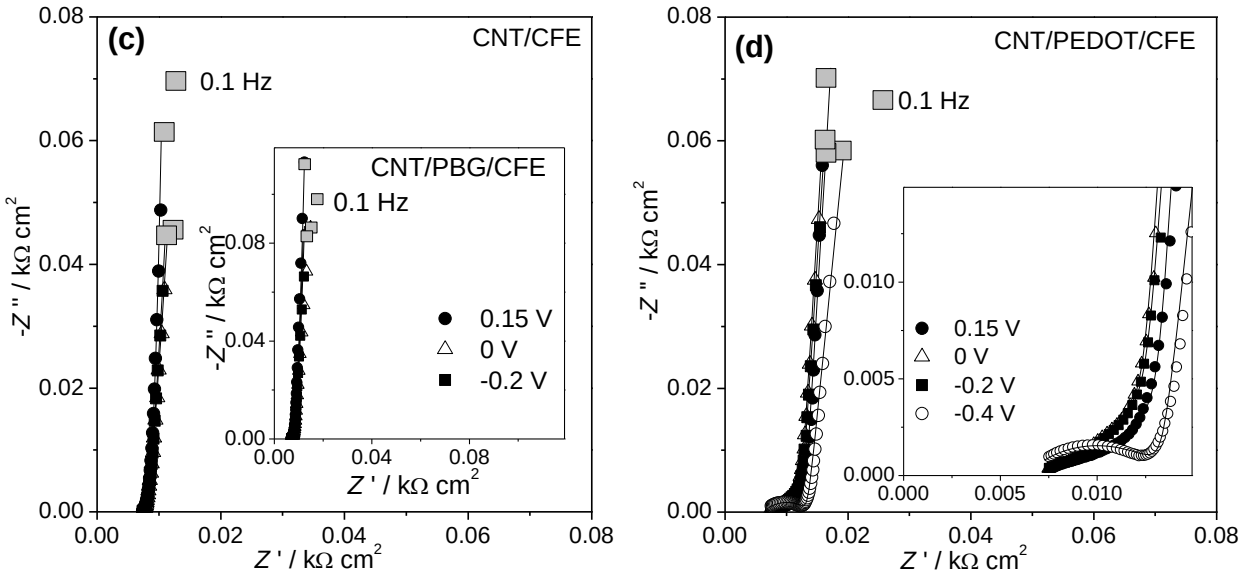

Figure 5.3. Complex plane impedance plots recorded in KCl 0.1 M for the electrodes PBG/CFE, PEDOT/CFE, CNT/CFE, CNT/PEDOT/CFE; the lines represent equivalent circuit fitting.

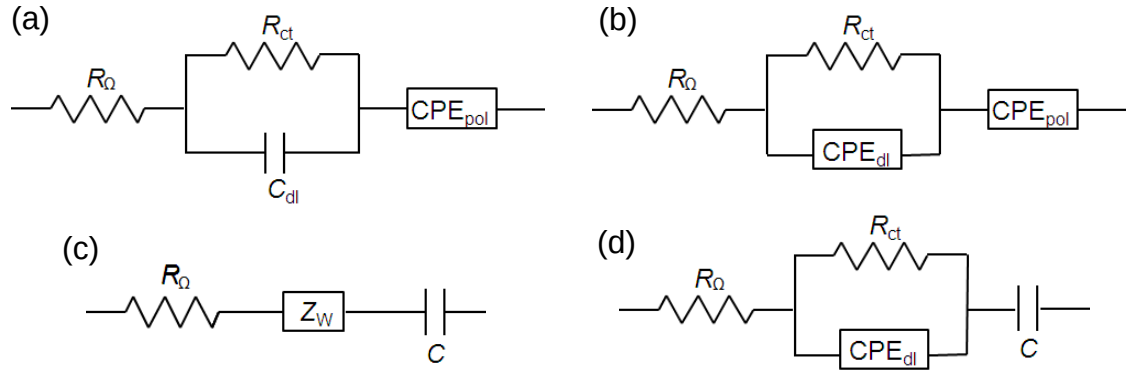

Figure 5.4. Equivalents circuits used to fit EIS spectra.

Table 4.2. Values of the parameters obtained by fitting impedance spectra for PBG/CFE, PEDOT/CFE, CNT/CFE, CNT/PBG/CFE, CNT/PEDOT/CFE.

Electrode	E_{ap} vs SCE / V	CPE_{dl} / mF cm^{-2} $s^{\alpha-1}$	α_{dl}	R_{ct} / Ω cm^2	CPE_{pol} / mF cm^{-2} $s^{\alpha-1}$	α_{pol}	R_{pol} / Ω cm^2	R_w / Ω cm^2	τ / s	α	C / mF cm^{-2}
PBG/CFE	0.15	10.7×10^{-3}	1	2.5	46.9×10^{-3}	0.84	-	-	-	-	-
	0	5.5×10^{-3}	1	2.4	19.3×10^{-3}	0.73	-	-	-	-	-
	-0.2	2.5×10^{-3}	1	6.2	26.7×10^{-3}	0.73	-	-	-	-	-
	-0.4	0.7×10^{-3}	1	10.2	64.7×10^{-3}	0.81	6.7	-	-	-	-
PEDOT/CFE	0.15	3.1	0.51	10.1	3.6	0.97	-	-	-	-	-
	0	3.5	0.50	18.0	3.4	0.97	-	-	-	-	-
	-0.2	1.9	0.55	53.4	3.0	0.90	-	-	-	-	-
	-0.4	0.7	0.74	313.6	1.3	0.60	-	-	-	-	-
CNT/CFE	0.15	-	-	-	-	-	-	0.4	0.003	0.19	13.2
	0	-	-	-	-	-	-	1.8	0.094	0.37	21.1
	-0.2	-	-	-	-	-	-	2.0	0.136	0.34	20.0
CNT/PBG/CFE	0.15	-	-	-	-	-	-	0.9	0.016	0.19	14.2
	0	-	-	-	-	-	-	1.1	0.024	0.19	18.9
	-0.2	-	-	-	-	-	-	1.0	0.022	0.19	19.5
CNT/PEDOT/CFE	0.15	-	-	-	-	-	-	5.1	0.119	0.13	24.0
	0	-	-	-	-	-	-	4.0	0.080	0.16	29.9
	-0.2	-	-	-	-	-	-	4.4	0.113	0.16	30.7
	-0.4	1.8	0.52	7.8	-	-	-	-	-	-	25.5

The influence of oxygen was also studied, because redox polymers can be oxidized in the presence of O_2 and O_2 can be reduced at the interface, affecting the homogeneity of the film. For these reasons impedance spectra were also recorded in the absence of O_2, removed from the solution by bubbling N_2 for at least 20 minutes. In particular, PBG/CFE is affected by the absence of oxygen, since R_{CT} increases and CPE_{pol} decreases only at + 0.15 and – 0.4 V, where the polymer is electroactive. Probably, the redox activity of the polymer involves or is favoured by oxygen. In the case of PEDOT/CFE, oxygen has a lower influence, showing a R_{CT} increase probably due to few hydroxyl ion formation, which may help the electron transfer at the surface. Moreover, CNT modified electrodes are not influenced at all by oxygen, showing again advantages in the use of CNT for (bio)sensor design.

The characterization of the electrodes demonstrates that each type of material used to modify the bare electrode can strongly influence its performances and its properties. To further investigate the best architecture for electroanalytical purposes, a study of electrode behaviour towards hydrogen peroxide was performed. The choice of hydrogen peroxide (W. Chen, Cai, Ren, Wen, & Zhao, 2012) is justified by its importance in pharmaceutical, clinical, environmental, mining, textile and food manufacturing applications. Moreover, hydrogen peroxide is a side product of many biochemical reactions catalyzed by many oxidase enzymes. For these reasons, H_2O_2 appears to be the best species to demonstrate the possible electrode application in the field of sensors and biosensors.

Initially, potential cycling between – 0.7 V and + 0.7 V in 0.1 M NaPBS (pH = 7) was performed for each electrode in the absence and presence of H_2O_2. Cyclic voltammograms for electrodes without carbon nanotubes do not exhibit a significant response when H_2O_2 is present, while CNT-modified electrodes show activity towards the reduction of hydrogen peroxide at around – 0.1 V, as shown

in Figure 5.5. For this reason and considering CV and EIS results, electrodes without carbon nanotubes were excluded from further studies and applications.

Chronoamperometries were performed at all the CNT-modified electrodes at 0.0 V (SCE), since at this potential electrodes still exhibit good performances and the majority of possible interferences is avoided. Figure 5.5 shows a typical chronoamperometric spectrum in the range 5-50 μM in H_2O_2 and the corresponding calibration plots.

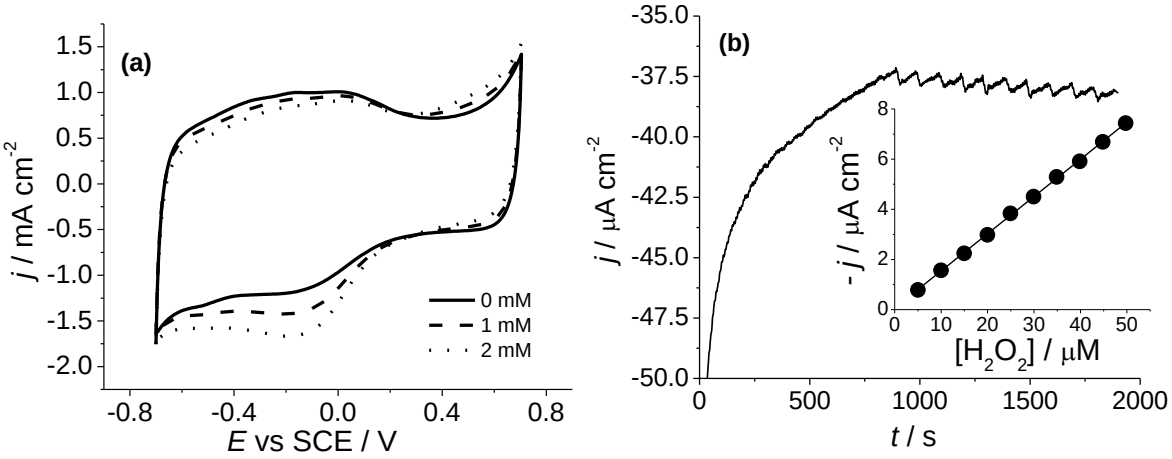

Figure 5.5. (a) Cyclic voltammograms recorded in a solution containing NaPBS 0.1 M before and after addition of H_2O_2 and (b) Amperometric response to H_2O_2 at CNT/PBG/CFE with the corresponding calibration plot shown in the inset.

For electrodes with polymers on the top (PEDOT/CNT/CFE and PBG/CNT/CFE) sensitivities are smaller, 91.4 ± 0.4 and 113.5 ± 0.6 μA cm^{-2} mM^{-1}, and detection limits are higher, 2.40 and 1.45 μM, than in the case of CNT/CFE (124.5 ± 0.4 μA cm^{-2} mM^{-1}, 1.19 μM), demonstrating that covering CNT with polymers reduces electrode activity, probably because of a decrease of active sites and surface area. On the other hand, electrodes with CNT on the top (CNT/PEDOT/CFE and CNT/PBG/CFE) show higher sensitivities and smaller limits of detection compared with CNT alone. In the case of CNT/PEDOT/CFE the improvement in sensitivity, 131.9 ± 0.5 μA cm^{-2} mM^{-1}, and LoD, 0.89 μM was expected as predicted by the high values of capacitance obtained from CV and EIS. For CNT/PBG/CFE, the detection limit of 0.91 μM is comparable with CNT/PEDOT/CFE and the best

sensitivity is obtained (151.8 ± 0.6 µA cm^{-2} mM^{-1}), indicating that PBG improves hydrogen peroxide determination, even if it does not contribute to the total capacitance.

Repeatability was also tested, preparing three new electrodes for each type and using the same conditions. In Figure 5.6 calibration plots in the low concentration range for CNT/PEDOT/CFE and CNT/PBG/CFE are shown; the points were obtained as mean values of the three electrodes and error bars represent the standard deviation of each point. Repeatability is excellent, RSD values being lower than 1 %. In the inset, an example of calibration plot for higher concentration is presented and all the electrodes show in general saturation at 6 µM H_2O_2.

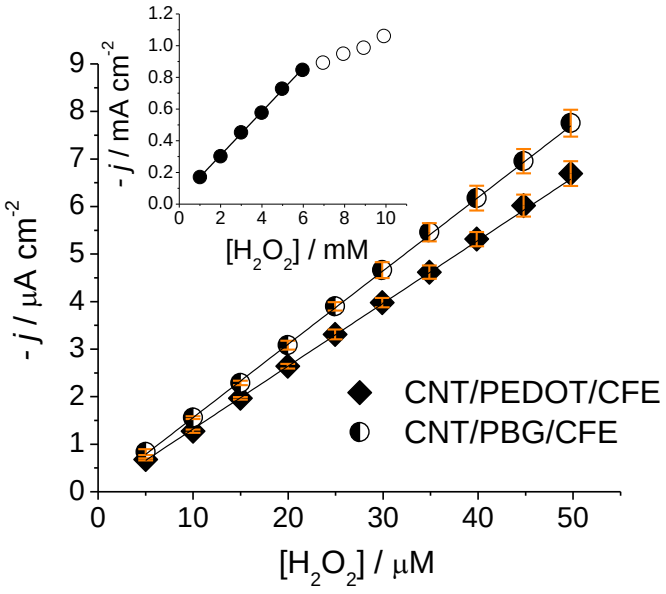

Figure 5.6. Linear calibration plots corresponding to CNT/PBG/CFE and CNT/PEDOT/CFE in NaPBS 0.1 M at 0.0 V obtained in the concentration range from 5 to 50 µM H_2O_2. Inset: typical calibration plot obtained for high concentration range.

Stability was also evaluated recording a calibration plots of 7 points in the low concentration range three times a week. The sensitivity decreases by only 10 % from its initial value after 20 days. After this period it decreases faster.

Comparison with recent (2010-2012) Literature data on hydrogen peroxide sensing at modified electrodes was also considered (Table 5.3). The values of sensitivities and operational ranges are

comparable with other types of sensors and LoDs are very similar, but this new electrode has the advantage of 0.0 V working potential, allowing the avoidance of the majority of interferences.

Table 5.3. Performance parameters of hydrogen peroxide sensors for different modified electrodes recently reported in the literature.

Electrode	Concentration Range / mM	*S* / μA $cm^{-2}mM^{-1}$	LOD / μM	Potential / V	Ref.
MnO_2/VACNTs	0.001-1.8	1001.0	0.80	+0.45	(B. Xu, Ye, Yu, & Zhang, 2010)
SiNW/AgNPs	0.2-70	57.5	0.20	-0.45	(Yin et al., 2011)
HRP/PAM/MWCNT COOH/Au	0.086-10	194.9	26.0	-0.35	(Hua, Lin, Tsai, Chen, & Liu, 2011)
HRP/AuNPs/BC	0.0003-1.00	610.0	0.10	+0.15	(W. Wang et al., 2011)
HRP/Sulf-G	0.003-0.33	557.0	1.17	-0.35	(Q. Zhang et al., 2011)
HRP/3DAuNW	0.1-15	45.9	0.42	-0.1	(J. Xu, Shang, Luong, Razeeb, & Glennon, 2010)
Graphene/PB	0.1-15.5	408.7	0.34	+0.1	(Yao Zhang, Sun, Zhu, Shen, & Jia, 2011)
N-CNTs	0.002-0.14	24.5	0.37	+0.3	(X. Xu, Jiang, Hu, & Liu, 2010)
PB/MWCNT	0.001-5	856.0	0.02	+0.1	(Du, Wang, Qin, & Lin, 2010)
PAA-BO/Au	0.025-2.5	311.2	5.00	-0.5	(Hua, Chen, et al., 2011)
Ag-UTPNSs	0.1-90	4.5	0.57	-0.35	(Mahmoudian, Alias, Basirun, & Ebadi, 2012)
PPy/Magnetite hybrid	0-0.4	72.0	-	-0.3	(Bencsik, Janáky, Endrődi, & Visy, 2012)
CNT/PBG/CFE	0.0005-6	151.8	0.91	0.0	this work

Considering the results obtained towards hydrogen peroxide detection, the electrode with the best performance (CNT/PBG/CFE) was chosen for application in biosensoristic field and CNT/PEDOT/CFE was selected for comparison.

Among all the types of biosensors, those for the detection of glucose (J Wang, 2008) are ideal to evaluate the performances of new developed electrodes in the biosensor field and have also the potential application in food and medical areas (Oliver, Toumazou, Cass, & Johnston, 2009). Glucose Oxidase (GOx) can be considered a model enzyme since it permits the production of simple and cheap biosensors, which allow a fast evaluation of electrode performance without the addition of a cofactor, as in the case of Glucose Dehydrogenase.

Ethanol is another important analyte and its detection is required in many different areas, clinical and forensic analysis, food, pulp and beverage industries, agricultural and environmental measurements. Many analytical methods (Azevedo, Prazeres, Cabral, & Fonseca, 2005) have been developed during the years for the determination of ethanol and include the use of chemical methods, colorimetric methods, specific gravity and refractive index measurements, chromatographic and spectroscopic methods. The disadvantages of these methods are complexity, time consuming steps and requirement of previous separation processes, expensive instrumentation and trained operators, which can be overcome by the use of enzymatic methods. In particular, two enzymes have been extensively used in the determination of ethanol, Alcohol Dehydrogenase (ADH), which require the cofactor NAD+, and Alcohol Oxidase (AlOx), which already contains the cofactor FAD^{2+}. The development of ethanol biosensors usually requires a redox mediator, since the active sites of these enzymes are deeply buried in the protein limitating the electron transfer. Electroactive polymers represent an interesting solution to this problem (Barsan & Brett, 2008).

Oxygen is a very important parameter to be considered during the planning of a new biosensor based on enzymes, since it can strongly influence the performances of the electrode. In fact, the first studies about biosensors for glucose (J Wang, 2008) and also for ethanol (Azevedo et al., 2005) showed oxygen acting as cosubstrate during the enzymatic reactions. Furthermore, the

types of microorganism from which the enzyme is extracted has to be taken into consideration. In particular, GOx belongs to *Aspergillus Niger* (Geiser, 2009), which is a highly aerobic species, while AlOx is extracted by *Hansenula sp* (Gellissen et al., 2005; Ramezani-Rad et al., 2003), which is principally anaerobic. Another key point is the possibility that oxygen can influence not only the performances of enzymes, but also the behaviour of the electroactive polymer during its redox process, as already discussed (Valentina Pifferi, Barsan, Ghica, Falciola, & Brett, 2013).

The operative potential and pH conditions play an important role in biosensor activity, since they can influence the sensitivity of the detection and the possible interferences. For these reasons, these conditions were firstly taken into consideration and optimized.

In the case of glucose biosensors, 0.1 M NaPB + 0.05 M NaCl pH = 7 was chosen as supporting electrolyte (Barsan & Brett, 2009; Barsan, Carvalho, Zhong, Sun, & Brett, 2012). Figure 5.7 shows the study of working potential for CNT/PEDOT/CFE and CNT/PBG/CFE from -0.4 V to 0.0 V (SCE). For both electrodes the intensity of the signal is higher for -0.4 V, closer to the formal potential of $FAD/FADH_2$ couple, and decreases rapidly when potential is increased, reflecting the behaviour of other biosensors with GOx (Barsan & Brett, 2009; Barsan et al., 2012). A potential of -0.3 V was chosen for further amperometric experiments with the aim of minimising possible interferences, ensuring a good intensity of the signal.

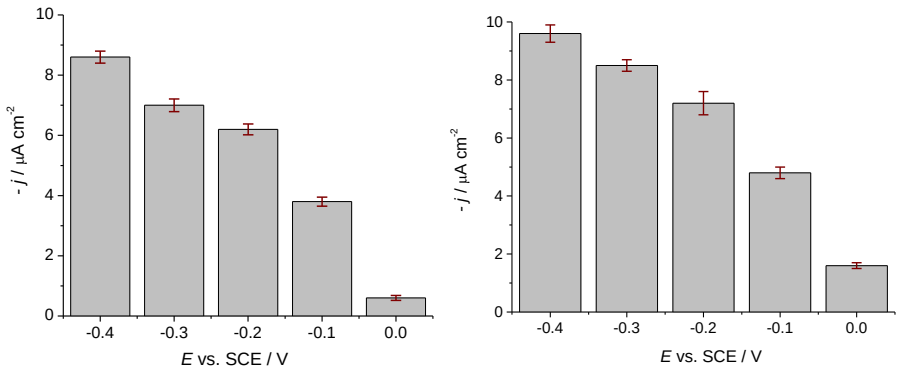

Figure 5.7. Study of applied potential for a) GOx/CNT/PEDOT/CFE and b) GOx/CNT/PBG/CFE in 0.1 M NaPBS M pH=7.

In the case of AlOx, the behaviour of the biosensor is very different for the two types of electrodes, considering the operative pH and the working potential.

Figure 5.8 reports the intensity of the signal increasing the pH from 6.5 to 9.0 for CNT/PEDOT/CFE and CNT/PBG/CFE, showing that in the case of CNT/PEDOT/CFE the optimum operative pH is 7.0, while in the case of CNT/PBG/CFE is 8.5. Another important difference is presented in Figure 5.9, where the intensity of the signal is reported varying the potential. For CNT/PEDOT/CFE the current decreases increasing the potential and it reaches the highest value closer to the formal potential of FAD/$FADH_2$ couple, as already reported for other similar biosensors (Barsan & Brett, 2008). For CNT/PBG/CFE the behaviour is completely different, since the current increases from -0.4 V to -0.2 V, with a small decrease at -0.1 V. This fact can be explained considering that PBG is a redox polymer and thanks to its redox activity it gives a good answer even at -0.1 V, where the signal of PEDOT is very low, considering its non electroactive nature.

The operative potential chosen for CNT/PEDOT/CFE was -0.3 V with the aim of minimizing possible interferences but maintaining a good response, while for CNT/PBG/CFE was -0.1 V, since the signal is already good and the potential very close to 0 V allows to avoid the majority of interferences.

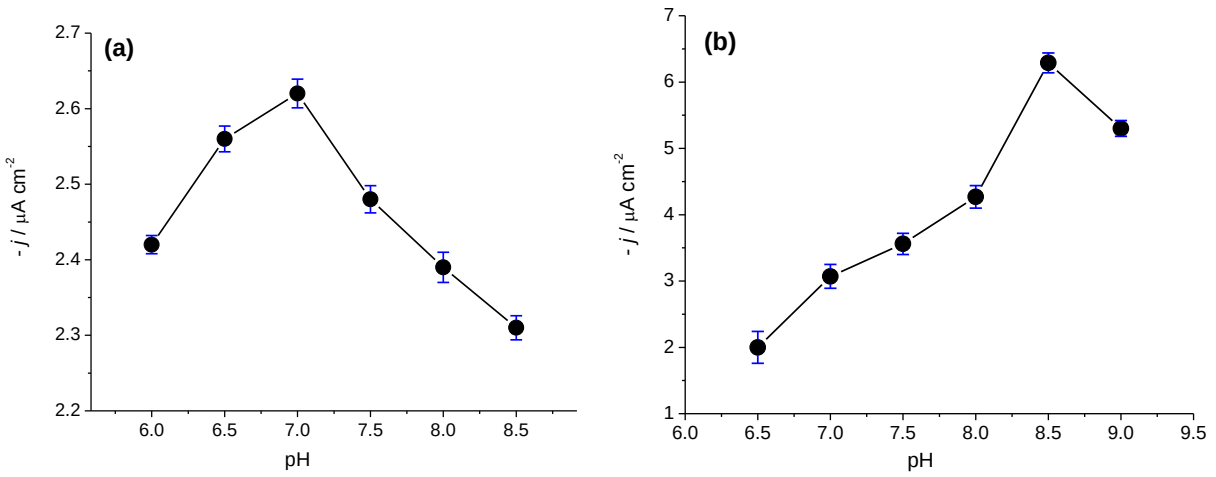

Figure 5.8. Study of solution pH at -0.3 V vs SCE for a) AlOx/CNT/PEDOT/CFE and b) AlOx/CNT/PBG/CFE.

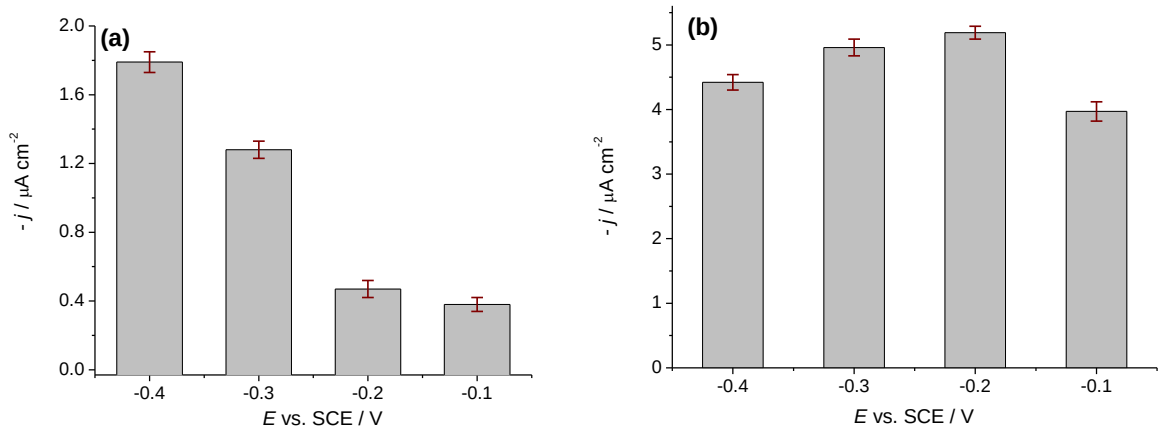

Figure 5.9. Study of potential at optimum pH of 8.5 of 0.1 M NaPBS for a) AlOx/CNT/PEDOT/CFE and b) AlOx/CNT/PBG/CFE.

After the optimization of experimental conditions, analytical parameters were evaluated.

In the case of glucose detection, calibration plots were obtained for both electrodes in 0.1 M NaPBS + 0.05 M NaCl pH = 7 at the working potential of -0.3 V for consecutive additions of 0.1 M Glucose. The typical amperometric signal is shown in Figure 5.10 with the corresponding calibration plot, which presents a dynamic range of linearity from 0.05 mM to 1.25 mM. After this value the electrode reaches saturation. Reproducibility, which was also tested preparing three different electrodes for each type, appears to be very good considering the small error bars shown in the calibration plot.

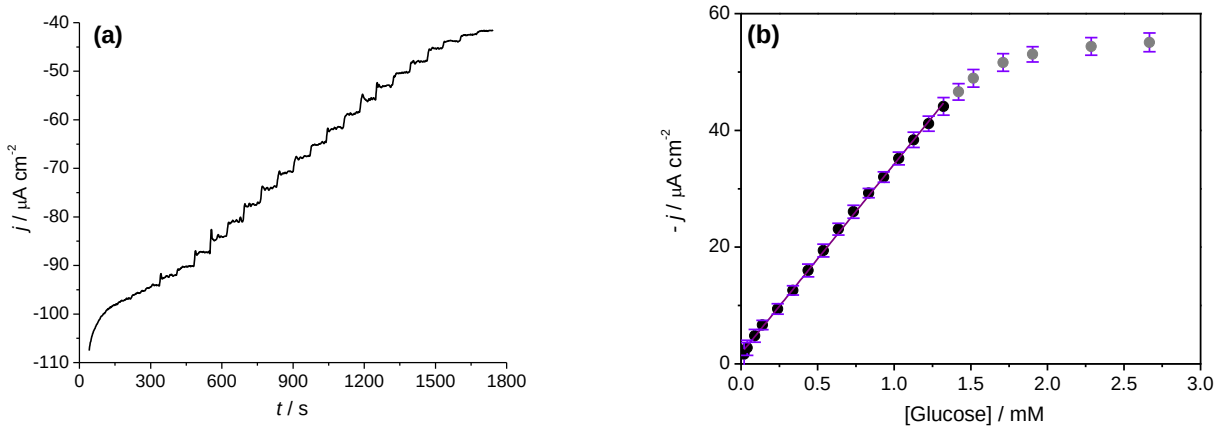

Figure 5.10. a) Amperometric response to glucose at -0.3 V vs. SCE in 0.1 M NaPBS pH=7.0 at GOx/CNT/PBG/CFE and b) the corresponding calibration plot.

In the case of ethanol determination, the chosen experimental conditions were different for the two types of electrodes. For CNT/PEDOT/CFE the supporting electrolyte was 0.1 NaPBS + 0.05 NaCl pH = 7 and the working potential was -0.3 V, while for CNT/PBG/CFE the supporting electrolyte was 0.1 NaPBS + 0.05 NaCl pH = 8.5 and the working potential was -0.1 V. Figure 5.11 shows the amperometric signal for CNT/PBG/CFE, which increases for consecutive additions of 0.1 M ethanol solution without the typical amperometric steps, but according to other amperometric measurements of ethanol presented in other papers (Barsan & Brett, 2008). The corresponding calibration plot (Figure 5.11) can be obtained considering the current increase at each addition. The range of linearity covers the interval between 0.1 mM and 0.7 mM; after that the electrode reaches saturation. Reproducibility, tested on three different electrodes, was very good, as small error bars in the calibration plot show.

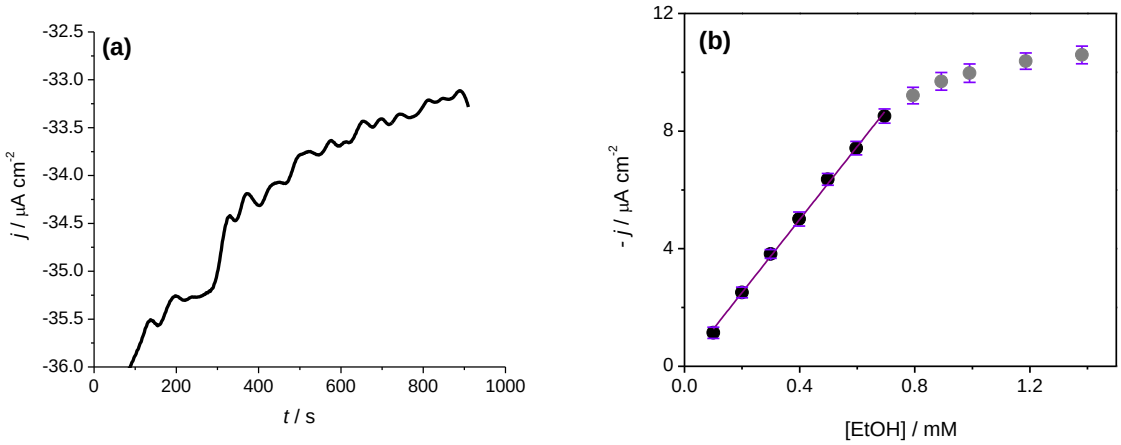

Figure 5.11. a) amperometric response to ethanol at -0.1 V vs. SCE in 0.1 M NaPBS pH=8.5 for AlOx/CNT/PBG/CFE and b) the corresponding calibration plot.7

Table 5.4 reports sensitivity and detection limits for all the electrodes and for both types of biosensors, also comparing the values with bare CFE. Sensitivity was obtained from the slope of the calibration plot, while LoD was calculated as three times the signal-to-noise ratio. For all the electrodes, sensitivity values recorded the first day (after 4 hours of drying) are smaller than for the second day (stored after the first measurement at 4 °C in its own electrolyte), probably

because of necessary hydration of the enzyme. Sensitivity values are higher and LoD values are lower for modified electrodes than for bare CFE, both for glucose and ethanol, which can not be detected at bare electrode. CNT/PBG/CFE shows better values than CNT/PEDOT/CFE. These results are in accordance with precedent results obtained for the detection of hydrogen peroxide (Valentina Pifferi, Barsan, et al., 2013), where the electrode with PBG, also if it is less capacitive than PEDOT modified electrode, shows higher sensitivity and lower detection limit, probably due to its redox nature, which can amplify the signal, allowing electrocatalysis.

Relative standard deviation was lower than 5 % for all the electrodes.

Stability was also evaluated, testing electrodes for five weeks, three times a week. GOx electrodes were stable for all the 40 days period, while for AlOx electrodes after 20 days the sensitivity began to decrease.

Table 5.4. Sensitivities and detection limits obtained at different glucose and ethanol biosensors under the optimized experimental conditions (GOx: 0.1 M NaPBS pH=7, -0.3 V vs. SCE; AlOx/CNT/PEDOT/CFE: 0.1 M NaPBS pH=7, -0.3 V vs. SCE and AlOx/CNT/PBG/CFE: 0.1 M NaPBS pH=8.5 and -0.1 V vs. SCE).

Electrode	S / μAcm^{-2}mM^{-1}		LOD / μM
	First day	Second day	
GOx/CFE	0.436 ± 0.004	0.431 ± 0.001	105.2
GOx/CNT/PEDOT/CFE	23.2 ± 0.2	40.3 ± 0.7	37.0
GOx/CNT/PBG/CFE	23.5 ± 0.2	43.6 ± 0.6	13.3
AlOx/CFE	-	-	-
AlOx/CNT/PEDOT/CFE	4.4 ± 0.1	9.3 ± 0.2	70.0
AlOx/CNT/PBG/CFE	9.2 ± 0.5	12.4 ± 0.2	29.0

Oxygen is a key parameter to be consider in biosensor field, since it can influence not only the enzymatic reaction, but also the behaviour of the electroactive polymer.

For these reasons, the influence of oxygen was studied for both biosensors considering the better architecture (CNT/PBG/CFE). Calibration plots (Figure 5.12) in different atmospheres (N_2, O_2, air) were collected with the same conditions used before, while the corresponding sensitivities are presented in Table 5.5. In the case of glucose biosensor, the presence of oxygen deeply influences the detection of glucose, since the sensitivity is higher under O_2 atmosphere, while under N_2 it decreases by 60 %. In the case of ethanol biosensor the best sensitivity is obtained in the absence of oxygen, but the difference in sensitivity is not so relevant as in the case of glucose. Probably this behaviour can be explained considering the enzymatic source, a completely aerobic bacterium for GOx and a principally anaerobic bacterium, which in same cases can behave also in the aerobic way, for AlOx. In fact, the change in sensitivity is more relevant and evident in the case of GOx.

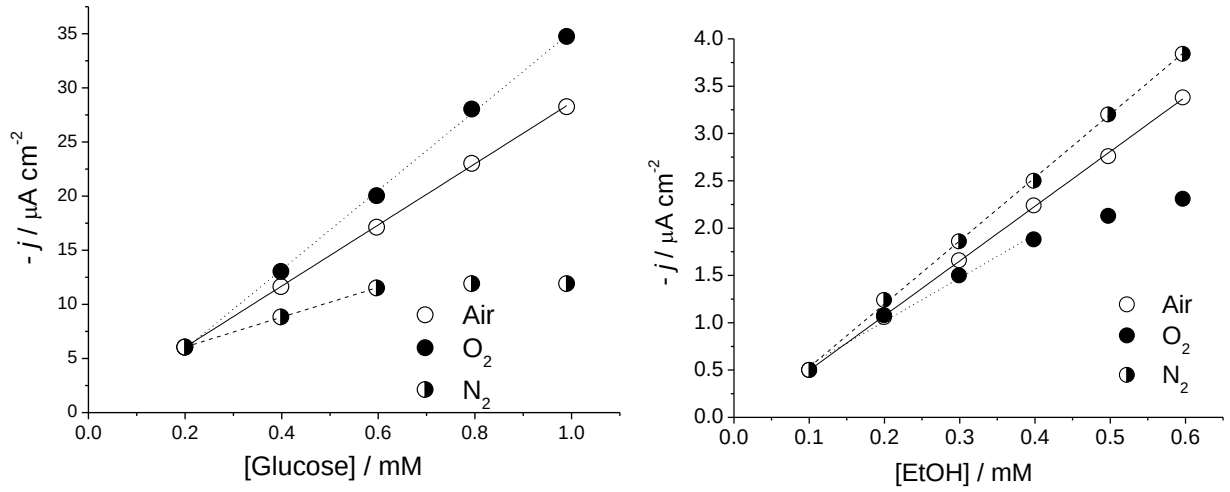

Figure 5.12. Calibration plot in buffer solutions with different oxygen content (air, oxygen and nitrogen) for GOx/CNT/PBG/CFE (-0.3 V, pH = 7) and AlOx/CNT/PBG/CFE (-0.1 V, pH = 8.5).

Table 5.5. Sensitivities obtained at GOx and AlOx CNT/PBG/CFE in 0.1 M NaPBS buffer solutions of different oxygen contents (GOx: pH=7, -0.3 V vs. SCE and AlOx: pH=8.5, -0.1 V vs. SCE).

Oxygen content %	S / µAcm^{-2}mM^{-1}	
	GOx	AlOx
100	56.7 ± 0.8	9.8 ± 0.2
21	43.6 ± 0.6	12.4 ± 0.2
0	21.4 ± 0.3	14.4 ± 0.2

The amperometric response at -0.3 V (SCE) to glucose and -0.1 V (SCE) to ethanol in the presence of acetic acid, ascorbic acid, tartaric acid, dopamine, catechol, fructose and uric acid, electroactive compounds which can probably interfere in the determination of glucose or ethanol in real samples, was measured using the CNT/PBG/CFE biosensor (Figure 5.13). Glucose or ethanol were injected before and after addition of the interfering compounds, in the same concentration of the interferents; results are shown in Table 5.6. As observed, some compounds did not give any response, particularly in the case of glucose, despite the high interferent-to-glucose or ethanol concentration ratio. The decrease of the response to glucose or ethanol was only between 2-6 %, where small oxidation currents were observed. All these results evidence the applicability of the developed biosensors for the determination of glucose or ethanol in complex matrices.

Table 5.6. Interferences at GOx and AlOx CNT/PBG/CFE biosensors; ratio of interfering compounds to glucose or ethanol 1:1.

Interfering compounds	Biosensor response in the presence of interfering compound / %	
	GOx	AlOx
Acetic acid	97	98
Ascorbic acid	94	96
Tartaric acid	100	94
Dopamine	100	98
Catechol	98	100
Fructose	100	94
Uric acid	100	95

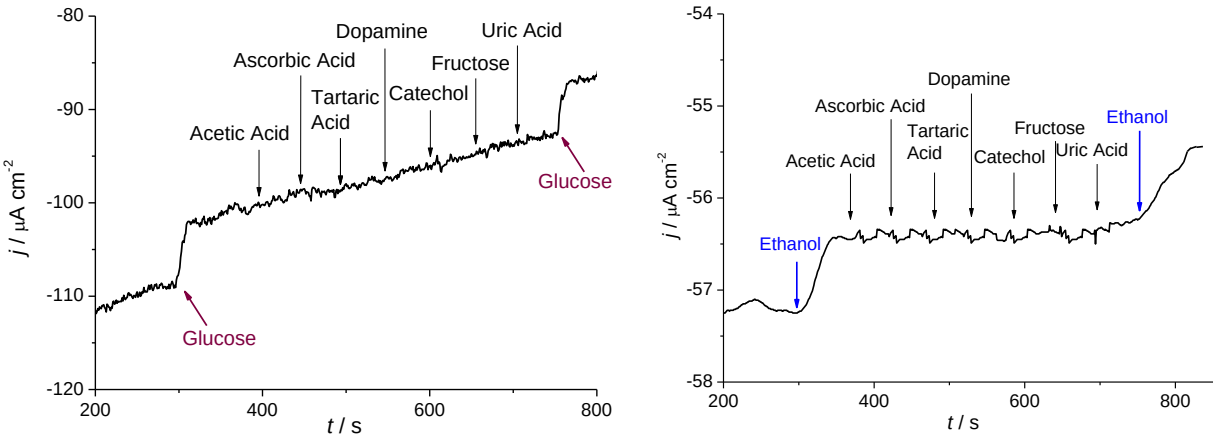

Figure 5.13. Interference studies for a) GOx/CNT/PBG/CFE (-0.3 V vs. SCE, 0.1 M NaPBS pH=7) and b) AlOx/CNT/PBG/CFE (-0.1 V vs. SCE, 0.1 M NaPBS pH=8.5).

5.2.4. Conclusions

Brilliant Green, belonging to the triphenylmethane family, has been successfully electropolymerized for the first time on bare carbon electrode (CFE) and on modified (with CNT and PEDOT) electrodes. The polymerisation is completed during the first four cycles, allowing the formation of a very compact film, as demonstrated by cyclic voltammetric studies that show lower diffusion coefficients and capacitances for the electrodes with PBG. On the contrary, when CNT are on the top of the electrode (CNT/PEDOT/CFE and CNT/PBG/CFE) the diffusion is facilitated. In general, CNT and PEDOT increase the capacitance values with the highest value recorded for CNT/PEDOT/CFE. EIS experiments confirm the results of CV, additionally showing the influence of oxygen on PBG-based electrodes.

Hydrogen peroxide determination was chosen to demonstrate the applicability of these types of electrodes and to find the best architecture. In particular, only CNT-based electrodes show activity towards H_2O_2 at 0.0 V, potential which permits to avoid the majority of interferences, and when CNT are placed on PEDOT or PBG higher sensitivities were obtained in comparison with CNT alone. The best performance was registered for CNT/PBG/CFE, indicating that PBG effectively improves H_2O_2 determination thanks to its redox activity. Reproducibility studies gave excellent results with

RSD lower than 1 % and together with electrode stability demonstrate the applicability for the development of electrochemical sensors.

The results towards hydrogen peroxide determination suggested also the applicability of these electrodes in the field of biosensors, since H_2O_2 is a side product of various biological reactions catalyzed by enzymes. In particular, among the different electrode architectures studied, CNT/PBG/CFE, which reached the best results for the determination of hydrogen peroxide, was chosen and CNT/PEDOT/CFE was used as comparison for the design of new biosensors for glucose and ethanol. Glucose oxidase from *Aspergillus Niger*, a completely aerobic bacterium, and Alcohol oxidase from *Hansenula sp*, a principally anaerobic bacterium, were chosen as enzymes.

The electrolyte pH and the operative potential were optimized, showing in the case of AlOx different behaviour for CNT/PBG/CFE and CNT/PEDOT/CFE. In fact, for PBG, the operative potential is lower than for PEDOT, showing the importance of the redox polymer in the electrode process. The electrode with the redox polymer (PBG) showed the best performance for both glucose and ethanol determination, with good sensitivity and detection limits, considering also other biosensors in the recent literature. In particular, sensitivity reached maximum values after hydration and was in general higher than in the case of the bare electrode. Reproducibility, stability and relative standard deviations were very good for both types of electrodes. The influence of oxygen was also studied, showing a relevant decrease in sensitivity for glucose detection and a slightly increase for ethanol determination under nitrogen atmosphere. This situation could be explained considering the enzyme source. Furthermore, interference studies showed the applicability of electrodes based on PBG in real samples.

5.3. Cation Conducting Polymers

5.3.1. Poly(Aryl Ether Sulfone)

Poly(Aryl Ether Sulfone)s (Figure 5.14), commonly called PES, are well-known engineered thermoplastic materials, with excellent properties thanks to their aromatic skeleton and charged groups, such as thermal and mechanical strength, resistance to oxidation and acid catalyzed hydrolysis (Herbert, Ghassemi, & Hay, 1997; Lakshmi et al., 2006). Moreover, they present high glass transition temperature, good solubility in polar aprotic and halogenated solvents, radiation stability, low flammability and toughness, and they are inexpensive compounds (Herbert et al., 1997). For their properties, they are used in many fields, as materials for composite matrices, high temperature films, adhesive and electronic parts, electrodialysis, desalination, gas separation process and water purification (Klaysom, Moon, Ladewig, Lu, & Wang, 2011a; F. Wang, Hickner, Kim, Zawodzinski, & McGrath, 2002), finding a larger application particularly as proton exchange membranes for fuel cells (S. Feng, Savage, & Voth, 2012). Nafion membrane is usually employed for this purpose with very good performances, but it has the disadvantages of significant decrease in proton conductivity over 90 °C, poor barrier properties with methanol and high cost (S. Feng et al., 2012). For these reasons, alternative compounds have been studied in the last years and poly(Aryl Ether Sulfone)s seem to be the most promising, together with sulfonated poly(ether sulfone)s, poly(ether ether ketone)s and polyimides. Thanks to the presence of aromatic rings, functionalities can be easily introduced in the structure, yielding to a potential infinite number of materials with flexible properties. These additional groups can be introduced in the polymer structure using different types of strategies, such as crosslinking and grafting of the side chain, performed prior or post synthesis. The introduction prior synthesis has the disadvantages of undesired side reactions, while the post synthesis method needs usually multiple time consuming

and difficult reactions. Therefore, the use of monomer with functionalizable moieties which are inert to the polymerization conditions seems to be the most attractive alternative (Cameron & Sherrington, 1997; Herbert et al., 1997; Meng, Hay, Jian, & Tjong, 1998). Moreover, inorganic fillers can be introduced in the polymer chain, improving the retain of water, the conductivity and the ion exchange capacity (Klaysom, Moon, Ladewig, Lu, & Wang, 2011b).

In the study of PES, various parameters have to be taken into consideration to understand the different properties and behaviour of these polymers (GUAN et al., 2006). First of all, the ion exchange capacity (IEC) is an important value to describe the milliequivalent of ions which can be exchanged per gram of polymer. This parameter is also described as the reciprocal of the polymer equivalent weight. Furthermore, the casting solvent is another key factor, since it remains as residual in the polymer structure. The study of different solvents showed morphological changes depending on the type of casting solvent. In particular, each solvent interacts quite differently with the polymer, in terms of hydrogen bondings, number of solvent-polymer interactions and size of polymer grains. For example, high volatile solvents, as dimethylformamide, give stronger hydrogen bondings, a big number of polymer-solvent interactions and a large grains formation, causing the production of less conductive and hydrophilic material in comparison with less volatile solvents, like *N*-Methyl-2-Pyrrolidone. Finally, other important characteristics are porosity, since small porosity gives less conductive materials, and solvation structure, depending on the distances of sulfonated groups, both easily controllable (Klaysom et al., 2011a).

In the Literature, no mention about the use of PES in electroanalysis can be found, while Nafion is extensively used for this purpose. In fact, its properties of chemical stability, preventing agglomeration and corrosion of guest species and easyness of handling, makes this compound very attractive as dispersive host membrane for nanomaterials, also helping to avoid anion interferences. Moreover, its conductivity demonstrates the possibility of direct application as

sensor, even if only one example can be found in the Literature for the detection of dyes microparticles (Moretto, Montagner, Ganzerla, & Ugo, 2013). In this context, the study of the electrochemical behaviour of different types of PES, synthesized by Prof. Di Silvestro group of the University of Milan for application in electroanalytical field as cheaper and more active alternative to Nafion seems to be very attractive.

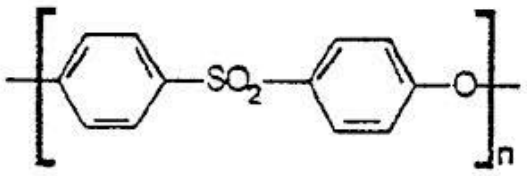

Figure 5.14. Chemical structure of Aryl Ether Sulfone monomer.

5.3.2. Materials and Methods

Glassy Carbon electrode was modified by drop casting using 1 % of PES dispersed in the desired solvent. Different solvents were employed, since they can influence the conformation of the polymer on the electrode, and also different configurations of PES were studied, linear with IEC = 1, linear with IEC = 1.33 and bramched with IEC = 1. The electrodes tested were:

- Glassy Carbon electrode without any modification (GC);
- GC/aPES-NMP electrode, modified with linear PES (IEC = 1) in the acidic form dissolved in *N*-Methylpyrrolidone;
- GC/aPES-DMSO electrode, modified with linear PES (IEC = 1) in the acidic form dissolved in dymethylsulfoxide;
- GC/aPES-DMF electrode, modified with linear PES (IEC = 1) in the acidic form dissolved in dymethylformamide;

- GC/sPES-NMP electrode, modified with linear PES (IEC = 1) in the salt form dissolved in *N*-Methylpyrrolidone;
- GC/sPES-DMSO electrode, modified with linear PES (IEC = 1) in the salt form dissolved in dymethylsulfoxide;
- GC/sPES-DMF electrode, modified with linear PES (IEC = 1) in the salt form dissolved in dymethylformamide;
- GC/aPES-NMP-1.33 electrode, modified with linear PES (IEC = 1.33) in the acidic form dissolved in *N*-Methylpyrrolidone;
- GC/aPES-NMP-br electrode, modified with branched PES (IEC = 1) in the acidic form dissolved in *N*-Methylpyrrolidone.

0.1 M KCl aqueous solution was used as supporting electrolyte and $Ru(NH_3)_6Cl_3$ was employed as model probe molecule.

5.3.3. Results and Discussion

Initially, linear PES with IEC = 1 was studied to find the optimized conditions (quantity, form, solvent and drying time) which give the best electrochemical performances. The results were also compared with Nafion.

The percentage of polymer was varied between 0.5 and 5 %, using DMF as solvent. Figure 5.15 reports the height of anodic and cathodic peaks for each polymer percentage and a comparison with Nafion . The highest value is obtained for 1 % PES, which shows also peak current values higher than Nafion. The following experiments were carried out using electrodes at this polymer percentage.

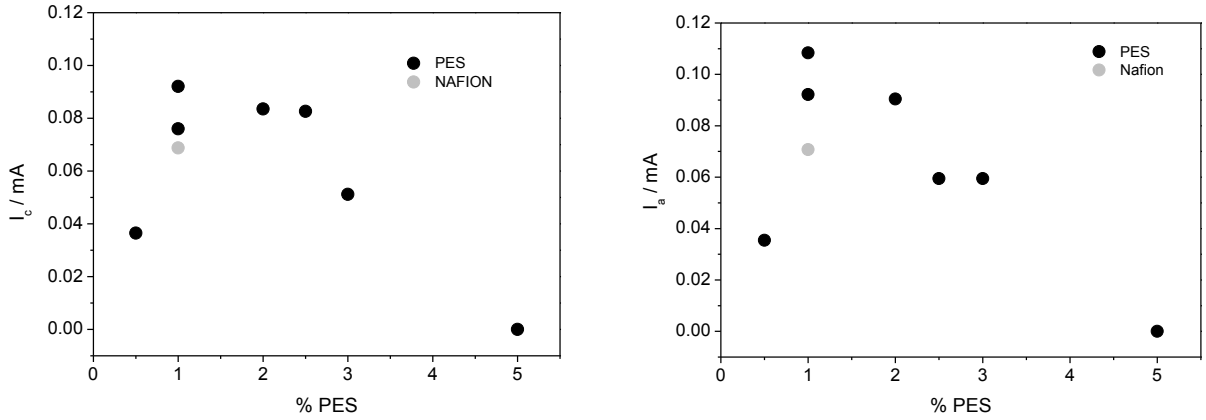

Figure 5.15. Intensity of anodic and cathodic peak current for different PES concentration in DMF and comparison with Nafion.

Figure 5.16-5.17 shows cyclic voltammograms obtained in the presence of the redox probe for 1 % PES in acidic or salt form dissolved in different solvents and dried in oven at 25 °C. The acidic form shows in general higher peak current intensity than the salt form and also than Nafion; the best performance is obtained when NMP is used as solvent. This fact is probably ascribable to the nature of the solvent; in fact NMP has the highest boiling point, followed by DMSO and DMF, in the same order of peak currents. The hypothesis is that when the boiling point is high, a bigger quantity of solvent remains in the structure of the polymer and causes a different configuration, as described also in the Literature (GUAN et al., 2006), which influences electrode performance.

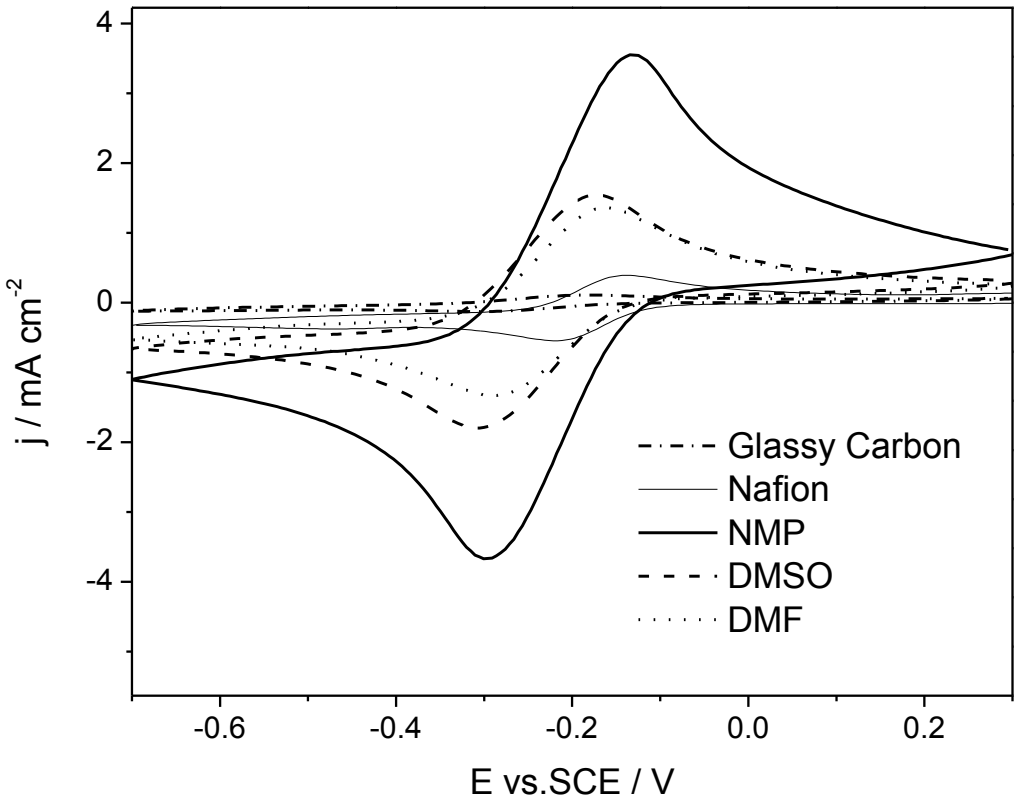

Figure 5.16. Cyclic voltammograms of glassy carbon, Nafion and PES 1% in acidic form in the presence of redox probe.

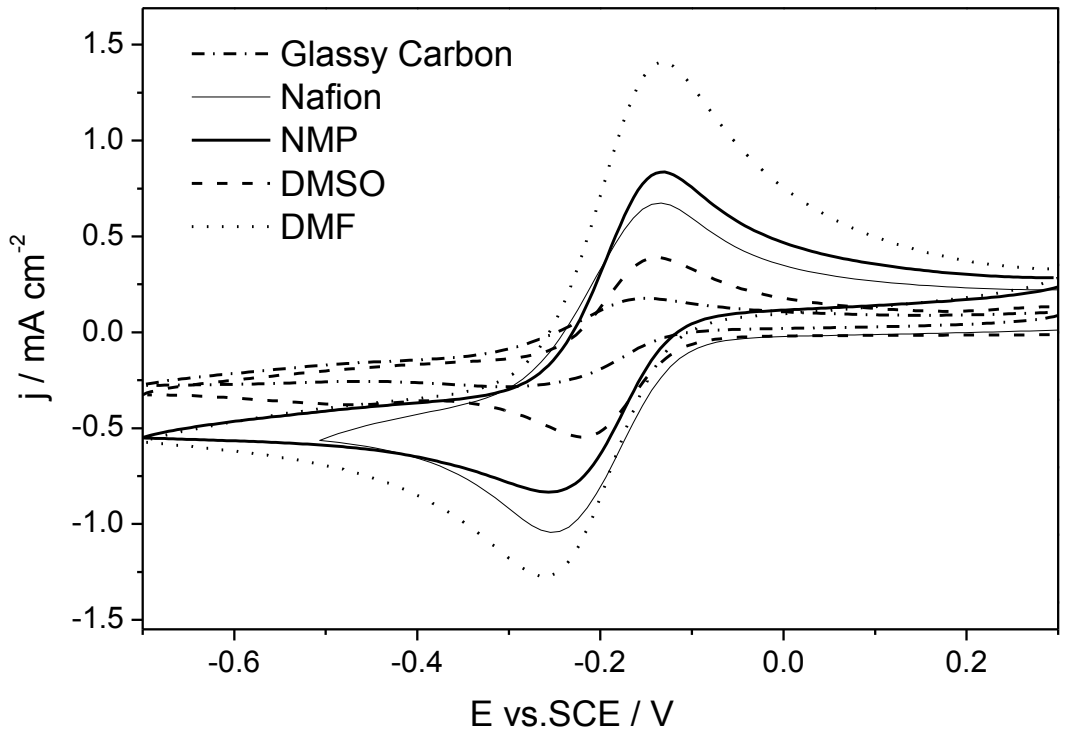

Figure 5.17. Cyclic voltammograms of glassy carbon, Nafion and PES 1% in salt form in the presence of redox probe.

Electrodes were also tested after drying in a vacuum oven, to obtain completely dried samples. Figure 5.18 shows the cyclic voltammograms obtained for PES in the acidic form dissolved in the three solvent and dried in a vacuum oven. The intensity of the peaks collapses of one order of magnitude and peaks are not so well defined as in samples dried in a normal oven. This confirms that effectively a small quantity of solvent can remain in the structure of the polymer giving a different conformation and consequent activity of the electrode. Moreover, the storage of the electrode was studied, leaving the electrode in air or in water after each measurement and results are presented in Figure 5.18. In the first case the membrane moves away the support after two measurements, while in the second case the membrane is stable for days giving the same signal.

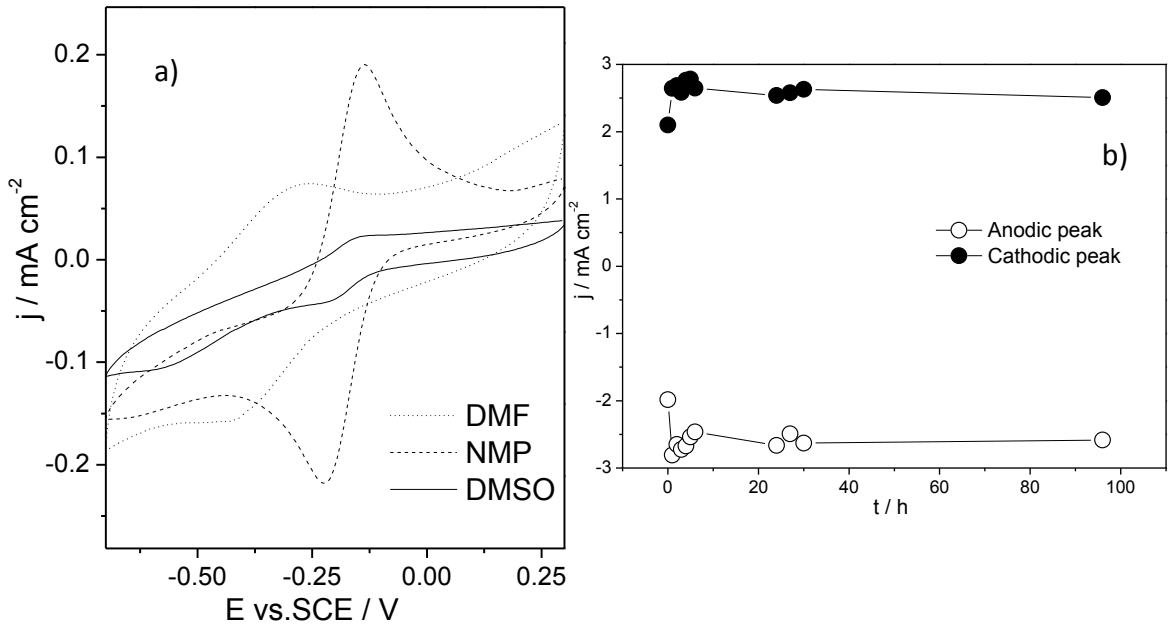

Figure 5.18. Cyclic voltammograms of PES 1% modified electrodes dried in a vacuum oven (a) and study of the variation of the signal with time (b).

Table 5.7 reports the voltammetric parameters obtained from scan rate studies in the presence or absence of redox probe. Surprisingly, calculated capacitance is very similar or even less than GC values and reversibility is in part lost for all the electrodes, but the slope of the Randles-Sevcik plot is one order of magnitude higher for all the acidic forms. This fact is probably due to higher values

of surface area in the case of acidic form and/or to a change in the diffusion mechanism of the redox probe inside the membrane. The last hypothesis is confirmed considering the slope of the logarithmic plot of intensity and scan rate, since for the acidic form this value indicates a total diffusive behaviour, while for the salt form these values show the partial loss of diffusive mechanism.

Table 5.7. Voltammetric parameters obtained from cyclic voltammograms of PES 1% modified electrodes.

CV parameters	GC	Acidic form			Salt form		
		NMP	DMSO	DMF	NMP	DMSO	DMF
C / mF cm^{-2}	0.08	0.01	0.02	0.02	0.04	0.03	0.08
E_c-$E_{c/2}$ / mV	61	91	89	80	68	74	74
E_a-$E_{a/2}$ / mV	59	85	89	81	81	117	76
ΔE_P / mV	78	156	131	122	117	137	122
Slope i_a *vs* $v^{0.5}$ / µA mV$^{-0.5}$ cm^{-2} s$^{0.5}$	47	272	148	120	66	24	96
Slope i_c *vs* $v^{0.5}$ / µA mV$^{-0.5}$ cm^{-2} s$^{0.5}$	-51	-285	-157	-114	-58	-19	-86
Slope Ln i_c *vs* ln v	0.49	0.44	0.49	0.49	0.35	0.43	0.42
Slope Ln i_a *vs* ln v	0.47	0.50	0.50	0.51	0.37	0.35	0.41

Electrochemical impedance spectroscopy was performed in the presence or absence of the model probe molecule at + 0.25 V (SCE), in the capacitive area of the cyclic voltammetry, and at – 0.15 V and – 0.25 V (SCE), where the redox reaction takes place.

Figure 5.19 shows impedance spectra obtained for the acidic and salt form for each type of solvent in the absence of redox probe. Complex plane spectra present a semicircle for higher frequencies, corresponding to the formation of the double layer, and a semicircle for lower frequencies, indicating the diffusion process inside the polymer, which becomes a straight line for all the salt forms and for the acidic form with DMF. Bode plots show very similar trend for all the electrodes with a time dependent process for medium frequencies ascribable to the formation of double layer.

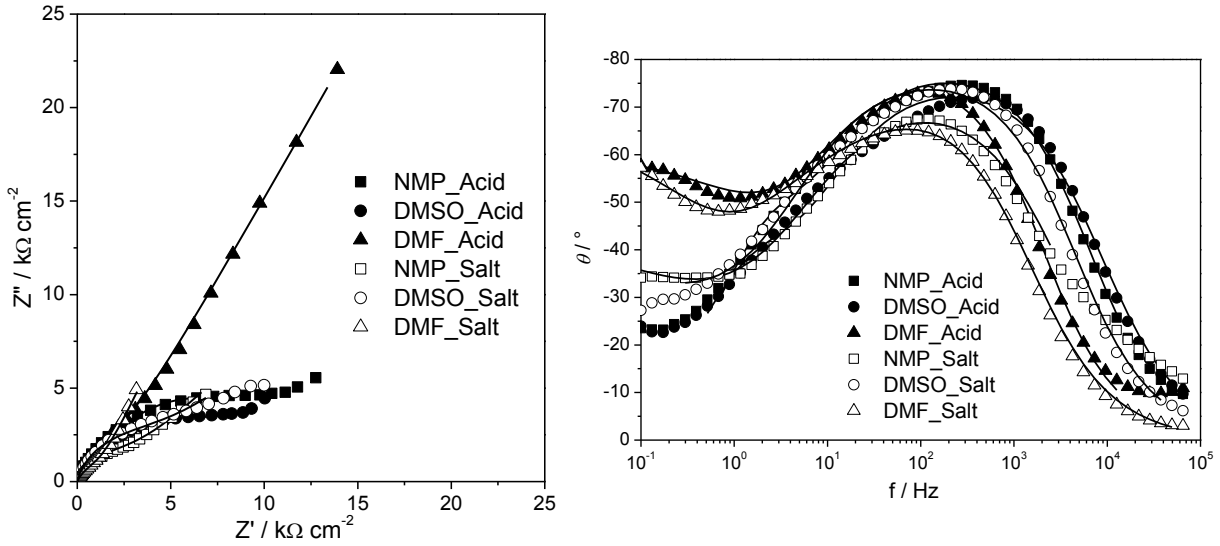

Figure 5.19. Complex plane plot and Bode plot at + 0.25 V in the absence of redox probe.

Figure 5.20 shows the equivalent circuits used to fit impedance data and Table 5.8 reports the values obtained from the fitting procedure. Values of double layer capacitance are in accordance with those obtained by cyclic voltammetry and decrease from negative to positive potentials, together with the increase of charge transfer resistance. Also polarization capacitance decreases and polarization and Warburg resistance increase in the same way, probably because negative potentials are more favourable for the electrochemical activity of the polymer. The resistance to charge transfer is lower for the acidic form dissolved in NMP and for this reason this electrode shows the best electrochemical performance. On the other hand, higher resistance and lower capacitance are obtained for the acidic form in DMF and the salt form in DMSO, which have the worst performance.

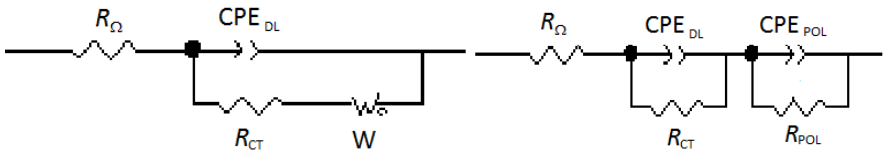

Figure 5.20. Equivalent circuits used to fit impedance data.

Table 5.8. Impedance parameters obtained by impedance fitting in the absence of redox probe.

Electrodes	E / V	R_Ω / Ω cm^2	CPE_{DL} / μF cm^{-2} $s^{\alpha-1}$	α_{DL}	R_{CT} / Ω cm^2	CPE_{POL} / μF cm^{-2} $s^{\alpha-1}$	α_{POL}	R_{POL} / Ω cm^2	R_w / Ω cm^2	τ / s	α
NMP_Acid	-0.25	8.87	21.5	0.85	420	27.5	0.89	7023	-	-	-
	-0.15	8.87	20.2	0.86	720	25.8	0.87	8469	-	-	-
	0.25	8.66	17.1	0.89	1420	21.9	0.88	10524	-	-	-
DMSO_Acid	-0.25	7.88	31.0	0.83	710	31.1	0.83	6390	-	-	-
	-0.15	8.02	24.2	0.84	852	28.0	0.84	7100	-	-	-
	0.25	7.88	16.2	0.85	2130	26.0	0.86	8311	-	-	-
DMF_Acid	-0.25	16.54	11.6	0.88	1420	-	-	-	3290	0.1	0.49
	-0.15	16.87	14.2	0.88	1863	-	-	-	3717	0.1	0.42
	0.25	17.39	11.6	0.90	2229	-	-	-	4627	0.1	0.42
NMP_Salt	-0.25	12.78	36.7	0.83	1528	13.0	0.70	8586	-	-	-
	-0.15	12.42	32.7	0.84	1615	12.2	0.70	12604	-	-	-
	0.25	13.49	22.1	0.82	2406	-	-	-	1706	0.1	0.44
DMSO_Salt	-0.25	9.37	16.4	0.86	2698	-	-	-	2419	0.1	0.40
	-0.15	9.29	14.7	0.86	3195	-	-	-	2824	0.1	0.48
	0.25	9.37	13.6	0.87	3550	-	-	-	3563	0.1	0.43
DMF_Salt	-0.25	8.66	82.9	0.81	497	-	-	-	921	0.1	0.45
	-0.15	8.59	82.4	0.80	571	-	-	-	1864	0.1	0.42
	0.25	7.95	51.0	0.85	667	-	-	-	4077	0.1	0.45

In the presence of model probe molecule, the situation is really different and interesting. In Figure 5.21-5.22-5.23 impedance spectra are presented. Complex plane spectra show a semicircle for higher frequencies, corresponding to the formation of the double layer, and a semicircle or straight line for lower frequencies, indicating the diffusion process. Only for the acidic form in NMP at – 0.15 V and – 0.25 V (SCE) and for the acidic form in DMSO at – 0.25 V (SCE) the first semicircle is not present, but is substituted by a straight line with slope < 0.5, indicating that only the diffusion process takes place, without the formation of double layer. On the other hand, for all the electrodes at + 0.25 V the complex plane spectrum is formed by two semicircles or one semicircle. In general, values of impedance decreases of two orders of magnitude when the redox reaction takes place. Bode plots show the same trend at + 0.25 V, with one time-dependent process corresponding to the formation of double layer, while at – 0.15 V and at – 0.25 V the trend changes the shape, with a less evident time dependent process. Moreover, no process is present at – 0.15 V and – 0.25 V for the acidic form in NMP and at – 0.25 V for the acidic form in DMSO and for the salt form peaks are present only at – 0.25 V.

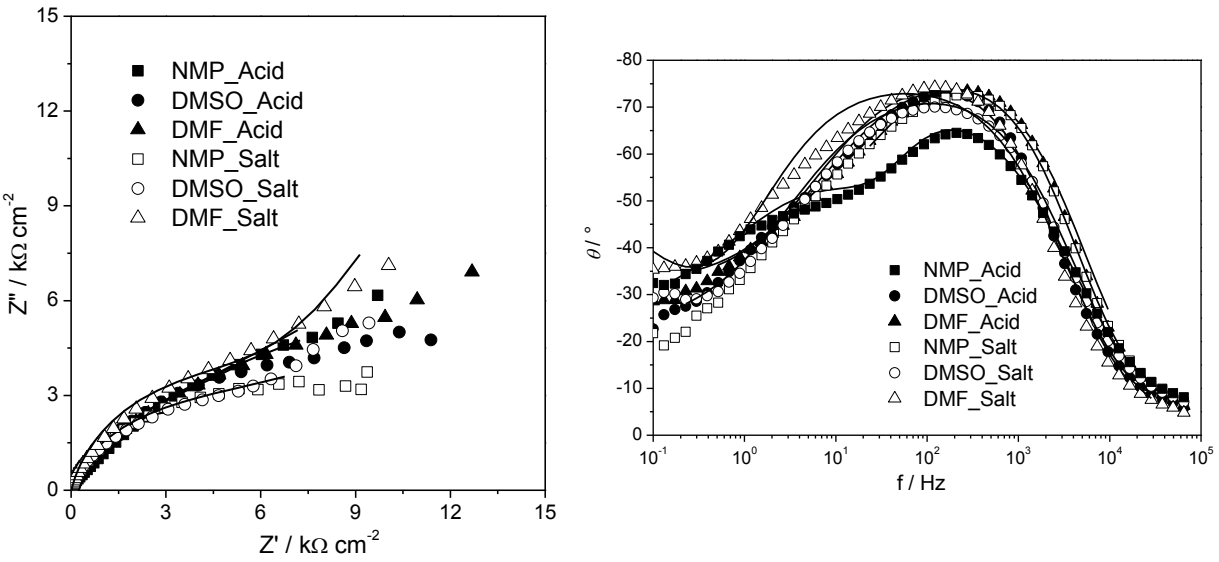

Figure 5.21. Complex plane plot and Bode plot at + 0.25 V in the presence of redox probe.

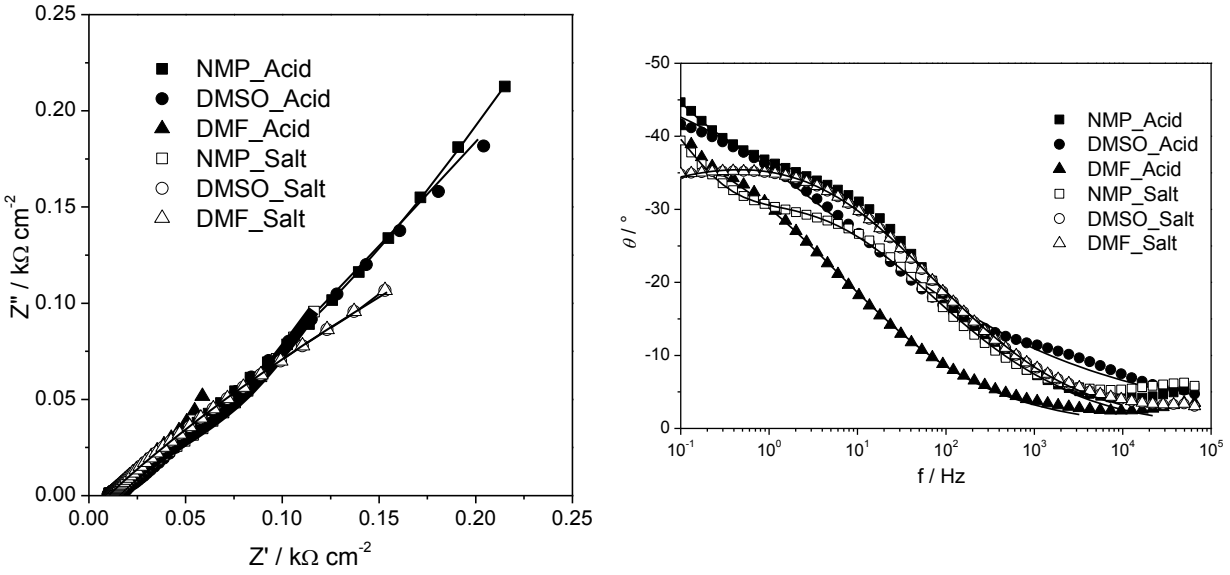

Figure 5.22. Complex plane plot and Bode plot at – 0.15 V in the presence of redox probe.

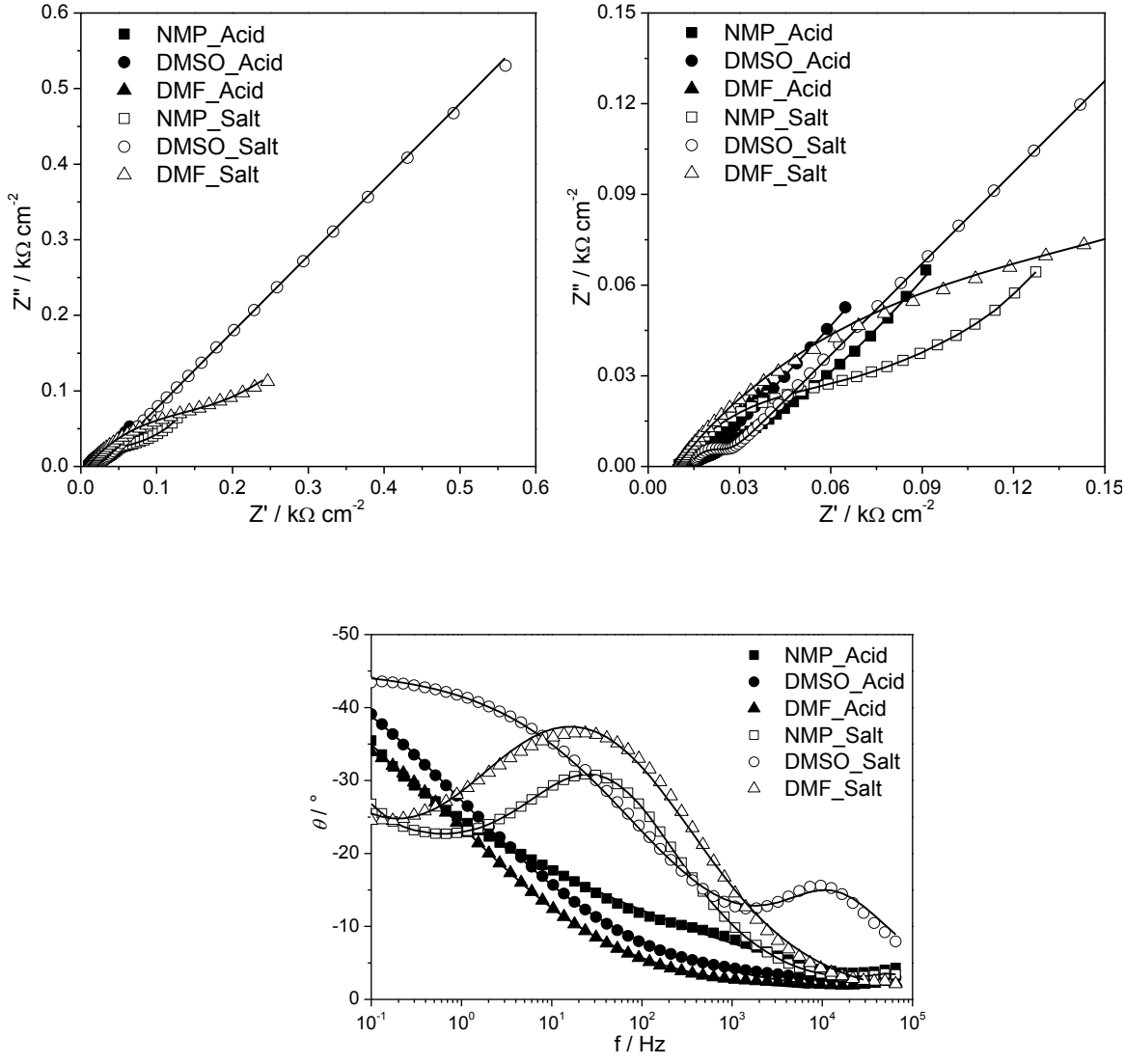

Figure 5.23. Complex plane plot and Bode plot at – 0.25 V in the presence of redox probe.

The different behaviour at capacitive potential and at redox potentials can be observed also considering the fitting parameters. In Figure 5.24 equivalent circuits used to fit the data are presented and in Table 5.9 the corresponding fitting parameters are reported. Capacitance values are very low at + 0.25 V and are in accordance with values obtained from cyclic voltammetry, but at the others two potentials this value increases of two order of magnitude, lowering also the resistance. This behaviour confirms the previous results about the low capacitances and the high Randles-Sevcik slopes obtained by cyclic voltammetry. Moreover, the best electrode is the acidic form in NMP, since the absence of double layer allows an easy electron transfer during redox reaction, without resistance problems, but only with diffusive mechanism. In fact, this electrode shows also low diffusion resistance and high polarization capacitance, explaining the reason of the excellent performance, also in comparison with Nafion, and confirming the different membrane structure which causes a different diffusion of the redox probe. The acidic form in DMSO has a mixed behaviour, since it behaves as NMP at – 0.25 V and as DMF at – 0.15 V and also in cyclic voltammetry shows intermediate performance. For the salt forms, double layer is formed in all cases with lower capacitances, explaining the worst electrochemical performances.

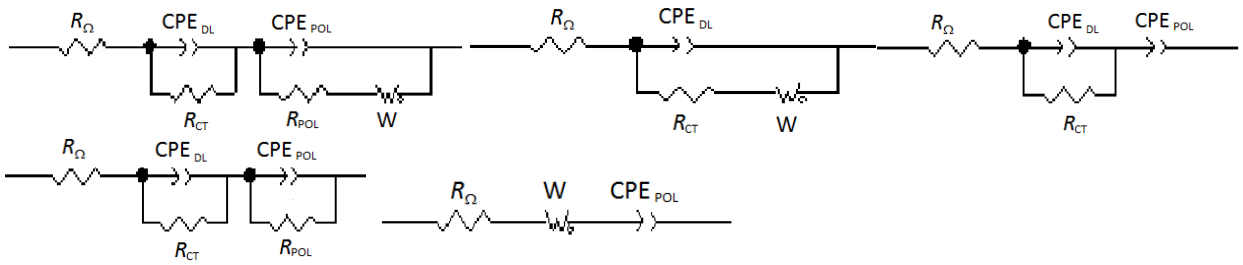

Figure 5.24. Equivalent circuits used to fit impedance data.

Table 5.9. Impedance parameters obtained by impedance fitting in the presence of redox probe.

Electrodes	E / V	R_Ω / Ω cm^2	CPE_{DL} / mF cm^{-2} s$^{\alpha-1}$	α_{DL}	R_{CT} / Ω cm^2	CPE_{POL} / mF cm^{-2} s$^{\alpha-1}$	α_{POL}	R_{POL} / Ω cm^2	R_w / Ω cm^2	τ / s	α
NMP_Acid	-0.25	8.40	-	-	-	33.20	0.50	-	2.40	0.1	0.45
	-0.15	9.51	-	-	-	19.48	0.51	-	3.91	0.1	0.47
	0.25	8.74	1.74E-2	0.89	511	-	-	-	4358	0.1	0.49
DMSO_Acid	-0.25	10.78	-	-	-	27.80	0.59	-	6.93	0.1	0.46
	-0.15	11.41	2.05	0.56	8.37	4.85	0.58	-	-	-	-
	0.25	12.84	1.21e-02	0.89	1425	-	-	-	3759	0.1	0.49
DMF_Acid	-0.25	13.30	1.94	0.51	11.33	-	-	-	176	0.1	0.40
	-0.15	15.34	4.14	0.51	147	6.69	0.70	-	-	-	-
	0.25	13.99	1.82e-02	1	202	4.06e-02	0.75	3709	3503	0.1	0.46
NMP_Salt	-0.25	9.23	1.35	0.6	213	-	-	-	32.61	0.1	0.46
	-0.15	9.94	5.46	0.49	213	-	-	-	249	0.1	0.40
	0.25	9.22	2.45E-2	085	7270	-	-	-	1292	0.1	0.43
DMSO_Salt	-0.25	13.92	0.85e-02	0.86	9.33	1.66	0.50	-	-	-	-
	-0.15	13.19	1.09e-02	0.84	23.09	4.63	0.50	-	-	-	-
	0.25	10.26	1.84e-02	0.85	2197	-	-	-	602	0.1	0.44
DMF_Salt	-0.25	10.06	1.46	0.63	71	-	-	-	22.98	0.1	0.45
	-0.15	11.28	6.10	0.47	252	-	-	-	32.53	0.1	0.41
	0.25	10.32	1.94E-2	0.89	710	2.11E-2	0.90	5680	-	-	-

After this extensive characterization, the acidic form of 1 % PES in NMP resulted the best electrode in terms of diffusion of the model probe molecule, high capacitance, low resistance and high current, and was chosen for further investigation about different IEC values and the possibility to use branched polymers.

Figure 5.25 shows cyclic voltammograms obtained using linear PES with IEC = 1 in comparison with linear PES with IEC = 1.33 and branched PES with IEC = 1. The new types of polymer present a very similar voltammetric response, with lower peak current than linear PES with IEC = 1, but always better than Nafion and GC.

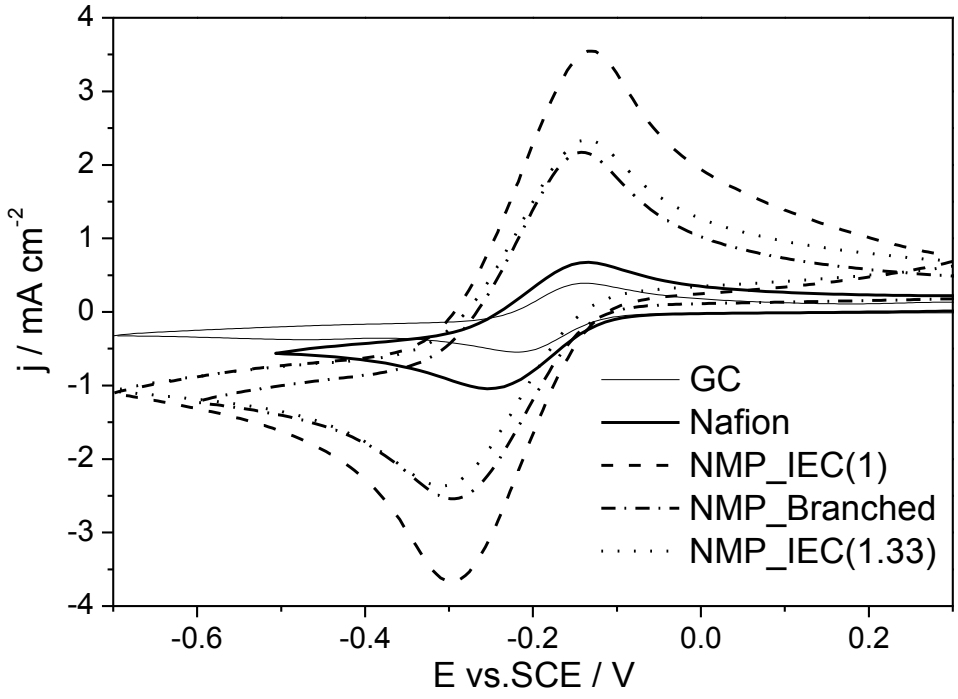

Figure 5.25. Cyclic voltammograms of glassy carbon, Nafion and different forms of PES 1% in the presence of redox probe.

Table 5.10 reports the voltammetric parameters which also in this case, show capacitance values very similar to GC; reversibility is partially lost. The slopes of the Randles-Sevcik plot remain two orders of magnitude higher than GC and the mechanism is more diffusive for linear PES with IEC =

1, followed by the ramified one, confirming a good diffusion in an open but not too charged structure.

Table 5.10. Voltammetric parameters obtained from cyclic voltammograms of PES 1% modified electrodes.

CV parameters	GC	NMP		
		IEC (1)	IEC (1.33)	Branched
C / mF cm^{-2}	0.08	0.01	0.07	0.07
E_c-$E_{c/2}$ / mV	61	91	89	79
E_a-$E_{a/2}$ / mV	59	85	89	89
ΔE_P / mV	78	156	131	142
Slope i_a *vs* $v^{0.5}$ / µA mV$^{-0.5}$ cm^{-2} s$^{0.5}$	47	272	167	157
Slope i_c *vs* $v^{0.5}$ / µA mV$^{-0.5}$ cm^{-2} s$^{0.5}$	-51	-285	-148	-167
Slope Ln i_c *vs* ln v	0.49	0.44	0.37	0.42
Slope Ln i_a *vs* ln v	0.47	0.50	0.40	0.44

Figure 26 shows impedance spectra obtained in the absence of the redox probe in the same manner of the previous discussion and at the same potentials. Complex plane spectra report a semicircle for higher frequencies followed by a second semicircle in the case of linear PES with IEC = 1 or by a straight line with slope < 0.5 for the other two cases. Bode plots show lower phase angle changes in the two new electrodes, but with two time dependent processes.

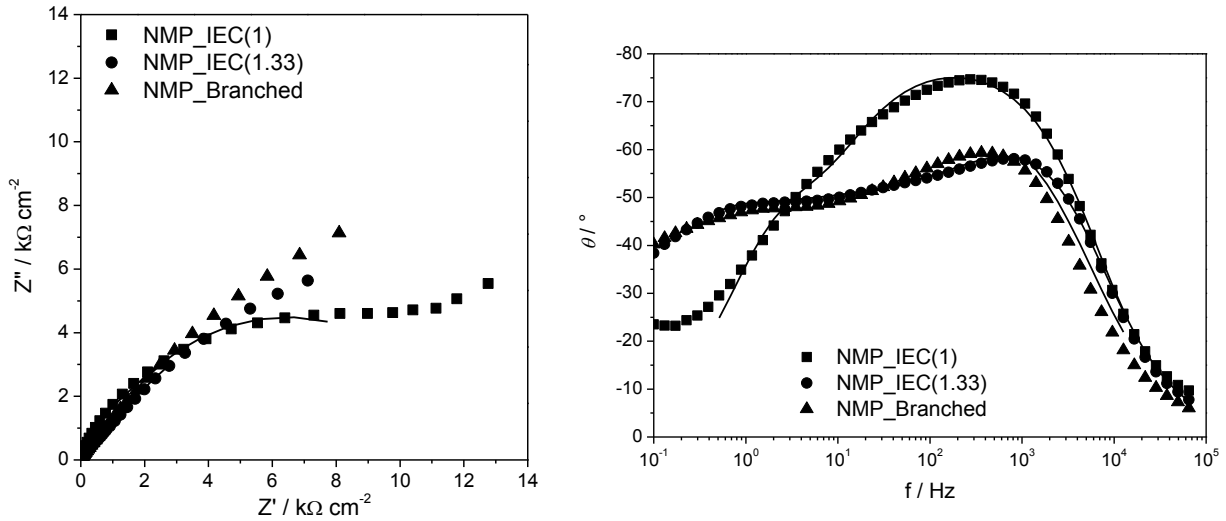

Figure 5.26. Complex plane plot and Bode plot at + 0.25 V in the absence of redox probe.

Figure 5.27 reports the equivalent circuits used to fit impedance data and in Table 5.11 fitting parameters are reported. Double layer capacitance is higher for branched PES, followed by linear PES with IEC = 1, since the branched gives an extended structure and the polymer with IEC = 1.33 is more disordered for the presence of more negative groups. For this last reason, charge transfer resistance is lower for IEC = 1.33 polymer, but diffusive resistance for both new electrodes is higher than polarization resistance of linear PES with IEC = 1.

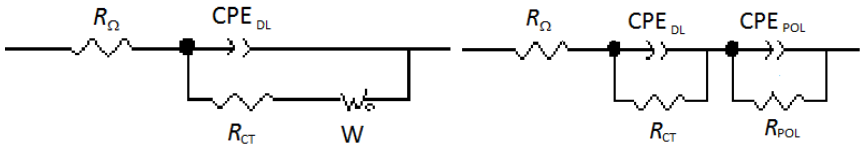

Figure 5.27. Equivalent circuits used to fit impedance data.

Table 5.11. Impedance parameters obtained by impedance fitting in the absence of redox probe.

Electrodes	E / V	R_Ω / Ω cm^2	CPE_{DL} / μF cm^{-2} s$^{\alpha-1}$	α_{DL}	R_{CT} / Ω cm^2	CPE_{POL} / μF cm^{-2} s$^{\alpha-1}$	α_{POL}	R_{POL} / Ω cm^2	R_w / Ω cm^2	τ / s	α
NMP_IEC(1)	-0.25	8.87	21.5	0.85	420	27.5	0.89	7023	-	-	-
	-0.15	8.87	20.2	0.86	720	25.8	0.87	8469	-	-	-
	0.25	8.66	17.1	0.89	1420	21.9	0.88	10524	-	-	-
NMP_IEC(1.33)	-0.25	8.99	11.8	0.86	105	-	-	-	10800	0.1	0.45
	-0.15	8.95	12.8	0.85	134	-	-	-	11161	0.1	0.49
	0.25	8.95	10.0	0.80	137	-	-	-	13991	0.1	0.51
NMP_Branched	-0.25	8.60	36.2	0.78	703	-	-	-	8642	0.1	0.47
	-0.15	8.51	36.0	0.78	837	-	-	-	11086	0.1	0.48
	0.25	8.46	19.4	0.84	372	-	-	-	14435	0.1	0.43

Figure 5.28-5.29-5.30 reports impedance spectra in the presence of model probe molecule, showing a complex plane spectra based on a semicircle or for linear PES with IEC = 1 a straight line with slope < 0.5 for higher frequencies and a straight line for lower frequencies. Bode plots have a very similar trend at + 0.25 V with a time dependent process, while at – 0.15 V no double layer is formed for all the electrodes. At – 0.25 V only for linear PES with IEC = 1, there is no formation of the double layer, showing another time its superior performance.

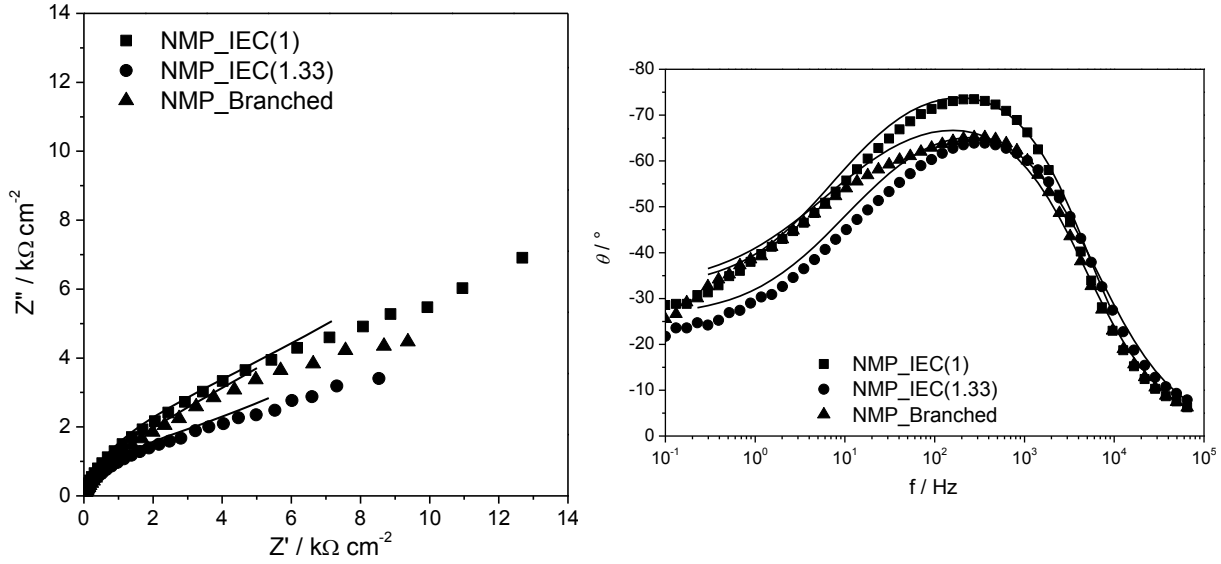

Figure 5.28. Complex plane plot and Bode plot at + 0.25 V in the presence of redox probe.

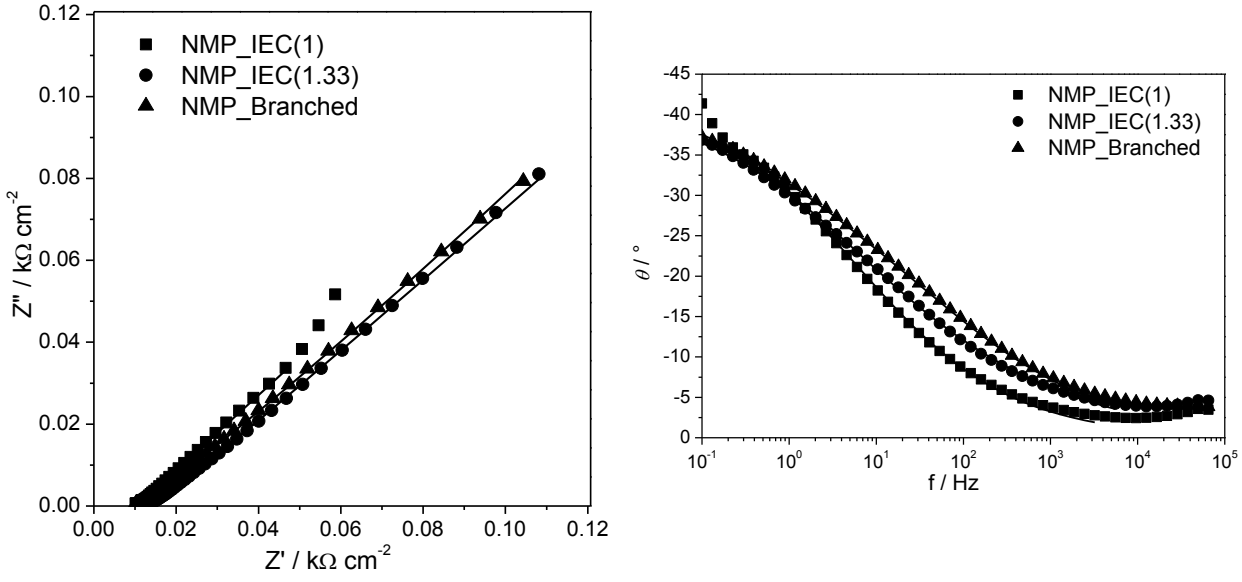

Figure 5.29. Complex plane plot and Bode plot at – 0.15 V in the presence of redox probe.

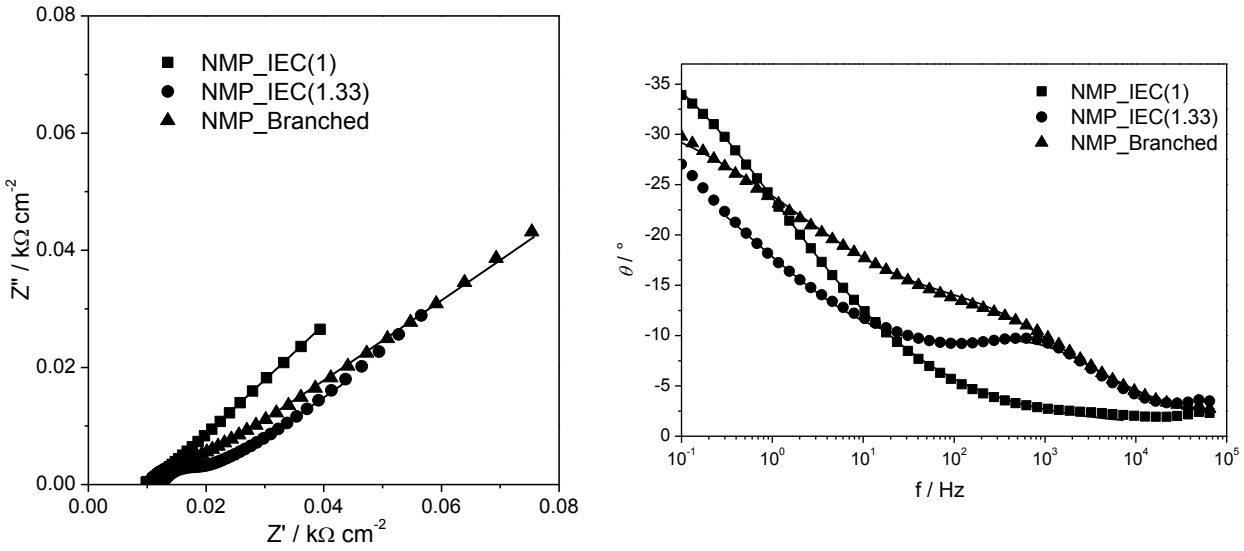

Figure 5.30. Complex plane plot and Bode plot at – 0.25 V in the presence of redox probe.

Figure 5.31 shows the equivalent circuits used in the fitting of impedance data and Table 5.12 reports the parameters obtained from the fitting. As in the previous discussion, capacitance is very low at + 0.25 V, but increases of two orders of magnitude at the other two potentials. The highest capacitance values are obtained for linear PES with IEC = 1.

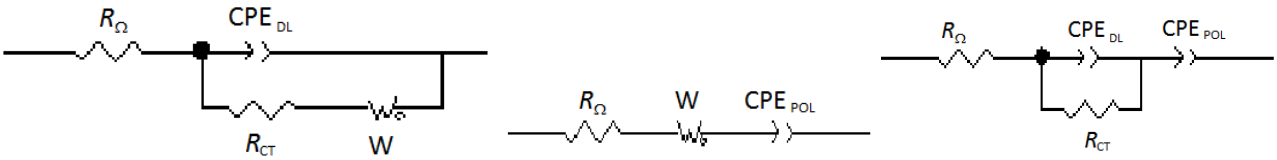

Figure 5.31. Equivalent circuits used to fit impedance data.

Table 5.12. Impedance parameters obtained by impedance fitting in the presence of redox probe.

Electrodes	E / V	R_Ω / Ω cm^2	CPE_{DL} / μF cm^{-2} s$^{\alpha-1}$	α_{DL}	R_{CT} / Ω cm^2	CPE_{POL} / μF cm^{-2} s$^{\alpha-1}$	α_{POL}	R_w / Ω cm^2	τ / s	α
NMP_IEC(1)	-0.25	8.40	-	-	-	16.13	0.49	2.40	0.1	0.45
	-0.15	9.51	-	-	-	11.22	0.51	3.91	0.1	0.47
	0.25	8.74	1.74E-2	0.89	511	16.13	0.49	4358	0.1	0.49
NMP_IEC(1.33)	-0.25	12.27	0.33	0.69	3.39	-	-	15.31	0.1	0.42
	-0.15	12.91	-	-	-	13.61	0.51	6.97	0.1	0.47
	0.25	11.91	1.60E-2	0.81	392	-	-	2908	0.1	0.45
NMP_Branched	-0.25	9.44	3.75	0.57	5.40	16.13	0.49	-	-	-
	-0.15	10.36	-	-	-	11.22	0.51	3.34	0.1	0.46
	0.25	9.68	2.11e-2	0.83	362	-	-	2931	0.1	0.48

5.3.4. Conclusions

In this work, linear poly(arylethersulfones) PES with IEC = 1 were tested in comparison with Nafion as electroactive negative membrane for use in electroanalysis.

Numerous parameters, such as quantity of the dissolved polymer, solvent used for dissolution, form of the polymer, method of drying and storage could influence the performances of the membrane and were taken into consideration. The ideal quantity of polymer was 1 %, because this quantity allowed to obtain the maximum peak current, while the optimum method of drying was at 25 °C in a normal oven, since if the polymer was dried in a vacuum oven, the signal of the model probe molecule decreased or was completely lost, probably due to total removal of the solvent from the membrane structure. Moreover, the membrane loses its characteristics when the electrode is stored in air after use, but it maintains its performances for days if stored in the supporting electrolyte solution. This fact confirms that probably the membrane needs hydration to maintain its activity.

The type of solvent and the polymer form are key factors, since interactions between the polymer and the solvent influence the final configuration and the consequent electroactivity of the membrane. Results showed that the acidic form was the most electroactive for all the solvent used, probably due to major availability of charged groups in this form, and that the solvent with the highest boiling point, NMP, provided the best performances, probably since this solvent allows a higher organization of the polymer, yielding to a more ordered and extended structure.

The behaviour of this polymer is very interesting, since the capacitance is comparable with that of glassy carbon, but when the redox probe is present capacitance increases of two orders of magnitude, resistance to electron transfer decreases and the process is governed only by diffusion without the formation of double layer. The hypothesis is that the polymer conformation changes

the mechanism of diffusion of the analyte, probably for the presence and availability/affinity of charged groups in the structure.

This polymer used as new membrane for application in electrochemistry showed superior activity in comparison with Nafion, since it was more stable, more capacitive, less resistive and gave higher peak currents, maintaining the partial reversibility and the diffusive control.

Moreover, linear PES with IEC = 1.33 and branched PES with IEC = 1 were also studied, to see the influence of ramification and of the different quantity of sulphonic groups on the electrochemical performances. In these cases the peak current was lower than linear PES with IEC = 1 and diffusive mechanism, capacitance and resistance remained better in the first case. However, the electrochemical performances of these new two types of polymer were good and superior with respect to Nafion.

Future developments will consider the analysis of linear and branched PES with different IEC and casting solvents to understand and rationalize how each parameter can influence the electrochemical response towards different types of analytes. The idea is the production of electroactive membranes with *ad hoc* properties, designed for the specific type of analyte and application. Moreover, these polymers can be considered as host species for nanomaterials.

6. Conclusions

In this PhD thesis, two quite recent technological developments were used for the design of new electrodes and new electroanalytical methodologies for trace detection of organic and inorganic relevant compounds and pollutants.

The first technological approach is based on the screen-printing microfabrication technology, which allows the production of accurate, sensitive, low cost, easy to use and disposable sensors. In particular, four types of electrodes and different voltammetric techniques were tested, demonstrating the importance of the method choice and the material affinity for the analyte.

Platinum-based screen-printed electrodes in combination with Square-Wave Voltammetry were used for the determination of furan (Falciola, Pifferi, Possenti, et al., 2012), obtaining good detection limits (0.52 ppm) and accuracy (Apparent Recovery Factors > 95 %), even using coffee as real matrix. Carbon-based screen-printed electrodes and Differential Pulse Voltammetry were employed for the detection of four types of benzidines (Falciola, Pifferi, & Mascheroni, 2012) with excellent limits of detection (ppb range) and Apparent Recovery Factors (very close to 100 %). Analysis using polluted water and experiments with the contemporaneous presence of all the analytes were performed with very good promising results. Bismuth-based screen-printed electrodes were tested using Square-Wave Voltammetry for chromium (VI) trace analysis (V Pifferi et al., 2013), as alternative to mercury-based electrodes, with pyrocathecol violet as complexing agent for chromium, showing electroactivity both in the free and complexed forms. The technique was presented as valid alternative to mercury, obtaining detection limit of 0.28 ppb and Apparent Recovery Factors around 102 %, and was applied for the determination of Cr(VI) during its photoremoval mediated by three different titania photocatalysts, with excellent results. Gold-based screen-printed electrodes and Linear Sweep Adsorptive Stripping Voltammetry were

employed for the electroanalytical detection of arsenic (III) (Valentina Pifferi, Ardizzone, et al., 2013), showing detection limits in the range of ppb and allowing application for As(III) determination during its photooxidation operated by three different titania photocatalysts. Screen-printed electrodes were always used in comparison with the corresponding conventional bulk electrodes, showing comparable or even better results.

The second technological approach concerns the use of innovative materials for the preparation of modified electrodes, in particular nanomaterials and polymeric membranes, allowing specificity for the analytes, high accuracy, excellent repeatability and very low detection limits.

Nanomaterials show peculiar properties in comparison with the corresponding bulk material and different nanomaterials-modified electrodes can be obtained varying shape, size, composition and functionalities of nanoelements, with different detection applications. Carbon nanotubes were studied and characterized considering various methods of purification. The best results were obtained with the sulphonitric mixture (24 h treatment) after removal of amorphous carbon, showing higher peak currents and capacitance, higher surface area and mesoporosity, higher covalent acidity and lower resistance to charge transfer. These optimized electrodes were used to detect *o*-toluidine, obtaining low detection limits (0.16 ppm) and excellent accuracy, allowing the study of its photoremoval by ZnO photocatalyst, showing results comparable with HPLC, and of its absorption by cyclodextrine-based polymeric resins. Benzidine and furan were also determined with promising preliminary results. Colloidal gold nanoparticles on carbon nanotubes were characterized, showing the gold nanoparticles beneficial effect in terms of peak currents, capacitance and charge transfer resistance, and used for the detection of glycerol with promising preliminary results. Colloidal silver nanoparticles on Nafion (Valentina Pifferi, Marona, Longhi, & Falciola, 2013) and on carbon nanotubes were studied, obtaining in the first case electrodes with a very small double layer very useful for halothane and dichloromethane determination, and in the

second case an extended potential window in the cathodic region. Titanium dioxide nanorods on single-walled carbon nanotubes were also characterized in the dark and under UV illumination, considering the photoactivity of titania, obtaining a change in the diffusion mechanism of the redox probe probably ascribable to excited electrons produced by titanium dioxide.

In the last part of the PhD Thesis, polymeric membranes with promising applicability in electroanalysis were studied, allowing the production of biosensors and the change in the analyte diffusion mechanism.

An electron conducting electroactive polymer, poly(Brilliant Green) was studied in combination with carbon nanotubes and PEDOT, an electron conducting non-electroactive polymer (Valentina Pifferi, Barsan, et al., 2013). The different architectures were evaluated, demonstrating the fundamental role of PEDOT for the determination of hydrogen peroxide (LoD 30 ppb) and for the production of glucose and ethanol biosensors (LoD 2 ppm and 1 ppm respectively).

A proton conducting polymer, poly(Aryl Ether Sulfone), was studied in comparison with Nafion, showing better electrochemical performances in terms of affinity for the analyte and small double layer formation, even if capacitance is comparable with glassy carbon. The properties of the membrane were influenced by the type of casting solvent and the form of the polymer (acidic or salt), which probably resulted in a different membrane structure during solvent evaporation, causing a change in the analyte diffusion mechanism.

In conclusion, this PhD Thesis has demonstrated the importance of the new technological developments in electroanalysis for trace determination of organic and inorganic relevant and pollutant compounds. The production of *ad hoc* electrodes together with the optimization of electroanalytical procedures have shown their potentialities for application as standard detection methods in environmental, medical and food analysis.

Future developments will consider the production of home-made screen-printed electrodes modified with nanomaterials and/or polymeric membranes to further improve the simplicity of use and extend the applicability of these sensors. Moreover, new nanomaterials and conducting polymers will be studied alone or in combination for the development of new electrodes and new electroanalytical techniques for trace determination of other relevant compounds.

7. References

Papers and books:

Abirama Sundari, P., & Manisankar, P. (2010). Development of ultrasensitive surfactants doped poly(3,4-ethylenedioxythiophene)/multiwalled carbon nanotube sensor for the detection of pyrethroids and an organochlorine pesticide. *Journal of Applied Electrochemistry*, *41*(1), 29–37. doi:10.1007/s10800-010-0204-9

Agüí, L., Yáñez-Sedeño, P., & Pingarrón, J. M. (2008). Role of carbon nanotubes in electroanalytical chemistry: a review. *Analytica chimica acta*, *622*(1-2), 11–47. doi:10.1016/j.aca.2008.05.070

Ahuja, T., & Kumar, D. (2009). Recent progress in the development of nano-structured conducting polymers/nanocomposites for sensor applications. *Sensors and Actuators B: Chemical*, *136*(1), 275–286. doi:10.1016/j.snb.2008.09.014

Altaki, M. S., Santos, F. J., & Galceran, M. T. (2007). Analysis of furan in foods by headspace solid-phase microextraction-gas chromatography-ion trap mass spectrometry. *Journal of chromatography. A*, *1146*(1), 103–9. doi:10.1016/j.chroma.2007.01.104

Alvarez-lcaza, M., & Bilitewski, U. (1993). Mass Production of Biosensors. *Analytical Chemistry*, *65*(11), 525A–533A. doi:10.1021/ac00059a717

Ambrosi, A., & Pumera, M. (2011). Amorphous Carbon Impurities Play an Active Role in Redox Processes of Carbon Nanotubes. *The Journal of Physical Chemistry C*, *115*(51), 25281–25284. doi:10.1021/jp209734t

Amini, M., Abbaspour, K. C., Berg, M., Winkel, L., Hug, S. J., Hoehn, E., … Johnson, C. A. (2008). Statistical Modeling of Global Geogenic Arsenic Contamination in Groundwater. *Environmental Science & Technology*, *42*(10), 3669–3675. doi:10.1021/es702859e

Anezaki, K., Nukatsuka, I., & Ohzeki, K. (1999). Determination of arsenic(III) and total arsenic(III,V) in water samples by resin suspension graphite furnace atomic absorption spectrometry. *Analytical Sciences*, *15*(9), 829–834. doi:DOI 10.2116/analsci.15.829

Ates, M. (2013). A review study of (bio)sensor systems based on conducting polymers. *Materials science & engineering. C, Materials for biological applications*, *33*(4), 1853–9. doi:10.1016/j.msec.2013.01.035

Ates, M., & Sarac, a. S. (2009). Conducting polymer coated carbon surfaces and biosensor applications. *Progress in Organic Coatings*, *66*(4), 337–358. doi:10.1016/j.porgcoat.2009.08.014

Atmeh, M., & Alcock-Earley, B. E. (2011). A conducting polymer/Ag nanoparticle composite as a nitrate sensor. *Journal of Applied Electrochemistry*, *41*(11), 1341–1347. doi:10.1007/s10800-011-0354-4

Azevedo, A. M., Prazeres, D. M. F., Cabral, J. M. S., & Fonseca, L. P. (2005). Ethanol biosensors based on alcohol oxidase. *Biosensors & Bioelectronics*, *21*(2), 235–247. doi:DOI 10.1016/j.bios.2004.09.030

Bănică, F.-G. (2012). *Chemical Sensors and Biosensors*. Chichester, UK: John Wiley & Sons, Ltd. doi:10.1002/9781118354162

Banks, C. E., & Compton, R. G. (2006). New electrodes for old: from carbon nanotubes to edge plane pyrolytic graphite. *The Analyst*, *131*(1), 15. doi:10.1039/b512688f

Banks, C. E., Ji, X., Crossley, A., & Compton, R. G. (2006). Understanding the Electrochemical Reactivity of Bamboo Multiwalled Carbon Nanotubes: the Presence of Oxygenated Species at Tube Ends May not Increase Electron Transfer Kinetics. *Electroanalysis*, *18*(21), 2137–2140. doi:10.1002/elan.200603633

Banks, C. E., Moore, R. R., Davies, T. J., & Compton, R. G. (2004). Investigation of modified basal plane pyrolytic graphite electrodes: definitive evidence for the electrocatalytic properties of the ends of carbon nanotubes. *Chemical communications (Cambridge, England)*, *129*(16), 1804–5. doi:10.1039/b406174h

Bard, A. J. (Ed.). (2007). *Encyclopedia of Electrochemistry*. Weinheim, Germany: Wiley-VCH Verlag GmbH & Co. KGaA. doi:10.1002/9783527610426

Bard, A. J., & Faulkner, L. R. (2001). *Electrochemical Methods: Fundamentals and Applications* (p. 864).

Barek, J, Cvacka, J., Muck, A., Quaiserová, V., & Zima, J. (2001). Electrochemical methods for monitoring of environmental carcinogens. *Fresenius' journal of analytical chemistry*, *369*(7-8), 556–62. Retrieved from http://www.ncbi.nlm.nih.gov/pubmed/11371047

Barek, Jiri, Jandová, K., Pecková, K., & Zima, J. (2007). Voltammetric determination of aminobiphenyls at a boron-doped nanocrystalline diamond film electrode. *Talanta*, *74*(3), 421–6. doi:10.1016/j.talanta.2007.08.039

Barek, Jiri, Peckova, K., & Vyskocil, V. (2008). Adsorptive Stripping Voltammetry of Environmental Carcinogens. *Current Analytical Chemistry*, *4*(3), 242–249. doi:10.2174/157341108784911325

Barek, Jiří, Pumera, M., Muck, A., Kadeřábková, M., & Zima, J. (1999). Polarographic and voltammetric determination of selected nitrated polycyclic aromatic hydrocarbons. *Analytica Chimica Acta*, *393*(1-3), 141–146. doi:10.1016/S0003-2670(99)00057-4

Barsan, M. M., & Brett, C. M. A. (2008). An alcohol oxidase biosensor using PNR redox mediator at carbon film electrodes. *Talanta*, *74*(5), 1505–1510. doi:DOI 10.1016/j.talanta.2007.09.027

Barsan, M. M., & Brett, C. M. A. (2009). A new modified conducting carbon composite electrode as sensor for ascorbate and biosensor for glucose. *Bioelectrochemistry*, *76*(1-2), 135–140. doi:DOI 10.1016/j.bioelechem.2009.03.004

Barsan, M. M., Carvalho, R. C., Zhong, Y., Sun, X. L., & Brett, C. M. A. (2012). Carbon nanotube modified carbon cloth electrodes: Characterisation and application as biosensors. *Electrochimica Acta*, *85*, 203–209. doi:DOI 10.1016/j.electacta.2012.08.048

Bellomunno, C., Bonanomi, D., Falciola, L., Longhi, M., Mussini, P. R., Doubova, L. M., & Di Silvestro, G. (2005). Building up an electrocatalytic activity scale of cathode materials for organic halide reductions. *Electrochimica Acta*, *50*(11), 2331–2341. doi:10.1016/j.electacta.2004.10.047

Bencsik, G., Janáky, C., Endrődi, B., & Visy, C. (2012). Electrocatalytic properties of the polypyrrole/magnetite hybrid modified electrode towards the reduction of hydrogen peroxide in the presence of dissolved oxygen. *Electrochimica Acta*, *73*, 53–58. doi:10.1016/j.electacta.2011.10.100

Benvenuto, P., Kafi, A. K. M., & Chen, A. (2009). High performance glucose biosensor based on the immobilization of glucose oxidase onto modified titania nanotube arrays. *Journal of Electroanalytical Chemistry*, *627*(1-2), 76–81. doi:10.1016/j.jelechem.2008.12.022

Berg, M., Tran, H. C., Nguyen, T. C., Pham, H. V., Schertenleib, R., & Giger, W. (2001). Arsenic Contamination of Groundwater and Drinking Water in Vietnam: A Human Health Threat. *Environmental Science & Technology*, *35*(13), 2621–2626. doi:10.1021/es010027y

Bergamini, M. F., dos Santos, D. P., & Zanoni, M. V. B. (2007). Development of a voltammetric sensor for chromium(VI) determination in wastewater sample. *Sensors and Actuators B: Chemical*, *123*(2), 902–908. doi:10.1016/j.snb.2006.10.062

Bosworth, T., Setford, S., Heywood, R., & Saini, S. (2001). Pulsed amperometric detection of furan compounds in transformer oil. *Analytica Chimica Acta*, *450*(1-2), 253–261. doi:10.1016/S0003-2670(01)01377-0

Bouzige, M., Legeay, P., Pichon, V., & Hennion, M. C. (1999). Selective on-line immunoextraction coupled to liquid chromatography for the trace determination of benzidine, congeners and related azo dyes in surface water and industrial effluents. *Journal of chromatography. A*, *846*(1-2), 317–29. Retrieved from http://www.ncbi.nlm.nih.gov/pubmed/10420617

Breiby, D. A. G. W., Samuelsen, E. J., Groenendaal, L. B., & Struth, B. (2002). Smectic Structures in Electrochemically Prepared Poly (3 , 4- ethylenedioxythiophene) Films, 945–952.

Brett, C. M. a. (2001). Electrochemical sensors for environmental monitoring. Strategy and examples. *Pure and Applied Chemistry*, *73*(12), 1969–1977. doi:10.1351/pac200173121969

Brett, C. M. A., Alves, V. A., & Fungaro, D. A. (2001). Nafion-Coated Mercury Thin Film and Glassy Carbon Electrodes for Electroanalysis: Characterization by Electrochemical Impedance. *Electroanalysis*, *13*(3), 212–218. doi:10.1002/1521-4109(200103)13:3<212::AID-ELAN212>3.0.CO;2-Z

Brett, C. M. A., & Oliveira Brett, A. M. (1993). *Electrochemistry: Principles, Methods, and Applications* (p. 456).

Calvo-Pérez, A., Domínguez-Renedo, O., Alonso-Lomillo, M. A., & Arcos-Martínez, M. J. (2010). Simultaneous Determination of Cr(III) and Cr(VI) by Differential Pulse Voltammetry Using Modified Screen-Printed Carbon Electrodes in Array Mode. *Electroanalysis*, *22*(24), 2924–2930. doi:10.1002/elan.201000350

Cameron, N. R., & Sherrington, D. C. (1997). Synthesis and Characterization of Poly(aryl ether sulfone) PolyHIPE Materials. *Macromolecules*, *30*(19), 5860–5869. doi:10.1021/ma961403f

Campbell, F. W., & Compton, R. G. (2010). The use of nanoparticles in electroanalysis: an updated review. *Analytical and bioanalytical chemistry*, *396*(1), 241–59. doi:10.1007/s00216-009-3063-7

Cañete-Rosales, P., Ortega, V., Álvarez-Lueje, A., Bollo, S., González, M., Ansón, A., & Martínez, M. T. (2012). Influence of size and oxidative treatments of multi-walled carbon nanotubes on their electrocatalytic properties. *Electrochimica Acta*, *62*, 163–171. doi:10.1016/j.electacta.2011.12.043

Cappelletti, G., Bianchi, C. L., & Ardizzone, S. (2008). Nano-titania assisted photoreduction of Cr(VI). *Applied Catalysis B: Environmental*, *78*(3-4), 193–201. doi:10.1016/j.apcatb.2007.09.022

CARP, O. (2004). Photoinduced reactivity of titanium dioxide. *Progress in Solid State Chemistry*, *32*(1-2), 33–177. doi:10.1016/j.progsolidstchem.2004.08.001

Carrington, N. a, Yong, L., & Xue, Z.-L. (2006). Electrochemical deposition of sol-gel films for enhanced chromium(VI) determination in aqueous solutions. *Analytica chimica acta*, *572*(1), 17–24. doi:10.1016/j.aca.2006.05.020

Carvalho, R. C., Gouveia-Caridade, C., & Brett, C. M. a. (2010). Glassy carbon electrodes modified by multiwalled carbon nanotubes and poly(neutral red): a comparative study of different brands and application to electrocatalytic ascorbate determination. *Analytical and bioanalytical chemistry*, *398*(4), 1675–85. doi:10.1007/s00216-010-3966-3

Chatzitheodorou, E., Economou, A., & Voulgaropoulos, A. (2004). Trace Determination of Chromium by Square-Wave Adsorptive Stripping Voltammetry on Bismuth Film Electrodes. *Electroanalysis*, *16*(21), 1745–1754. doi:10.1002/elan.200403051

Chen, D., & K. Ray, A. (2001). Removal of toxic metal ions from wastewater by semiconductor photocatalysis. *Chemical Engineering Science*, *56*(4), 1561–1570. doi:http://dx.doi.org/10.1016/S0009-2509(00)00383-3

Chen, S.-M., Chen, J.-Y., & Thangamuthu, R. (2007). Electrochemical Preparation of Poly(Malachite Green) Film Modified Nafion-Coated Glassy Carbon Electrode and Its Electrocatalytic Behavior Towards NADH, Dopamine and Ascorbic Acid. *Electroanalysis*, *19*(14), 1531–1538. doi:10.1002/elan.200703861

Chen, W., Cai, S., Ren, Q.-Q., Wen, W., & Zhao, Y.-D. (2012). Recent advances in electrochemical sensing for hydrogen peroxide: a review. *The Analyst*, *137*(1), 49–58. doi:10.1039/c1an15738h

Chen, Y., Lunsford, S., & Dionysiou, D. D. (2008). Photocatalytic activity and electrochemical response of titania film with macro/mesoporous texture. *Thin Solid Films*, *516*(21), 7930–7936. doi:10.1016/j.tsf.2008.05.019

Chiang, I. W., Brinson, B. E., Smalley, R. E., Margrave, J. L., & Hauge, R. H. (2001). Purification and Characterization of Single-Wall Carbon Nanotubes. *The Journal of Physical Chemistry B*, *105*(6), 1157–1161. doi:10.1021/jp003453z

Chiu, J.-Y., Yu, C.-M., Yen, M.-J., & Chen, L.-C. (2009). Glucose sensing electrodes based on a poly(3,4-ethylenedioxythiophene)/Prussian blue bilayer and multi-walled carbon nanotubes. *Biosensors & bioelectronics*, *24*(7), 2015–20. doi:10.1016/j.bios.2008.10.010

Cho, Y., Kyung, H., & Choi, W. (2004). Visible light activity of TiO2 for the photoreduction of CCl4 and Cr(VI) in the presence of nonionic surfactant (Brij). *Applied Catalysis B: Environmental*, *52*(1), 23–32. doi:10.1016/j.apcatb.2004.03.013

Chou, A., Bocking, T., Singh, N. K., & Gooding, J. J. (2005). Demonstration of the importance of oxygenated species at the ends of carbon nanotubes for their favourable electrochemical properties. *Chemical communications (Cambridge, England)*, (7), 842–4. doi:10.1039/b415051a

Chu, L., & Zhang, X. (2012). Electrochemical detection of chloride at the multilayer nano-silver modified indium-tin oxide thin electrodes. *Journal of Electroanalytical Chemistry*, *665*, 26–32. doi:10.1016/j.jelechem.2011.11.012

Chun, K.-Y., Oh, Y., Rho, J., Ahn, J.-H., Kim, Y.-J., Choi, H. R., & Baik, S. (2010). Highly conductive, printable and stretchable composite films of carbon nanotubes and silver. *Nature nanotechnology*, *5*(12), 853–7. doi:10.1038/nnano.2010.232

Chung, K.-T., Chen, S.-C., & Claxton, L. D. (2006). Review of the Salmonella typhimurium mutagenicity of benzidine, benzidine analogues, and benzidine-based dyes. *Mutation research*, *612*(1), 58–76. doi:10.1016/j.mrrev.2005.08.001

Crispin, X., Jakobsson, F. L. E., Crispin, A., Grim, P. C. M., Andersson, P., Volodin, A., … Berggren, M. (2006). The Origin of the High Conductivity of Poly(3,4-ethylenedioxythiophene)−Poly(styrenesulfonate) (PEDOT−PSS) Plastic Electrodes. *Chemistry of Materials*, *18*(18), 4354–4360. doi:10.1021/cm061032+

Currie, L. A. (1995). Nomenclature in evaluation of analytical methods including detection and quantification capabilities (IUPAC Recommendations 1995). *Pure and Applied Chemistry*, *67*(10), 1699–1723. doi:10.1351/pac199567101699

Curulli, A., Cesaro, S. N., Coppe, A., Silvestri, C., & Palleschi, G. (2005). Functionalization and Dissolution of Single-Walled Carbon Nanotubes by Chemical-Physical and Electrochemical Treatments. *Microchimica Acta*, *152*(3-4), 225–232. doi:10.1007/s00604-005-0440-6

Dai, X., Wildgoose, G. G., & Compton, R. G. (2006). Apparent "electrocatalytic" activity of multiwalled carbon nanotubes in the detection of the anaesthetic halothane: occluded copper nanoparticles. *The Analyst*, *131*(8), 901–6. doi:10.1039/b606197d

Daniele, S., Battistel, D., Gerbasi, R., Benetollo, F., & Battiston, S. (2007). Titania-Coated Platinum Thin Films by MOCVD: Electrochemical and Photoelectrochemical Properties. *Chemical Vapor Deposition*, *13*(11), 644–650. doi:10.1002/cvde.200706599

Datsyuk, V., Kalyva, M., Papagelis, K., Parthenios, J., Tasis, D., Siokou, A., … Galiotis, C. (2008). Chemical oxidation of multiwalled carbon nanotubes. *Carbon*, *46*(6), 833–840. doi:10.1016/j.carbon.2008.02.012

Demirboğa, B., & Önal, A. M. (1999). Electrochemical polymerization of furan and 2-methylfuran. *Synthetic Metals*, *99*(3), 237–242. doi:10.1016/S0379-6779(98)01509-4

Desimoni, E., & Brunetti, B. (2012). Glassy Carbon Electrodes Film-Modified with Acidic Functionalities. A Review. *Electroanalysis*, *24*(7), 1481–1500. doi:10.1002/elan.201200125

Devi, P., Reddy, P., Arora, S., Singh, S., Ghanshyam, C., & Singla, M. L. (2012). Sensing behavior study of silica-coated Ag nanoparticles deposited on glassy carbon toward nitrobenzene. *Journal of Nanoparticle Research*, *14*(10), 1172. doi:10.1007/s11051-012-1172-2

Diesel, E., Schreiber, M., & van der Meer, J. R. (2009). Development of bacteria-based bioassays for arsenic detection in natural waters. *Analytical and Bioanalytical Chemistry*, *394*(3), 687–693. doi:DOI 10.1007/s00216-009-2785-x

Domínguez, O., & Arcos, M. J. (2000). Speciation of Chromium by Adsorptive Stripping Voltammetry Using Pyrocatechol Violet. *Electroanalysis*, *12*(6), 449–458. doi:10.1002/(SICI)1521-4109(20000401)12:6<449::AID-ELAN449>3.0.CO;2-J

Domínguez, O., Asunción Alonso, M., & Arcos, M. J. (2002). Application of an Optimization Procedure in Adsorptive Stripping Voltammetry for the Determination of Chromium with Ammonium Pyrrolidine Dithiocarbamate. *Electroanalysis*, *14*(15-16), 1083–1089. doi:10.1002/1521-4109(200208)14:15/16<1083::AID-ELAN1083>3.0.CO;2-P

Domínguez, O., & Julia Arcos, M. (2002). Simultaneous determination of chromium(VI) and chromium(III) at trace levels by adsorptive stripping voltammetry. *Analytica Chimica Acta*, *470*(2), 241–252. doi:10.1016/S0003-2670(02)00757-2

Domínguez, O., Sanllorente, S., Alonso, M. A., & Arcos, M. J. (2001). Application of an Optimization Procedure for the Determination of Chromium in Various Water Types by Catalytic-Adsorptive Stripping Voltammetry. *Electroanalysis*, *13*(18), 1505–1512. doi:10.1002/1521-4109(200112)13:18<1505::AID-ELAN1505>3.0.CO;2-N

Domínguez-Renedo, O., Ruiz-Espelt, L., García-Astorgano, N., & Arcos-Martínez, M. J. (2008). Electrochemical determination of chromium(VI) using metallic nanoparticle-modified carbon screen-printed electrodes. *Talanta*, *76*(4), 854–8. doi:10.1016/j.talanta.2008.04.036

Du, D., Ding, J., Cai, J., & Zhang, A. (2007). Electrochemical thiocholine inhibition sensor based on biocatalytic growth of Au nanoparticles using chitosan as template. *Sensors and Actuators B: Chemical*, *127*(2), 317–322. doi:10.1016/j.snb.2007.04.023

Du, D., Wang, M., Qin, Y., & Lin, Y. (2010). One-step electrochemical deposition of Prussian Blue–multiwalled carbon nanotube nanocomposite thin-film: preparation, characterization and evaluation for H2O2 sensing. *Journal of Materials Chemistry*, *20*(8), 1532. doi:10.1039/b919500a

Dumitrescu, I., Wilson, N. R., & Macpherson, J. V. (2007). Functionalizing Single-Walled Carbon Nanotube Networks: Effect on Electrical and Electrochemical Properties. *Journal of Physical Chemistry C*, *111*(35), 12944–12953. doi:10.1021/jp067256x

Dura, J. a., Murthi, V. S., Hartman, M., Satija, S. K., & Majkrzak, C. F. (2009). Multilamellar Interface Structures in Nafion. *Macromolecules*, *42*(13), 4769–4774. doi:10.1021/ma802823j

Fajerwerg, K., Ynam, V., Chaudret, B., Garçon, V., Thouron, D., & Comtat, M. (2010). An original nitrate sensor based on silver nanoparticles electrodeposited on a gold electrode. *Electrochemistry Communications*, *12*(10), 1439–1441. doi:10.1016/j.elecom.2010.08.003

Falciola, L., Pifferi, V., & Mascheroni, E. (2012). Platinum-Based and Carbon-Based Screen Printed Electrodes for the Determination of Benzidine by Differential Pulse Voltammetry. *Electroanalysis*, *24*(4), 767–775. doi:10.1002/elan.201200007

Falciola, L., Pifferi, V., Possenti, M. L., & Carrara, V. (2012). Square Wave Voltammetric detection of furan on platinum and platinum-based Screen Printed Electrodes. *Journal of Electroanalytical Chemistry*, *664*, 100–104. doi:10.1016/j.jelechem.2011.10.021

Fang, H.-T., Liu, C.-G., Liu, C., Li, F., Liu, M., & Cheng, H.-M. (2004). Purification of Single-Wall Carbon Nanotubes by Electrochemical Oxidation. *Chemistry of Materials*, *16*(26), 5744–5750. doi:10.1021/cm035263h

Feng, S., Savage, J., & Voth, G. A. (2012). Effects of Polymer Morphology on Proton Solvation and Transport in Proton-Exchange Membranes. *The Journal of Physical Chemistry C*, *116*(36), 19104–19116. doi:10.1021/jp304783z

Feng, Y. L., Chen, H. Y., Tian, L. C., & Narasaki, H. (1998). Off-line separation and determination of inorganic arsenic species in natural water by high resolution inductively coupled plasma mass spectrometry with hydride generation combined with reaction of arsenic(V) and L-cysteine. *Analytica Chimica Acta*, *375*(1-2), 167–175. doi:Doi 10.1016/S0003-2670(98)00285-2

Ferruti, P., Mauro, N., Falciola, L., Pifferi, V., Bartoli, C., Gazzarri, M., … Ranucci, E. (2013). Amphoteric, Prevailingly Cationic L -Arginine Polymers of Poly(amidoamino acid) Structure:

Synthesis, Acid/Base Properties and Preliminary Cytocompatibility and Cell-Permeating Characterizations. *Macromolecular Bioscience*, n/a–n/a. doi:10.1002/mabi.201300387

Fujishima, A., Rao, T. N., & Tryk, D. A. (2000). Titanium dioxide photocatalysis. *Journal of Photochemistry and Photobiology C: Photochemistry Reviews*, *1*(1), 1–21. doi:10.1016/S1389-5567(00)00002-2

Geiser, D. M. (2009). Sexual structures in Aspergillus: morphology, importance and genomics. *Medical Mycology*, *47*(s1), S21–S26. doi:doi:10.1080/13693780802139859

Gellissen, G., Kunze, G., Gaillardin, C., Cregg, J. M., Berardi, E., Veenhuis, M., & van der Klei, I. (2005). New yeast expression platforms based on methylotrophic Hansenula polymorpha and Pichia pastoris and on dimorphic Arxula adeninivorans and Yarrowia lipolytica – A comparison. *FEMS Yeast Research*, *5*(11), 1079–1096. doi:http://dx.doi.org/10.1016/j.femsyr.2005.06.004

Gerard, M., Chaubey, A., & Malhotra, B. D. (2002). Application of conducting polymers to biosensors. *Biosensors & bioelectronics*, *17*(5), 345–59. Retrieved from http://www.ncbi.nlm.nih.gov/pubmed/11888724

Ghica, M. Emilia, Wintersteller, Y., & Brett, C. M. A. (2013). Poly(brilliant green)/carbon nanotube-modified carbon film electrodes and application as sensors. *Journal of Solid State Electrochemistry*, *17*(6), 1571–1580. doi:10.1007/s10008-013-2040-4

Ghica, Mariana Emilia, & Brett, C. M. a. (2010). The influence of carbon nanotubes and polyazine redox mediators on the performance of amperometric enzyme biosensors. *Microchimica Acta*, *170*(3-4), 257–265. doi:10.1007/s00604-010-0325-1

Ghilane, J., Fan, F.-R. F., Bard, A. J., & Dunwoody, N. (2007). Facile electrochemical characterization of core/shell nanoparticles. Ag core/Ag(2)O shell structures. *Nano letters*, *7*(5), 1406–12. doi:10.1021/nl070268p

Giacomino, A., Abollino, O., Lazzara, M., Malandrino, M., & Mentasti, E. (2011). Determination of As(III) by anodic stripping voltammetry using a lateral gold electrode: Experimental conditions, electron transfer and monitoring of electrode surface. *Talanta*, *83*(5), 1428–1435. doi:DOI 10.1016/j.talanta.2010.11.033

Goldmann, T., Périsset, A., Scanlan, F., & Stadler, R. H. (2005). Rapid determination of furan in heated foodstuffs by isotope dilution solid phase micro-extraction-gas chromatography--mass spectrometry (SPME-GC-MS). *The Analyst*, *130*(6), 878–83. doi:10.1039/b419270b

Golka, K., Kopps, S., & Myslak, Z. W. (2004). Carcinogenicity of azo colorants: influence of solubility and bioavailability. *Toxicology letters*, *151*(1), 203–10. doi:10.1016/j.toxlet.2003.11.016

Gómez, V., & Callao, M. P. (2006). Chromium determination and speciation since 2000. *TrAC Trends in Analytical Chemistry*, *25*(10), 1006–1015. doi:10.1016/j.trac.2006.06.010

Gonçalves, a. R., Ghica, M. E., & Brett, C. M. a. (2011). Preparation and characterisation of poly(3,4-ethylenedioxythiophene) and poly(3,4-ethylenedioxythiophene)/poly(neutral red) modified carbon film electrodes, and application as sensors for hydrogen peroxide. *Electrochimica Acta*, *56*(10), 3685–3692. doi:10.1016/j.electacta.2010.11.056

Gooding, J. J. (2005). Nanostructuring electrodes with carbon nanotubes: A review on electrochemistry and applications for sensing. *Electrochimica Acta*, *50*(15), 3049–3060. doi:10.1016/j.electacta.2004.08.052

Gouveia-caridade, C., Brett, C. M. A., & Liess, H. (2006). Development and Interfacial Properties of Novel Polymer-modified Carbon Film Electrodes, *516*, 1313–1317.

Grabarczyk, M. (2008). Protocol for Extraction and Determination of Cr(VI) in Solid Materials with a High Cr(III)/Cr(VI) Ratio Using EDDS as a Leaching Agent for Cr(VI) and a Masking Agent for Cr(III). *Electroanalysis*, *20*(17), 1857–1862. doi:10.1002/elan.200804256

Grabarczyk, M., Baś, B., & Korolczuk, M. (2008). Application of a renewable silver based mercury film electrode to the determination of Cr(VI) in soil samples. *Microchimica Acta*, *164*(3-4), 465–470. doi:10.1007/s00604-008-0087-1

Grabarczyk, M., Kaczmarek, L., & Korolczuk, M. (2004). Determination of Cr(VI) by Catalytic Adsorptive Stripping Voltammetry with Application of Nitrilotriacetic Acid as a Masking Agent. *Electroanalysis*, *16*(18), 1503–1507. doi:10.1002/elan.200402977

Groenendaal, L., Zotti, G., Aubert, P. H., Waybright, S. M., & Reynolds, J. R. (2003). Electrochemistry of poly(3,4-alkylenedioxythiophene) derivatives. *Advanced Materials*, *15*(11), 855–879. Retrieved from http://www.scopus.com/inward/record.url?eid=2-s2.0-0038608197&partnerID=40&md5=27d8efdacae4aa66994601f15c07eaa8

GUAN, R., DAI, H., LI, C., LIU, J., & XU, J. (2006). Effect of casting solvent on the morphology and performance of sulfonated polyethersulfone membranes. *Journal of Membrane Science*, *277*(1-2), 148–156. doi:10.1016/j.memsci.2005.10.025

Hallam, P. M., Kampouris, D. K., Kadara, R. O., & Banks, C. E. (2010). Graphite screen printed electrodes for the electrochemical sensing of chromium(VI). *The Analyst*, *135*(8), 1947–52. doi:10.1039/c0an00228c

Han, Y., Zheng, J., & Dong, S. (2013). A novel nonenzymatic hydrogen peroxide sensor based on Ag–MnO2–MWCNTs nanocomposites. *Electrochimica Acta*, *90*, 35–43. doi:10.1016/j.electacta.2012.11.117

Hanelt, S., Orts-Gil, G., Friedrich, J. F., & Meyer-Plath, A. (2011). Differentiation and quantification of surface acidities on MWCNTs by indirect potentiometric titration. *Carbon*, *49*(9), 2978–2988. doi:10.1016/j.carbon.2011.03.016

Hanrahan, G., Patil, D. G., & Wang, J. (2004). Electrochemical sensors for environmental monitoring: design, development and applications. *Journal of environmental monitoring : JEM*, *6*(8), 657–64. doi:10.1039/b403975k

Harden, J., Donaldson, F. P., & Nyman, M. C. (2005). Concentrations and distribution of 3,3'-dichlorobenzidine and its congeners in environmental samples from Lake Macatawa. *Chemosphere*, *58*(6), 767–77. doi:10.1016/j.chemosphere.2004.09.081

Harris, P. J. F. (2009). *Carbon Nanotube Science*. Cambridge: Cambridge University Press. doi:10.1017/CBO9780511609701

Heras, A., Colina, A., López-Palacios, J., Ayala, P., Sainio, J., Ruiz, V., & Kauppinen, E. I. (2009). Electrochemical purification of carbon nanotube electrodes. *Electrochemistry Communications*, *11*(7), 1535–1538. doi:10.1016/j.elecom.2009.05.052

Herbert, C. G., Ghassemi, H., & Hay, A. S. (1997). Introduction of amino, aliphatic, and aliphatic carboxylic acid side groups onto poly(arylene ether sulfone)s via transimidization reactions. *Journal of Polymer Science Part A: Polymer Chemistry*, *35*(6), 1095–1108. doi:10.1002/(SICI)1099-0518(19970430)35:6<1095::AID-POLA13>3.0.CO;2-1

Hernández-Santos, D., González-García, M. B., & García, A. C. (2002). Metal-Nanoparticles Based Electroanalysis. *Electroanalysis*, *14*(18), 1225–1235. doi:10.1002/1521-4109(200210)14:18<1225::AID-ELAN1225>3.0.CO;2-Z

Hodes, G. (Ed.). (2001). *Electrochemistry of Nanomaterials*. Weinheim, Germany: Wiley-VCH Verlag GmbH. doi:10.1002/9783527612789

Hopenhayn-Rich, C., Biggs, M. Lou, & Smith, A. H. (1998). Lung and kidney cancer mortality associated with arsenic in drinking water in Córdoba, Argentina. *International Journal of Epidemiology*, *27*(4), 561–569. doi:10.1093/ije/27.4.561

Hou, P.-X., Liu, C., & Cheng, H.-M. (2008). Purification of carbon nanotubes. *Carbon*, *46*(15), 2003–2025. doi:10.1016/j.carbon.2008.09.009

Hsu, F. F., Lakshmi, V., Rothman, N., Bhatnager, V. K., Hayes, R. B., Kashyap, R., … Davis, B. (1996). Determination of benzidine, N-acetylbenzidine, and N,N'-diacetylbenzidine in human urine by capillary gas chromatography/negative ion chemical ionization mass spectrometry. *Analytical biochemistry*, *234*(2), 183–9. doi:10.1006/abio.1996.0070

Hu, X., Jiao, K., Sun, W., & You, J.-Y. (2006). Electrochemical and Spectroscopic Studies on the Interaction of Malachite Green with DNA and Its Application. *Electroanalysis*, *18*(6), 613–620. doi:10.1002/elan.200503438

Hua, M.-Y., Chen, H.-C., Chuang, C.-K., Tsai, R.-Y., Jeng, J.-L., Yang, H.-W., & Chern, Y.-T. (2011). The intrinsic redox reactions of polyamic acid derivatives and their application in hydrogen peroxide sensor. *Biomaterials*, *32*(21), 4885–95. doi:10.1016/j.biomaterials.2011.03.051

Hua, M.-Y., Lin, Y.-C., Tsai, R.-Y., Chen, H.-C., & Liu, Y.-C. (2011). A hydrogen peroxide sensor based on a horseradish peroxidase/polyaniline/carboxy-functionalized multiwalled carbon nanotube modified gold electrode. *Electrochimica Acta*, *56*(25), 9488–9495. doi:10.1016/j.electacta.2011.08.043

Huang, H. L., & Dasgupta, P. K. (1999). A field-deployable instrument for the measurement and speciation of arsenic in potable water. *Analytica Chimica Acta*, *380*(1), 27–37. doi:Doi 10.1016/S0003-2670(98)00649-7

Hung, D. Q., Nekrassova, O., & Compton, R. G. (2004). Analytical methods for inorganic arsenic in water: a review. *Talanta*, *64*(2), 269–277. doi:DOI 10.1016/j.talanta.2004.01.027

Inzelt, G., Pineri, M., Schultze, J. ., & Vorotyntsev, M. . (2000). Electron and proton conducting polymers: recent developments and prospects. *Electrochimica Acta*, *45*(15-16), 2403–2421. doi:10.1016/S0013-4686(00)00329-7

Isse, Abdirisak A, Falciola, L., Mussini, P. R., & Gennaro, A. (2006). Relevance of electron transfer mechanism in electrocatalysis: the reduction of organic halides at silver electrodes. *Chemical communications (Cambridge, England)*, (3), 344–6. doi:10.1039/b513801a

Isse, Abdirisak Ahmed, Berzi, G., Falciola, L., Rossi, M., Mussini, P. R., & Gennaro, A. (2009). Electrocatalysis and electron transfer mechanisms in the reduction of organic halides at Ag. *Journal of Applied Electrochemistry*, *39*(11), 2217–2225. doi:10.1007/s10800-008-9768-z

Janáky, C., & Visy, C. (2013). Conducting polymer-based hybrid assemblies for electrochemical sensing: a materials science perspective. *Analytical and bioanalytical chemistry*, *405*(11), 3489–511. doi:10.1007/s00216-013-6702-y

Jannasch, P. (2003). Recent developments in high-temperature proton conducting polymer electrolyte membranes. *Current Opinion in Colloid & Interface Science*, *8*(1), 96–102. doi:10.1016/S1359-0294(03)00006-2

Jia, M., Wang, T., Liang, F., & Hu, J. (2012). A Novel Process for the Fabrication of a Silver-Nanoparticle-Modified Electrode and Its Application in Nonenzymatic Glucose Sensing. *Electroanalysis*, *24*(9), 1864–1868. doi:10.1002/elan.201200273

Jones, C. P., Jurkschat, K., Crossley, A., Compton, R. G., Riehl, B. L., & Banks, C. E. (2007). Use of high-purity metal-catalyst-free multiwalled carbon nanotubes to avoid potential experimental misinterpretations. *Langmuir : the ACS journal of surfaces and colloids*, *23*(18), 9501–4. doi:10.1021/la701522p

Jorge, E. O., Rocha, M. M., Fonseca, I. T. E., & Neto, M. M. M. (2010). Studies on the stripping voltammetric determination and speciation of chromium at a rotating-disc bismuth film electrode. *Talanta*, *81*(1-2), 556–64. doi:10.1016/j.talanta.2009.12.043

Kajitvichyanukul, P., Ananpattarachai, J., & Pongpom, S. (2005). Sol–gel preparation and properties study of TiO 2 thin film for photocatalytic reduction of chromium(VI) in photocatalysis process. *Science and Technology of Advanced Materials*, *6*(3-4), 352–358. doi:10.1016/j.stam.2005.02.014

Kakhki, S., Barsan, M. M., Shams, E., & Brett, C. M. a. (2012). Development and characterization of poly(3,4-ethylenedioxythiophene)-coated poly(methylene blue)-modified carbon electrodes. *Synthetic Metals*, *161*(23-24), 2718–2726. doi:10.1016/j.synthmet.2011.10.007

Khairy, M., Kampouris, D. K., Kadara, R. O., & Banks, C. E. (2010). Gold Nanoparticle Modified Screen Printed Electrodes for the Trace Sensing of Arsenic(III) in the Presence of Copper(II). *Electroanalysis*, *22*(21), 2496–2501. doi:DOI 10.1002/elan.201000226

Klaine, S. J., Alvarez, P. J. J., Batley, G. E., Fernandes, T. F., Handy, R. D., Lyon, D. Y., … Lead, J. R. (2008). NANOMATERIALS IN THE ENVIRONMENT: BEHAVIOR, FATE, BIOAVAILABILITY, AND EFFECTS. *Environmental Toxicology and Chemistry*, *27*(9), 1825. doi:10.1897/08-090.1

Klaysom, C., Moon, S.-H., Ladewig, B. P., Lu, G. Q. M., & Wang, L. (2011a). Preparation of porous ion-exchange membranes (IEMs) and their characterizations. *Journal of Membrane Science*, *371*(1-2), 37–44. doi:10.1016/j.memsci.2011.01.008

Klaysom, C., Moon, S.-H., Ladewig, B. P., Lu, G. Q. M., & Wang, L. (2011b). The effects of aspect ratio of inorganic fillers on the structure and property of composite ion-exchange membranes. *Journal of colloid and interface science*, *363*(2), 431–9. doi:10.1016/j.jcis.2011.07.071

Kochmann, S., Hirsch, T., & Wolfbeis, O. S. (2012). Graphenes in chemical sensors and biosensors. *TrAC Trends in Analytical Chemistry*, *39*, 87–113. doi:10.1016/j.trac.2012.06.004

Korolczuk, M. (1999). Voltammetric Determination of Cr(VI) in Natural Water in the Presence of Bipyridine Following Its Deposition to the Metallic State. *Electroanalysis*, *11*(16), 1218–1221. doi:10.1002/(SICI)1521-4109(199911)11:16<1218::AID-ELAN1218>3.0.CO;2-Q

Ku, Y., & Jung, I. L. (2001). Photocatalytic reduction of Cr(VI) in aqueous solutions by UV irradiation with the presence of titanium dioxide. *Water research*, *35*(1), 135–42. Retrieved from http://www.ncbi.nlm.nih.gov/pubmed/11257867

Kumaravel, a., & Chandrasekaran, M. (2010). A novel nanosilver/nafion composite electrode for electrochemical sensing of methyl parathion and parathion. *Journal of Electroanalytical Chemistry*, *638*(2), 231–235. doi:10.1016/j.jelechem.2009.11.002

La Pera, L., Liberatore, A., Avellone, G., Fanara, S., Dugo, G., & Agozzino, P. (2009). Analysis of furan in coffee of different provenance by head-space solid phase microextraction gas chromatography-mass spectrometry: effect of brewing procedures. *Food additives & contaminants. Part A, Chemistry, analysis, control, exposure & risk assessment*, *26*(6), 786–92. doi:10.1080/02652030902751712

Lacorte, S, Guiffard, I., Fraisse, D., & Barcelo, D. (2000). Broad spectrum analysis of 109 priority compounds listed in the 76/464/CEE Council Directive using solid-phase extraction and GC/EI/MS. *Analytical chemistry*, *72*(7), 1430–40. Retrieved from http://www.ncbi.nlm.nih.gov/pubmed/10763237

Lacorte, Sílvia, Perrot, M.-C., Fraisse, D., & Barceló, D. (1999). Determination of chlorobenzidines in industrial effluent by solid-phase extraction and liquid chromatography with electrochemical and mass spectrometric detection. *Journal of Chromatography A*, *833*(2), 181–194. doi:10.1016/S0021-9673(98)00834-6

Lakshmi, R. T. S. M., Meier-Haack, J., Schlenstedt, K., Komber, H., Choudhary, V., & Varma, I. K. (2006). Synthesis, characterisation and membrane properties of sulphonated poly(aryl ether sulphone) copolymers. *Reactive and Functional Polymers*, *66*(6), 634–644. doi:10.1016/j.reactfunctpolym.2005.10.016

Laschi, S, Bagni, G., Palchetti, I., & Mascini, M. (2007). As(III) voltammetric detection by means of disposable screen-printed gold electrochemical sensors. *Analytical Letters*, *40*(16-18), 3002–3013. doi:Doi 10.1080/00032710701645703

Laschi, Serena, Fránek, M., & Mascini, M. (2000). Screen-Printed Electrochemical Immunosensors for PCB Detection. *Electroanalysis*, *12*(16), 1293–1298. doi:10.1002/1521-4109(200011)12:16<1293::AID-ELAN1293>3.0.CO;2-5

Leary, R., & Westwood, A. (2011). Carbonaceous nanomaterials for the enhancement of TiO2 photocatalysis. *Carbon*, *49*(3), 741–772. doi:10.1016/j.carbon.2010.10.010

Leermakers, M., Baeyens, W., De Gieter, M., Smedts, B., Meert, C., De Bisschop, H. C., … Quevauviller, P. (2006). Toxic arsenic compounds in environmental samples: Speciation and validation. *Trac-Trends in Analytical Chemistry*, *25*(1), 1–10. doi:DOI 10.1016/j.trac.2005.06.004

Li, C., Bai, H., & Shi, G. (2009). Conducting polymer nanomaterials: electrosynthesis and applications. *Chemical Society reviews*, *38*(8), 2397–409. doi:10.1039/b816681c

Li, J., Kuang, D., Feng, Y., Zhang, F., Xu, Z., Liu, M., & Wang, D. (2013). Green synthesis of silver nanoparticles-graphene oxide nanocomposite and its application in electrochemical sensing of tryptophan. *Biosensors & bioelectronics*, *42*, 198–206. doi:10.1016/j.bios.2012.10.029

LI, L., & LI, F. (2011). The effect of carbonyl, carboxyl and hydroxyl groups on the capacitance of carbon nanotubes. *New Carbon Materials*, *26*(3), 224–228. doi:10.1016/S1872-5805(11)60078-4

Li, M., Li, Y.-T., Li, D.-W., & Long, Y.-T. (2012). Recent developments and applications of screen-printed electrodes in environmental assays--a review. *Analytica chimica acta*, *734*, 31–44. doi:10.1016/j.aca.2012.05.018

Li, Q., Zhang, Q., Ding, L., Zhou, D., Cui, H., Wei, Z., & Zhai, J. (2013). Synthesis of silver/multi-walled carbon nanotubes composite and its application for electrocatalytic reduction of bromate. *Chemical Engineering Journal*, *217*, 28–33. doi:10.1016/j.cej.2012.12.005

Li, X., Wang, Y., Yang, X., Chen, J., Fu, H., & Cheng, T. (2012). Conducting polymers in environmental analysis. *TrAC Trends in Analytical Chemistry*, *39*, 163–179. doi:10.1016/j.trac.2012.06.003

Lin, L., Lawrence, N. S., Thongngamdee, S., Wang, J., & Lin, Y. (2005). Catalytic adsorptive stripping determination of trace chromium (VI) at the bismuth film electrode. *Talanta*, *65*(1), 144–8. doi:10.1016/j.talanta.2004.05.044

Litster, S., & McLean, G. (2004). PEM fuel cell electrodes. *Journal of Power Sources*, *130*(1-2), 61–76. doi:10.1016/j.jpowsour.2003.12.055

Liu, B., Deng, Y., Hu, X., Gao, Z., & Sun, C. (2012). Electrochemical sensing of trichloroacetic acid based on silver nanoparticles doped chitosan hydrogel film prepared with controllable electrodeposition. *Electrochimica Acta*, *76*, 410–415. doi:10.1016/j.electacta.2012.05.046

Liu, B., Lu, L., Wang, M., & Zi, Y. (2008). A study of nanostructured gold modified glassy carbon electrode for the determination of trace Cr(VI). *Journal of Chemical Sciences*, *120*(5), 493–498. doi:10.1007/s12039-008-0077-1

Liu, G., Lin, Y.-Y., Wu, H., & Lin, Y. (2007). Voltammetric Detection of Cr(VI) with Disposable Screen-Printed Electrode Modified with Gold Nanoparticles. *Environmental Science & Technology*, *41*(23), 8129–8134. doi:10.1021/es071726z

Lota, G., Fic, K., & Frackowiak, E. (2011). Carbon nanotubes and their composites in electrochemical applications. *Energy & Environmental Science*, *4*(5), 1592. doi:10.1039/c0ee00470g

Lu, W., Liao, F., Luo, Y., Chang, G., & Sun, X. (2011). Hydrothermal synthesis of well-stable silver nanoparticles and their application for enzymeless hydrogen peroxide detection. *Electrochimica Acta*, *56*(5), 2295–2298. doi:10.1016/j.electacta.2010.11.053

Lubert, K.-H., & Kalcher, K. (2010). History of Electroanalytical Methods. *Electroanalysis*, *22*(17-18), 1937–1946. doi:10.1002/elan.201000087

Luo, X. L., Morrin, A., Killard, A. J., & Smyth, M. R. (2006). Application of nanoparticles in electrochemical sensors and biosensors. *Electroanalysis*, *18*(4), 319–326. doi:DOI 10.1002/elan.200503415

Mahmoudian, M. R., Alias, Y., Basirun, W. J., & Ebadi, M. (2012). Preparation of ultra-thin polypyrrole nanosheets decorated with Ag nanoparticles and their application in hydrogen peroxide detection. *Electrochimica Acta*, *72*, 46–52. doi:10.1016/j.electacta.2012.03.144

Maino, G., Meroni, D., Pifferi, V., Falciola, L., Soliveri, G., Cappelletti, G., & Ardizzone, S. (2013). Electrochemically assisted deposition of transparent, mechanically robust TiO2 films for advanced applications. *Journal of Nanoparticle Research*, *15*(11), 2087. doi:10.1007/s11051-013-2087-2

Makena, P., & Chung, K.-T. (2007). Evidence that 4-aminobiphenyl, benzidine, and benzidine congeners produce genotoxicity through reactive oxygen species. *Environmental and molecular mutagenesis*, *48*(5), 404–13. doi:10.1002/em.20288

Manivannan, S., & Ramaraj, R. (2013). Silver nanoparticles embedded in cyclodextrin-silicate composite and their applications in Hg(II) ion and nitrobenzene sensing. *The Analyst*, *138*(6), 1733–9. doi:10.1039/c3an36488g

Manova, A., Humenikova, S., Strelec, M., & Beinrohr, E. (2007). Determination of chromium(VI) and total chromium in water by in-electrode coulometric titration in a porous glassy carbon electrode. *Microchimica Acta*, *159*(1-2), 41–47. doi:10.1007/s00604-007-0751-x

Mardegan, A., Scopece, P., Lamberti, F., Meneghetti, M., Moretto, L. M., & Ugo, P. (2012). Electroanalysis of Trace Inorganic Arsenic with Gold Nanoelectrode Ensembles. *Electroanalysis*, *24*(4), 798–806. doi:DOI 10.1002/elan.201100555

Mauter, M. S., & Elimelech, M. (2008). Environmental Applications of Carbon-Based Nanomaterials. *Environmental Science & Technology*, *42*(16), 5843–5859. doi:10.1021/es8006904

Mazov, I., Kuznetsov, V. L., Simonova, I. a., Stadnichenko, A. I., Ishchenko, A. V., Romanenko, A. I., … Anikeeva, O. B. (2012). Oxidation behavior of multiwall carbon nanotubes with different diameters and morphology. *Applied Surface Science*, *258*(17), 6272–6280. doi:10.1016/j.apsusc.2012.03.021

Melamed, D. (2005). Monitoring arsenic in the environment: a review of science and technologies with the potential for field measurements. *Analytica Chimica Acta*, *532*(1), 1–13. doi:DOI 10.1016/j.aca.2004.10.047

Meng, Y. Z., Hay, A. A., Jian, X. G., & Tjong, S. C. (1998). Synthesis and properties of poly(aryl ether sulfone)s containing the phthalazinone moiety. *Journal of Applied Polymer Science*, *68*(1), 137–143. doi:10.1002/(SICI)1097-4628(19980404)68:1<137::AID-APP15>3.0.CO;2-Y

Meroni, D., Ardizzone, S., Cappelletti, G., Ceotto, M., Ratti, M., Annunziata, R., … Raimondi, L. (2011). Interplay between Chemistry and Texture in Hydrophobic TiO2 Hybrids. *Journal of Physical Chemistry C*, *115*(38), 18649–18658. doi:Doi 10.1021/Jp205142b

Meroni, D., Pifferi, V., Sironi, B., Cappelletti, G., Falciola, L., Cerrato, G., & Ardizzone, S. (2012). Block copolymers for the synthesis of pure and Bi-promoted nano-TiO2 as active photocatalysts. *Journal of Nanoparticle Research*, *14*(8), 1086. doi:10.1007/s11051-012-1086-z

Metters, J. P., Kadara, R. O., & Banks, C. E. (2011). New directions in screen printed electroanalytical sensors: an overview of recent developments. *The Analyst*, *136*(6), 1067–76. doi:10.1039/c0an00894j

Mittal, A., Kaur, D., & Mittal, J. (2008). Applicability of waste materials--bottom ash and deoiled soya--as adsorbents for the removal and recovery of a hazardous dye, brilliant green. *Journal of colloid and interface science*, *326*(1), 8–17. doi:10.1016/j.jcis.2008.07.005

Moores, A., & Goettmann, F. (2006). The plasmon band in noble metal nanoparticles: an introduction to theory and applications. *New Journal of Chemistry*, *30*(8), 1121. doi:10.1039/b604038c

Moraes, F. C., Cabral, M. F., Mascaro, L. H., & Machado, S. a. S. (2011). The electrochemical effect of acid functionalisation of carbon nanotubes to be used in sensors development. *Surface Science*, *605*(3-4), 435–440. doi:10.1016/j.susc.2010.11.014

Moretto, L. M., Montagner, F., Ganzerla, R., & Ugo, P. (2013). Nafion® as advanced immobilisation substrate for the voltammetric analysis of electroactive microparticles: the case of some artistic colouring agents. *Analytical and bioanalytical chemistry*, *405*(11), 3603–10. doi:10.1007/s00216-013-6796-2

Nandi, B. K., Goswami, A., & Purkait, M. K. (2009). Adsorption characteristics of brilliant green dye on kaolin. *Journal of hazardous materials*, *161*(1), 387–95. doi:10.1016/j.jhazmat.2008.03.110

Narang, J., Chauhan, N., Jain, P., & Pundir, C. S. (2012). Silver nanoparticles/multiwalled carbon nanotube/polyaniline film for amperometric glutathione biosensor. *International journal of biological macromolecules*, *50*(3), 672–8. doi:10.1016/j.ijbiomac.2012.01.023

Noked, M., Soffer, A., & Aurbach, D. (2011). The electrochemistry of activated carbonaceous materials: past, present, and future. *Journal of Solid State Electrochemistry*, *15*(7-8), 1563–1578. doi:10.1007/s10008-011-1411-y

Nordstrom, D. K. (2002). Worldwide Occurrences of Arsenic in Ground Water. *Science*, *296*(5576), 2143–2145. doi:10.1126/science.1072375

Oliver, N. S., Toumazou, C., Cass, A. E. G., & Johnston, D. G. (2009). Glucose sensors: a review of current and emerging technology. *Diabetic medicine : a journal of the British Diabetic Association*, *26*(3), 197–210. doi:10.1111/j.1464-5491.2008.02642.x

Orazem, M. E., & Tribollet, B. (2008). *Electrochemical Impedance Spectroscopy* (p. 560).

Pal, P., Sarkar, P., Bhattacharyay, D., & Pal, S. (2010). Development of Some Electrochemical Systems for Detection of Arsenic in Drinking Water. *Sensor Letters*, *8*(4), 577–583. doi:Doi 10.1166/Sl.2010.1314

Paoli, E., Cappelletti, G., & Falciola, L. (2010). Electrochemistry as a tool for nano-TiO2 deposition and for photoremediation pollutant monitoring. *Electrochemistry Communications*, *12*(8), 1013–1016. doi:http://dx.doi.org/10.1016/j.elecom.2010.05.012

Park, J.-A., Kim, B.-K., Choi, H.-N., & Lee, W. (2010). Electrochemical Determination of Dopamine Based on Carbon Nanotube-Sol-Gel Titania-Nafion Composite Film Modified Electrode. *Bulletin of the Korean Chemical Society*, *31*(11), 3123–3127. doi:10.5012/bkcs.2010.31.11.3123

Park, T., Banerjee, S., Hemraj-Benny, T., & Wong, S. S. (2006). Purification strategies and purity visualization techniques for single-walled carbon nanotubes. *Journal of Materials Chemistry*, *16*(2), 141. doi:10.1039/b510858f

Patel, G., & Agrawal, Y. . (2003). Separation and trace estimation of benzidine and its macromolecular adducts using supercritical fluid chromatography. *Journal of Chromatography B*, *795*(2), 157–165. doi:10.1016/S1570-0232(03)00558-0

Pauliukaite, R., Ghica, M. E., Barsan, M. M., & Brett, C. M. a. (2010). Phenazines and Polyphenazines in Electrochemical Sensors and Biosensors. *Analytical Letters*, *43*(10-11), 1588–1608. doi:10.1080/00032711003653791

Pena, M. E., Korfiatis, G. P., Patel, M., Lippincott, L., & Meng, X. (2005). Adsorption of As(V) and As(III) by nanocrystalline titanium dioxide. *Water Research*, *39*(11), 2327–2337. doi:http://dx.doi.org/10.1016/j.watres.2005.04.006

Peña, R. C., Bertotti, M., & Brett, C. M. a. (2011). Methylene Blue/Multiwall Carbon Nanotube Modified Electrode for the Amperometric Determination of Hydrogen Peroxide. *Electroanalysis*, *23*(10), 2290–2296. doi:10.1002/elan.201100324

Pichler, T., Veizer, J., & Hall, G. E. M. (1999). Natural Input of Arsenic into a Coral-Reef Ecosystem by Hydrothermal Fluids and Its Removal by Fe(III) Oxyhydroxides. *Environmental Science & Technology*, *33*(9), 1373–1378. doi:10.1021/es980949+

Pierce, D. T., & Zhao, J. X. (Eds.). (2010). *Trace Analysis with Nanomaterials*. Weinheim, Germany: Wiley-VCH Verlag GmbH & Co. KGaA. doi:10.1002/9783527632015

Pifferi, V, Spadavecchia, F., Cappelletti, G., Paoli, E. A., Bianchi, C. L., & Falciola, L. (2013). Electrodeposited nano-titania films for photocatalytic Cr(VI) reduction. *Catalysis Today*, *209*(0), 8–12. doi:http://dx.doi.org/10.1016/j.cattod.2012.08.031

Pifferi, Valentina, Ardizzone, S., Cappelletti, G., Falciola, L., & Meroni, D. (2013). Ultra-Traces Detection by Gold-Based Electrodes in As(III) Novel Photoremediation. *Electrocatalysis*, *4*(4), 306–311. doi:10.1007/s12678-013-0163-0

Pifferi, Valentina, Barsan, M. M., Ghica, M. E., Falciola, L., & Brett, C. M. A. (2013). Synthesis, characterization and influence of poly(brilliant green) on the performance of different electrode architectures based on carbon nanotubes and poly(3,4-ethylenedioxythiophene). *Electrochimica Acta*, *98*, 199–207. doi:10.1016/j.electacta.2013.03.048

Pifferi, Valentina, Marona, V., Longhi, M., & Falciola, L. (2013). Characterization of polymer stabilized silver nanoparticles modified Glassy Carbon electrodes for electroanalytical applications. *Electrochimica Acta*, *109*, 447–453. doi:10.1016/j.electacta.2013.07.194

Pigani, L., Culetu, A., Ulrici, A., Foca, G., Vignali, M., & Seeber, R. (2011). Pedot modified electrodes in amperometric sensing for analysis of red wine samples. *Food Chemistry*, *129*(1), 226–233. doi:10.1016/j.foodchem.2011.04.046

Pop, A., Manea, F., Radovan, C., Dascalu, D., Vaszilcsin, N., & Schoonman, J. (2012). Non-enzymatic electrochemical detection of glycerol on boron-doped diamond electrode. *The Analyst*, *137*(3), 641–7. doi:10.1039/c2an15645h

Prakash, S., Chakrabarty, T., Singh, A. K., & Shahi, V. K. (2012). Silver nanoparticles built-in chitosan modified glassy carbon electrode for anodic stripping analysis of As(III) and its removal from water. *Electrochimica Acta*, *72*, 157–164. doi:10.1016/j.electacta.2012.04.025

Pumera, M. (2009). The electrochemistry of carbon nanotubes: fundamentals and applications. *Chemistry (Weinheim an der Bergstrasse, Germany)*, *15*(20), 4970–8. doi:10.1002/chem.200900421

Pumera, M. (2012). Voltammetry of carbon nanotubes and graphenes: excitement, disappointment, and reality. *Chemical record (New York, N.Y.)*, *12*(1), 201–13. doi:10.1002/tcr.201100027

Pumera, M., Sánchez, S., Ichinose, I., & Tang, J. (2007). Electrochemical nanobiosensors. *Sensors and Actuators B: Chemical*, *123*(2), 1195–1205. doi:10.1016/j.snb.2006.11.016

Pumera, M., Šmíd, B., & Veltruská, K. (2009). Influence of Nitric Acid Treatment of Carbon Nanotubes on Their Physico-Chemical Properties. *Journal of Nanoscience and Nanotechnology*, *9*(4), 2671–2676. doi:10.1166/jnn.2009.031

Qin, X., Lu, W., Luo, Y., Chang, G., Asiri, A. M., Al-Youbi, A. O., & Sun, X. (2012). Synthesis of Ag nanoparticle-decorated 2,4,6-tris(2-pyridyl)-1,3,5-triazine nanobelts and their application for H2O2 and glucose detection. *The Analyst*, *137*(4), 939–43. doi:10.1039/c2an15996a

Quan, H., Park, S.-U., & Park, J. (2010). Electrochemical oxidation of glucose on silver nanoparticle-modified composite electrodes. *Electrochimica Acta*, *55*(7), 2232–2237. doi:10.1016/j.electacta.2009.11.074

Qureshi, A., Kang, W. P., Davidson, J. L., & Gurbuz, Y. (2009). Review on carbon-derived, solid-state, micro and nano sensors for electrochemical sensing applications. *Diamond and Related Materials*, *18*(12), 1401–1420. doi:10.1016/j.diamond.2009.09.008

Ramezani-Rad, M., Hollenberg, C. P., Lauber, J., Wedler, H., Griess, E., Wagner, C., … Gellissen, G. (2003). The Hansenula polymorpha (strain CBS4732) genome sequencing and analysis. *FEMS Yeast Research*, *4*(2), 207–215. doi:http://dx.doi.org/10.1016/S1567-1356(03)00125-9

Rani, S., Roy, S. C., Paulose, M., Varghese, O. K., Mor, G. K., Kim, S., … Grimes, C. A. (2010). Synthesis and applications of electrochemically self-assembled titania nanotube arrays. *Physical chemistry chemical physics : PCCP*, *12*(12), 2780–800. doi:10.1039/b924125f

Rao, C. N. R., Müller, A., & Cheetham, A. K. (Eds.). (2004). *The Chemistry of Nanomaterials*. Weinheim, FRG: Wiley-VCH Verlag GmbH & Co. KGaA. doi:10.1002/352760247X

Rao, C. N., Satishkumar, B. C., Govindaraj, A., & Nath, M. (2001). Nanotubes. *Chemphyschem : a European journal of chemical physics and physical chemistry*, *2*(2), 78–105. doi:10.1002/1439-7641(20010216)2:2<78::AID-CPHC78>3.0.CO;2-7

Rassaei, L, Amiri, M., Cirtiu, C. M., Sillanpaa, M., & Marken, F. (2011). Nanoparticles in electrochemical sensors for environmental monitoring. *Trac-Trends in Analytical Chemistry*, *30*(11), 1704–1715. doi:DOI 10.1016/j.trac.2011.05.009

Rassaei, Liza, Marken, F., Sillanpää, M., Amiri, M., Cirtiu, C. M., & Sillanpää, M. (2011). Nanoparticles in electrochemical sensors for environmental monitoring. *TrAC Trends in Analytical Chemistry*, *30*(11), 1704–1715. doi:10.1016/j.trac.2011.05.009

Ratinac, K. R., Yang, W., Gooding, J. J., Thordarson, P., & Braet, F. (2011). Graphene and Related Materials in Electrochemical Sensing. *Electroanalysis*, *23*(4), 803–826. doi:10.1002/elan.201000545

Ravichandran, R., Sundarrajan, S., Venugopal, J. R., Mukherjee, S., & Ramakrishna, S. (2012). Advances in Polymeric Systems for Tissue Engineering and Biomedical Applications. *Macromolecular Bioscience*, *12*(3), 286–311. doi:DOI 10.1002/mabi.201100325

Rawal, R., Chawla, S., & Pundir, C. S. (2011). Polyphenol biosensor based on laccase immobilized onto silver nanoparticles/multiwalled carbon nanotube/polyaniline gold electrode. *Analytical biochemistry*, *419*(2), 196–204. doi:10.1016/j.ab.2011.07.028

Ren, X., Meng, X., Chen, D., Tang, F., & Jiao, J. (2005). Using silver nanoparticle to enhance current response of biosensor. *Biosensors & bioelectronics*, *21*(3), 433–7. doi:10.1016/j.bios.2004.08.052

Renedo, O. D., & Julia Arcos Martínez, M. (2007). A novel method for the anodic stripping voltammetry determination of Sb(III) using silver nanoparticle-modified screen-printed electrodes. *Electrochemistry Communications*, *9*(4), 820–826. doi:10.1016/j.elecom.2006.11.016

Riggin, R. M., & Howard, C. C. (1979). Determination of benzidine, dichlorobenzidine, and diphenylhydrazine in aqueous media by high performance liquid chromatography. *Analytical Chemistry*, *51*(2), 210–214. doi:10.1021/ac50038a014

Rondinini, S., & Vertova, A. (2004). Electrocatalysis on silver and silver alloys for dichloromethane and trichloromethane dehalogenation. *Electrochimica Acta*, *49*(22-23), 4035–4046. doi:10.1016/j.electacta.2003.12.061

Rosca, I. D., Watari, F., Uo, M., & Akasaka, T. (2005). Oxidation of multiwalled carbon nanotubes by nitric acid. *Carbon*, *43*(15), 3124–3131. doi:10.1016/j.carbon.2005.06.019

Sadeghi, S., Hemmati, M., & Garmroodi, A. (2013). Preparation of Ag-Nanoparticles/Ionic-Liquid Modified Screen-Printed Electrode and Its Application in the Determination of Metronidazole. *Electroanalysis*, *25*(1), 316–322. doi:10.1002/elan.201200412

Sander, S., Navrátil, T., & Novotný, L. (2003). Study of the Complexation, Adsorption and Electrode Reaction Mechanisms of Chromium(VI) and (III) with DTPA Under Adsorptive Stripping Voltammetric Conditions. *Electroanalysis*, *15*(19), 1513–1521. doi:10.1002/elan.200302735

Satheesh Babu, T. G., Suneesh, P. V, Ramachandran, T., & Nair, B. (2010). Gold Nanoparticles Modified Titania Nanotube Arrays for Amperometric Determination of Ascorbic Acid. *Analytical Letters*, *43*(18), 2809–2822. doi:10.1080/00032711003725615

Scheibe, B., Borowiak-Palen, E., & Kalenczuk, R. J. (2010). Oxidation and reduction of multiwalled carbon nanotubes — preparation and characterization. *Materials Characterization*, *61*(2), 185–191. doi:10.1016/j.matchar.2009.11.008

Schmid, G. (Ed.). (2003). *Nanoparticles*. Weinheim, FRG: Wiley-VCH Verlag GmbH & Co. KGaA. doi:10.1002/3527602399

Scott, C. L., & Pumera, M. (2011). Carbon nanotubes can exhibit negative effects in electroanalysis due to presence of nanographite impurities. *Electrochemistry Communications*, *13*(5), 426–428. doi:10.1016/j.elecom.2011.02.011

Sharma, V. K., Dutta, P. K., & Ray, A. K. (2007). Review of kinetics of chemical and photocatalytical oxidation of Arsenic(III) as influenced by pH. *Journal of Environmental Science and Health, Part A*, *42*(7), 997–1004. doi:10.1080/10934520701373034

Sharma, V. K., & Sohn, M. (2009). Aquatic arsenic: Toxicity, speciation, transformations, and remediation. *Environment International*, *35*(4), 743–759. doi:http://dx.doi.org/10.1016/j.envint.2009.01.005

Shervani, Z., Ikushima, Y., Sato, M., Kawanami, H., Hakuta, Y., Yokoyama, T., … Aramaki, K. (2007). Morphology and size-controlled synthesis of silver nanoparticles in aqueous surfactant polymer solutions. *Colloid and Polymer Science*, *286*(4), 403–410. doi:10.1007/s00396-007-1784-8

Shin, H.-S., & Ahn, H.-S. (2006). Analysis of Benzidine and Dichlorobenzidine at Trace Levels in Water by Silylation and Gas Chromatography–Mass Spectrometry. *Chromatographia*, *63*(1-2), 77–84. doi:10.1365/s10337-005-0692-7

Simm, A O, Banks, C. E., Wilkins, S. J., Karousos, N. G., Davis, J., & Compton, R. G. (2005). A comparison of different types of gold-carbon composite electrode for detection of arsenic(III). *Analytical and Bioanalytical Chemistry*, *381*(4), 979–985. doi:DOI 10.1007/s00216-004-2960-z

Simm, Andrew O, Ward-Jones, S., Banks, C. E., & Compton, R. G. (2005). Novel methods for the production of silver microelectrode-arrays: their characterisation by atomic force microscopy and application to the electro-reduction of halothane. *Analytical sciences : the international journal of the Japan Society for Analytical Chemistry*, *21*(6), 667–71. Retrieved from http://www.ncbi.nlm.nih.gov/pubmed/15984203

Smith, A. H., Lopipero, P. A., Bates, M. N., & Steinmaus, C. M. (2002). Arsenic Epidemiology and Drinking Water Standards. *Science*, *296*(5576), 2145–2146. doi:10.1126/science.1072896

Song, Y., & Swain, G. M. (2007). Total inorganic arsenic detection in real water samples using anodic stripping voltammetry and a gold-coated diamond thin-film electrode. *Analytica Chimica Acta*, *593*(1), 7–12. doi:DOI 10.1016/j.aca.2007.04.033

Spadavecchia, F., Cappelletti, G., Ardizzone, S., Bianchi, C. L., Cappelli, S., Oliva, C., … Fermo, P. (2010). Solar photoactivity of nano-N-TiO2 from tertiary amine: role of defects and paramagnetic species. *Applied Catalysis B: Environmental*, *96*(3–4), 314–322. doi:http://dx.doi.org/10.1016/j.apcatb.2010.02.027

Spadavecchia, F., Cappelletti, G., Ardizzone, S., Ceotto, M., Azzola, M. S., Presti, L. Lo, … Falciola, L. (2012). Role of Pr on the Semiconductor Properties of Nanotitania. An Experimental and First-Principles Investigation. *The Journal of Physical Chemistry C*, *116*(43), 23083–23093. doi:10.1021/jp307303n

Svancara, I., Foret, P., & Vytras, K. (2004). A study on the determination of chromium as chromate at a carbon paste electrode modified with surfactants. *Talanta*, *64*(4), 844–52. doi:10.1016/j.talanta.2004.03.062

Švancara, I., Prior, C., Hočevar, S. B., & Wang, J. (2010). A Decade with Bismuth-Based Electrodes in Electroanalysis. *Electroanalysis*, *22*(13), 1405–1420. doi:10.1002/elan.200970017

Švancara, I., Vytřas, K., Kalcher, K., Walcarius, A., & Wang, J. (2009). Carbon Paste Electrodes in Facts, Numbers, and Notes: A Review on the Occasion of the 50-Years Jubilee of Carbon Paste in Electrochemistry and Electroanalysis. *Electroanalysis*, *21*(1), 7–28. doi:10.1002/elan.200804340

Tamburri, E., Orlanducci, S., Terranova, M. L., Valentini, F., Palleschi, G., Curulli, A., … Rossi, M. (2005). Modulation of electrical properties in single-walled carbon nanotube/conducting polymer composites. *Carbon*, *43*(6), 1213–1221. doi:10.1016/j.carbon.2004.12.014

Tessonnier, J.-P., Rosenthal, D., Hansen, T. W., Hess, C., Schuster, M. E., Blume, R., … Schlögl, R. (2009). Analysis of the structure and chemical properties of some commercial carbon nanostructures. *Carbon*, *47*(7), 1779–1798. doi:10.1016/j.carbon.2009.02.032

Thiagarajan, S., Rajkumar, M., & Chen, S. (2012). Nano TiO 2 -PEDOT Film for the Simultaneous Detection of Ascorbic Acid and Diclofenac, *7*, 2109–2122.

Thomas, P., & Sniatecki, K. (1995). Determination of Trace Amounts of Arsenic Species in Natural-Waters by High-Performance Liquid-Chromatography Inductively-Coupled Plasma-Mass Spectrometry. *Journal of Analytical Atomic Spectrometry*, *10*(9), 615–618. doi:Doi 10.1039/Ja9951000615

Thompson, M., Ellison, S. L. R., & Wood, R. (2002). Harmonized guidelines for single-laboratory validation of methods of analysis (IUPAC Technical Report). *Pure and Applied Chemistry*, *74*(5), 835–855. doi:10.1351/pac200274050835

Trasatti, S., & Petrii, O. A. (1991). Real surface area measurements in electrochemistry. *Pure and Applied Chemistry*, *63*(5), 711–734. doi:10.1351/pac199163050711

Tsai, Y.-C., & Huang, J.-D. (2006). Poly(vinyl alcohol)-assisted dispersion of multiwalled carbon nanotubes in aqueous solution for electroanalysis. *Electrochemistry Communications*, *8*(6), 956–960. doi:10.1016/j.elecom.2006.04.003

Umasankar, Y., Periasamy, A. P., & Chen, S.-M. (2011). Electrocatalysis and simultaneous determination of catechol and quinol by poly(malachite green) coated multiwalled carbon nanotube film. *Analytical biochemistry*, *411*(1), 71–9. doi:10.1016/j.ab.2010.12.002

Valcárcel, M., Simonet, B. M., Cárdenas, S., & Suárez, B. (2005). Present and future applications of carbon nanotubes to analytical science. *Analytical and bioanalytical chemistry*, *382*(8), 1783–90. doi:10.1007/s00216-005-3373-3

Valentini, F., Amine, A., Orlanducci, S., Terranova, M. L., & Palleschi, G. (2003). Carbon nanotube purification: preparation and characterization of carbon nanotube paste electrodes. *Analytical chemistry*, *75*(20), 5413–21. Retrieved from http://www.ncbi.nlm.nih.gov/pubmed/14710820

Valentini, F., Biagiotti, V., Lete, C., Palleschi, G., & Wang, J. (2007). The electrochemical detection of ammonia in drinking water based on multi-walled carbon nanotube/copper nanoparticle composite paste electrodes. *Sensors and Actuators B: Chemical*, *128*(1), 326–333. doi:10.1016/j.snb.2007.06.010

Vertova, A., Barhdadi, R., Cachet-Vivier, C., Locatelli, C., Minguzzi, A., Nedelec, J.-Y., & Rondinini, S. (2008). Cavity microelectrodes for the voltammetric investigation of electrocatalysts: the electroreduction of volatile organic halides on micro-sized silver powders. *Journal of Applied Electrochemistry*, *38*(7), 965–971. doi:10.1007/s10800-008-9507-5

Volpe, G., Draisci, R., Palleschi, G., & Compagnone, D. (1998). 3,3’,5,5’-Tetramethylbenzidine as electrochemical substrate for horseradish peroxidase based enzyme immunoassays. A comparative study. *The Analyst*, *123*(6), 1303–1307. doi:10.1039/a800255j

Vukomanovic, D. V., Vanloon, G. W., Nakatsu, K., & Zoutman, D. E. (1997). Determination of Chromium (VI) and (III) by Adsorptive Stripping Voltammetry with Pyrocatechol Violet. *Microchemical Journal*, *57*(1), 86–95. doi:10.1006/mchj.1997.1495

Wan, Q., Wang, X., Wang, X., & Yang, N. (2006). Poly(malachite green) film: Electrosynthesis, characterization, and sensor application. *Polymer*, *47*(22), 7684–7692. doi:10.1016/j.polymer.2006.09.002

Wanekaya, A. K. (2011). Applications of nanoscale carbon-based materials in heavy metal sensing and detection. *The Analyst*, *136*(21), 4383–91. doi:10.1039/c1an15574a

Wang, F., Hickner, M., Kim, Y. S., Zawodzinski, T. a., & McGrath, J. E. (2002). Direct polymerization of sulfonated poly(arylene ether sulfone) random (statistical) copolymers: candidates for new proton exchange membranes. *Journal of Membrane Science*, *197*(1-2), 231–242. doi:10.1016/S0376-7388(01)00620-2

Wang, J. (2008). Electrochemical glucose biosensors. *Chemical Reviews*, *108*(2), 814–825. doi:Doi 10.1021/Cr068123a

Wang, Jing. (2012). Electrochemical biosensing based on noble metal nanoparticles. *Microchimica Acta*, *177*(3-4), 245–270. doi:10.1007/s00604-011-0758-1

Wang, Joseph, Tian, B., Nascimento, V. B., & Angnes, L. (1998). Performance of screen-printed carbon electrodes fabricated from different carbon inks. *Electrochimica Acta*, *43*(23), 3459–3465. doi:10.1016/S0013-4686(98)00092-9

Wang, L., Ambrosi, A., & Pumera, M. (2013). Carbonaceous impurities in carbon nanotubes are responsible for accelerated electrochemistry of cytochrome c. *Analytical chemistry*, *85*(13), 6195–7. doi:10.1021/ac4010748

Wang, Qi, & Yun, Y. (2012). Nonenzymatic sensor for hydrogen peroxide based on the electrodeposition of silver nanoparticles on poly(ionic liquid)-stabilized graphene sheets. *Microchimica Acta*, *180*(3-4), 261–268. doi:10.1007/s00604-012-0921-3

Wang, Qing, Shang, J., Zhu, T., & Zhao, F. (2011). Efficient photoelectrocatalytic reduction of Cr(VI) using TiO2 nanotube arrays as the photoanode and a large-area titanium mesh as the photocathode. *Journal of Molecular Catalysis A: Chemical*, *335*(1-2), 242–247. doi:10.1016/j.molcata.2010.11.040

Wang, W., Zhang, T.-J., Zhang, D.-W., Li, H.-Y., Ma, Y.-R., Qi, L.-M., … Zhang, X.-X. (2011). Amperometric hydrogen peroxide biosensor based on the immobilization of heme proteins on gold nanoparticles-bacteria cellulose nanofibers nanocomposite. *Talanta*, *84*(1), 71–7. doi:10.1016/j.talanta.2010.12.015

Wang, Xiaoling, Pehkonen, S. O., & Ray, A. K. (2004). Removal of Aqueous Cr(VI) by a Combination of Photocatalytic Reduction and Coprecipitation. *Industrial & Engineering Chemistry Research*, *43*(7), 1665–1672. doi:10.1021/ie030580j

Wang, Xiaoxia, Yang, N., Wan, Q., & Wang, X. (2007). Catalytic capability of poly(malachite green) films based electrochemical sensor for oxidation of dopamine. *Sensors and Actuators B: Chemical*, *128*(1), 83–90. doi:10.1016/j.snb.2007.05.036

Welch, C M, Banks, C. E., Simm, A. O., & Compton, R. G. (2005). Silver nanoparticle assemblies supported on glassy-carbon electrodes for the electro-analytical detection of hydrogen peroxide. *Analytical and Bioanalytical Chemistry*, *382*(1), 12–21. doi:DOI 10.1007/s00216-005-3205-5

Welch, Christine M, Nekrassova, O., & Compton, R. G. (2005). Reduction of hexavalent chromium at solid electrodes in acidic media: reaction mechanism and analytical applications. *Talanta*, *65*(1), 74–80. doi:10.1016/j.talanta.2004.05.017

Wood, D. L., Chlistunoff, J., Majewski, J., & Borup, R. L. (2009). Nafion structural phenomena at platinum and carbon interfaces. *Journal of the American Chemical Society*, *131*(50), 18096–104. doi:10.1021/ja9033928

Xia, Y., & Liu, J. (2004). An overview on chronic arsenism via drinking water in PR China. *Toxicology*, *198*(1–3), 25–29. doi:http://dx.doi.org/10.1016/j.tox.2004.01.016

Xiao, X., Zhou, B., Zhu, L., Xu, L., Tan, L., Tang, H., … Yao, S. (2012). An reagentless glucose biosensor based on direct electrochemistry of glucose oxidase immobilized on

poly(methylene blue) doped silica nanocomposites. *Sensors and Actuators B: Chemical*, *165*(1), 126–132. doi:10.1016/j.snb.2012.02.029

Xie, Y., Zhou, L., & Huang, H. (2007). Bioelectrocatalytic application of titania nanotube array for molecule detection. *Biosensors & bioelectronics*, *22*(12), 2812–8. doi:10.1016/j.bios.2006.11.016

Xing, S. J., Xu, H., Chen, J. S., Shi, G. Y., & Jin, L. T. (2011). Nafion stabilized silver nanoparticles modified electrode and its application to Cr(VI) detection. *Journal of Electroanalytical Chemistry*, *652*(1-2), 60–65. doi:DOI 10.1016/j.jelechem.2010.03.035

Xing, S., Xu, H., Chen, J., Shi, G., & Jin, L. (2011). Nafion stabilized silver nanoparticles modified electrode and its application to Cr(VI) detection. *Journal of Electroanalytical Chemistry*, *652*(1-2), 60–65. doi:10.1016/j.jelechem.2010.03.035

Xu, B., Ye, M.-L., Yu, Y.-X., & Zhang, W.-D. (2010). A highly sensitive hydrogen peroxide amperometric sensor based on MnO2-modified vertically aligned multiwalled carbon nanotubes. *Analytica chimica acta*, *674*(1), 20–6. doi:10.1016/j.aca.2010.06.004

Xu, J., Shang, F., Luong, J. H. T., Razeeb, K. M., & Glennon, J. D. (2010). Direct electrochemistry of horseradish peroxidase immobilized on a monolayer modified nanowire array electrode. *Biosensors & bioelectronics*, *25*(6), 1313–8. doi:10.1016/j.bios.2009.10.018

Xu, X., Jiang, S., Hu, Z., & Liu, S. (2010). Nitrogen-doped carbon nanotubes: high electrocatalytic activity toward the oxidation of hydrogen peroxide and its application for biosensing. *ACS nano*, *4*(7), 4292–8. doi:10.1021/nn1010057

Xu, Z., & Meng, X. (2009). Size effects of nanocrystalline TiO2 on As(V) and As(III) adsorption and As(III) photooxidation. *Journal of Hazardous Materials*, *168*(2–3), 747–752. doi:http://dx.doi.org/10.1016/j.jhazmat.2009.02.084

Yáñez-Sedeño, P., Pingarrón, J. M., Riu, J., & Rius, F. X. (2010). Electrochemical sensing based on carbon nanotubes. *TrAC Trends in Analytical Chemistry*, *29*(9), 939–953. doi:10.1016/j.trac.2010.06.006

Yang, H. (2012). Enzyme-based ultrasensitive electrochemical biosensors. *Current opinion in chemical biology*, *16*(3-4), 422–8. doi:10.1016/j.cbpa.2012.03.015

Yi, H., Qu, W., & Huang, W. (2007). Electrochemical determination of malachite green using a multi-wall carbon nanotube modified glassy carbon electrode. *Microchimica Acta*, *160*(1-2), 291–296. doi:10.1007/s00604-007-0814-z

Yiğitoğlu, M., & Temoçin, Z. (2010). Removal of benzidine-based azo dye from aqueous solution using amide and amine-functionalized poly(ethylene terephthalate) fibers. *Fibers and Polymers*, *11*(7), 996–1002. doi:10.1007/s12221-010-0996-6

Yilmaz, E., Memon, S., & Yilmaz, M. (2010). Removal of direct azo dyes and aromatic amines from aqueous solutions using two beta-cyclodextrin-based polymers. *Journal of hazardous materials*, *174*(1-3), 592–7. doi:10.1016/j.jhazmat.2009.09.093

Yin, J., Qi, X., Yang, L., Hao, G., Li, J., & Zhong, J. (2011). A hydrogen peroxide electrochemical sensor based on silver nanoparticles decorated silicon nanowire arrays. *Electrochimica Acta*, *56*(11), 3884–3889. doi:10.1016/j.electacta.2011.02.033

Zhang, D., Shi, L., Fang, J., Li, X., & Dai, K. (2005). Preparation and modification of carbon nanotubes. *Materials Letters*, *59*(29-30), 4044–4047. doi:10.1016/j.matlet.2005.07.081

Zhang, K., & Zhang, Y. (2010). Electrochemical behavior of adriamycin at an electrode modified with silver nanoparticles and multi-walled carbon nanotubes, and its application. *Microchimica Acta*, *169*(1-2), 161–165. doi:10.1007/s00604-010-0331-3

Zhang, L., Duan, X., Wen, Y., Xu, J., Yao, Y., Lu, Y., … Zhang, O. (2012). Electrochemical behaviors of roxithromycin at poly(3,4-ethylenedioxythiophene) modified gold electrode and its electrochemical determination. *Electrochimica Acta*, *72*, 179–185. doi:10.1016/j.electacta.2012.04.019

Zhang, Q., Qiao, Y., Zhang, L., Wu, S., Zhou, H., Xu, J., & Song, X.-M. (2011). Direct Electrochemistry and Electrocatalysis of Horseradish Peroxidase Immobilized on Water Soluble Sulfonated Graphene Film via Self-assembly. *Electroanalysis*, *23*(4), 900–906. doi:10.1002/elan.201000614

Zhang, Yao, Sun, X., Zhu, L., Shen, H., & Jia, N. (2011). Electrochemical sensing based on graphene oxide/Prussian blue hybrid film modified electrode. *Electrochimica Acta*, *56*(3), 1239–1245. doi:10.1016/j.electacta.2010.11.011

Zhang, Yuzhong, Zhang, K., & Ma, H. (2009). Electrochemical DNA biosensor based on silver nanoparticles/poly(3-(3-pyridyl) acrylic acid)/carbon nanotubes modified electrode. *Analytical biochemistry*, *387*(1), 13–9. doi:10.1016/j.ab.2008.10.043

Zhu, Y., Wang, M., Du, H., Wang, F., Mou, S., & Haddad, P. R. (2002). Organic analysis by ion chromatography. 1. Determination of aromatic amines and aromatic diisocyanates by cation-exchange chromatography with amperometric detection. *Journal of chromatography. A*, *956*(1-2), 215–20. Retrieved from http://www.ncbi.nlm.nih.gov/pubmed/12108653

Zima, Jiri, Dejmkova, H., & Barek, J. (2007). HPLC Determination of Naphthalene Amino Derivatives Using Electrochemical Detection at Carbon Paste Electrodes. *Electroanalysis*, *19*(2-3), 185–190. doi:10.1002/elan.200603690

Zima, Jiří, Švancara, I., Barek, J., & Vytřas, K. (2009). Recent Advances in Electroanalysis of Organic Compounds at Carbon Paste Electrodes. *Critical Reviews in Analytical Chemistry*, *39*(3), 204–227. doi:10.1080/10408340903011853

Documents

- The Stockholm Convention on Persistent Organic Pollutants, 22 May 2001. <http://chm.pops.int/>.
- Report of the scientific panel on contaminants in the food chain on provisional findings on furan in food, EFSA J. 137 (2004) 1–20.
- home cooked food products and ready-to-eat products, Report of the EFSA CFP/DATEX/2007/03 project (2009) 1–49.
- C. Crews, Consumer exposure to furan from heat-processed foods and kitchen air, Scientific/technical report submitted to EFSA (2009) 1–65.
- Technical report of EFSA prepared by Data Collection and Exposure Unit (DATEX) on ‘‘Monitoring of furan levels in food’’, The EFSA Scientific Report 304 (2009) 1–23.
- US FDA, Report on Exploratory Data on furan in food (2004) 1–11.
- Swiss Federal Office of Public Health, Report on Furan in Lebensmitteln, 2004.
- USA EPA Priority Pollutant List, www.epa.gov.
- European Parliament and Council 2006/11/CE Directive, http://www.eea.europa.eu.
- IARC Special Report: Policy, Vol. 9, April 2008
- WHO, 17th Model List of Essential Medicines of World Health Organization,March 2011.
- EU, Commission Regulation 276/2010 31 March 2010.

- SCOEL/SUM/130, in: Scientific Committee on Occupational Exposure Limits formethylene chloride &LPKT;dichloromethane&RPKT; June 2009.

- J. Wang, “Electrochemical sensors for environmental monitoring: a review of recent technology”, Solicitation No. LV-94-012.

8. Appendixes

8.1. Analytical Parameters

All the analytical parameters were determined according to the IUPAC protocols:

- Limit of detection: inferior limit of concentration where the analyte can be distinguished from the blank.

  $LoD = \frac{3.29\times \sigma_{Blank}}{S}$, where *S*, indicating the method calibration sensitivity, is the slope of the linear calibration plot, and σ_{blank} is the blank standard deviation. When no blank signal could be detected, σ_{blank} was estimated by the standard deviation of 10 repeated scans on the same solution of the lowest available standard;

- Limit of quantification: inferior limit of analyte concentration measured with an acceptable precision and accuracy level.

  $LoQ = \frac{10\times \sigma_{Blank}}{S}$, where *S*, indicating the method calibration sensitivity, is the slope of the linear calibration plot, and σ_{blank} is the blank standard deviation. When no blank signal could be detected, σ_{blank} was estimated by the standard deviation of 10 repeated scans on the same solution of the lowest available standard;

- Relative standard deviation: absolute value of the coefficient of variation.

  $RSD\ \% = \frac{\sigma_{Blank}}{\bar{x}} \times 100$, where σ_{blank} is the blank standard deviation, estimated by the standard deviation of 10 repeated scans on the same solution of the lowest available standard, and $\bar{x}$ is the average value, calculated on the 10 repeated scans;

- Apparent recovery factor: observed value, x_{obs}, derived from an analytical procedure by means of a calibration graph divided by reference value, x_{ref}, indicating the accuracy of the method (higher accuracy when close to 100%)

$$RF = \frac{x_{obs}}{x_{ref}} \times 100$$

8.2. Electroanalytical Techniques (outlines)

8.2.1. Cyclic Voltammetry (CV)

In this technique, the potential of a working electrode is varied linearly with time until a step potential, where the potential ramp is inverted, and the resulting current is measured. This method allows characterizing the electrodes, in terms of capacitance, surface area, diffusion coefficient of the analyte, rate determining steps and reversibility.

Electrode capacitance *C* can be calculated varying the scan rate without the presence of the analyte, from the slope of the plot Δ*i vs* scan rate, derived from the equation $\frac{i_{cat}-i_{an}}{2} = Cv$.

When the analyte is present and is electroactive, if the plot i_p *vs* $v^{0.5}$, obtained by Randles-Sevcik equation $i_p = 0.4463\, nFAC \left(\frac{nFvD}{RT}\right)^{0.5}$, [where i_p is the peak current, *n* the number of electrons transferred in the redox event, *A* the electrode area, *F* the Faraday Constant, *D* the diffusion coefficient, *C* the concentration and *v* the scan rate], is linear, the rate determining step is the diffusion of the analyte to the electrode. On the other hand, if the peak current is proportional to the scan rate the rate determining step is the absorption of the analyte on the electrode. Moreover, the slope of the Randles-Sevcik plot can give information about the diffusion coefficient of the analyte and the surface area of the electrode.

Information about the diffusion mechanism can be obtained also from the slope of the $\ln i_p$ *vs* $\ln v$ plot, since the perfect diffusional behaviour gives a slope of 0.5.

A detailed description of the technique can be found in many dedicated books (Bard & Faulkner, 2001; Bard, 2007; C. M. A. Brett & Oliveira Brett, 1993).

8.2.2. Electrochemical Impedance Spectroscopy (EIS)

This technique measures the impedance (Z) of a system over a range of frequencies as a result of the perturbation of an applied potential or current. In this thesis, only the applied potential was employed to characterize electrodes. Impedance data can be presented using two types of plot: complex plane or Nyquist plot, the imaginary part of impedance (Z'') *vs* the real part (Z'), and the Bode plots: $|Z|$ *vs* frequency or phase angle *vs* frequency. Moreover, from the fitting of impedance data, information about the morphology and the electrical properties can be obtained, after the choice of the electrical circuit corresponding to the electrochemical system.

In the equivalent circuit, R_Ω is the cell resistance, R_{ct} represents the charge transfer resistance at the solid-liquid interface and R_{pol} the polarization resistance of the material. CPE_{dl} and CPE_{pol} are constant phase elements constituting the charge separation of the double layers and the polarization of the material, respectively. $CPE = [(Ci\omega)^{\alpha}]^{-1}$, is modelled as pure capacitor in the case of α=1 or as non-ideal capacitor, due to the porosity and non-homogeneity of the surface, for $0.5 < \alpha < 1$. The diffusional resistance R_W and the diffusional time constant τ are parameters of the Open Warburg Element, resulting from the equation $Z_W = R_W \mathrm{cth}[(\tau i\omega)^{\alpha}](\tau i\omega)^{-\alpha}$, where $\alpha < 0.5$.

A detailed description of the technique can be found in many dedicated books (Bard, 2007; Orazem & Tribollet, 2008).

8.2.3. Other voltammetric or amperometric techniques

This is the list of all the employed electrochemical techniques with a brief description. A detailed description of all the techniques can be found in many dedicated books (Bard & Faulkner, 2001; Bard, 2007; C. M. A. Brett & Oliveira Brett, 1993) and it is out of the scope of this Thesis:

- Linear Sweep Voltammetry (LSV): the potential of a working electrode is varied linearly with time and the resulting current is measured;
- Linear Sweep Adsorptive Stripping Voltammetry (LSAdSV): preconcentration deposition is performed before LSV stripping;
- Square-Wave Voltammetry (SWV): a square-wave is superimposed on the potential linear sweep and the resulting current is measured at the end of each potential change, minimising the capacitive currents;
- Differential Pulse Voltammetry (DPV): a series of regular voltage pulses is superimposed on the potential linear sweep and the resulting current is measured immediately before each potential change;
- Chronoamperometry: the potential is maintained at a chosen value and the resulting current is measured during time.

8.3. List of papers and Congress Communications

Papers:

- Luigi Falciola, Valentina Pifferi, Maria Luisa Possenti, Veronica Carrara
  "*Square Wave Voltammetric detection of furan on platinum and platinum-based Screen Printed Electrodes*"
  Journal of Electroanalytical Chemistry, 664 (1), (2012), 100-104
  DOI: 10.1016/j.jelechem.2011.10.021
- Luigi Falciola, Valentina Pifferi, Elisabetta Mascheroni

"*Platinum-based and Carbon-based Screen Printed Electrodes for the determination of benzidine by Differential Pulse Voltammetry*"
Electroanalysis, 24 (4), (2012), 767-775
DOI: 10.1002/elan.201200007

- Daniela Meroni, Valentina Pifferi, Beatrice Sironi, Giuseppe Cappelletti, Luigi Falciola, Giuseppina Cerrato, Silvia Ardizzone
"*Block copolymers for the synthesis of pure and Bi-promoted nano-TiO2 as active photocatalysts*"
Journal of Nanoparticles Research, 14 (8), (2012), 1086-1101
DOI: 10.1007/s11051-012-1086-z

- Valentina Pifferi, Francesca Spadavecchia, Giuseppe Cappelletti, Elisa A. Paoli, Claudia L. Bianchi, Luigi Falciola
"*Electrodeposited nano-titania films for photocatalytic Cr(VI) reduction*"
Catalysis Today, 209, (2013), 8-12
DOI: 10.1016/j.cattod.2012.08.031

- Valentina Pifferi, Madalina M. Barsan, M. Emilia Ghica, Luigi Falciola, Christopher M.A. Brett
"*Synthesis, characterization and influence of poly(brilliant green) on the performance of different electrode architectures based on carbon nanotubes and poly(3,4 ethylenedioxythiophene)*"
Electrochimica Acta, 98, (2013), 199-207
DOI: 10.1016/j.electacta.2013.03.048

- Valentina Pifferi, Valeria Marona, Mariangela Longhi, Luigi Falciola
"*Characterization of polymer stabilized silver nanoparticles modified Glassy Carbon electrodes for electroanalytical applications*"
Electrochimica Acta, 109, (2013), 447-453
DOI: 10.1016/j.electacta.2013.07.194

- Giulia Maino, Daniela Meroni, Valentina Pifferi, Luigi Falciola, Guido Soliveri, Giuseppe Cappelletti, Silvia Ardizzone
"*Electrochemically assisted deposition of transparent,mechanically robust TiO2 films for advanced applications*"
Journal of Nanoparticles Research, 15, (2013), 2087-2097
DOI: 10.1007/s11051-013-2087-2

- Valentina Pifferi, Silvia Ardizzone, Giuseppe Cappelletti, Luigi Falciola, Daniela Meroni
"*Ultra-Traces Detection by Gold-Based Electrodes in As(III)Novel Photoremediation*"
Electrocatalysis, 4, (2013), 306-311
DOI: 10.1007/s12678-013-0163-0

- Paolo Ferruti, Nicolò Mauro, Luigi Falciola, Valentina Pifferi, Cristina Bartoli, Matteo Gazzarri, Federica Chiellini, Elisabetta Ranucci
"*Amphoteric, Prevailingly Cationic L-Arginine Polymers of Poly(amidoamino acid) Structure: Synthesis, Acid/Base Properties and Preliminary Cytocompatibility and Cell-Permeating Characterizations*"

Macromolecular Bioscience, (2013), accepted, in press
DOI: 10.1002/mabi.201300387

Communications:

- Valentina Pifferi, Giuseppe Cappelletti, Luigi Falciola, Elisa Paoli, Francesca Spadavecchia
  "*Electrochemical capabilities in both photoreduction and detection of toxic Cr(VI) pollutant*"
  XXIV Congresso Nazionale della Società Chimica Italiana (Lecce, Italia 11-16 September 2011)

- Luigi Falciola, Valentina Pifferi, Elisabetta Mascheroni, Alice Ballerini, Marta Decio
  "*Electroanalytical determination of benzidine by differential pulse voltammetry on different electrodes*"
  XXIV Congresso Nazionale della Società Chimica Italiana (Lecce, Italia 11-16 September 2011)

- Luigi Falciola, Valentina Pifferi, Chiara Di Bari, Giuseppe Cappelletti, Francesca Spadavecchia, Elena Ferrari, Paolo Ferruti, Amedea Manfredi, Elisabetta Ranucci
  "*Carbon-based electrodes for the electroanalytical monitoring of o-toluidine*"
  GS 2013 (Sestri Levante, Italia 19-20 September 2013)

- Luigi Falciola, Valentina Pifferi, Stefano Bonacina, Chiara Di Bari, Giuseppe Cappelletti
  "*Electroanalytical monitoring of o-toluidine at carbon based electrodes. Application to its photocatalytic oxidation mediated by ZnO*"
  GEI 2013 (Pavia, Italia 22-27 September 2013)

- Daniela Meroni, Valentina Pifferi, Luigi Falciola, Guido Soliveri, Giuseppe Cappelletti, Silvia Ardizzone
  "*Electrochemical Synthesis And Applications of Transparent Titania Layers*"
  GEI 2013 (Pavia, Italia 22-27 September 2013)

9. Acknowledgements

At the end of these long and at the same time short three years, it is time to express my gratitude to all the people who have shared with me the work and the life.

My first thank goes to my supervisor, Dr. Luigi Falciola, who gave me the opportunity to work in his laboratory and the possibility to discover the new world of electrochemistry, also being my mentor for scientific and personal life.

My deepest gratitude goes to Prof. Silvia Ardizzone and Dr. Giuseppe Cappelletti, from my Master Thesis Laboratory, who continue to collaborate with me and support me, not only from the research, but also from the personal point of view.

I would like to thank Prof. C.M.A. Brett from Coimbra University, where I studied for a period of six months, who has given me the opportunity to work in its laboratory, learning fundamental concepts and methodologies which today I apply in my research.

My deep thanks to Dr. Daniela Meroni and Dr. Francesca Spadavecchia, who have welcomed me during my Master Thesis, and today are still part of my life. Daniela, who continue to share with me the work and she is not only a scientific mates, but also a friend; Francesca, who, even we don't meet at work, is still present as confidant.

A special thank to Iole, always helpful to solve my scientific problems, but also always ready to listen and give advice to me.

A deep thank to Guido, for our interesting collaboration and our pleasant culinary chats.

My acknowledgements go to all people who collaborate with me, Prof. Prati and Dr. Villa for the synthesis of nanoparticles supported on carbon nanotubes, Prof. Ranucci and Prof. Ferruti for the

synthesis of cyclodextrine-based nanosponges, Prof. Di Silvestro for the synthesis of poly(aryl ether sulfone)s, Prof. Agostiano and Dr. Comparelli for the synthesis of titanium dioxide nanorods. A big thank to Elena, not only for the samples who prepared for me, but also for our friendly chats.

A special thank to all my students of the lab (Monica, Erica, Maria, Marta, Nicolò, Valeria, Jessica, Mattia, Stefano, Simone, Luca, Maurizio, Fulvia, Marika, Eleni, Paola, Ilaria, Serena, Alberto, Elisabetta, Veronica, Francesca,…), but also to those of close laboratory (Chiara, Alice, Chiara, Federico, Miriam, Beatrice,…) for the passion and the effort they had in their job, always ready to listen to me, to work with me and to laugh.

My gratitude goes to all the laboratory mates of Coimbra, Madi, Carolina, Carla, Ricardo, who have make me feel welcome and have make those months unforgettable. A special thank to Madalina, who teaches me everything in the lab, but who was and is a special friend (estou com saudade!).

My thanks to all my friends of the theatre and of the gym, and in particular to my best friend Vanessa, who always supports me.

My gratitude to all my grandparents and uncles, who always want to know what I do and how I feel.

Last, but not least, my infinite gratitude to my parents and my brother, who support me with love and who are proud of me, and to Nicolò, who shared with me the last three years and more.